Multiphase Flow and Control of Fluid Path in Microsystems

By

Manish Jhunjhunwala

Submitted to the Department of Chemical Engineering in partial fulfillment of the requirements for the degree of

Doctor of Philosophy in Chemical Engineering Practice

at the

MASSACHUSETTS INSTITUTE OF TECHNOLOGY

[February 2005]
August 2003

Author.....
Manish Jhunjhunwala
Department of Chemical Engineering

Certified by.....
Klavs F. Jensen
Lammot duPont Professor of Chemical Engineering
Professor of Materials Science and Engineerng
Thesis Supervisor

Accepted by.....
Daniel Blankschtein
Professor of Chemical Engineering
Chairman, Committee for Graduate Students

Abstract

Miniaturized chemical-systems are expected to have advantages of handling, portability, cost, speed, reproducibility and safety. Control of fluid path in small channels between processes in a chemical/biological network is crucial for connecting process elements. We show complete separation of individual phases (phase routing) from two-phase gas-liquid and liquid-liquid (aqueous-organic) mixtures on microscale. To provide for robust interfacing of operations in a network, we demonstrate this ability over a wide range of two-phase flow conditions, including transient ones.

Enabled by the technique for complete separation of individual phases from two-phase mixtures, we show mixing of liquids by introduction of a passive gas-phase and demonstrate integration of mixing, reaction and phase separation on a single platform. Additionally, we use the principles developed for phase routing to design microfluidic valves that do not rely on elastic deformation of material. Such valves can be used in a variety of chemical environments, where polymer-based deformable materials would fail. We show a concept for realization of logic-gates on microscale using appropriate connections for these valves, paving the way for design of automation and computational control directly into microfluidic analysis without use of electronics.

Further, we use the phase separation concept for sampling liquid from gas-liquid and liquid-liquid mixtures. Such sampling ability, when coupled with a suitable analysis system, can be used for retrieving process information (example mass-transfer coefficients, chemical kinetics) from multiphase-processes. We provide evidence of this through estimation of mass-transfer coefficients in a model oxygen-water system and show at least an order-of-magnitude improvement over macroscale systems.

Controlled definition of fluid path enabled by laminar flow on microscale is used in a large number of applications. We examine the role of gravity in determining flow path of fluids in a microchannel. We demonstrate density-gradient-driven flows leading to complete reorientation of fluids in the gravitational field. We provide estimates of the time and velocity scales for different parameter ranges through two-dimensional and three-dimensional finite-element models, in agreement with experimental observations. We believe this thesis addresses a number of both: system and fundamental issues, advancing applications and understanding of microfluidic networks.

Acknowledgements

Before I acknowledge the people directly connected with this work I would like to acknowledge the love and support of my family, especially my father. I am indebted to him for my education.

I found in Prof. Klavs Jensen a remarkable advisor. Without his encouragement and advice this work would be unfathomable. Apart from being an exemplary tutor he is a wonderful person and I think I have learnt a lot more from him than I can thank him for. I literally do not have the words to express the gratitude I feel for everything.

I would like to thank Prof. Marty Schmidt for his guidance, especially with the silicon microfabricated device. To have someone with his expertise help with a long sequential process, even at the design stage, is invaluable. Without his advice realization of the devices presented here would have been severely jeopardized.

Prof. Pat Doyle always had a ready ear and provided valuable suggestions with experiments at all stages, and I am thankful for his comments.

I started with the microreactor group under the mentorship of Matt Losey. Matt not only allowed me to use his devices initially when I had no clue how to make them, but also took the pains to go through his process with me. I continued to use his tips with success and am obliged to him for his inputs.

Large portions of this work were carried out in collaboration with Axel Guenther, a postdoctoral associate in the group. I am thankful for his insights and help at all stages of the work including the details, especially his help with multiphase flow imaging and microscopy, where his experience was invaluable.

I want to thank Zhiyu Zhang for collaboration with the work on realization of valves. He continues to investigate their integration in his system and his patience convinces me about the results.

Tobias Kraus helped with the error analysis and in developing the methodology for mass transfer measurements and I appreciate his efforts.

I also want to thank Brian Yen for providing the quantum dots that were used in the quantification of the extent of mixing, we can only appreciate the amount of work that he must have put in their preparation while always providing them graciously.

I am also thankful to members of the group for empathizing with my failures in the laboratory and the fab, and the MTL community for help and advice with the fabrication. It is definitely a great fortune to be able to learn from their experience.

Finally I would like to thank all my friends for being around when I needed, especially Nitesh, Manish and Pooja, I feel fortunate to have such friends.

List of Figures

1. Introduction

1.1. Motivation

The potential for increased performance from miniaturization of a system is tremendous. The impact realized in efficient interaction of multiple such systems even more promising. The ability to capture increasing number of capabilities in a smaller space provides an opportunity for realization of high performance sophisticated systems through increased interactions between complex components. The revolution that the electronics industry has seen from integration is evident in the decreasing size and an exponential increase in functionality of electronic devices. The impact this evolution has made in various aspects of human life is truly incredible.

Micro-Electro-Mechanical-Systems (MEMS) and Microchemical Systems have been identified to represent similar, though unique opportunities, with the latter carrying the potential to alter the pace as well as practice of biology and chemistry through miniaturization of chemical processing systems. Opportunities for such systems exist in delivering the technology required both for creating a consumer or mass market for these devices, for example through easy-to-use diagnostic solutions, developing capabilities required for their use in specialized functions, and research and development tools. In addition to the inherent advantages of high speed, low cost and safety, initial efforts with microchemical systems quickly realized benefits from improved with heat and mass transfer processes for reactions otherwise limited by heat/mass transfer. The initial success and intrigue attracted considerable interest from people in different disciplines and led to a fast growth and evolution of this field over the past few years. As is

symptomatic of most positive evolutions, the success of processes or components demands transformation into systems. These evolve into more complex systems or networks, which when packaged and the economic perspective incorporated gives rise to solutions.

As a result, a positively evolving field stresses two requirements: the need to build increasingly sophisticated systems by integration with other successful systems through efficient interactions, and the need to continuously add to the basic level of knowledge in the field. The latter allows better understanding of concepts necessary for efficient evolution to more complicated systems.

Recent years has seen an increased thrust in both directions for the field of microchemical systems. There is continued interest in development of techniques for characterization and understanding of chemical processes of increased complexity on microscale, one such example being increased interest in multiphase chemistry compared to single phase chemical systems. At the same time, attraction from being able to perform multiple operations on a single platform or a chip continues to grow. Increasing number of efforts in the field are addressing the need to create systems capable of multiple sequential operations, catering to specific application requirements. The functionality of a complex system hinges on the nature of interaction of its parts, which implies that the functionality of a system emerges from the efficiency of interaction that can be provided among the components.

For chemistry on microscale, this means the ability to transfer fluids between processes in a complex system or a network. Multistep chemical processes requiring mixing, heat/mass transfer, reactions and separation are common across chemical,

biochemical and pharmaceutical industries. A model multistep synthesis sequence is suggested in Figure 1-1. Such a sequence represents a small part of the chemical/biological processing networks that combine interaction with analysis and control devices necessary for an automated system. Valves to shuttle fluids between elements of the network and capable of operation in variety of chemical environments are important for realization of these complex chemical sequences. In addition, processes for routing or separation of individual phases from a two-phase mixture, under varying conditions and for a wide range of operating conditions is crucial to realization of such networks, and they represent an opportunity for enhancement of microscale chemical processing capabilities. Thus *control of fluid path between different processes in a network* is essential for evolving present abilities into complete microsystems and solutions on microscale. Continued development will require automation, ideally accompanied with the ability to program the required manipulations through miniaturized fluidic logic without the use of electronic interfacing [1]. In addition, the opportunity available in terms of increased characterization of microscale multiphase systems for the purpose of extracting useful process information is growing. Microscale chemical systems used to derive process information have improved basic understanding of multiphase applications including catalysis and have also expanded the knowledge base that impacts performance of large scale systems. The ability to partly draw out one of the phases through *control of fluid path between a multiphase process and the sensing and information analysis section* could be used as a valuable source of information retrieved from a multiphase system. The existence of these opportunities and the concomitant

potential revolution in the practice of chemistry and biology at a progressively faster speed, serve as motivations for this work.

The development of devices manipulating fluid volumes inside a small channel and among networks of small channels, must be preceded by refinement of understanding for the nature of interaction between forces of inertia, viscosity, buoyancy and those arising at the interface of two phases. Increased understanding of fluid flow and physical parametric conditions in which the different forces serve as source of fluid motion and govern the path of fluid on microscale is necessary to be able to provide the tools for manipulating these forces. This thesis aims to provide this understanding as a step towards realizing control of fluid path on microscale.

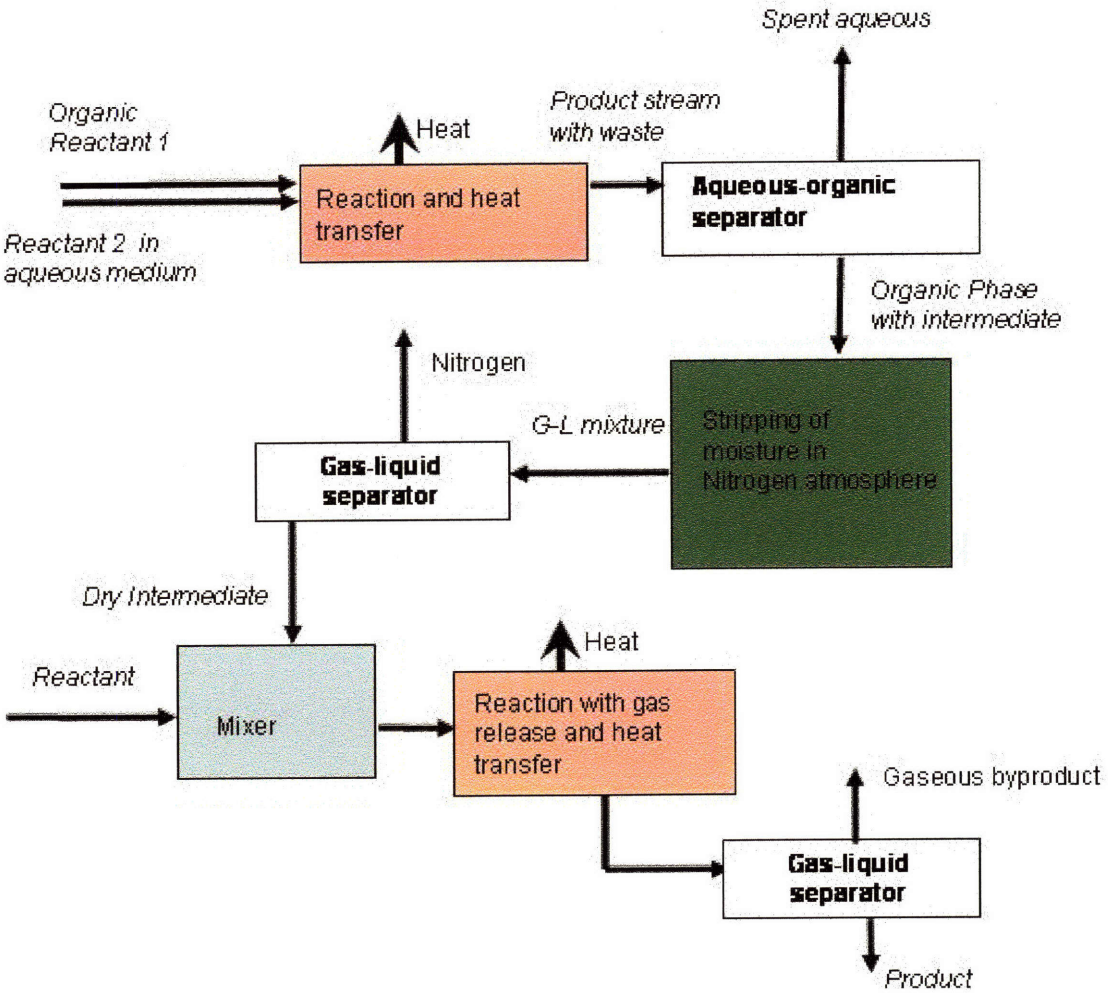

Figure 1-1. An example of a multistep synthesis sequence, potentially representing only a section of a miniaturized multistage chemical/biological processing network of tomorrow

1.2. Thesis Objectives

The objectives of this thesis are to provide for the understanding required for an improved ability to control the fluid path in microscale systems. One goal is demonstration of separately routing individual phases from two-phase gas-liquid and liquid-liquid mixtures over a range of flow velocities and individual fractions of the two-phases. Another goal is to use the generalized understanding developed in this to demonstrate its applicability to relevant problems of interest on microscale. Examples include deriving information from multiphase processes, realization of valves useful in shuttling fluids between processes for a large range of chemical environments, the concept for realization of fluid logic required for building in automation through fluidics rather than electronics and methodologies based on multiphase systems for mixing liquids and demonstration of multiple processing steps on a single platform. Yet another aim is to use the basic understanding of forces to emphasize situations in which one might be more relevant than the other, especially for buoyancy forces. Additionally to demonstrate the effect that this interaction might have on the path of fluids on microscale, and the conditions under which they are important.

1.3. Thesis Outline

Chapter 2 of this thesis describes the basic principles for the construction of a device capable of phase separation or routing individual phases from two-phase gas-liquid and liquid-liquid mixtures. It also details the experiments carried out to develop this understanding and characterization with respect to relevant parameters. The principles laid out, Chapter 3 describes the devices used in this thesis. The details for silicon microfabrication of device for demonstration of phase separation, information retrieval, on-chip gas-liquid mass transfer measurement, mixing and studying the interaction of different forces on microscale is provided. This chapter also describes the realization of devices using alternative techniques of metal/plastic machining. We use these for demonstration of microfluidic valves, development of concept of fluid logic and in general as proof-of-concept devices in other studies. Chapter 4 presents the results for separately routing individual phases from gas-liquid and liquid-liquid two-phase mixtures using the devices described in Chapter 3 and based on the principles outlined in Chapter 2. It also shows the use of the separation and routing concept in sampling a small fraction of liquid phase from a two-phase flow stream, and emphasizes the general applicability of this technique in retrieving multiphase microscale process information. The chapter further outlines general applications of the understanding developed in routing of phases. It uses the concept in realization of valves on microscale, without involvement of deformable/elastic structures common to other microscale valve designs. It further shows how these valves can be connected to realize microfluidic logic-gates. The use of developed technique for retrieval of information from multiphase systems, described in Chapter 4, is demonstrated through a model gas (oxygen)-liquid (water) system in

Chapter 5. This chapter details the on-chip integration of a sensor for measurement of oxygen concentration and the subsequent estimation of mass transfer coefficient for this system. A comparison of the obtained results with measurements in the literature for larger scale is drawn and the advantages arising from chemical processing on microscale are delineated. Chapter 6 describes a novel strategy for mixing liquids on microscale that uses introduction of gas phase into two liquid streams to obtain a transient gas-liquid slug flow. It demonstrates the efficient mixing of the liquids obtained in the transient two-phase regime. This chapter also briefly describes the methodology used for estimation of the extent of mixing, discussed in detail elsewhere, but focuses on integration of the sequential processing steps of mixing (through this novel strategy), reaction and subsequent separation of individual phases from the two-phase mixture (using the phase routing principle developed).

Chapter 7 is devoted to the study of role of buoyancy force on microscale in determining the path of multiphase miscible fluids. It presents the results from experiments on miscible liquids with a density difference coflowing in a microchannel and identifies the important parameters controlling buoyancy driven flows on microscale. 2-dimensional transient and 3-dimensional steady state finite element models are used to understand the system and confirming the experimental observations. The thesis concludes with a summary of major contributions highlighted in Chapter 8. This chapter also lays out some of the potential future opportunities with microscale chemical systems.

2. *Principles for phase routing on microscale*

2.1.Background

Multistep, microscale chemical/biological processing networks capture capabilities of mixing, mass/heat transfer, reaction, separation, and analysis on a single platform on microscale. They are altering the pace as well as practice of biology and chemistry [2]. However, control of fluid path from output node of one process to the input node of another, without disturbing other parts of the network sequence, remains a challenge. The efficiency of this fluid routing limits the extent to which a network can be interconnected and its functionality.

Networks with integrated micromechanical valves and pumps for controlling the fluid flow between microscale processing steps, have recently been developed [3, 4], and they partially addressed the problem of integration. The need to transfer different types of fluid phase (data packets) received at a node in a network, to different processing or storage steps remains unanswered. In data networks, routers receive information from different parts of the network and direct it to the appropriate destination address. This increases the efficiency of data flow within the network manifold as a specific data packet does not engage the capacity of all the different nodes on a network before reaching its destination. The concept is indispensable for the present day Internet and its performance is critical to the efficient functioning of any network. In chemical/biological networks two-phase gas-liquid and liquid-liquid mixtures occur commonly and need to be separated and transferred to subsequent processing steps.

Fluidic-phase routers for separately directing individual phases from a gas-liquid or liquid-liquid mixture over a large range of flow conditions, are critical to the realization of networks that can address needs of connectivity.

2.2. Dominance of Surface Force on Microscale

Surface forces dominate on microscale, and can be used to overcome viscous and gravitational forces to generate inertia. For a drop of liquid with viscosity μ, density ρ, moving at a velocity U in a microchannel of length scale L, (L = diameter d for a channel of circular cross-section, or the hydraulic diameter for other cross-sectional shapes), the inertial, viscous and buoyancy forces normalized by the liquid-vapor interfacial tension, γ, can be expressed in terms of the dimensionless Capillary number (*Ca*), Weber number (*We*) and Bond number (*Bo*) respectively:

$$We = \rho U^2 L / \gamma,\ Ca = \mu U / \gamma,\ Bo = \Delta\rho U L^2 / \gamma \tag{2.1}$$

Here, $\Delta\rho$ is the density difference between liquid and vapor (for most cases $\Delta\rho \sim \rho$). A plot for these dimensionless numbers for liquid water (ρ= *1000 kg/m^3*, μ = *1e-3 kg/(m-s)*, γ = *0.072 N/m*), on length scales from *10 μm -1 mm* over a range of velocities (*100 μm/s to 1 cm/s*) commonly encountered in microscale applications, shows the dominance of surface forces on microscale, (Figure 2-1).

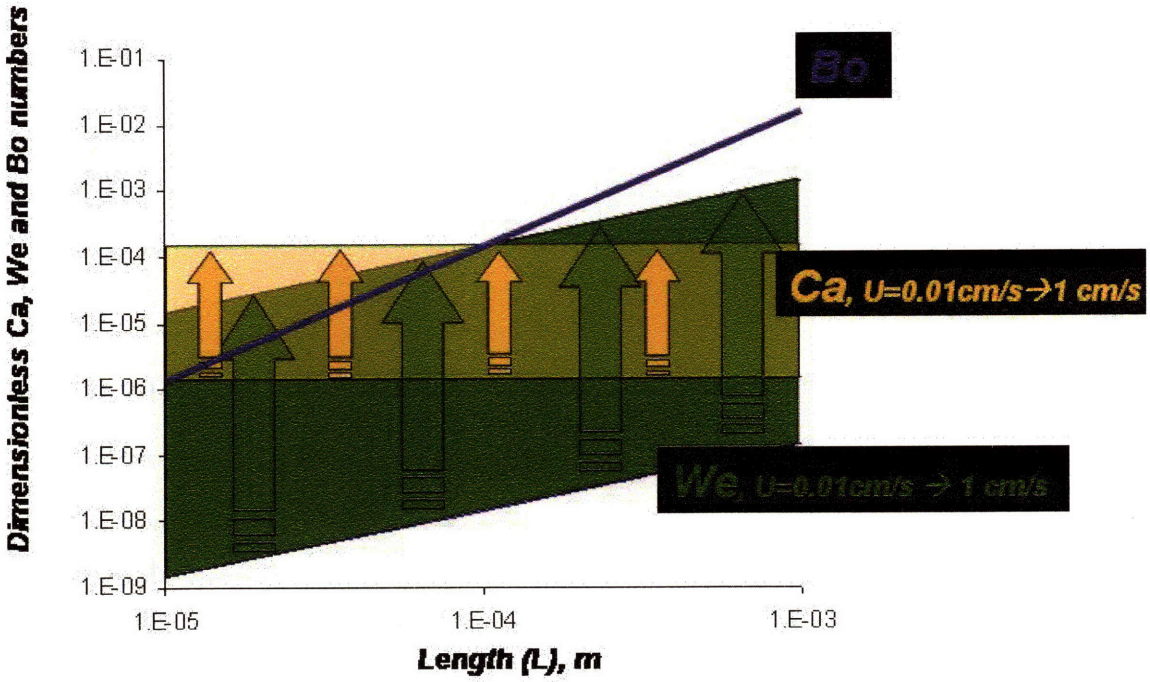

Figure 2-1. On microscale the inertial, viscous and buoyancy forces are much smaller than the interfacial force.

Consider a drop of liquid φ_1 resting on a solid surface S, (Figure 2-2). A contact line is formed at the intersection of the solid, liquid and vapor, V, phases. Young's equation, [5]

$$\gamma_{\varphi_1-V}\cos(\theta_{ce}) = \gamma_{S-V} - \gamma_{S-\varphi_1} \tag{2.2}$$

relates the equilibrium contact angle, θ_{ce} (measured from the liquid side of the contact line), to the interfacial free energies, γ_{ij}, between the three phases.

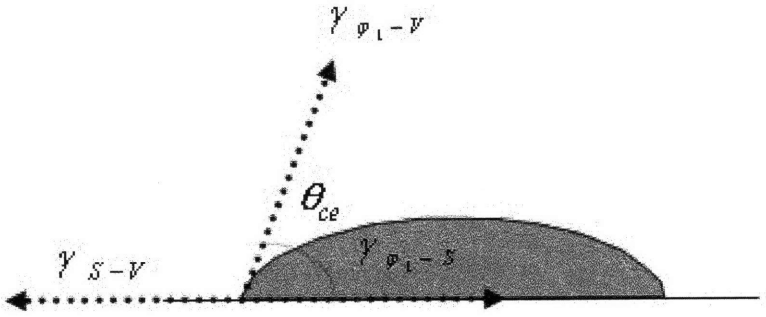

$$\gamma_{S-V} = \gamma_{\varphi_1-V} \cos\theta_{ce} + \gamma_{\varphi_1-S}$$

Figure 2-2. The equilibrium between forces acting at the 3 phase contact line formed at the solid-liquid-vapor boundary. This equilibrium defines the contact angle θ_{ce} for a given 3 phase system. The liquid is said to wet the surface for $\theta_{ce} < 90°$, and has a stabilizing effect on the solid surface. For these cases the $\gamma_{S-V} > \gamma_{\varphi_1-S}$ and the liquid is said to stabilize the solid surface. The presence of liquid on the solid being energetically favored, it spreads on solid. For $\theta_{ce} > 90°$, liquid does not wet the surface and $\gamma_{S-V} > \gamma_{\varphi_1-S}$, and the liquid tends to ball-up on the surface.

Local modification of the interfacial energies at different parts of the contact line can be used to generate an unbalanced force and can produce motion of the drop. The direction in which force is generated can be designed, and correspondingly the movement/positioning of fluids controlled by suitable modification of surface forces through utilization of thermal, [6, 7], [8], chemical and electrochemical [9-12], optical [13], electrical energy [14, 15] or by combinations of these. Confining liquid flow along patterned surfaces has been demonstrated [16], and it has been possible to maintain a flow of immiscible streams with a steady interface using this strategy [17]. However, such schemes are not designed to address the need for receiving a two-phase mixture from one part of a processing network under variable inflow conditions of pressure, phase velocities or distributions and transferring them separately to subsequent processes in the network.

2.3. Overview of strategy

Fluid flow in a channel is defined by interaction between inertial, viscous, interfacial and body (gravitational, magnetic, electrical) forces. Surface tension force at the interface of miscible (similar) fluids is negligible while immiscible (dissimilar) fluids have large energy associated with the interface. We demonstrate the concept of a phase-router that uses this essential difference between interface of miscible and immiscible fluids for switching between two states. The router does not contain any moving parts and operates in a binary mode. It switches 'on' to be completely-open allowing flow of 'select phase' through it and switches 'off' to completely close, directing the 'second phase' along a different fluidic path. We use it to separate individual phases from gas-liquid and liquid-liquid two phase mixtures.

The phase separation strategy aims at selectively removing one liquid phase, the 'select phase', φ_1, completely from the mixture through the fluid-phase router, thereby also obtaining a separate stream for the other fluid phase, the 'second phase', φ_2. We design the router as a capillary tube of diameter, $d \sim 10\ \mu m$ and operate it with φ_1 filling the router. When φ_2 fraction of the two-phase mixture arrives at the router, a meniscus is formed at its inlet. We choose the router surface, *S*, such that φ_2 is non-wetting while φ_1 wets the surface. This sets the meniscus curvature such that pressure on the φ_1 side of inlet, P_{φ_1}, is lower than the pressure at the router inlet, P_i, the side with φ_2. This pressure drop across the meniscus, $\Delta P_m \equiv P_i - P_{\varphi_1}$, can be expressed by the Young-Laplace equation as,

$$\Delta P_m = \gamma_{\phi_1-\phi_2} C \qquad (2.3)$$

where C is the meniscus curvature. For a cylindrical capillary tube a spherical shape of the meniscus can be assumed and $C = 4\cos\theta_{ce}/d$, [18].

The difference in pressure between the router inlet and the outlet, $\Delta P_i \equiv P_i - P_o = \Delta P_m - \Delta P_h + \Delta P_f$, where P_o is pressure at the outlet (often a common port from multiple routers where φ_1 directed through the routers is collected and a constant pressure may be maintained), $\Delta P_h = h\rho_{\varphi_1} g$ is the hydrostatic head due to an elevation h of the inlet with respect to the outlet, ρ_{φ_1} the φ_1 density, and ΔP_f the pressure drop due to flow through the router. Liquid flows in the router when $\Delta P_f > 0$, or $\Delta P_T - \Delta P_m > 0$, where $\Delta P_T = \Delta P_i + \Delta P_h$, is the total pressure head applied between the inlet and the outlet and equals the sum of excess pressure at the router inlet over the outlet and the hydrostatic head applied.

We show that the meniscus adjusts itself to resist any flow of φ_2 thereby directing φ_2 to an alternate fluidic path for all ΔP_T less than a maximum pressure ΔP_{max}. In this case with presence of φ_2 fraction at the router inlet, $\Delta P_m = \Delta P_T$ and $\Delta P_f = 0$. However, when portions of the mixture containing φ_1 arrive at the router inlet, the meniscus vanishes. In absence of any interfacial force $\Delta P_m = 0$ and $\Delta P_f = \Delta P_T$, the router switches 'on' and completely opens to allow the φ_1 fraction in the mixture to flow through it under the influence of unbalanced ΔP_T. We use an array of routers to obtain the required flow capacity for directing φ_1 completely from the two-phase mixture, through the routers. We design a router of small length, $l_c \sim 1\ mm$, to obtain a low pressure drop for the flow of φ_1 through it. Then the ΔP_T required for expected flow capacity, can be designed as a small fraction of ΔP_{max}. Assuming a fixed P_o, the meniscus then adapts to pressure fluctuations at the inlet smaller than $(\Delta P_{max} - \Delta P_T)$.

Due to presence of interfacial forces, the flow of immiscible fluids, like an organic and an aqueous phase or a gas and liquid, can assume different patterns: bubbly flow, with small bubbles of one phase dispersed in the other phase, plug/slug flow with bubble size comparable to the channel diameter, and annular with one phase forming the core of channel while the other surrounds and flows at the periphery, and are all observed on microscale [19-25]. These regimes are commonly encountered, and attractive in various chemical processing applications, including those requiring good contacting between immiscible phases. We show that the capability of meniscus to adapt to pressure disturbances and spontaneously self-actuate between the two states, allows separation of two-phase mixtures across different flow patterns, including transient 'bubbly' and 'slug' regimes.

2.4. Adaptation of meniscus in a single capillary

We observe the spontaneous self-adaptation of the liquid meniscus using a single capillary tube. When one end of a capillary tube is dipped in a trough containing liquid that wets the capillary wall, the liquid rises inside the tube to a level higher than the level of liquid in the trough. This capillary rise is due to a pressure difference, $\Delta P_m = 4\gamma_{\phi_1-V}\cos(\theta_{ce})/d$, created across the meniscus. The liquid rises in the capillary to a height h_{ce} such that the hydrostatic pressure drop in the column of liquid in capillary, $\Delta P_h = \rho_{\phi_1} g h_{ce}$, is equal to ΔP_m and $h_{ce} = 4\gamma_{\phi_1-V}\cos(\theta_{ce})/(\Delta\rho g d)$, where g is the gravitational acceleration and the pressure contribution due to gravitational head of air is neglected in comparison to that of liquid (assuming $\rho_{\phi_1} >> \rho_{air}$). θ_{ce} being an equilibrium property is determined solely by the thermodynamic parameters and for a certain solid-

liquid-fluid system, for a capillary of a given diameter the capillary rise, h_{ce}, must be fixed.

However, the influence of contact angle is indirect, as contact angle in small diameter capillaries controls the radius of curvature of the meniscus which in turn regulates ΔP_m, [26]. Then the curvature C can be expressed as, $C = 4\sin\alpha/d$ and the radius of curvature, $R = d/(2\sin\alpha)$, where $\alpha = \pi/2 - \theta_{ce}$, is the angle of curvature, (Figure 2-3). We use a 340 μm diameter glass capillary tube, with one end lowered in a trough containing water, $\gamma_{\text{water-air}} = 72$ dynes/cm, $\theta_{ce} \sim 0$ ° and $h_{ce} = 8.4$ cm. When the height, h, between the capillary-top and the liquid free surface in the trough is kept less than h_{ce}, the liquid rises through the entire length of the capillary and the meniscus rests at its top. At the capillary top, the meniscus still has a contact angle θ_{ce} and $\Delta P_m = \rho_{\varphi_1} g h_{ce}$, is still greater than the downward hydrostatic force, $\Delta P_h = \rho_{\varphi_1} g h$, corresponding to height h. At the top of a capillary when the surface suddenly changes angle, the curvature attempting to advance under the influence of $(\Delta P_m - \Delta P_h)$, adapts to establish the contact angle at the next surface, beyond the edge. Here the contact line remains pinned at the edge while α decreases from $(\pi/2\text{-}\theta_{ce})$ to a value $\alpha' = \pi/2 - \theta_{app}$, where θ_{app} is the apparent contact angle. As a result, the pressure drop across the meniscus decreases and new $\Delta P_m = 4\gamma_{\phi_1 - V} \cos(\theta_{app}) / d = \rho_{\varphi_1} g h$, (Figure 2-3).

Adaptation of curvature when the contact line remains fixed is called *pinning* and is observed when the contact line is at an edge on a surface and the surface changes angle due to microscopic roughness or otherwise, [27, 28]. If the capillary is moved vertically up or down to vary the height h, the meniscus at the top of capillary adjusts to balance the hydrostatic head in the liquid column for all $h <$ the maximum height, h_{cmax}, (Figure 2-4).

Then for any such h, $\Delta P_h = \rho_{\varphi_1} gh = \Delta P_m$, and must be balanced by a reduced upward component of the surface tension force due to an apparent contact angle $\theta_{app} > \theta_{ce}$, so that $h = 4\gamma_{\varphi_1 - V} \cos(\theta_{app}) / (\rho_{\varphi_1} gd)$.

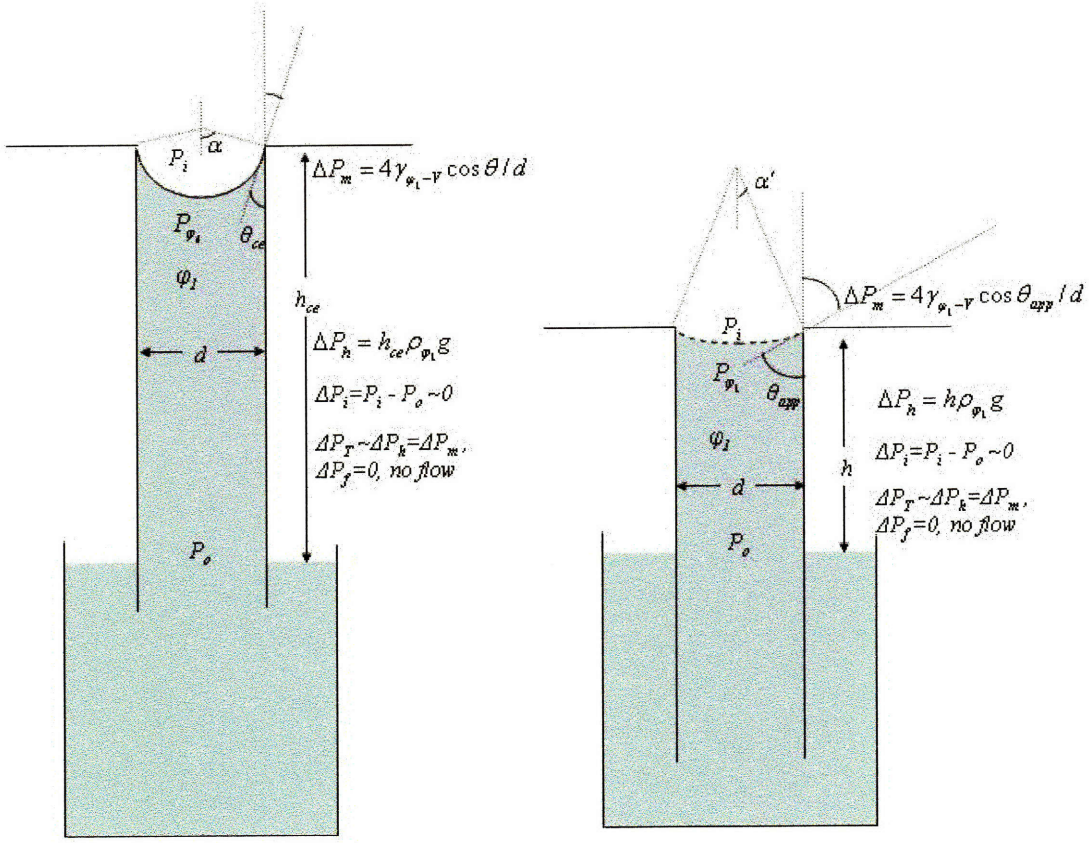

Figure 2-3. Schematic showing the adjustment of meniscus in a single capillary.

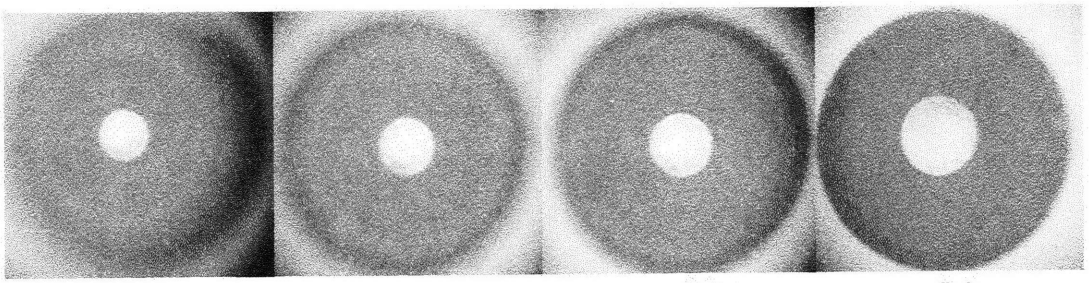

Figure 2-4. Top view of an adapting water meniscus in a single circular capillary (d = *340 μm*, $h_{ce} \sim 8.4$ *cm*), observed with a *20X* magnification, in response to changing h, (i) $h = 0.68h_{ce}$ (ii) $h = 0.59h_{ce}$ (iii) $h = 0.53h_{ce}$ (iv) $h = 0.41h_{ce}$. The central flatter part of the meniscus appears bright due to light refracted out through it, while the peripheral region appears dark as most light in this region undergoes reflection at the meniscus, back into the liquid in the capillary. As h is decreased the meniscus assumes a flatter shape and the central bright region that transmits the light becomes larger, case (i) to (iv). In addition when the meniscus becomes more curved, the meniscus depth increases and the focal planes of two regions become more distant. As a result, when the central part is focused the peripheral region appears blurred, cases (i)-(iii). Flatter meniscus implies when the central part is brought into focus the peripheral portion also appears sharp, case (iv).

2.5. Adaptation of meniscus in an array

We show the same adaptation of meniscus using an array of capillaries and model water (φ_1)-air (φ_2) and ethanol (φ_1)-air (φ_2) systems. We use a *10.4 mm* diameter glass-array, *0.762 mm* thick, containing capillaries of diameter *10 μm* (*Collimated Holes Inc*). The length of each capillary in the array is equal to the array thickness. Single capillaries, of long length, can be used to study the adaptation of liquid meniscus at the top as described, and the difference in height between the meniscus in the capillary and the liquid free surface in the trough is altered by moving the capillary vertically up/down. For short capillaries in the array as above, we use a setup consisting of a 'U' shaped flexible tube, *5 mm* in diameter and filled with liquid. The glass-array is attached to a conical casing at the fixed end of tube in arm '1', while the other end in arm '2' is kept free to

move up or down along a scale, (Figure 2-5). Due to capillary rise, the liquid quickly rises through the small length of the capillaries and forms a meniscus at their inlets when the 'U' tube and the conical casing are filled. Using this setup we maintain and vary a difference in level, h, and the hydrostatic head, ($\Delta P_h = h\rho_{\varphi_1} g$),between the liquid meniscus in the capillaries and the free surface of liquid, at the outflow, in arm '2'. The large inner diameter of the U-tube is used so that the interfacial force acting at the outflow is negligible compared to that in the capillaries.

The liquid meniscus becomes flatter when $\Delta P_h = h\rho_{\varphi_1} g$ is reduced while becomes more concave, assuming a smaller contact angle when ΔP_h is increased, as shown for the two systems, (Figure 2-6). The meniscus has an ability to self-adjust to different curvatures and balance ΔP_h, so that $\Delta P_h = \Delta P_m$ at all points. The maximum ΔP_h, that can be supported before the meniscus collapses, and is forced out of the capillaries, ΔP_{max}, is $2\gamma_{\varphi_1-\varphi_2}\cos(\theta_r)/r$, corresponding to the receding contact angle θ_r, and the maximum height, $h_{c\max} = 4\gamma_{\varphi_1-\varphi_2}\cos(\theta_r)/(\rho_{\varphi_1} gd)$. For r = *5* µm, for ethanol-air system, $\gamma_{\varphi_1-\varphi_2} = 0.022$ N/m at 20 ° C, and, $cos(\theta_r) \sim 1$, ΔP_{max} = *8.9* kPa (~*0.9 m* of water) and h_{cmax} = *1.1* m, for water-air system, $\gamma_{\varphi_1-\varphi_2} = 0.072$ N/m at 20 ° C, $cos(\theta_r) \sim 1$, $\Delta P_{max} \sim$ *28.8* kPa (~*2.9* m of water) and h_{cmax} = *2.88 m.*

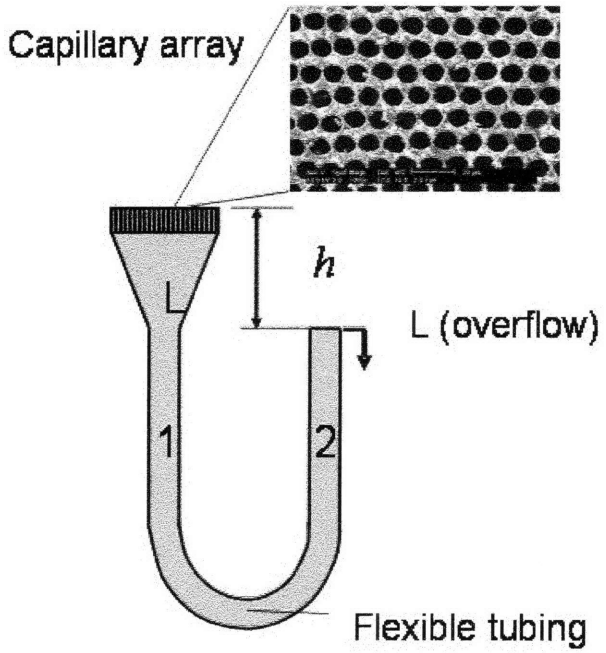

Figure 2-5. Schematic of the setup for observation of self-adaptation of meniscus.

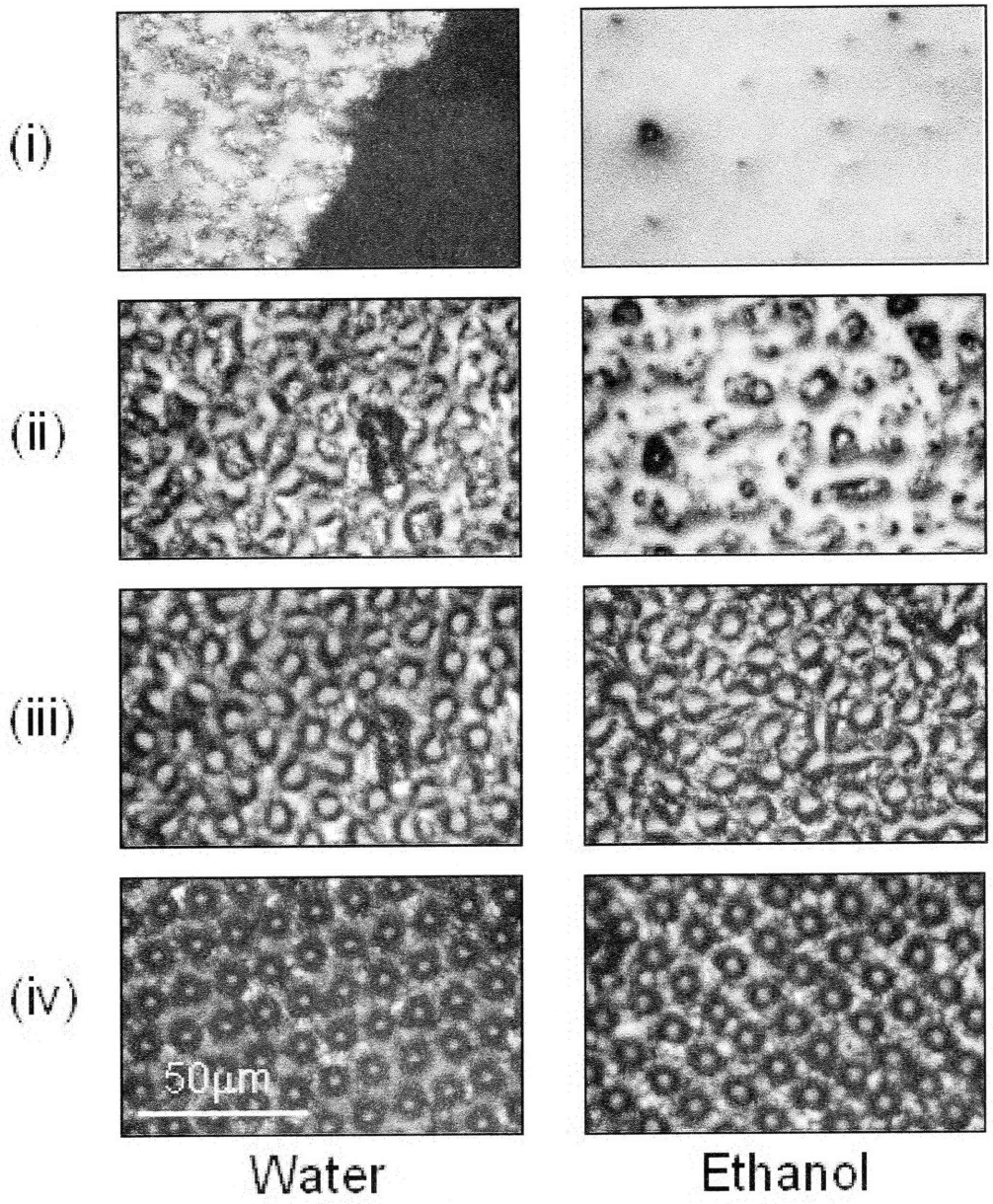

Figure 2-6. A section of the array observed with an interference, *40X* objective to record adaptation in the valve menisci at different $\Delta P_h'$, for water (left column) corresponding to (i) $h < 0$, flooding state, (ii) $h = 40\ cm$, (iii) $h = 80\ cm$ (iv) $h > 100\ cm$, and ethanol (right column) (i) $h < 0$, (ii) $h = 17\ cm$, (iii) $h = 29\ cm$ and (iv) $h = 45\ cm$. A balance is obtained between the adapting upward component of the surface tension force and the hydrostatic force for all $h_{cmax} > h > 0$. For $h > h_{cmax}$, the liquid menisci are forced out of the valves as the liquid flows out from the outflow in arm '2'.

2.6. Dynamics and flow capacity of array

The above setup used to vary the height difference between the liquid menisci in the capillaries of array and the liquid free surface in arm '2' creates the same effect on ΔP_T as the vertical movement of a single capillary in a trough, described earlier. We use this setup with liquid dispensed on the array surface to study the self-actuation and flow capacity of the routers at different ΔP_T, for model water (φ_1)-air (φ_2) system, (Figure 2-7). Here, $\Delta P_i \sim 0$ and $\Delta P_T = \Delta P_h$, as no excess pressure is applied between the air above the meniscus and that above the liquid free surface at the end of U-tube. Then in presence of a meniscus at the inlet, $\Delta P_m = \Delta P_T$ and $\Delta P_f = 0$. However, as the meniscus is destroyed by the incoming liquid, interfacial force disappears and the capillaries receiving the liquid allow it to flow out under the action of unbalanced ΔP_T as the meniscus vanishes. By choosing a large diameter for the U-tube, the pressure drop due to flow in the U-tube can be neglected in comparison to that in the valves. Then for these capillaries $\Delta P_m = 0$, $\Delta P_T = \Delta P_f$, and is varied through changes in h. The meniscus stays at rest in the remaining capillaries which still have an interface at the inlet. Thus each capillary in the array independently allows the flow of liquid through it when receiving liquid while has the air-liquid-solid interface reestablished and resists any gas to flow through in absence of liquid.

We increased the rate of incoming liquid to the array until a thin liquid film covered all the capillaries, thereby switching 'on' all of them. At this point the maximum flow capacity of φ_1 through the array for a particular ΔP_T, is reached. The diameter being small, Reynolds number is low and Stokes flow is obtained in the capillaries. The pressure drop ΔP_f due to liquid flow in the capillaries can then be calculated using the

Hagen-Poiseuille equation as $\Delta P_f = 32\mu u l_c / d^2$, while the velocity u through each capillary is $Q/(n\pi d^2)$, where Q is the total incoming liquid rate, and n is the number of capillaries in the array. Since ΔP_T must provide for ΔP_f, the maximum velocity in each valve, $u_{\max} = \Delta P_T d^2/(32\mu l_c)$ and maximum flow rate through the array, $Q_{\max} = u_{\max} n\pi d^2$, can be calculated for various ΔP_T, (Figure 2-8). The array size allows the choice of the number of routers that can be accommodated. This can be designed from the knowledge of the flow capacity desired from the array. Even for arrays of size ~ 500 μm, $\Delta P_T \sim 5\%$ of ΔP_{max} is sufficient for flow rates common on microscale (region μS). A single array can then be used for phase separation from a large number of parallel streams with separation being unaffected by disturbances in individual streams. This characteristic, combined with high resistance to flow of φ_2 and spontaneous actuation between two states makes the concept well suited for reliable phase separation and integration with different parts of a chemical/biological processing network.

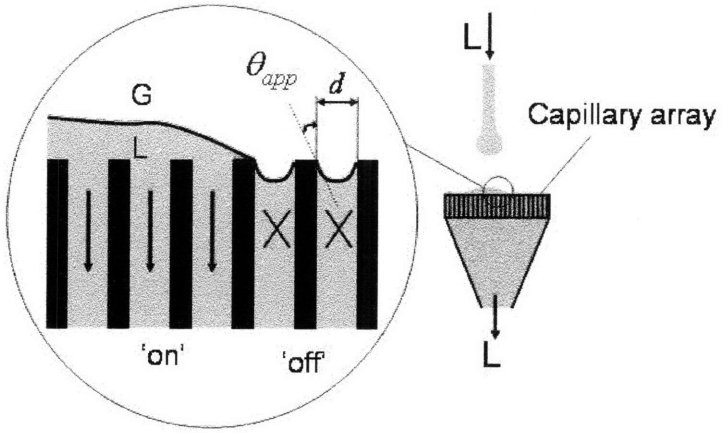

Figure 2-7. Schematic showing menisci of a wetting liquid (φ_1) inside individual capillaries. The spontaneous actuation from 'off' to 'on' state is prompted solely by the presence of φ_1 at the capillary inlet. The actuation back to 'off' state happens in presence of φ_2 at the inlet. Thus actuation of routers for phase separation is automatic

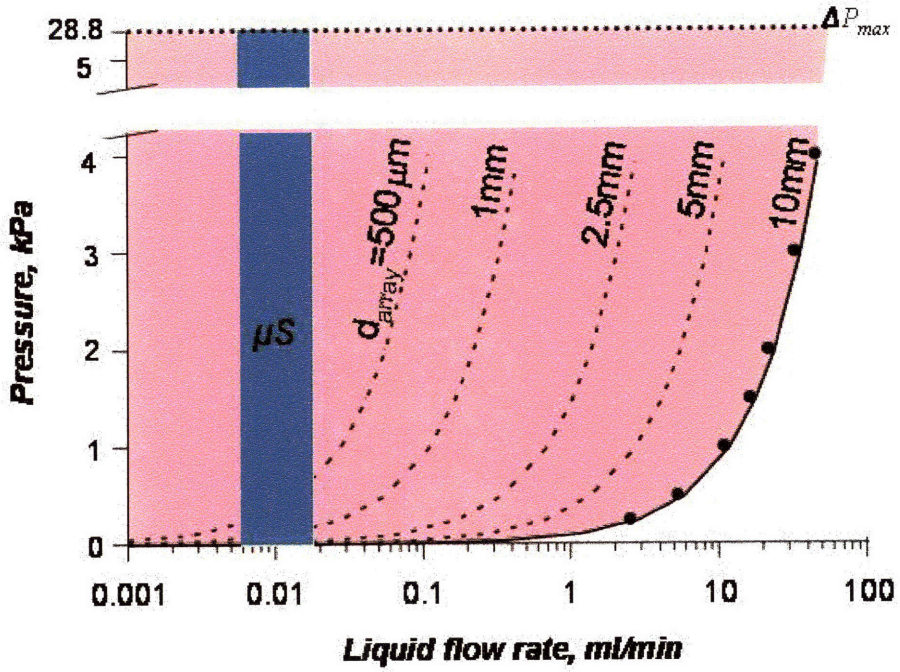

Figure 2-8. The small diameter (*~10 μm*) of the capillaries ensures that the resistance to flow of φ_2 is large, *=28.8 kPa* for water-air (ΔP_{max} indicated by dotted line), and *~ 10 kPa* for other gas-liquid and liquid-liquid systems. The variation of ΔP_T with the maximum flow capacity is shown for various array sizes (500 μm, 1 mm, 2.5 mm, and 5 mm diameter arrays) as dashed curves. The maximum flow-capacity at different ΔP_T, is experimentally measured (solid markers) to be in good agreement with that predicted theoretically (solid line), for array diameter *10.4 mm*.

2.7. Independence with orientation in gravitational field

The routing of individual phases from a two-phase mixture is desired to be independent of the orientation of the routers in the gravitational field. We use the above setup to show φ_1 directed through the routers irrespective of the array orientation. Liquid is drawn in and flows out the array in both instances; when dispensed downwards on the array and when directed upwards to the array positioned above the liquid nozzle, (Fig.

9).A $\Delta P_T = 0.05\ \Delta P_{max}$ is provided in each case.The downward gravitational force on liquid that comes in contact with any capillary in the array is much smaller than the force due to ΔP_T drawing the liquid into the capillary. Assuming ΔP_T is a fraction of the ΔP_{max} (depends on the interfacial force), then the Bond (Bo) number gives an estimate of the relative magnitude of the gravitational and the interfacial force. For water-air system, in a capillary $d = 10\ \mu m$, the density difference between two phases, $\Delta\rho \sim 10^3$ kg/m^3, $\gamma_{\varphi_1-\varphi_2}$ = 0.072 N/m, $g = 9.8\ m/s^2, Bo = \Delta\rho g d^2 / \gamma_{\varphi_1-\varphi_2} \sim 1e\text{-}6$ and thus the force due to $\Delta P_T >>$ gravitational acceleration. This independence with orientation in the gravitational field coupled with the robustness of operation with respect to pressure fluctuation in the two-phase flow makes the fluid phase routers well suited for convenient integration into microfluidic systems.

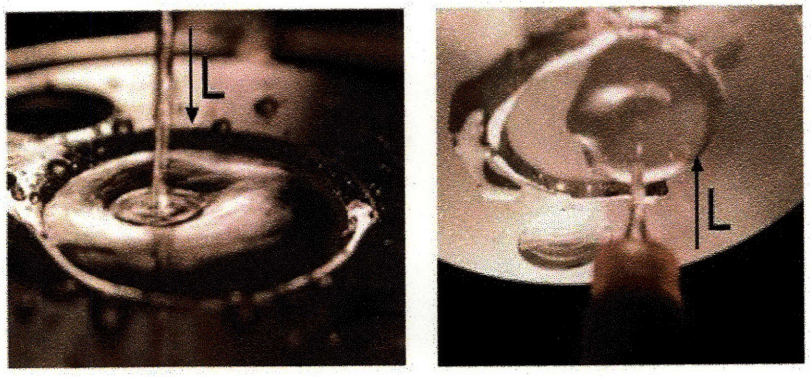

Figure 2-9. Independence of phase separation with orientation of array in gravitational field. Water jet impinging with (Left) and impinging against (Right), the direction of gravitational acceleration on the array while liquid is completely drawn into the capillaries for a $\Delta P_T \sim 4\ kPa$, both instances.

2.8. Summary

In this chapter we have developed and outlined the basic principles for design and operation of fluid-phase routing on microscale. We have shown how the dominance of

interfacial forces, combined with the choice of wetting behavior can be used to design the magnitude and direction of the interfacial force in the router. We have also demonstrated the ability of meniscus to adapt to changes in pressure and shown how this can be useful at the separator inlet. The independence of separator operation with respect to orientation in the gravitational field was illustrated. Finally we developed an understanding of the expected of flow rates and how the realization of desired flow capacity through use of an array. The theory developed and the experimental results point to design of a potentially robust concept of phase routing possible on microscale, well suited for interfacing different processes in a microfluidic network.

3. Construction of Microdevices

3.1. Background

This chapter describes details of devices used in this thesis and realized through silicon microfabrication or machining of metal/plastics. As the microscale industry is expanding, opportunities are being identified in an array of applications especially in the fields of biology and chemistry, with some of them already at a product stage while large numbers are actively at the research and development level. The variety of applications are characterized by very different requirements, however, the general ability to create a confined space of sub-millimeter dimensions and to be able to introduce fluids into or remove fluids from the confined space is desired. Specific application requirements additionally desire inertness of the device material/channel walls with respect to harsh chemical environment, feasibility of operation under the extremes of temperature, pressure or other operating conditions. In addition, the provision for integration of analytical abilities (in general the ability to derive process information), is becoming increasingly important. Such abilities range from optical access for microscopy (including fluorescence and confocal scan) and on-chip integration of sensing and measurement to allowing for direct interfacing with state-of-the-art instruments like the HPLC and GC/LC-MS.

However, before the perfect product for the market may be produced or a laboratory device with all the desired ability of a complex process demonstrated, it is sometimes desired to test the basic principles using a device that can be realized with a relatively small cost and in a much shorter time. Several alternative material technologies

for realization of microdevices are available, and companies/research efforts focusing on metal, plastics, rubber, soft polymers, glass and semiconductor materials exist.

Silicon microfabrication has developed considerably over the last few decades [29, 30]. The technology with the ability of photolithography, deep reactive ion etching (DRIE), wafer and die level bonding techniques for silicon to silicon and silicon to pyrex glass bonding and deposited metal coatings and growth of silicon oxide/nitride layers provides a strong base for the development of integrated, complex microdevices.

Some of the characteristics that provide a strong competitive edge to a silicon microfabrication based devices include:

- Photolithography is used to transfer pattern which is then realized through etching using an appropriate mask. The effort does not scale with the density of features. This is important during 'scale out' and in the applications that can use multiple devices on 1 wafer. In addition each device can have multiple features of different sizes, all this potentially realized in one step.
- Sealing of channel etched in silicon is achieved through anodic bonding of a glass wafer, which provides the desired optical access to the channel for flow visualization and microscopy.
- Chemical resistance of the channel walls can be achieved with the help of deposited coatings and growth of passivation layers (example silicon oxide and nitride).
- The technology for mass manufacturing is established on microscale and even smaller scales.

- Extremes of temperature and pressure can be worked with and depends largely on the efficiency of the packaging scheme, that is how the chip-to-world interface is carried out.

The MEMS fabrication process draws from the vast experience and expertise of the microelectronics fabrication, and hence the ease of development and integration of sensors, actuators and analyzers, apart from the ability to realize variety of structures.

Even though the different fabrication steps are standardized and extremely well-suited for the needs of mass-manufacturing in modern fabrication facilities, for personnel newly-trained on the instruments, silicon microfabrication is non-trivial. The sequential nature of the steps involved easily leads to low yields even for a relatively high performance efficiency in individual steps, and leaves less room for error than can be desired for an initial test device. We found the initial testing of concepts through devices realized from machining of plastics/metal to be an efficient way of rapid-prototyping. We used the understanding developed through experiments with these machined devices to develop integrated devices fabricated in silicon.

3.2. Test Devices realized using Standard Machining

3.2.1. Metal-machined device for testing of fluid-phase routing

Figure 3-1 shows a device for testing of fluid phase routing machined in aluminum and its different parts. The device realized consists of two-inlet channels leading to a main channel in a Y configuration machined in a *3 mm* thick Aluminum substrate (*MIT, Central Machine Shop*). The main and the inlet channels are each *1 mm* wide and *400 μm* deep. Limitations for the minimum feature size in machining of

channels in metal/plastic materials is governed by the hardness and size of the drill-bit used and the hardness of the material to be machined. Features greater than *400 μm* in width and ranging from a few hundred microns to a couple of millimeters in depth can be easily realized in this way.

The main channel is expanded to a diameter of about *5 mm*. Phase-routing requires the use of channels typically ~ *10-20 μm*. Glass capillary-arrays of more than *5 mm* in diameter are available commercially (*Collimated Holes Inc.*) We obtained a *5 mm* diameter array, *0.5 mm* thick containing *15 μm* diameter capillaries and affixed it with an epoxy glue (*Master Bond*), in a recess equal to the array size, machined in the aluminum substrate at the end of the channel.

Sealing the channel while providing for optical access and inertness to organic solvents is required. However, most metals are opaque while transparent plastics (example poly(methyl) methacrylate (PMMA), Polycarbonate) have a poor resistance to organic solvents. We used a glass cover (*3 mm thick*) and sandwiched it between the aluminum substrate and a top aluminum cover with a window cut out. Screw threads are provided in the aluminum substrate while clearance for the screws is provided in the aluminum top cover. The size and dimensions of the glass cover are selected such that it covers the channel machined in the aluminum substrate while stays clear of the screws tightened to compress the top aluminum cover against the bottom substrate. A through hole, *3 mm* in diameter, is machined in the glass cover at the point above the capillary-array. This serves as one of the two outlet ports required. The seal realized in this way is adequate for the small pressures in the channel, while providing good optical access to the channel and walls being chemically inert to organic solvents.

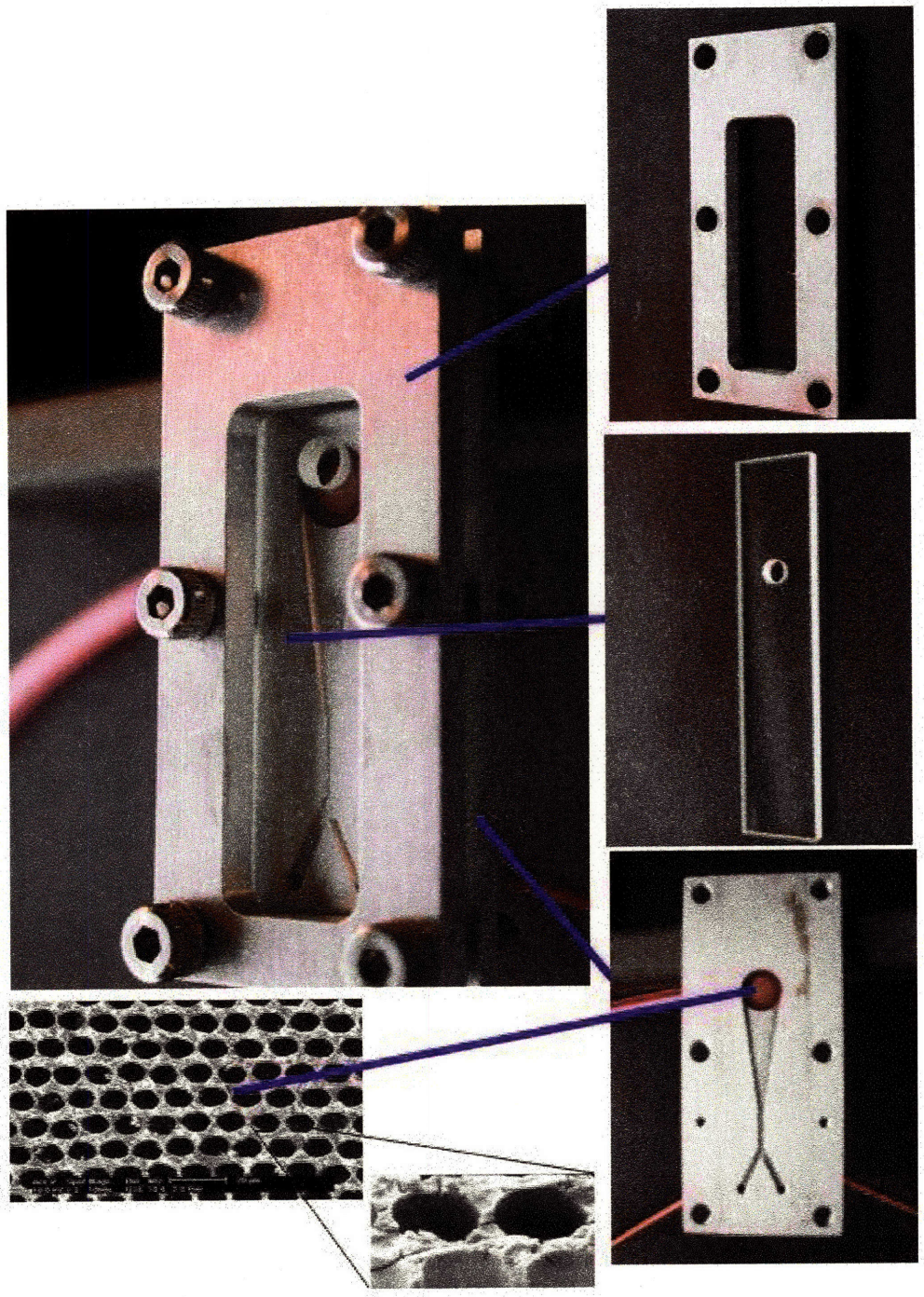

Figure 3-1. Device realized through metal machining consisting of a bottom substrate, top cover and a glass piece sandwiched in between the substrate and the top cover to seal the channel on the substrate as well as allowing optical access to it. A commercially available capillary array is affixed to the substrate at the end of channel.

Ports for introduction of fluids into the channel and removal at the end of channel are provided in the aluminum substrate, on its bottom side. Short pieces (about 2-3" length) of standard plastic tubing (PEEK/PTFE, Upchurch scientific), of appropriate size (1/16" for the inlet and 1/8" for outlet) is glued to the ports on the bottom side of the substrate using ferrule fittings, (Figure 3-2). Fluidic fittings attached to the short tube are then used to interface with the required fluid source (syringe pump for liquids and compressed air line with a Mass Flow Controller (MFC) for gases).

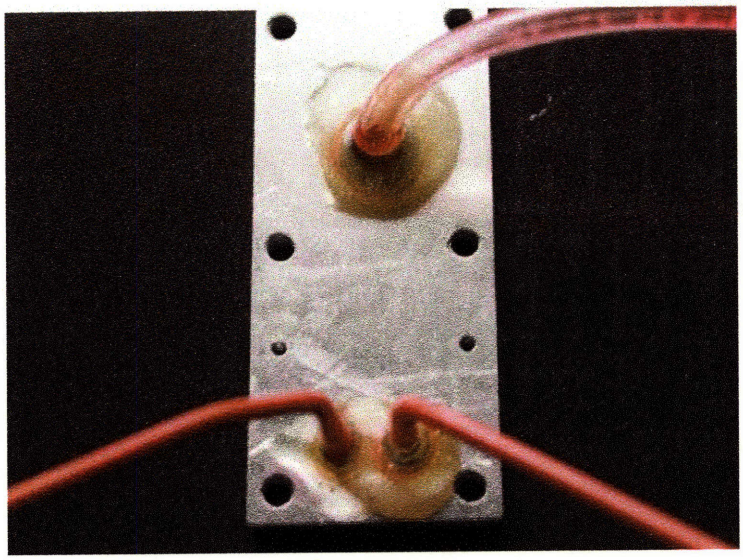

Figure 3-2. Connecting the inlet and outlet ports to the outside world

3.2.2. Devices realized from machining of plastic substrates

Channels with sub-millimeter dimensions can be machined in plastic substrates in the same way as in metal substrates. Figure 3-3 shows a geometry realized in PMMA containing two inlet channels leading to a main channel in a Y-configuration, each *400μm* deep and *1 mm* wide. The channel is capped with a PMMA piece, and the two pieces fastened together using screws. We used this device for the initial study of fluidic path of two miscible liquids inside a microchannel.

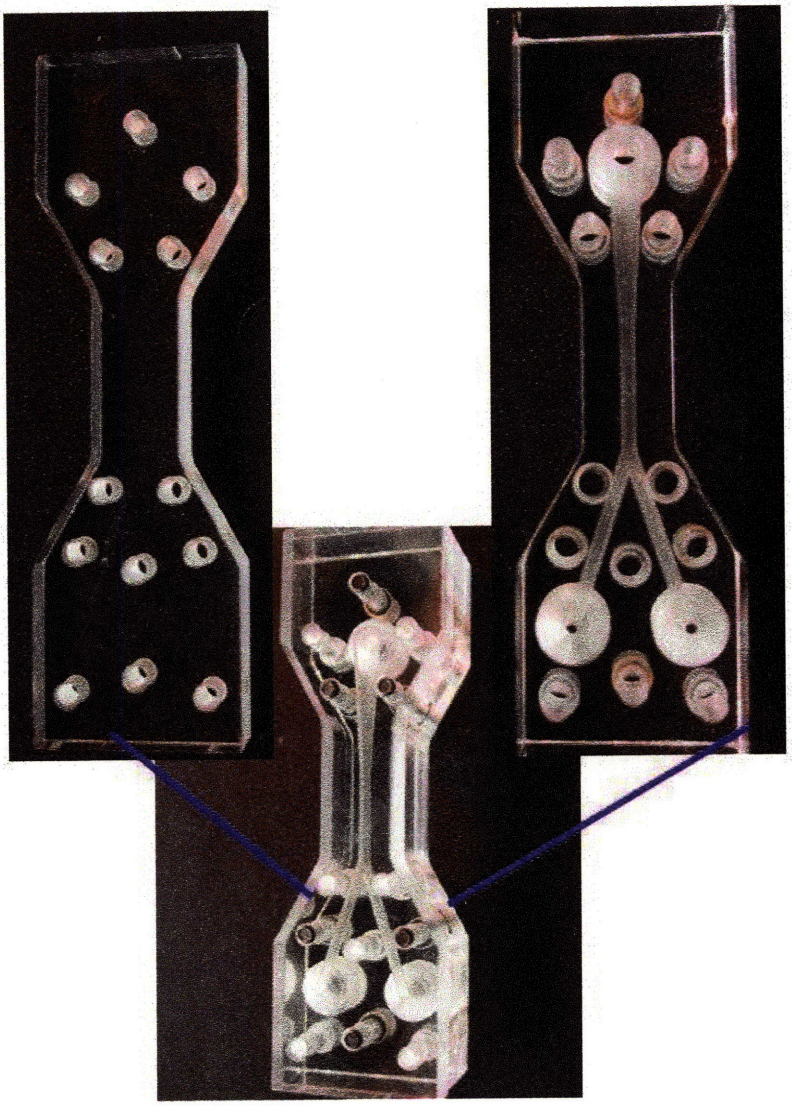

Figure 3-3. Channels of submillimeter dimension machined in plastic (PMMA) and capped with the same to realize plastic devices.

Figure 3-4 shows another device realized in PMMA. We use this for demonstration of the concept of a valve realized on micoscale, described in *Chapter 4*. This device consists of a channel machined in the plastic substrate, with capillary arrays integrated in the channel path along with an additional port used to connect the gas-line. The point to emphasize about such devices is that they can be realized in a matter of a day and serve as good candidates for proof-of-concept studies. The transparent plastic

allows visualization of the flow path. In the plastic devices the packaging required for introduction and removal of fluids is realized through screw threads (example 1/4 -28) compatible with standard fluid fittings directly machined on the port locations. Then a compression seal using a commercially available standard nut and a ferrule (Upchurch Scientific) can be created directly with the device at the port location and a tubing used with the nut to introduce/remove fluids.

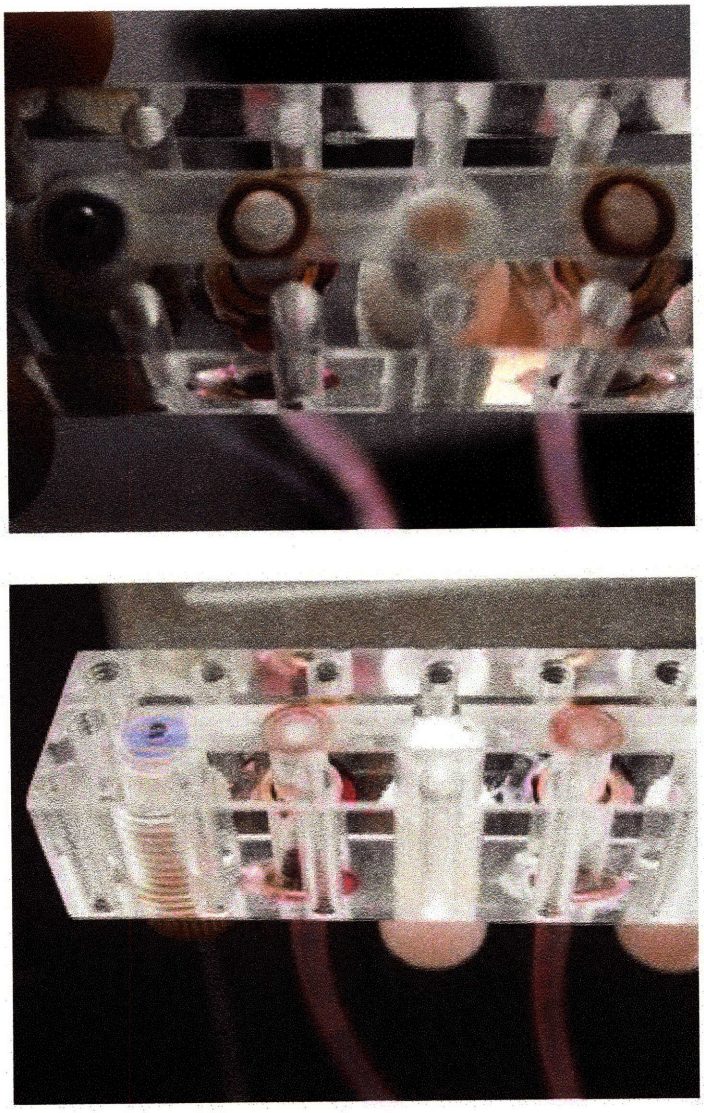

Figure 3-4. Channel machined in plastic integrated with commercially available capillary arrays for realization of proof-of-concept device.

3.3.Silicon Microfabricated Devices

3.3.1. Overview and description of the fabricated device

Figure 3-5 shows the silicon microfabricated device, consisting of inlet channels, a main channel, side channels and a capillary array for fluid-phase routing, at the end of the main channel. The *40 mm* long main channel is *400 μm* wide and *470 μm* deep, and is fed by two inlet channels of the same depth and width and each *1.2 cm* long. Different fluids can be introduced into the device from the two inlet channels so that they meet at the beginning of the main channel.

Side channels provided at *5 mm*, *15 mm* and *25 mm* points along the main channel are *40 μm* deep and *10 μm* wide at the point of intersection with the main channel. We use these side channels to introduce fluids or alternatively as routers to remove one of the phases exclusively from a two-phase flow in the main channel. The side channel though only *10 μm* at the point of intersection with the main channel is expanded to *500 μm* before branching into three smaller channels of *100 μm* dimension, (Figure 3-6). These three channels meet at a port with a window and a recess on the backside, (Figure 3-6), where the concentration sensor-foil is attached.

At the end of the main channel is an array of *20 μm* holes with a *10 μm* center-to-center spacing and arranged in a square pitch. Figure 3-7 shows an SEM (Scanning Electron Micrograph) of the array. A blowout is seen for the separator holes. For the size of capillary on the mask of *15 μm* the actual size of the holes is about *20 μm*. This is expected and for our purpose it is important that the two capillaries do not merge when etched. We accounted for this blowout in our design by providing enough center to center spacing (*30 μm*) between capillaries. It is also seen that the side walls are smooth only to

an accuracy of about $1\mu m$. This is also an expected feature of the high aspect ratio, DRIE used to etch silicon. A scale is etched at the side of the main channel and parallel to it and allows an estimate of the position along the main channel.

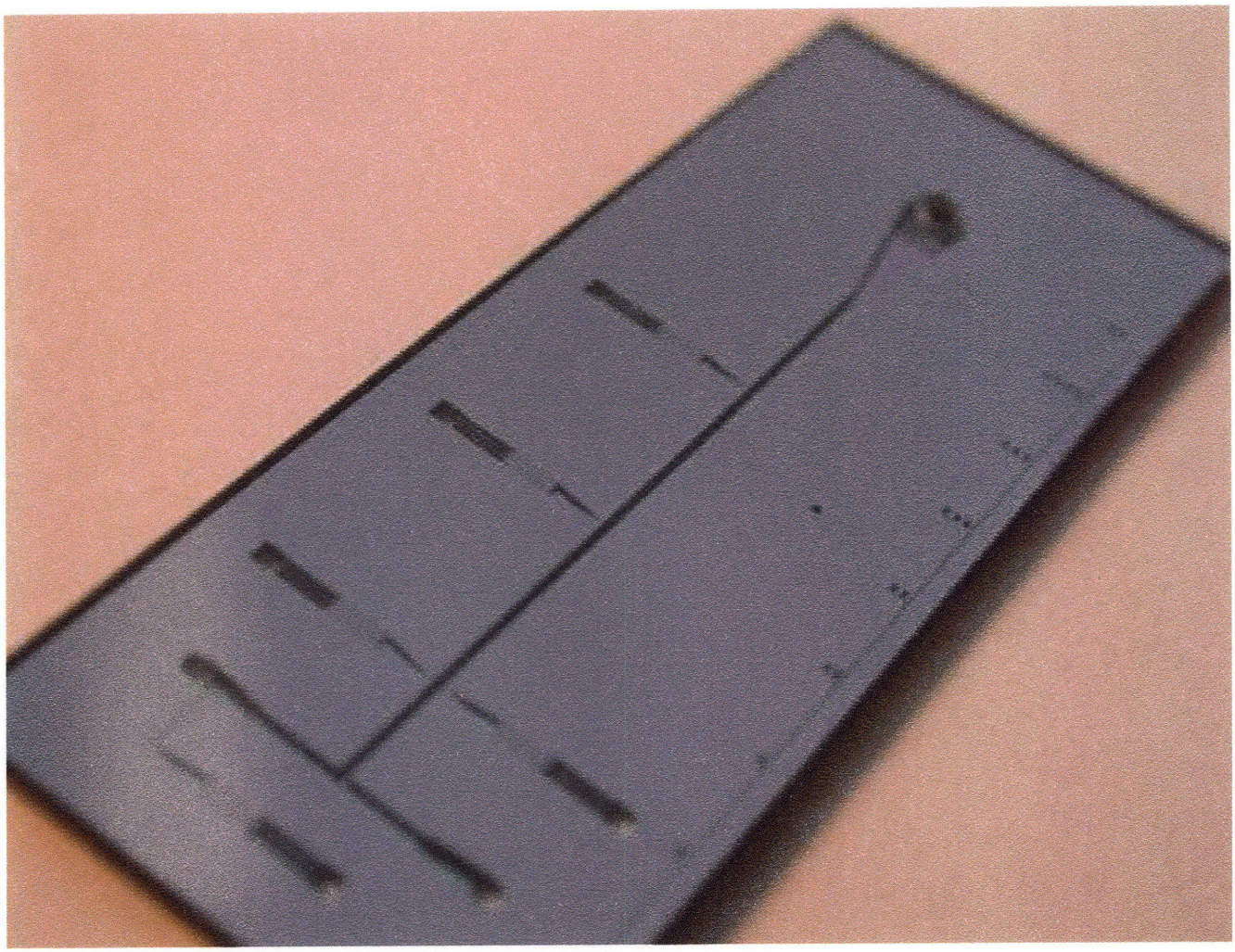

Fig. 3-5. Device microfabricated in silicon using MEMS and microelectronics industry processing techniques.

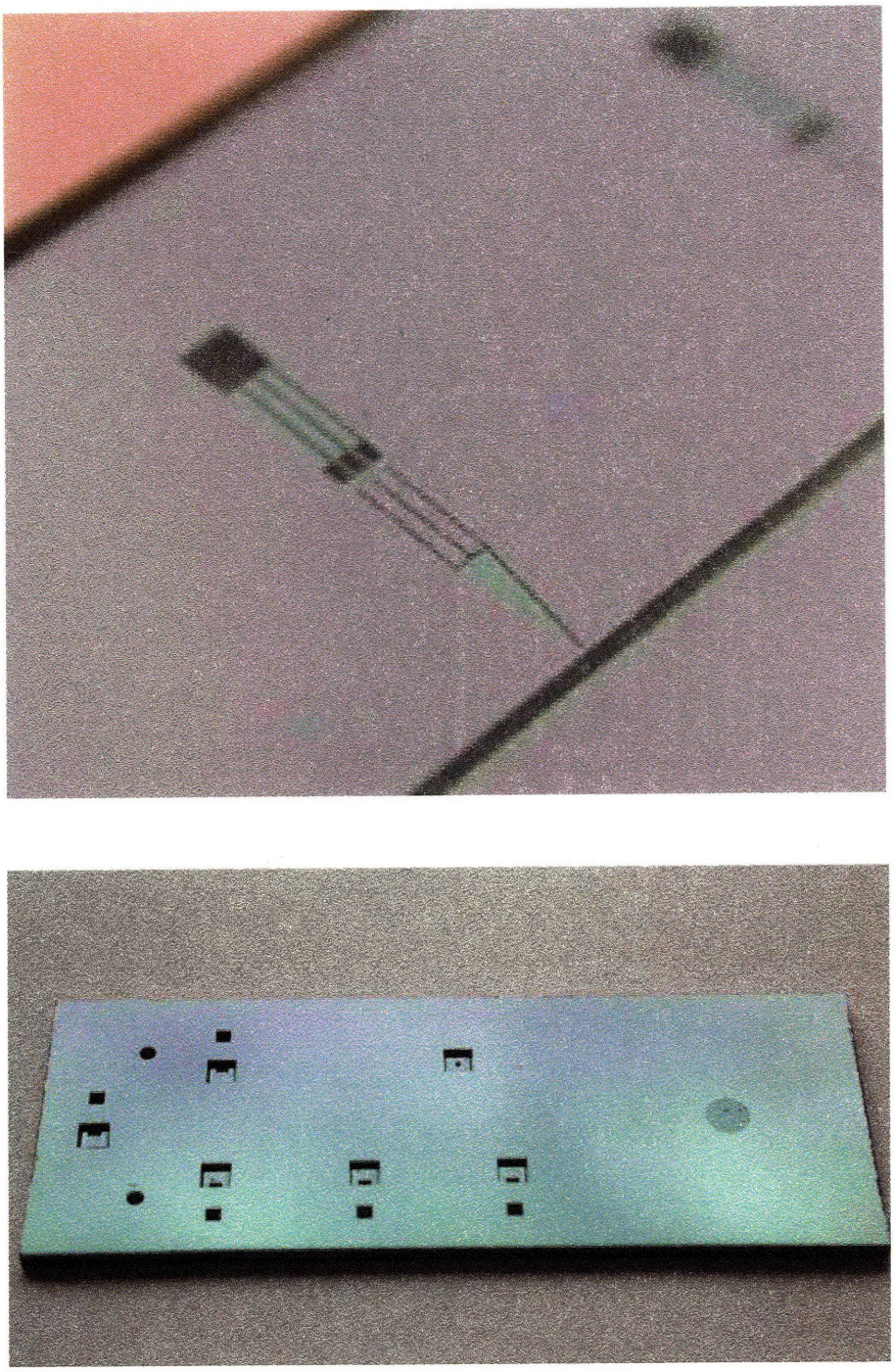

Figure 3-6. Closer view of a side-channel interfacing with the main channel. and backside of the microfabricated device with fluidic inlet and outlet ports and window for receiving sensing element.

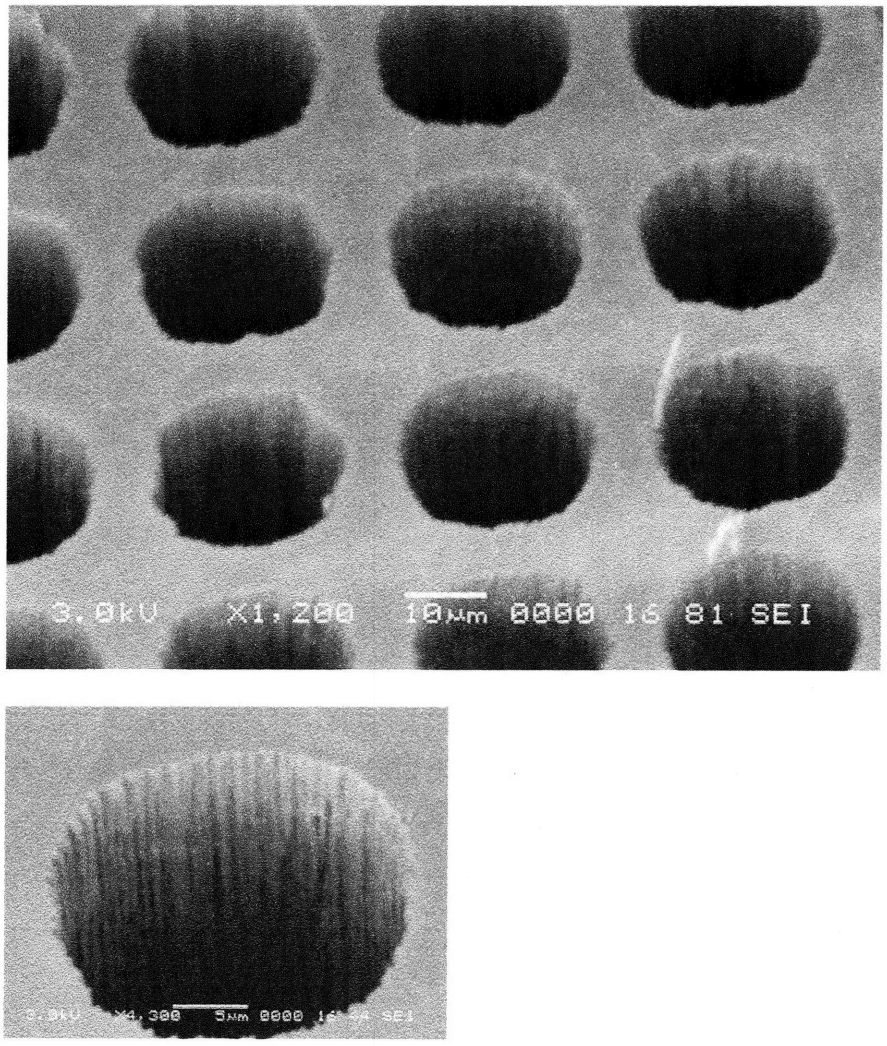

Figure 3-7. Scanning Electron Micrograph of a (A) section of capillary array and (B) a single capillary in the array fabricated at the end of main channel.

3.3.2. Silicon device fabrication

The fabrication process for the device described above involves photolithography and DRIE steps for the front and the backside of the wafer and a final anodic bond step to cap the channels. We start by growing a passivating oxide layer prior to photolithography.

We pattern the features on the backside of the device first followed by the patterning of the topside channels and anodic bonding. Thick resist (AZ4620, Hoechst

AG) is spin coated to *10 μm* thickness and a contact mask alignment procedure is used (Electronic Visions EV 450 Aligner) for transferring the pattern from the mask to the wafer. The oxide is then selectively removed from the exposed areas in a buffered oxide etch (BOE) etch solution. The exposed pattern is etched to a depth of about *400 μm*, by using a time-multiplexed inductively coupled plasma etch process using a Surface Technology Systems deep reactive ion etcher [31-33]. For the conditions used this takes between 150 to 180 minutes. The wafer is then cleaned in a piranha solution (mixture of H_2SO_4 and H_2O_2 in the ratio 3:1) and silicon oxide grown to prepare for patterning the front side. The front side of the device has features of two different depths: *40 μm* for the side channels and *470*μm for the main channel, which are realized by a nested mask concept. We first pattern the features with *40 μm* depth using thin resist and then spin-coat the thick resist to pattern the deeper features using the thick resist. The deeper pattern is then DRI etched to a depth of about 430 *μm*. Following this the resist is stripped off and the exposed shallow as well as deep features are etched together to a depth of *40 μm*, giving an overall depth of about 470 *μm* for the deep features and about 40 *μm* for the shallow ones. The DRIE method essentially involves etching a high aspect ratio feature by alternating between etch and passivation cycles. The rough side walls of the capillary array and the smooth top are characteristic of this etch. Due to difference in etch rates between features of different size the capillaries of the array 'break through' much later than the larger port holes used for fluidic inlets. The silicon wafer with the features for the front and back side of the device is cleaned again using a piranha solution and a final protective oxide layer grown. A pyrex *7740* glass wafer (Bullen Ultrasonics) is anodically bonded to the silicon wafer at a temperature of about 380° C and using a

force large enough to maintain good contact while bodning [34]. The silicon wafer at this stage is extremely fragile and a large force (*>2000 N,* for a 6" wafer*)* can easily crack the wafer. We find that a force of about *1000 N* is good enough to obtain desired bonding between glass and silicon. Finally the wafer is diced into individual devices.

3.3.3. Silicon device packaging

We package the fabricated silicon device for introduction and removal of fluids to in a way that allows optical access into the device channels for microscopy. We attach a short piece standard tubing (PEEK 1/8" or 1/16" depending on the port size, Upchurch scientific), inserted in appropriate ferrule fitting (Upchurch Scientific) using an epoxy glue (*Master Bond*), (Figure 3-8). In addition to the tubing for introduction and removal of fluids we attach the sensor-foils in the windows provided on the backside, (Figure 3-8). Attaching the foil is done with some care as it has two challenges, to fix and keep the foil in place during fluid flow and not allow the epoxy glue is used for this purpose to wick into the silicon channels from the backside while applying the glue. But the essential principle of glue relies on the ability of glue to wet the surfaces that it bonds to and then harden, if it does not wet /spread easily on the surface the strength after bonding is weak and is easily removed after hardening. Later this was also prevented by first taping down the foil with a scotch tape and then applying the glue on top of the tape to further strengthen thebond.

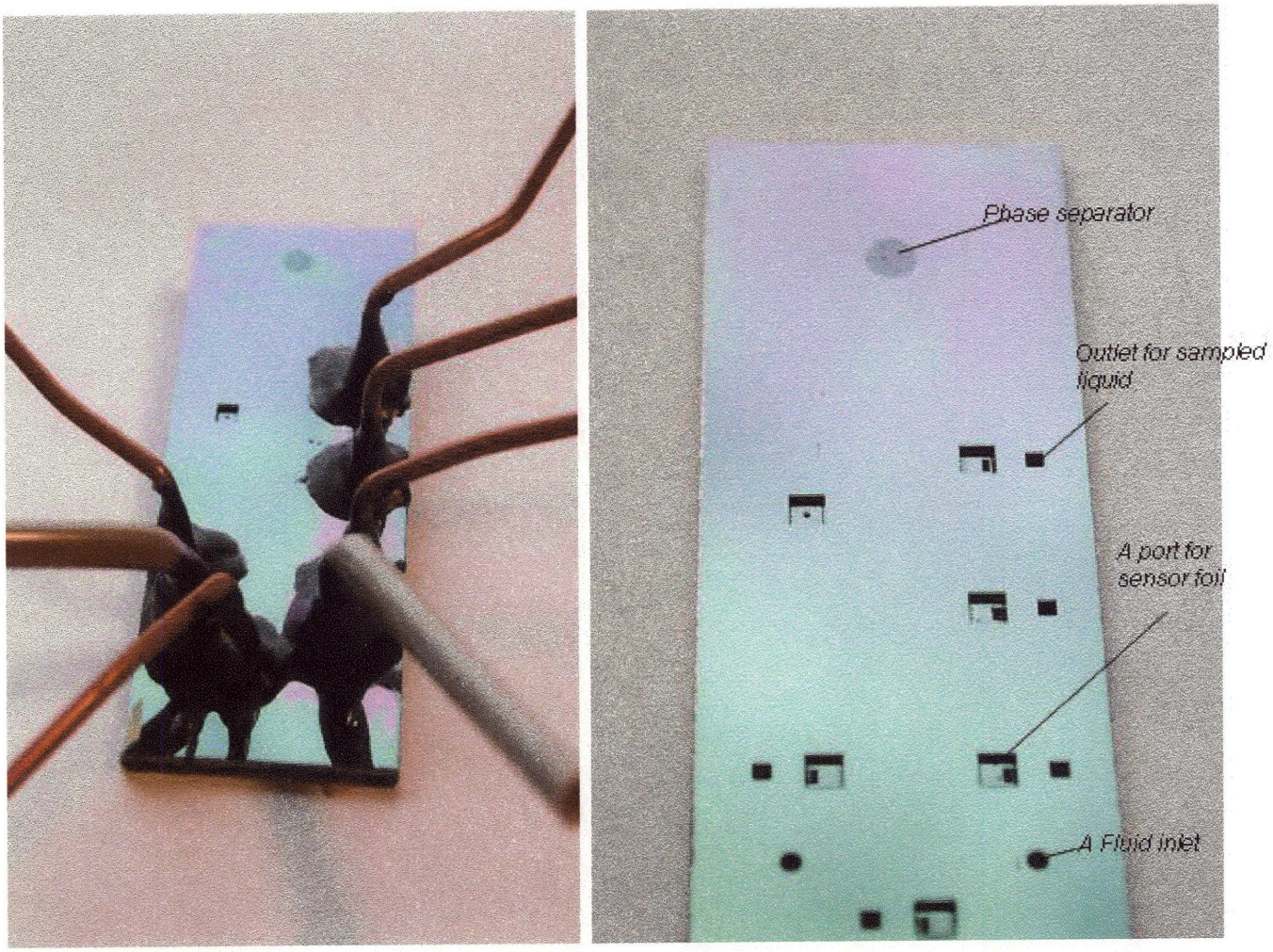

Figure 3-8 Short lengths of tubing attached to the inlet and outlet ports using glue (left), and the sensor foil affixed to larger square windows on the backside of device (right).

3.4. Summary

In this chapter the methodology for the different devices used in this thesis is detailed. We have shown the use of metal and plastic machining coupled with assembly of commercially available materials, for the purpose of rapid prototyping. To demonstrate the compatibility of developed concepts for integration with the existent capabilities of microscale devices on silicon template we used the improved understanding of the concepts, for a superior design using the silicon microfabrication technology. The chapter described the details of the fabrication and packaging techniques used in each case.

4. *Application of Router Principles*

The principle for operation of fluid-phase routers and the devices realized (through metal-machining and silicon microfabrication technology) are described earlier. In this chapter we use the concept for separately routing individual phases from gas-liquid and liquid-liquid two-phase mixtures for a range of flow regimes. We also show how the concept can be used to retrieve process information from a two-phase flow in microscale. Additionally we demonstrate the use of this concept in realization of valves on microscale without involvement of deformable/elastic structures, common to other microscale valve designs. The demonstrated valves are unique for being suitable in harsh chemical environments, a common attraction for microscale chemistry. Furthermore we show how microfluidic logic-gates can be realized by connecting these valves.

4.1. Routing of two-phase mixtures

4.1.1. Complete separation of phases in metal machined device

Figure 4-1 shows the schematic top view of the device machined in aluminum (detailed in Chapter 3), with two inlets for introduction of individual phases, a channel to mix the two phases and an array of routers for separation of individual phases at the end of the channel. For gas-liquid phase routing, we use the nitrogen-water combination as a model system while the toluene-water combination is used as an example system for routing of immiscible liquids on microscale. We use a syringe pump (Harvard PHD 2000, Harvard Apparatus), to pump liquid loaded into syringe of required size, to the device. Gas is introduced into the channel through a mass flow controller (MFC, Unit Instruments), of required flow capacity, fed from a pressurized cylinder. For liquids, the

flow rate is directly adjusted from the syringe pump settings whereas the gas-flow rate is controlled using the MFC. In this way we vary the superficial velocity, j_φ, of individual phases in the channel. Here,

$$j_\varphi = Q_\varphi / A_c \tag{4.1}$$

where Q_φ is the flow rate of phase φ, while A_c is the channel cross-section.

For gas-liquid separation we use a hydrophilic glass capillary array so that ethanol (φ_1) is wetting while nitrogen (φ_2) is the non-wetting phase. The two phases are contacted in the channel preceding the array, to obtain a two-phase flow. A sharp resolution of gas-liquid interface is obtained by using a frequency doubled Nd:YAG laser (532 nm, 25 mJ/pulse) and a full-frame, 12 bit CCD camera. Ethanol is colored with rhodamine dye for fluorescence. We vary the velocities of the two fluids to show complete separation for various fractions of the phases in the mixture ranging from pure liquid to gas only flow, including different steady and transient flow patterns, (Figure 4-2). We collect ethanol flowing out the capillaries of the array to a common port in a single large tube attached at the end of port. We maintain a liquid head of about *10 cm* between the inlet to the capillaries and the outlet at the end of tube, then the total pressure head driving the ethanol flow through the capillaries, $\Delta P_T = \Delta P_h = 10$ *cm* of ethanol (*14%* of ΔP_{max} for $d = 15\ \mu m$)

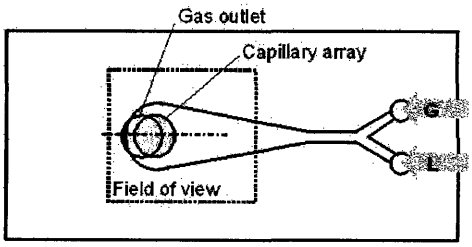

Figure 4-1 Top view of device for contacting and separation of two phases. The device consists of two inlets, one each for the two phases. The inlet section is 400 μm deep and 1 mm wide and is expanded to the capillary array diameter of 4 mm.

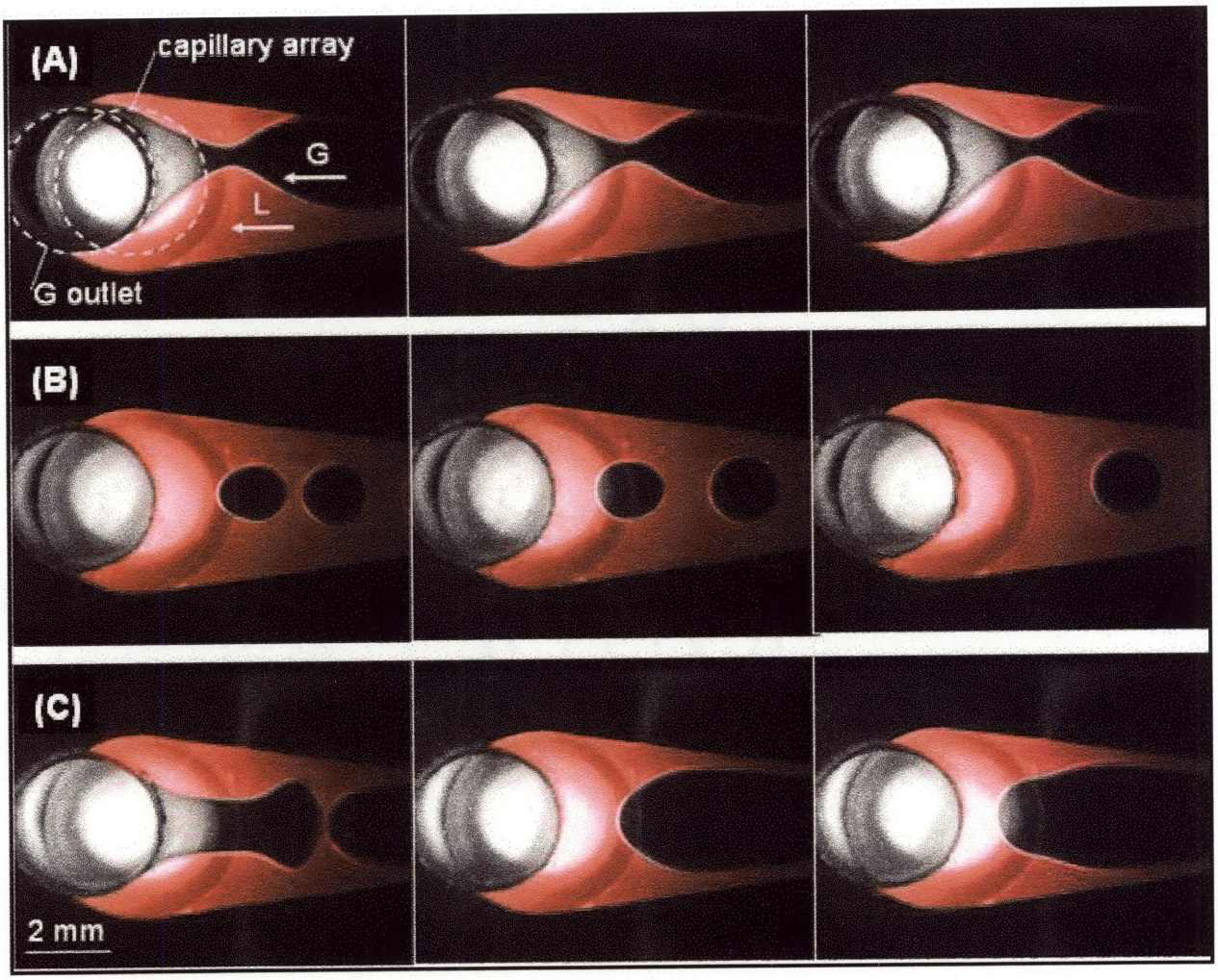

Figure 4-2 (A, B, C): Different gas-liquid flow regimes obtained with various combination of gas (nitrogen) and liquid (ethanol) velocities. The dark region within the channel is the gas phase, while the fluorescing region, the liquid phase. (A) Steady flow, gas-liquid interface unaltered with time, is obtained for high gas and low liquid superficial velocity (j_G = 3.8 m/s, j_L= 0.008 m/s). (B) For low gas and higher liquid superficial velocity (j_G = 0.027 m/s, j_L= 0.04 m/s) a transient regime with gas bubbles is obtained while for (C) moderate gas and liquid velocities (j_G = 0.7 m/s, j_L= 0.04 m/s) a highly transient slug flow regime is obtained. We obtain complete separation of the two-phase mixture for different velocity combinations of the phases.

Using a hydrophobic capillary-array a two-phase mixture between an aqueous (φ_2) and an organic (φ_1) phase can be separated analogous to a gas-liquid mixture. The metal device is coated with OTS (octadecyl trichlorosilane) to obtain a hydrophobic

surface. The device is first cleaned in an oxygen plasma cleaner for 2 min at 0.15-0.2 torr O_2 pressure. Silanization of the device is done in a 2% OTS solution in anhydrous toluene for 1 h at room temperature. After the coating, the device is rinsed sequentially with acetone and ethanol, and blown dry in a stream of nitrogen prior to use. Liquid-liquid flow is created in a microchannel by contacting model organic (toluene) and aqueous (water) phases. Here toluene wets while water is does not wet the hydrophobic surface. We obtain complete separation between the organic and aqueous phases as the organic phase in the mixture is directed through the array thus leaving a pure stream of the aqueous phase as well.

Separation devices have also been realized in silicon. The unique opportunity of handling of chemical systems and integration of unit operations presented by silicon microfabrication is demonstrated in Chapter 6 with a device integrating mixing, reaction and phase separation on a single-chip.

4.1.2. Complete separation of phases using silicon microfabricated device

The silicon microfabricated device with a router-array, is used for separation of nitrogen φ_2, and ethanol φ_1, from their mixture. We use a hydrophilic silicon oxide array surface so that ethanol is wetting while nitrogen fails to wet the surface. Individual phases are fed to the silicon device in the same way as described for metal-machined device. Once again we vary the velocities of the two fluids to show complete separation across different steady and transient regimes of the two-phase mixture, obtained for various combinations of phase velocities, (Figure 4-3). We use the total pressure head for driving the

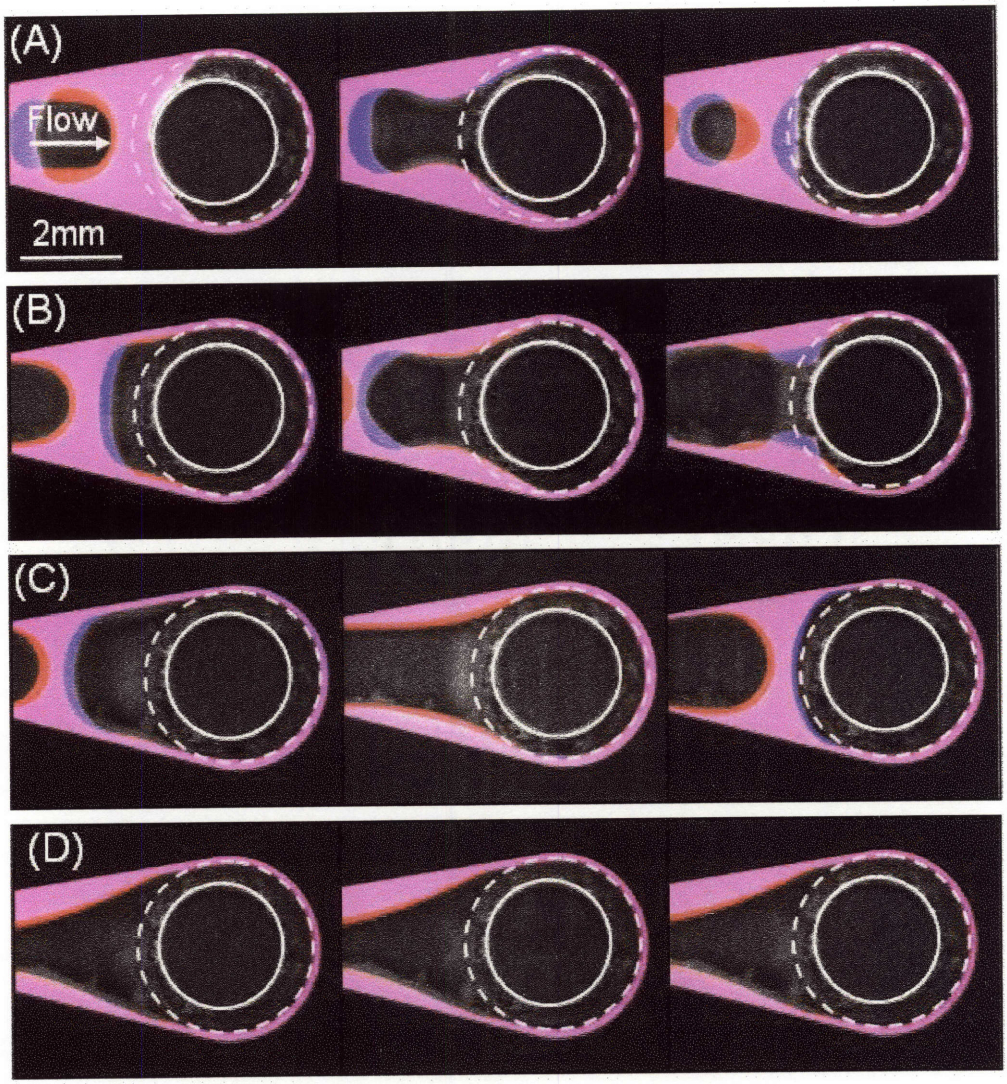

Figure 4-3. A model gas(N_2)-liquid (ethanol with rhodamine dye for fluorescence) two-phase system is used to obtain flow patterns in the main channel ranging from (A) liquid-rich and gas-deficient bubbly regime(j_G = 1.46 m/s, j_L= 0.3 m/s) with small bubbles shooting through the channel, through flow with large slugs (B) (j_G = 1.46 m/s, j_L= 0.1 m/s), (C) j_G = 1.46 m/s, j_L= 0.03 m/s, to (D) a liquid-deficient and gas-rich annular flow regime (j_G = 5.2 m/s, j_L= 0.01 m/s). Using a 12 bit CCD camera we captured images of the array (location in the channel indicated by the white-dashed circle) in operation under the different forms of approaching two-phase flow. Due to high liquid flow capacity of array all the liquid (fluorescent, colored region) is drawn into the capillaries in the initial portion of the array, while the gas (dark region within the channel boundary) continues to flow over the inlets of the remaining capillaries and is channeled separately (outlet indicated by white circle). The blue and red regions represent overlapping areas obtained in double exposure, used to estimate the velocity of bubbles/slugs.

flow in the same fashion as before, and $\Delta P_T = \Delta P_h = 10\ cm$ of ethanol = 18% of ΔP_{max} for $d = 20\ \mu m$. A sharp resolution of interface between phases is obtained by using two synchronized frequency doubled Nd:YAG lasers (532 nm, 25 mJ/pulse), which fire with time delay of 2 ms. The distance traveled by a gas-liquid interface divided by the time delay in firing of the lasers yields the estimate for the velocity of gas bubbles/slugs. In this way the double exposure allows freezing even high speed gas-liquid transient flows.

Separation of phases using the fluid-phase routers is realized by complete removal of the wetting phase (φ_1) through the routers, thereby also obtaining a separate stream for the non-wetting phase (φ_2) along a different fluidic path. The total head applied between the router inlet and the outlet point (where φ_1 is collected, and a pressure P_o is maintained), $\Delta P_T = \Delta P_h + \Delta P_i$, is the sum of the hydrostatic head, ΔP_h, and any applied pressure, ΔP_i. We have shown that φ_1 flows through the routers under this pressure while meniscus at the inlet resists this pressure with φ_2 present at the inlet. In the demonstrations above, ΔP_T required for flow was created through ΔP_h. Here $\Delta P_i = 0$ as both the inlet and the outlet were open to atmosphere. Some instances requiring integration of routers may desire the flexibility to provide the required ΔP_T through ΔP_i. We show complete separation for the ethanol(φ_1)-nitrogen(φ_2) system when ΔP_T required is provided by ΔP_i. On the silicon microfabricated device, we connect a small diameter tubing of known length to the fluid path for φ_2 at the capillaries, and control the φ_2 flow rate into the silicon device to maintain a desired pressure above the capillaries. The common port at the end of capillaries is connected to a tubing as before, for collection of φ_1. The tubing end is open to atmosphere, however, is maintained at the same level as the

capillary inlets such that there is no gravitational head applied and $\Delta P_h = 0$. Then the required ΔP_T for flow of φ_1 through the capillaries is provided by ΔP_i maintained through the pressure above the capillaries. Using this construct, we obtain complete separation of the two-phases for a range of φ_1 velocity from zero to a maximum, for each flow rate of φ_2 maintained to create the required ΔP_T. The maximum φ_1 velocity obtained is determined by the ΔP_T provided as described before. We increased ΔP_T, and for $\Delta P_T \sim$ 60% of ΔP_{max} realized φ_1 approach velocity to the capillaries > 1m/s, with complete separation of phases.

With $\Delta P_T \sim 0.6\Delta P_{max}$ maintained, we connected the outlet port receiving φ_1 to the inlet of a second silicon device, demonstrating complete separation of the phases and routing of the separated phase (φ_1), to a device in series, which can potentially be used to realize a second processing step. The maximum pressure drop in the fluid path carrying separated φ_1 is ΔP_{max} and for higher pressure drops required in this path a pump can be provided to transfer φ_1 to subsequent portions of the network, much like the pumping required between stages of a large scale distillation column.

4.2. Partial separation and Information retrieval

While an array of fluid-phase routers are shown to completely separate individual phases from a mixture and route them along different paths, individual ones can be used to sample a small quantity of liquid from a two-phase gas-liquid or a liquid-liquid flow inside a microchannel. The sampled liquid can be used as a source of local information (eg. composition) in the channel by coupling to a suitable on-chip/off-chip analysis device in the fluid path. Such a measurement at any point along a microchannel can then

used to obtain understanding of process efficiency parameters like, mass transfer performance, reaction kinetics and for characterization of catalysts in microscale multiphase systems.

We demonstrate routing a small portion of the organic phase from a two-phase organic (φ_1)-aqueous (φ_2) mixture flowing in the main-channel (*400 μm* wide and *470μm* deep) of the silicon device. A side-channel *10 μm* wide and *40 μm* deep at the point of intersection with the main channel serves as a router as described earlier. As before a hydrophobic surface coating is required such that the organic phase wets while the aqueous phase is non-wetting with the surface. This is realized through silanization of the device, done by continuously flowing through the microchannels a 2% OTS (octadecyl trichlorosilane) solution in anhydrous toluene for 1 h at room temperature. It is important that moisture does not come in contact with the coating solution inside the channel. Any contact with the moisture can lead to polymerization of solution resulting in precipitation and plugging of the channel. Thus airtight syringes are used and the entire system is flushed with pure toluene before silanization. After the coating, the device channels are washed sequentially with acetone and ethanol pumped through them and finally blown dry in a stream of nitrogen prior to use.

We use toluene (φ_1)–water(φ_2) as the model system. In operation the side-channel is filled with φ_1. Then the total head applied, ΔP_T, the difference in pressure between the point of intersection of the side and the main channel – the router inlet, and that at the outlet (at the end of a tube attached to the side channel), determines the rate of flow of sampled φ_1. Once again in presence of φ_2 at the router inlet, the pressure drop

across the meniscus, ΔP_m, balances ΔP_T, and prevents any φ_2 to flow through the side channel. For a rectangular cross-section of the capillary ΔP_m can be written as:

$$\sim 2\gamma_{\varphi_1-\varphi_2} \cos\theta_{app}[\frac{1}{w}+\frac{1}{h}] \tag{4.2}$$

where θ_{app} is the apparent contact angle determined by the angle of curvature of the meniscus, while w is the width and h the height of the side-channel.

We sample toluene from the mixture at different velocity combinations of the two phases. We color the water with rhodamine (fluorescent dye) for visualization purposes, and observe exclusive sampling of toluene from the two-phase mixture, (Figure 4-4).

The flow-rate of sampled liquid is given by:

$$Q = \frac{\Delta P_T d_h^{\,2}}{32\mu l}(\frac{\pi d_h^{\,2}}{4}) \tag{4.3}$$

where d_h is the average hydraulic diameter of the side-channel, l its length and μ viscosity of sampled liquid.

We control the flow rate of the sampled toluene by manipulating ΔP_T through variations in the elevation between the inlet and the outlet. Alternately, a suction applied to the outflow end connected to the syringe pump operated in the withdraw mode is used. Since this method continuously draws φ_1 from the main channel flow at a constant flow rate, it should be used when the two-phase flow in the channel is expected to contain φ_1. Attempting to withdraw liquid in absence of any φ_1 in the main channel, leads to development of increased pressure drop across the meniscus. When this exceeds ΔP_{max} the meniscus collapses and does not resist flow of φ_2 any more.

We manipulated the pressure at the outflow end of the side channel to obtain a desired sampling flow rate for φ_l, low enough (~ 5% of that in the main channel and lower), so that the main channel two-phase flow is undisturbed.

We also used the same concept for sampling water from an air-water two phase flow in the main channel. In this case we also demonstrate how information about concentration of the drawn liquid is derived by integrating a sensor on-chip in the path of the sampled liquid. Chapter 5 details the procedure and the liquid phase mass transfer coefficient for absorption of oxygen into water for two-phase gas-liquid flow in a microchannel with a model oxygen-water system.

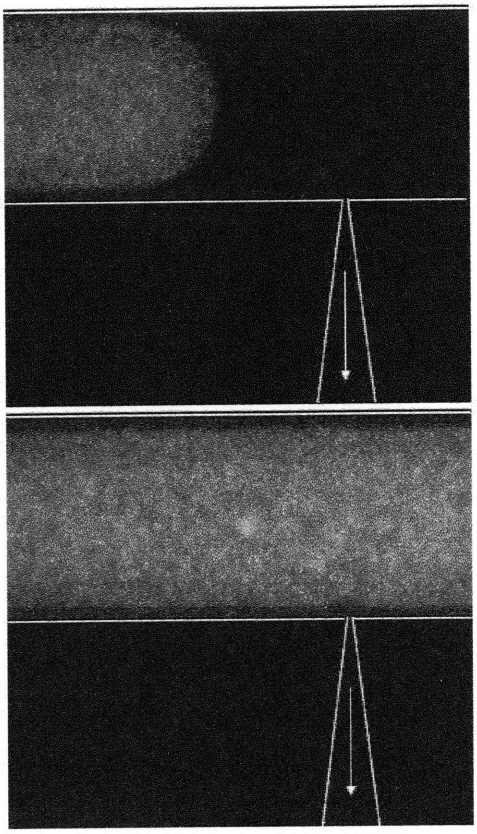

Figure 4-4. Sampling of the organic phase(toluene) exclusively from a two-phase toluene-water flow. The toluene (dark in the image) is removed from the side channel while the water (appears bright due to fluorescent dye rhodamine) flows past the channel, the meniscus at the inlet of the side-channel resisting its flow.

4.3. Valves

Integration of multiple fluidic functions in chemistry and biology on microscale requires transfer of fluids from one component of network to the other and valves are important in realization of such schemes, demonstrated by recent efforts [3, 4]. The basic function of a valve in a fluidic network is to allow the choice of transferring fluid from a common source to one of the branches fed by the source. The above efforts with microscale valve use air pressure to deflect the wall of a microfluidic channel made out of a flexible elastomer material to shut off one flow path, while opening the other. Releasing this air pressure causes the wall to deflect back and allows liquid to flow along the original path while shutting off the alternate. The method has been used to multiplex and control many fluid paths suitably connected.

This solution however has limitations. Flexible polymer materials, like the one used, have a poor chemical compatibility with organic solvents or other common chemicals used for microscale chemistry. They definitely do not address a common attraction cited for microscale chemistry, that of inherent safety in handling even the most hazardous chemistry. Relying on mechanical deformation of the elastomer material always comes with potential problems of incomplete shutoff and leakage. The ability of the fluid-phase router to resist the flow of one phase for pressures less than a maximum can be used to design valves on microscale that do not rely on deformation of flexible materials. Such valves can be realized in materials like silicon/glass and hence useful in virtually any chemical environment. In addition not relying on mechanical deformation the chances of material failure/fatigue are non-existent for a valve designed on this principle.

We have realized such a valve using commercially available glass capillary arrays and microchannels machined in plastic. The device realized and the schematic of the valve is shown in Figure 4-5. The device consists of two-glass capillary arrays (*A1* and *A2*), affixed to recesses in a plexiglass substrate. *A1* and *A2* are connected by a microchannel machined on the substrate top. The microchannel on the substrate extends to connect *A2* to a port on a substrate further connected to a gas (nitrogen) line, allowing application of a desired pressure through a compressed air source, input, *I*. In this way *A2* is between *I* and *A1*, all connected through the channel on the top surface. Additionally, from the bottom side of the plexiglass substrate *A1* is connected to a supply of liquid (water) from a fixed pressure source, *S*, (realized through a reservoir maintained at a certain elevation above the device). *A2* is also connected to an outlet, *O*, through a tubing. In operation, liquid fills the capillaries in *A1* and *A2*. A pressure P_S is maintained at the reservoir source *S*, and P_O at *O* while *A2* is maintained at a pressure higher than *O*, through a hydrostatic head ΔP_{h2}. In this configuration the pressure of air at the input, P_I is manipulated to control liquid flow to the outlet and the 'on' (when liquid flows to *O*, we identify this state of output as $O = 1$) and 'off' (when liquid is stopped at *A1* and does not flow to *O*, we identify this state of output as $O = 0$) states for the valve are realized. When $P_I < P_S$, (we identify this state of input as '$I=0$') liquid flows from the reservoir to *A2* and to the outlet *O* under the influence of ΔP_{h2}. The valve is switched to the 'off' state conveniently by increasing P_I such that $P_I > P_S$ (we identify this state of input as $I=1$), at which point air from the input drives liquid out from the fluid path on the substrate. Air cannot get to the outlet or through *A1* to *S*, due to the pressure drop across the liquid

meniscus formed in the capillaries of *A1* and *A2*. The menisci in the capillaries remain intact and resist air flow for:

$$P_I - P_S < \Delta P_{\max} \text{ , for menisci in } A1 \tag{4.4}$$

$$\Delta P_{h2} + (P_I - P_O) < \Delta P_{\max} \text{, for menisci in } A2 \tag{4.5}$$

where ΔP_{max} is the maximum possible pressure drop across the meniscus.

Figure 4-6 shows the schematic of two states of operation of the device and Figure 4-7 shows the valve in operation along with some of the intermediate actuation stages. Using this concept multiple liquid lines can also be controlled using a single compressed air line, (Figure 4-8).

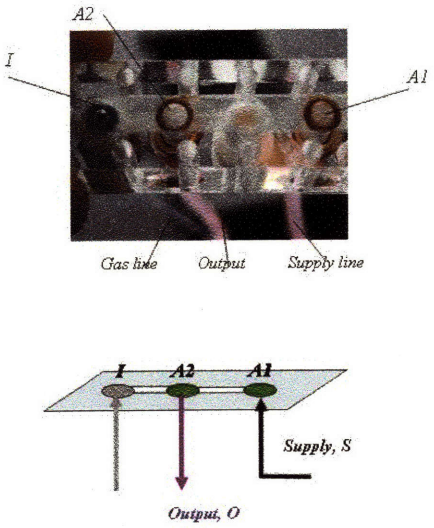

Figure 4-5. The device with the capillary arrays and the schematic of the device

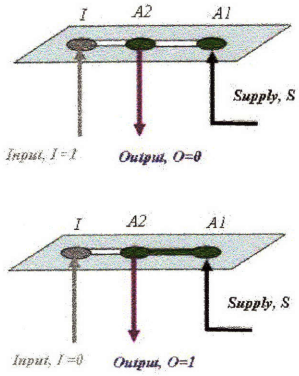

Figure 4-6. Schematic showing the two states of operation of valve.

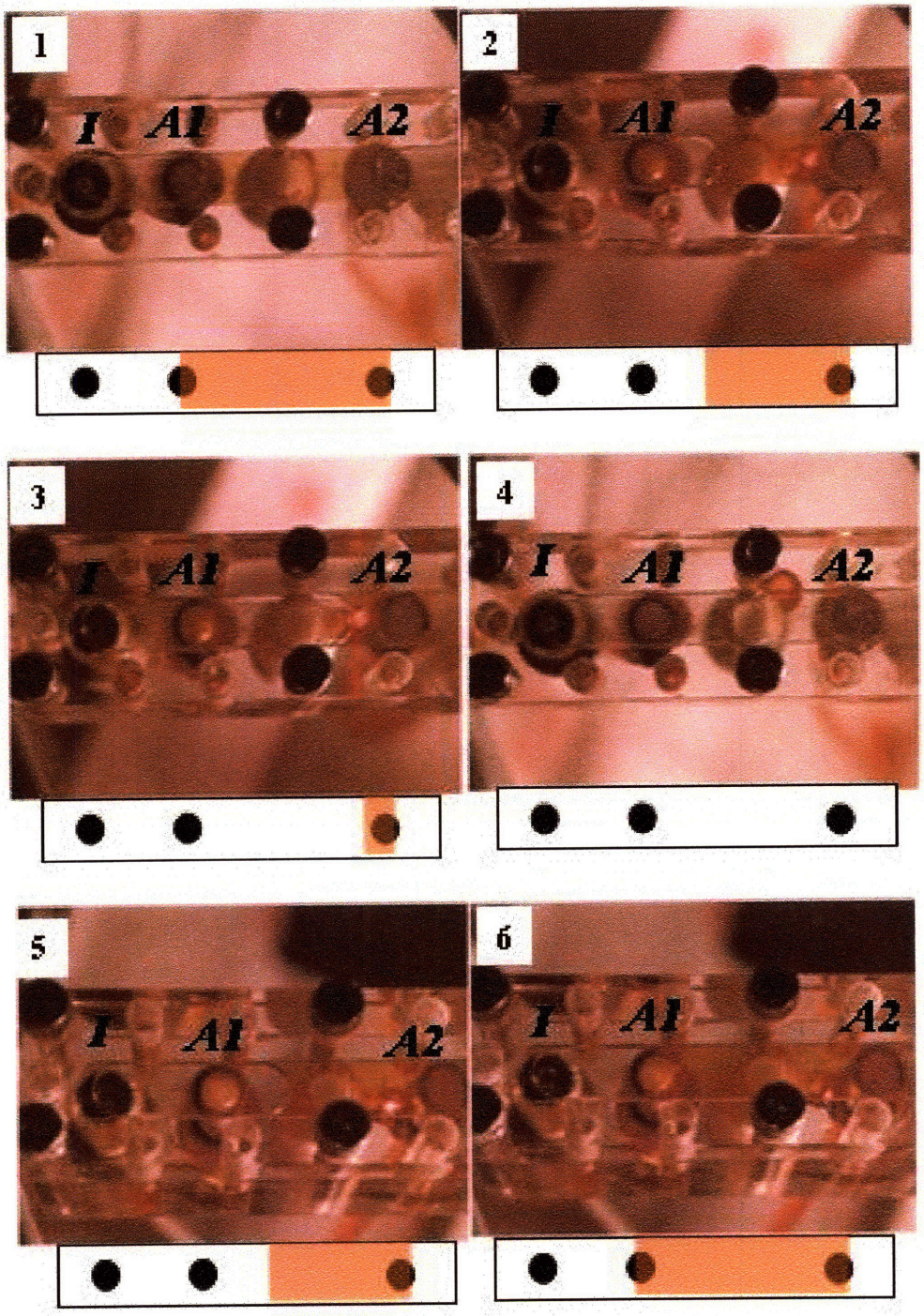

Figure 4-7. The different intermediate states in operation of the valve: State 1, *I=0* and *O = 1*. State 2 and 3, when *I =1* the meniscus in the microchannel on the substrate advances towards *A1*. State 4, *I =1* and *O =0*, the meniscus is stopped at *A1* and air cannot get into either *A1* or *A2* due to meniscus in the capillaries. State 5, when *I =0* the meniscus in the microchannel on the substrate advances back towards *A2*. State 6, once again the initial state: *I=0* and *O = 1* is restored, with liquid flow received at *O*.

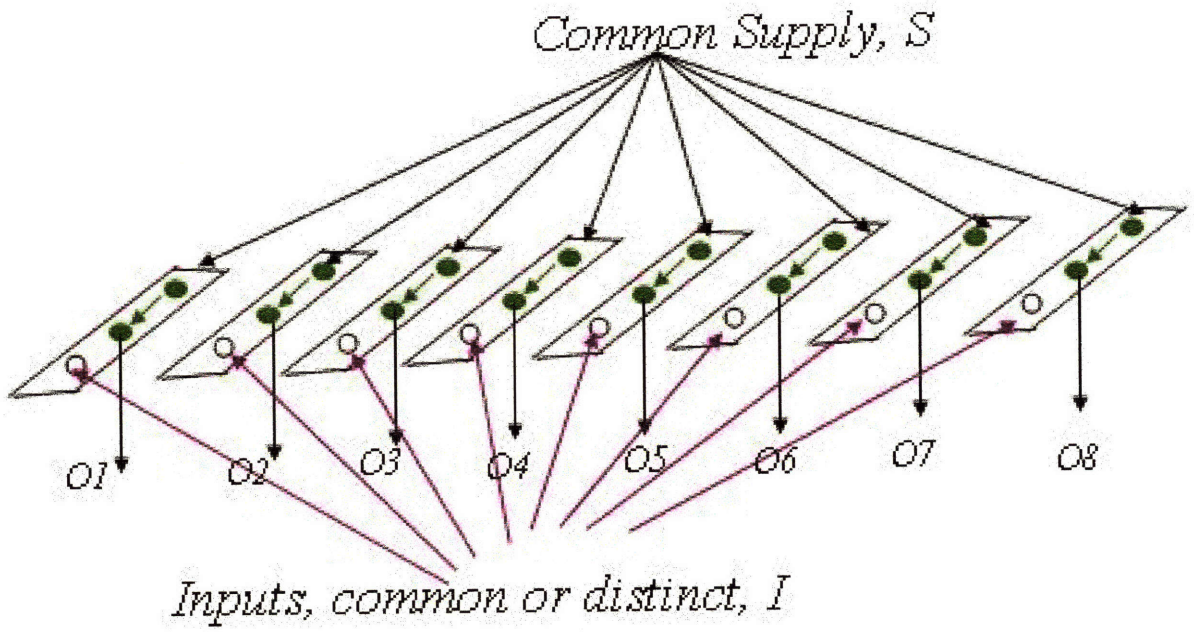

Figure 4-8. Schematic showing connection and control of multiple valves.

4.4.Fluid logic

Mathematical logic realized through fluidic manipulations is useful in situations where electrical connections are undesirable and a high speed for response is not critical. The attraction from the possibility of building computational control mechanisms directly into microfluidic systems developed for analysis, rather than using electronic microchips to control the flows, is recognized as perhaps the most attractive potential of microfluidic computation [1]. This could have strong implications for the development of a 'laboratory on a chip', for chemical analysis of very small liquid samples. The NAND and the NOR are fundamental logic gates and can be used as basic units to realize complicated logical functions. Let us consider a two input (*I1, I2*) and one output (*O*) mappings where the inputs and outputs can each assume two values (0 or 1). Such binary representation of

output and inputs in chemical systems can be associated with different levels of a physical variable like temperature, pressure concentration etc. A NAND gate is the complement of a logical AND function and for this gate O is equal to zero only when both $I1$ and $I2$ are equal to 1. For all other input level combinations $O = 0$, (Figure 4-9). The NOR gate is complement of the logical OR function and here O is equal to 1 only when $I1$ and $I2$ are both 0. Using the above developed valves we show the concept for microfluidics based fundamental logic-gates – the NAND and NOR, (Figure 4-9).

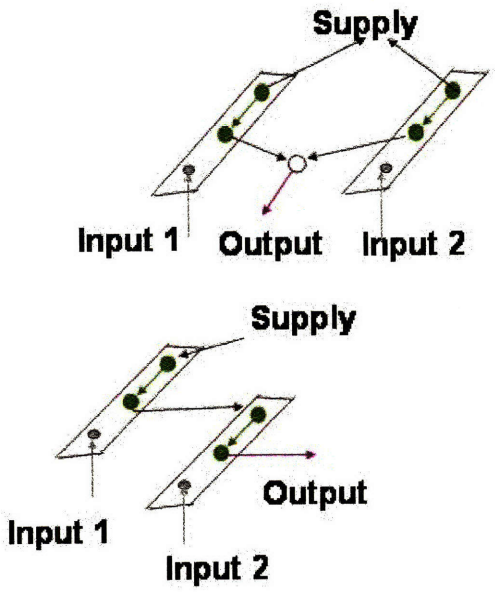

NAND

I1	I2	O
1	1	0
1	0	1
0	1	1
0	0	1

NOR

I1	I2	O
1	1	0
1	0	0
0	1	0
0	0	1

Figure 4-9. Basic logic gates, the NAND and NOR shown above, can be realized using the valves.

4.5.Summary

In this chapter we presented the experimental results for complete separation of gas-liquid and liquid-liquid two-phase mixtures, over a range of flow velocities and mixture fractions. Such a scheme can be used to remove water from anode of a fuel cell, redirect separately phases from a mass/heat transfer step to subsequent reaction, analysis step in a processing sequence. We also demonstrated partial routing or sampling from two-phase mixtures. We used the router principle to demonstrate realization of a microfluidic valve that does not depend on the deformation of an elastic material and is well suited for use in a variety of chemical environments. We showed how a completely different functionality of logic-gates, emerges through appropriate arrangement of these valves. Such logic-gates realized using fluids, pave the way for automation of microfluidic systems without use of electronic chips. In addition to automated multistage synthesis and analysis we believe this property of emergent functionality will be realized in much larger magnitudes through interfacing and automation of processes using fluid-phase routers, valves and logic-gates.

5. *Gas-Liquid Mass Transfer*

5.1.Background

Multiphase chemical processing includes reactions between immiscible liquids and gas-liquid reactions with/without the presence of solid catalyst. Due to limited solubility of one component in the other, the overall rate of these reactions is often determined by the efficiency of contacting between the immiscible phases, which determines the rate of mass transfer. Systems foe which the mass transfer rate is much slower than the intrinsic rate of chemical reaction, are common in industrial chemistry. Examples extend to applications ranging from commodity and fine/specialty chemicals to various emulsions, pharmaceuticals, polymers, personal care products, and petroleum based products, [35]-[36]. An improved mass transfer rate between immiscible phases depends on ability to create large interfacial area per unit volume between the phases and good mixing within each phase. Dispersions/finely distributed droplets of one phase within the other and high velocities are often used on large scale to realize large interfacial area and good mixing.

Microreactors present a unique opportunity for microchemical systems to address challenging problems of contacting, heat and mass transfer, good distribution, controlled reaction and sensing/analysis on microscale. Microfabrication capabilities of photolithography, DRIE, growth and deposition of thin films, multiple wafer bonding and ability to integrate sensing and actuation elements into the system enable this. Silicon microfabrication is unique in these respects in allowing for all on a single platform, [2]. Flow channels on microscale can be used as an efficient tool to create a large surface area

to volume ratio (~ 10^4 m^2/m^3), and a good contacting between immiscible phases can be achieved. In addition to large interfacial area small length scales provide good diffusive mixing even in the laminar flow regime. In addition mixing on microscale within individual phases, in two-phase gas-liquid and liquid-liquid flows, especially in the slug-flow regime where transverse velocity components are induced in each phase, has been found to be particularly rapid, [37-39]. Using gas-liquid reactions, advantages arising from these effects have been demonstrated in microsystems for reactions such as hydrogenation, fluorination, [25, 40-42].

For a gas-liquid system, assuming negligible resistance to diffusion in the gas phase, the absorption mass transfer efficiency in a channel can be measured in terms of the liquid phase mass transfer coefficient, $k_l a$. Gas and liquid enter the channel in cocurrent flow at $x = 0$ and leave at $x = L$. Consider a thin section of channel of thickness dx, at a point x along the channel length. The concentration, C, of gas in the liquid phase at any point x along the channel is assumed uniform for a cross-section and the gas-concentration changes from C at location x to $(C+dC)$ at $x+dx$, over the section dx. Then if C_{in}, C_s and C_{out} are the initial, saturation and the outlet concentration of gas phase in the liquid, $j_L = Q_l/A_c$, is the liquid superficial velocity in the channel with area of cross-section A_c, with a liquid flow rate Q_l, a mass balance on the gas over the section dx is written as:

Flux of dissolved gas out – Flux of dissolved gas in = Mass transfer rate, then

$$Q_l[(C+dC)-C] = k_l a(C_s - C)A_c dx \tag{5.1}$$

Rearranging and writing, $j_L = Q_L/A_c$, we get

$$\frac{dC}{(C_s - C)} = \frac{k_l a}{j_L} dx \tag{5.2}$$

Integrating over a length x of channel, the above is written as:

$$\int_{Ci_n}^{C} \frac{dC}{(C_s - C)} = \frac{k_l a}{j_L} \int_0^x dx \tag{5.3}$$

$$k_l a = \frac{j_L}{x} \ln \frac{C_s - C_{in}}{C_s - C} \tag{5.4}$$

Normally the liquid flow-rate, channel cross-section, inlet concentration of gas in liquid and the saturation concentration are known. Then, using the above equation the mass transfer performance of the system can be determined from the knowledge of the concentration of gas within the liquid, C, at any point x along the channel length.

We present a design and methodology which allows sampling of liquid exclusively from a two-phase gas-liquid flow in a microchannel, at any point along the channel length. We couple this sampling ability with an oxygen concentration sensor integrated on-chip to estimate liquid-phase absorption mass-transfer coefficients on microscale in an open-channel, for a model oxygen-water system and compare the mass transfer coefficients obtained to those measured on large scales. The solution of gaseous oxygen in water is a physical process and does not include a chemical reaction. Oxygen (in small quantities), is easy to handle and readily available. Moreover oxygen is of high importance in many applications, including aerobic growth of bacteria. Absorption of gas into the liquid phase and desorption from the liquid is key to a host of chemical processes. Exchange of oxygen and CO_2 gases between air in the lungs and the blood flowing in thin capillaries is key to supply of fresh oxygen to cells and sustains life. In light of the above, we considered the oxygen-water system as an appropriate model for mass-transfer studies, with characterization for such a system directly relevant to a number of areas.

5.2.Sensing methodology and theory

The measurement of oxygen concentration in liquids is done using a method based on the quenching of the fluorescence in dyes, commonly ruthenium based organic material. Such probes have been in use to monitor oxygen concentration as well as pH, nitrate, nitrous oxide and sulfite for more than twenty years, particularly in bioprocess monitoring [43]. They require only optical access which is advantageous in sterile environments where the opening for traditional electrochemical sensors is problematic.

Fluorescence dyes can be promoted to a state of higher energy by photons (excitation). The absorbed energy can then leave the dye either via the emission of a photon or on a dark path that does not lead to the emission of light. Dyes used for sensing purposes can transfer the energy to molecules, oxygen in the present case. They relax by transferring the energy during a collision with an oxygen molecule. Triplet ground state oxygen $^3O_2$ is promoted to excited singlet oxygen $^1O_2$ while the ligand to metal charge-transfer excited state is relaxed [44, 45]. The singlet oxygen relaxes later without fluorescence. Since the probability of such a collision depends on the concentration of oxygen, the time between the excitation of the dye and the quenching through oxygen (the fluorescence lifetime) is a statistical value connected with the concentration. It is possible to measure this lifetime of fluorescence directly using modulated light for excitation. Measurement of the overall intensity of fluorescence can also be used to measure the quenching and hence the oxygen concentration.

A model (originally derived empirically) to describe the relationship between fluorescence intensity and oxygen concentration is provided by the Stern-Volmer Equation:

$I_0/I = 1 + k\,\alpha C$

I_0: Intensity in absence of oxygen, (unquenched)

I: Intensity in presence of oxygen

k: Overall dynamic quenching constant

α: Henry-Dalton solubility coefficient

C: Oxygen Conc.

For intensity measurements at different concentrations, the equation can be written as:

$$I_0/I = 1 + KC \tag{5.5}$$

where $K = k\,\alpha$, thus requiring the determination of two parameters I_0 and K for a model predicting the dependency of fluorescent intensity on concentration.

It is useful to have the dye immobilized in a matrix so that the oxygen can reach it but the dye is not dissolved and washed out. The base material is critical for the performance of the sensor since the oxygen reaches the dye molecules through the matrix which can influence the measured concentration. Sometimes, a behavior exactly following the Stern-Volmer equation is not often observed in polymer encapsulated dyes. The deviations are explained by postulating a distribution of sites occupied by the dye molecules. These sites differ in oxygen solubility or diffusivity ("microheterogeneity",) [44]and can be described using multi-side models that assume certain distributions of the relevant properties of the sites. Different materials have been used for encapsulation, mostly polymers [46], and porous materials produced in sol-gel methods. We use a sensor film that has the dye embedded in an Ormosil (an organically modified silicate with tailored porosity), provided by *Presens (Germany)*, (Figure 5-1). Excitation takes

place at a wavelength, λ_{Ex} = 510 nm while the wavelength of emitted light has a maximum at λ_{Em} = 630 - 660 nm. The Ormosil is used as a thin film on a mylar polymer layer that provides mechanical stability. In this foil form we find the sensor well suited for integration in a microsystem.

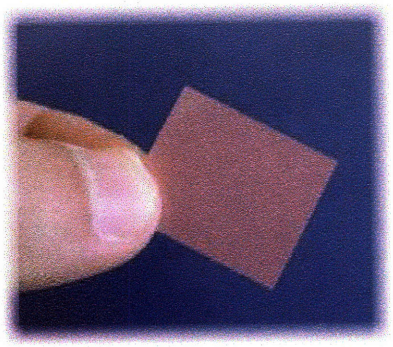

Figure 5-1. Oxygen sensor obtained in the form of a foil is well suited for on-chip integration and measurement of dissolved oxygen concentration.

Klimant et al, [47], find that a two parameter model is better suited for their purpose than the original Stern-Volmer for measured fluorescence quenching (obtained by them as the ratio of unquenched to quenched fluorescence lifetime t_0/t, equivalent to I_0/I). We tested both the two parameter model and the original Stern Volmer model in the initial phase of our study and found little difference in the fit for the two cases for our observations. We chose the original Stern Volmer model and tested its efficacy with our system in predicting concentrations of test samples successfully before using it for the mass-transfer coefficient estimation.

5.3. Experimental

5.3.1. Sampling

The microchannel used for the purpose of mass transfer measurements is shown in Figure 5-2. The fabricated microchannel has separate inlets for the introduction of liquid and gas phases. The two fluids flowing in from the inlet meet at the beginning of a main channel 470 um deep, 400 um wide and 4 cm long. A sampling port is provided at a point 25 mm along the main channel to draw liquid out exclusively from the gas-liquid mixture and in the liquid inlet line for measurement of the initial gas concentration of the liquid. Additional ports are provided at other points along the channel which can also be used for concentration measurements.

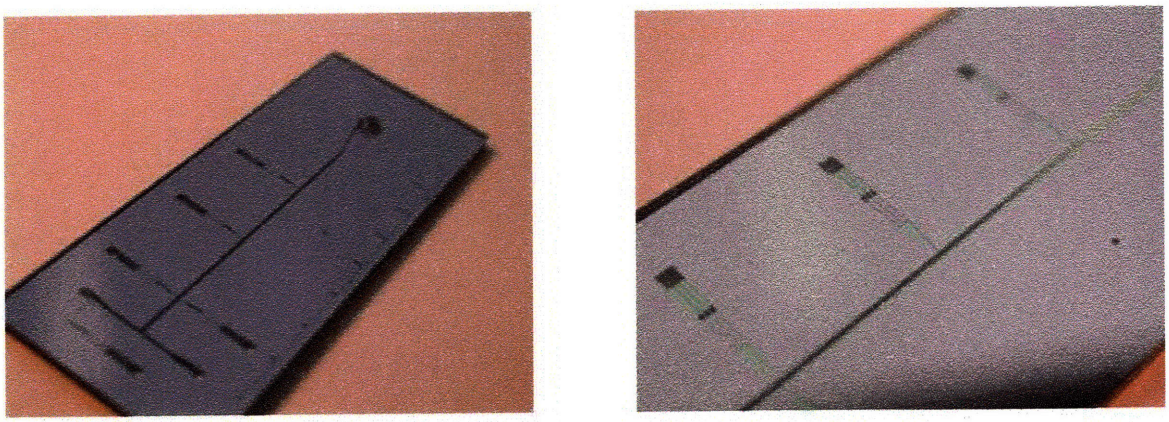

Figure 5-2 Silicon microfabricated device and closer view of the sampling port.

Figure 5-3 shows the schematic of sampling liquid from a transient gas-liquid flow. A smaller channel, (*10 μm* wide and *40 μm* deep at the point of intersection with the main channel, and expanded after a length of *50 μm*, to minimize pressure drop and accommodate a larger area for the sensor), is made to interface with the main channel. This channel is connected to a syringe pump using a 1/16" OD and 0.5 mm ID

transparent PTFE tubing. The smaller channel is filled with liquid, free of any air bubbles to continuously draw out about 5% of the liquid from the gas-liquid mixture. Alternatively liquid can also be drawn out by imposing a hydrostatic pressure difference between the point of intersection of the drawout channel with the main channel and the liquid outlet at the end of tubing connected to a port on-chip, after the sensing region. The surface tension force acting at the intersection of the main and the drawout channels prevents any gas from being drawn into the drawout channel, while liquid is continuously sampled. The sampling flow rate can be adjusted using the syringe pump or by adjusting the hydrostatic pressure applied. The theory of exclusive sampling of one of the phases from a two-phase mixture has been described in detail in Chapter 4.

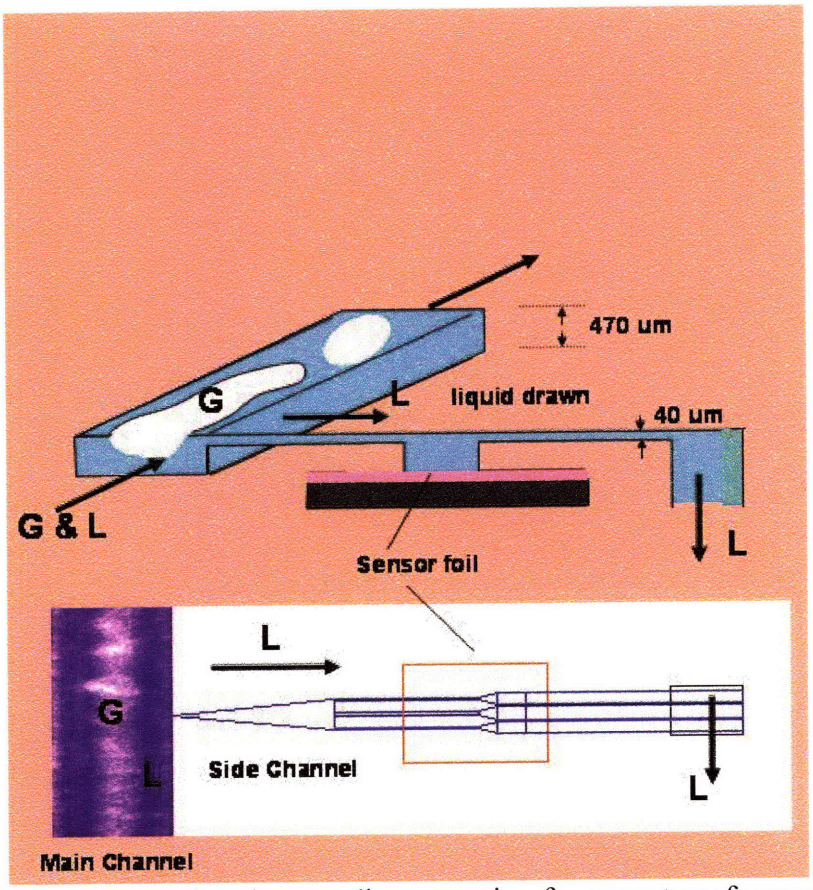

Figure 5-3. Schematic showing the sampling operation for mass-transfer measurement

5.3.2. Sensing setup

Providing for an on-chip sensing allows measurements free from delays due to dead volumes inherent to microscale fittings and connections required to carry the sample from the microchannel to an off-chip sensing system. This dead volume not only leads to a much slower response but also a possibility of larger errors due to a long path for the liquid sample before it reaches the sensor. The microchannel is mounted on an inverted fluorescence microscope (Zeiss Axiovert200). A countinuous white light source equipped with a Osram Sylvania HBO 103 W/2 100 W mercury discharge lamp is used. The light illuminates the sensor film after passing through a filter cube (Zeiss #12) that contains a dichroic mirror and the fluorescent light emerging from the film reaches a camera (Hamamatsu Orca 2, 12 bit full-frame cooled CCD, 1024 × 1280 pixels). Figure 5-4 shows the schematic of the optical setup used for sampling and sensing operations and the properties of the filter cube are shown in Figure 5-5. Combination of a 5×-Objective and a 1.6× base magnification lead is used to obtain a field of view of about $800\ \mu m \times 700\ \mu m$. The images are captured using a frame grabber card, exported to TIF image format files and the intensity of the pixels analyzed using a home-made program (in the IDL programing language, Research Systems Inc.).

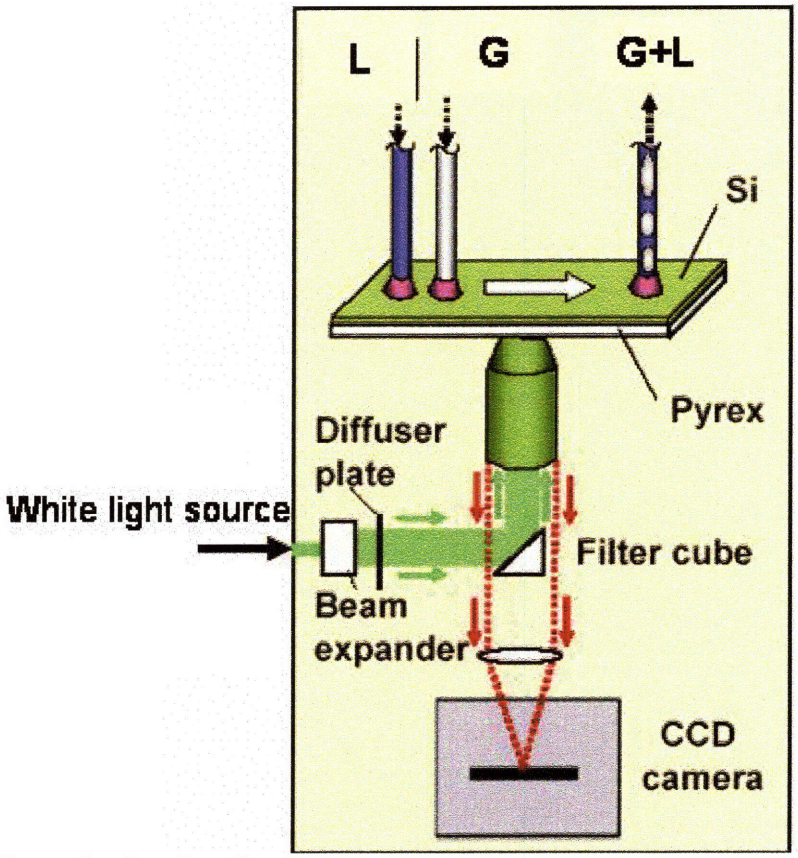

Figure 5-4. Schematic showing the optical setup for mass-transfer measurement

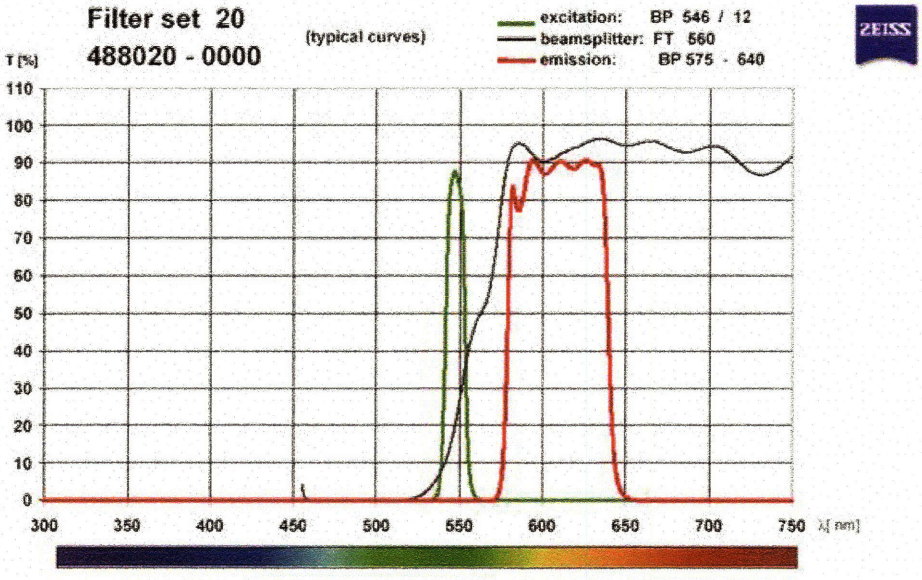

Figure 5-5. Emission and absorption properties of the filter cube used.

5.3.3. Identification of error-sources and error minimization

The accuracy of mass transfer coefficient depends upon the measurement of concentrations. It was therefore important to identify the sources of errors in the measurement procedure and to remove/minimize these errors.

The first set of measurements showed a sufficiently large difference in intensity measured from the sensor foil between the oxygen saturated water environment and an oxygen free environment, implying a good dynamic range of operation. However, large errors in repeatability and reliability were also observed. The following sources of error were identified and suitably tackled in order to improve the accuracy of the measurements. The tilt, stability and vibrations of the setup: The fluorescence intensity of the light reflected from the foil was altered on changing the tilt of the sample and in presence of mechanical disturbances. We carried out the measurements on a microscope stage, setup on an air table to minimize these effects. We used a continuous white light source to illuminate the sensor. It was found that the intensity of the light source fluctuated over short term (time period of fluctuation of the order of a few minutes), and drifted over long term (time scale for the drift is found to be of the order of a few days). A typical short term intensity fluctuation curve is plotted in Figure 5-6. In order to minimize the error due to these effects we averaged out the fluctuations by recording multiple measurements for each data point. A long term drift is inherent to the lamp, however we determined the drift that during a single day to be unimportant, with an introduced error in measured intensity of less than 0.3%. Thus the drift was compensated by calibrating the sensor foil the same day that the measurements were acquired.

Additionally we concluded from the measurements that even if a large area for a sensor foil was used each sensor foil must be calibrated independently due to heterogeneity in the distribution and nature of the fluorophores.

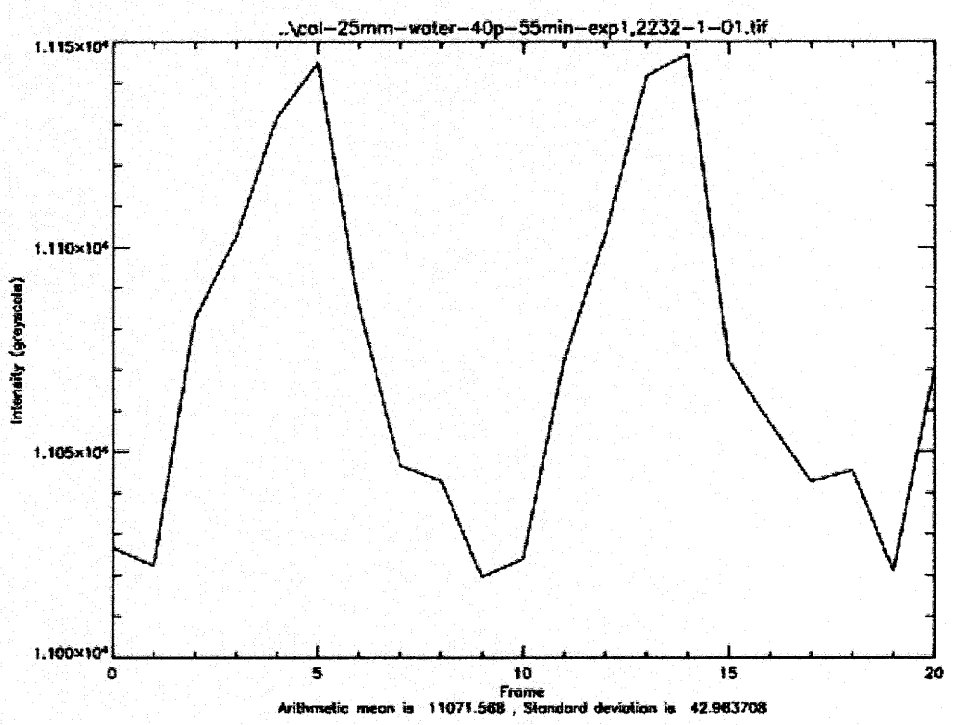

Figure 5-6. Short term intensity fluctuations of the lamp.

5.4. Analysis of Fitness of Methodology

5.4.1. Repeatability

We confirmed the repeatability of the intensity obtained for a particular oxygen concentration, over the entire range of concentration. For this purpose it is necessary to prepare water samples with known concentrations of oxygen. Desired proportions of nitrogen and oxygen gases are prepared by flowing nitrogen and oxygen from separate MFCs to a PEEK 'T' junction, (Upchurch scientific), and obtaining a mixture of the two

gases from the outlet of a tube connected to the 'T'. This air mixture with known proportions of nitrogen and oxygen is combined with water from a syringe pump using a second 'T' junction. The outlet of this 'T' leads into a 5m long tubing, 1/8" OD and 1 mm ID. This is used to obtain a two phase gas-liquid flow containing small liquid plugs separated by gas regions. The total gas and liquid flow rates are adjusted so that the length of the liquid plug is small enough and the liquid at the end of the long tubing is in equilibrium with the gaseous mixture. The equilibrated liquid sample is then fed into the microchannel through one of the inlets while the other inlet is plugged using a cap fitting (Upchurch Scientific). The liquid is drawn out from the sampling port and the fluorescence intensity estimated as described. The repeatability of the intensity measurements over different concentrations is shown in Figure 5-7. The variability between intensity measurements for a given concentration is low on each day, that is during a single lamp on-off cycle (each day represented by a different Run#). However intensities measured for a particular concentration on different days (beyond a single on-off cycle), are found to be very different. The intensity is especially different when the light source is changed, as is evident from comparison of intensities from *Run 4* taken using a different light source, with *Runs 1, 2* and *3* which use the same light source, (Figure 5-7).

We concluded that the intensities from different lamp on-off cycles or using different lamps should not be used to construct a common calibration and measurement graph. However, measurements performed during a single lamp on-off cycle are reliable and can be used for calibration and measurement of unknown concentrations.

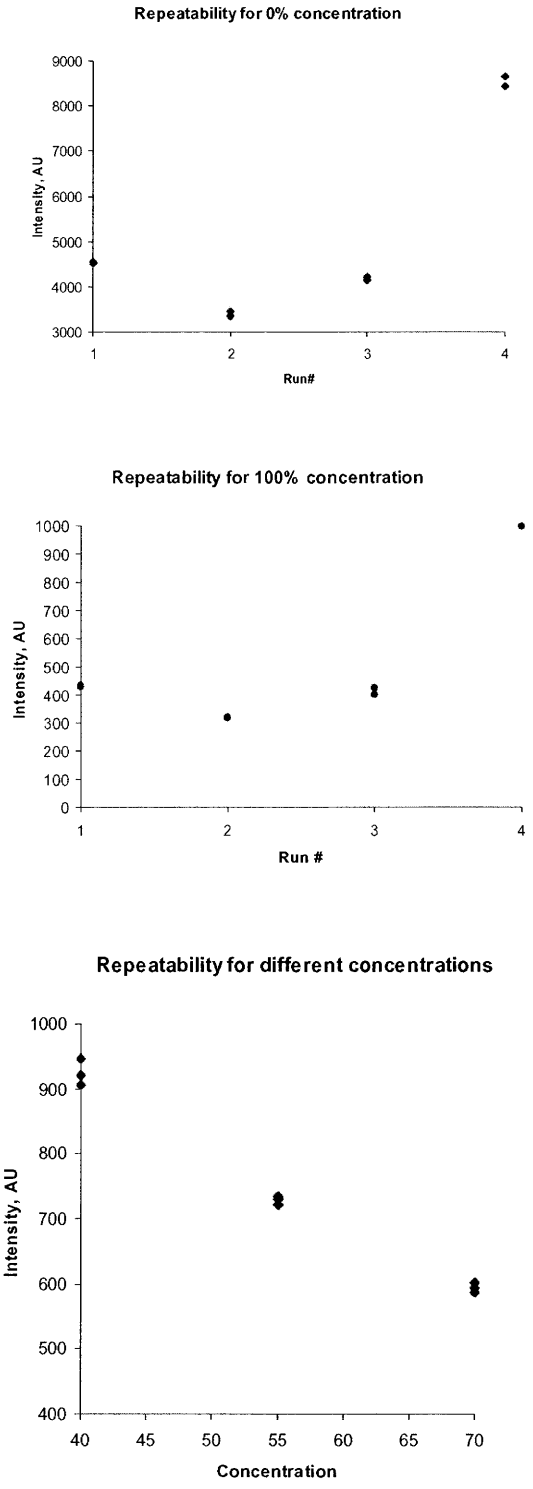

Figure 5-7. Repeatability of measurements in intensity tested at different concentrations.

5.4.2. Calibration and Prediction

The Stern Volmer equation needs the determination of 2 parameters and hence requires 2 intensity measurements at known concentrations for derivation of the calibration curve. We use the oxygen-free water ($C = 0\%$) and oxygen-saturated water ($C=100\%$) as the calibration points. Oxygen saturated water is obtained by equilibrating water with pure oxygen in a long tubing as described above. Oxygen free water is obtained by preparing a solution containing 10g of Na_2SO_3 per liter of water. The sulphite reacts with all the initial dissolved oxygen in the water and the oxygen free water is stored in an air tight flask. In addition the solubility of oxygen in water being low, the sulphite concentration used is high enough to maintain the water oxygen free while being used. Before using the developed sampling and sensing system for mass transfer measurements the ability of system to predict concentrations in known samples of liquid is tested. Once again water with known concentrations of oxygen is prepared and fed into the microchannel as described earlier. A calibration plot is derived using the intensity measurements of oxygen free water and oxygen saturated water, and fitted to the Stern-Volmer equation to calculate the parameters I_0 and k. Intensities measured for water samples with known concentration of oxygen are compared with predictions from the calibration plot. The results of the constructed calibration curve and the obtained prediction for different concentrations is shown in Figure 5-8. A good agreement (>95%) between the intensities predicted by calibration and the experimentally measured ones is obtained, confirming the appropriateness of the developed technique for concentration measurements.

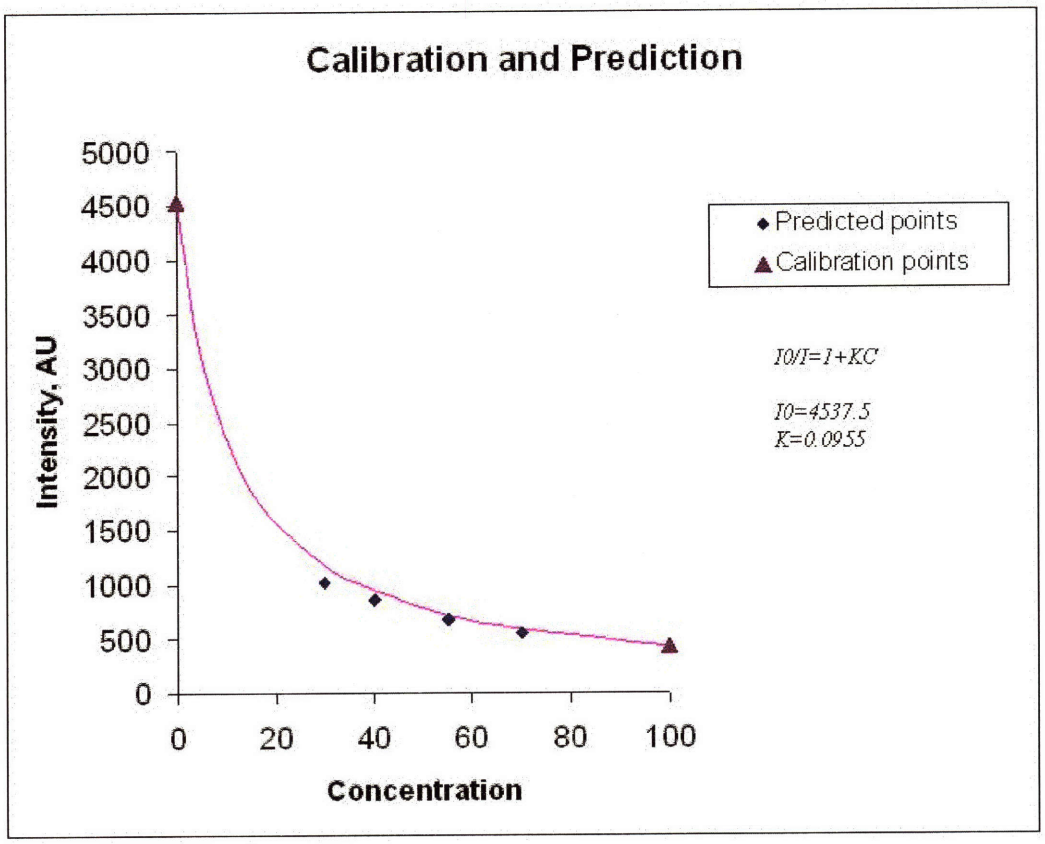

Figure 5-8. Calibration of sensor and prediction of intensities for samples with known concentration.

5.5. Mass transfer coefficient estimation and comparison

We use the above system to estimate the concentration and mass transfer coefficients. The oxygen free water provided by the sulphite solution and used for calibration purposes cannot be used as a solute free initial liquid in estimation of mass transfer coefficient, as the sulphite reacts with oxygen and interferes with the pure oxygen-water mass transfer dynamics. Oxygen free water is prepared by degassing with pure nitrogen and is contacted with pure oxygen from an MFC in the microdevice. A range of gas and liquid flowrates common on microscale is used and the concentration

measured for different gas-liquid velocity combinations to obtain the mass transfer coefficients in each case, Figure 5-9.

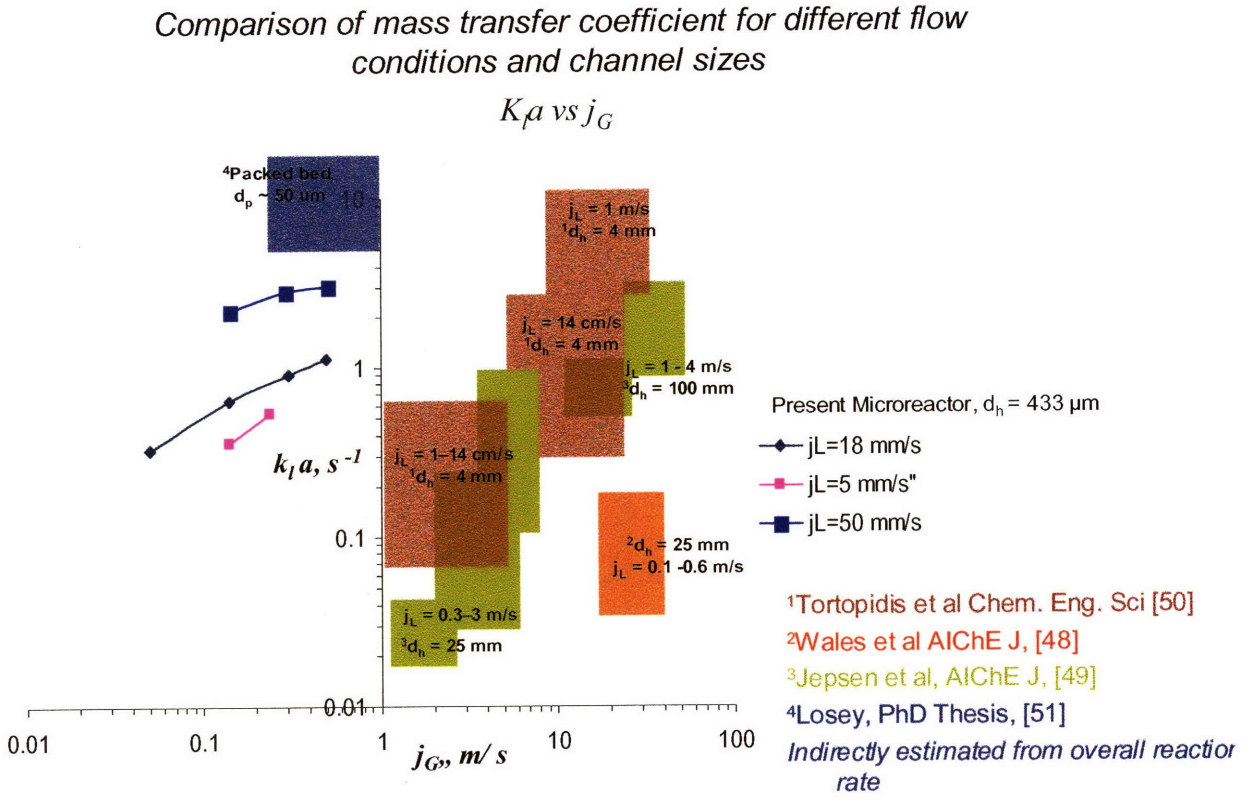

Figure 5-9. Mass transfer coefficients estimated for a range of gas-liquid flow combinations on microscale and compared with the literature data.

The mass transfer coefficient is seen to increase with increasing gas and liquid velocities. We compare the estimated mass transfer coefficients with those reported in the literature for large scale. [48-50]. The mass transfer coefficients obtained on small scale are at least an order of magnitude higher than those obtained with larger diameter pipes. On large scales much higher gas velocities are used in order to obtain improved mass transfer efficiency. However higher gas velocities lead to entrainment of the liquid in the gas phase, potentially resulting in loss of valuable product. Also shown for comparison is

gas phase, potentially resulting in loss of valuable product. Also shown for comparison is mass-transfer coefficients inferred from overall reaction rates with *25-50 μm* particles in packed bed microchannel, [51]. It is seen that the present values are smaller than the typical values reported for the packed bed microchannel. We attribute this to the larger length scale for our channel ($d_h \sim 433\ \mu m$) than the size of the packing particles, and a greater efficiency derived from smaller particles.

Mass transfer efficiency is a function of the energy expended in the flow process. It is desired that the energy expended goes to increase the interfacial area between the two phases and enhancement of mixing within individual phase. Thus a higher energy cost is expected to yield a higher mass transfer coefficient. Such an energy efficiency of mass transfer can be defined using an empirical energy dissipation term, ε, *[49]*:

$$\varepsilon = (j_G + j_L)\Delta P / L \tag{5.6}$$

where ΔP is the pressure drop in the channel over a length L. The mass transfer coefficients measured for the present case range from $0.3\text{ -}3\ s^{-1}$, that is $k_l\, a \sim 1$. The energy dissipation factor for the present case is of $\sim 10^4\ Pa\text{-}s^{-1}$, with $\Delta P_{measured} \sim 500\ Pa$, $j_G + j_L \sim 0.5\ m/s$, and length $L = 2.5\ cm$. Jepsen, *[49]*, correlated the energy dissipation parameter for a range of values on large scale (tubes >12 mm diameter). From this correlation, the predicted $k_l\, a$ value is ~ 0.1 for an ε of $\sim 10^4$. The same parameter evaluated by Tortopidis *et al, [50]*, for a 4 mm ID tube yields a value of $0.1 < k_l\, a < 1.0$. In addition to the improved mass transfer efficicency for small diameter tubes, the authors attributed the observed increase in the mass transfer coefficient partly to the entrance effect in short contactors used for their measurements. The short channel length is common to microscale processing and in the present case as well the length/diameter

ratio considered is small and higher efficiency of mixing at entrance is considered to be a contributing factor to the improved coefficients observed. However, the large improvement in mass transfer coefficient observed can hardly be accounted by this effect, and clearly points to the benefits of chemical processing on microscale.

5.6. Summary

In this chapter we used the developed ability for partial phase routing or sampling from two-phase mixtures to demonstrate the derivation of important process information. We coupled the sampling ability with an on-chip sensing system for a model oxygen-water to provide direct estimates of the gas-liquid mass transfer coefficients on microscale. We compared the estimated coefficients with their macroscale counterparts and report an improvement of at least an order-of-magnitude for microscale systems. Not only is this the first direct evidence of improved mass transfer performance on microscale but also provides evidence to strong opportunity for retrieval of information (example kinetic data and catalyst performance) from multiphase gas-liquid (with/without catalyst) and liquid-liquid systems through the developed methodology.

6. Integration of a Novel Mixing Strategy with reaction and Phase Separation on Microscale

6.1. Mixing Background

Mixing is one of the basic unit operations and necessary for an array of chemical and biological processing needs. Mixing of two process streams implies homogenization of their volume average properties and is sometimes indispensable while commonly helps accelerate the efficiency of a process (rate of reaction between two species, the mass transfer performance between two phases or the efficiency of thermal exchange). Mixing of liquids in microscale has received considerable attention recently. Significant efforts have been invested to solve the problem of mixing on microscale by reducing the effective length across which mixing must be diffusion limited, either by focusing streams [52-55] or by inducing chaotic advection [56-58], through a flow instability, [59-63]. Apart from these passive mixing concepts which rely on design and fabrication of specialized structures inside the channel (the increased surface area is likely to favor deposition of reactants, particles, or cells), active mixing concepts that use ultrasonic and acoustic actuation, [64, 65] have also been presented.Consider two liquids of density ρ, viscosity μ coflowing at a velocity U, in a microchannel of length scale (hydraulic diameter) L. The Reynolds number ($Re = LU\rho/\mu$) measuring the relative magnitude of the inertial and viscous forces is of $O(1)$. In microchannels the flow is laminar, viscous forces are dominant and the spontaneous velocity fluctuations are missing. Then the mixing between the two liquids in the radial direction is limited by diffusion across the channel. The Peclet number ($Pe= UL/D_{eff}$), where D_{eff} is the effective diffusivity of liquids,

measures the relative magnitudes of the convective and the diffusive velocities, (the diffusive velocity ~ D_{eff}/L while diffusive time scale, $\tau_D \sim L^2/D_{eff}$). Then an estimate of the axial distance required for complete mixing is reflected in the product of *Pe* and *L*. Commonly diffusion is slow in comparison to convection in the direction of flow (*Pe* ~100, for typical $L = 100\ \mu m$, $D_{eff} = 10^{-9}\ m^2/s$, $U = 10^{-3}\ m/s$,), and mixing in microchannels is a challenge [2]. A growing number of microscale applications like processing of large inorganic (e.g., nanoparticles) or organic molecules (e.g., proteins) in organic or aqueous solution, characterized by even lower diffusivities ($D_{eff} \sim 10^{-10}$ *to* 10^{-12} m^2/s) invite a more flexible solution to the problem of mixing on microscale.

6.2.Mixing Using Introduction of Gas Phase in Liquid Streams

Recirculations generated in a slug moving in a channel, stimulated by the shear between the stationery fluid at the wall and the slug axis, are known to enhance mixing within the liquid phase, [66]. Recent efforts on microscale with improved mixing using localization of liquids have used slug flow pattern in immiscible liquid-liquid systems to enhance mixing and reaction rates [37, 39]. We show on-chip mixing of two miscible liquids by introduction of an inert gas stream. Gas is introduced in the liquid flow path to obtain a two-phase gas-liquid slug flow pattern in the microchannel. As a result of a combined effect of focusing of streams and recirculatory motion induced in the liquid phase due to the inherently transient nature of gas-liquid two-phase flow we observe efficient mixing of the liquid streams. Efforts using an immiscible slug flow in liquid-liquid systems for enhancement of mixing and reaction rates have not addressed the problem of integration of proposed methodology with a potential downstream processing step. We demonstrate efficient mixing within the channel by introduction of a gas phase

and use the developed microfabricated fluid-phase router array that allows for the complete on-chip separation of a gas-liquid mixture into individual phases. The liquid phase separated from the gas phase can then be channeled to the next processing step in sequence with the mixing step.

We demonstrate the concept for two liquid rates differing by an order of magnitude, for a number of gas velocities. The methodology for the estimation of the extent of mixing is summarized and the details can be found elsewhere, [67]. Here we demonstrate with the help of a model reaction system, integration of the steps of mixing, reaction and phase separation on microscale.

We use the silicon microfabricated channel with two inlet channels, a main channel, side channels and a router-array integrated at the end of the main channel, described in Chapter 3. From one of the inlets we introduce ethanol while ethanol coloured with fluorescent dye (rhodamine) is introduced from the other inlet. Nitrogen gas from a compressed nitrogen cylinder is introduced through the side channel located at a point *5 mm* down the main channel. The flow rates of the ethanol streams are controlled using a syringe pump (Harvard, PHD 2000 series) and that of the nitrogen through a Mass Flow Controller (MFC). We observe the flow in the channel under an inverted microscope (Zeiss Axiovert200) by illuminating with a frequency doubled Nd:YAG laser (532 nm, 25 mJ/pulse) and capture the fluorescent light reflected from the liquid in the channel after passing through the filter cube (Zeiss #12) using a camera (Hamamatsu Orca 2, 12 bit full-frame cooled CCD, 1024 × 1280 pixels). Figure 6-1 shows the mixing observed due to gas introduction for the case with superficial liquid phase velocity in the channel, $j_L = Q_L/A_c = 0.006$ m/s for different velocities of gas phase. Figure 6-2 shows the

mixing observed at a much higher liquid superficial velocity, $j_L = Q_L/A_c = 0.06$ m/s, for a range of gas superficial velocities in the channel. It is seen that a sharp interface exists between the two ethanol streams in the channel until the point of introduction of gas phase for each condition. This is expected from two liquid streams in laminar flow and with mixing limited by diffusion, with τ_D here ~ *100 s*, much larger than time required for the streams to arrive at the point of gas introduction. Moving gas-bubbles inside the channels induce mixing between liquids as seen from images captured at different points along the channel length. It is also seen that an increase in gas velocity improves mixing, more apparent for the case with higher liquid velocity. In each case the gas and liquid phases are separated at the end of the main channel using the router array. The use of gas phase to mix liquids is found to be an efficient technique. The liquid phase often contains valuable products and loss of this during the mixing process is undesirable. In this method an inert gas phase is used and it is expected that some of the liquid (especially for volatile liquids) will be lost in the gas stream due to evaporation. We estimated the amount of liquid that may be lost based on the most conservative assumption that the gas phase exiting the channel is saturated with liquid. For the range of gas and liquid rates demonstrated here, we found this amount to be always < 1% of the initial liquid volume and conclude that this is an insignificant effect. Moreover, even this amount of potential evaporation can be minimized by using a gas phase that is already saturated with the solvent under consideration.

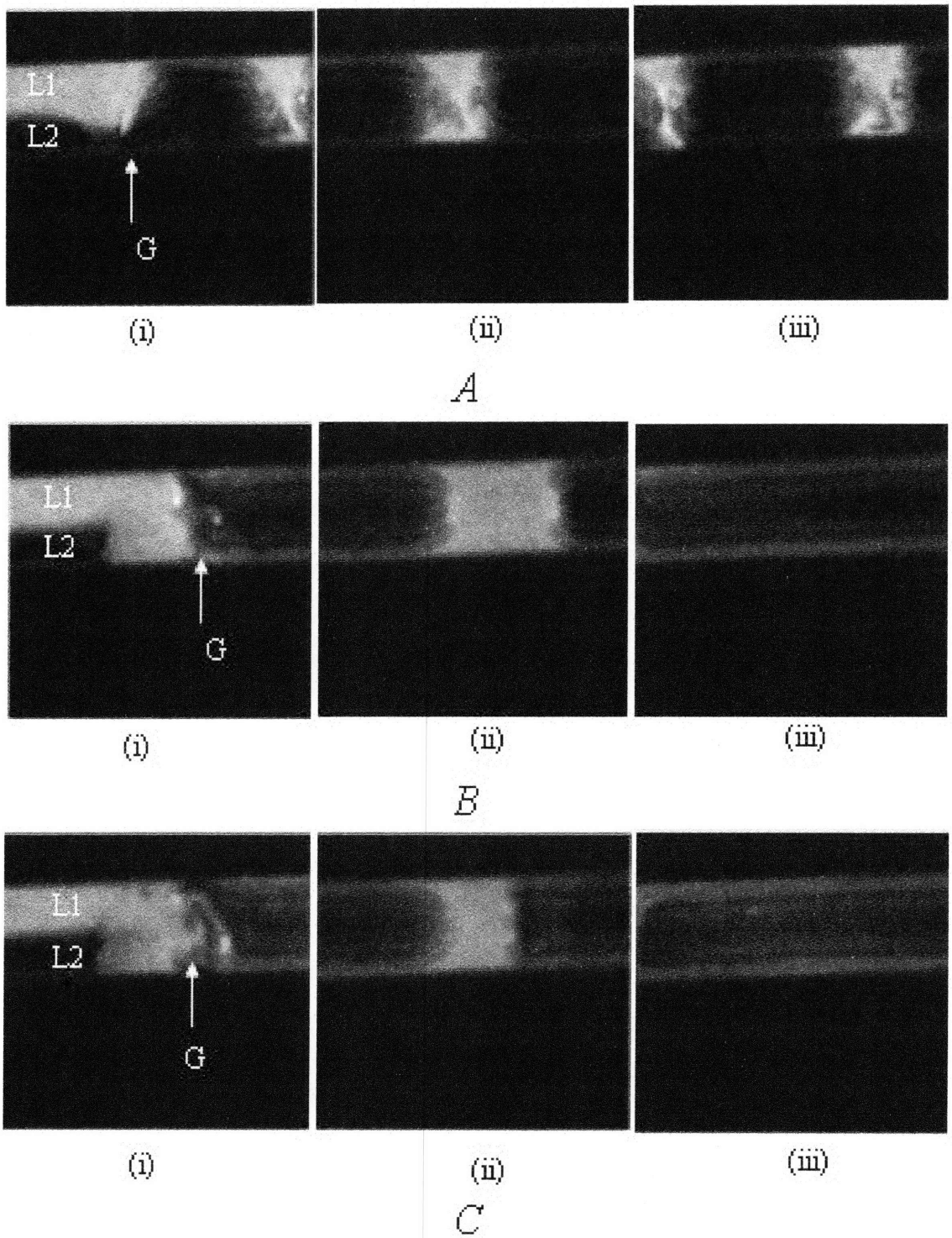

Figure 6-1. Visualization of flow with a gas phase introduced into two liquid streams for different combinations of gas and liquid superficial velocities and at different locations along the flow path: (A) j_L = 0.006 m/s, j_G = , (B) j_L = 0.006 m/s, j_G = , (C) j_L = 0.006 m/s, j_G = , with location (i) showing the point of introduction of gas phase while (ii) and (iii) taken 1 mm downstream from the point of gas introduction for each case

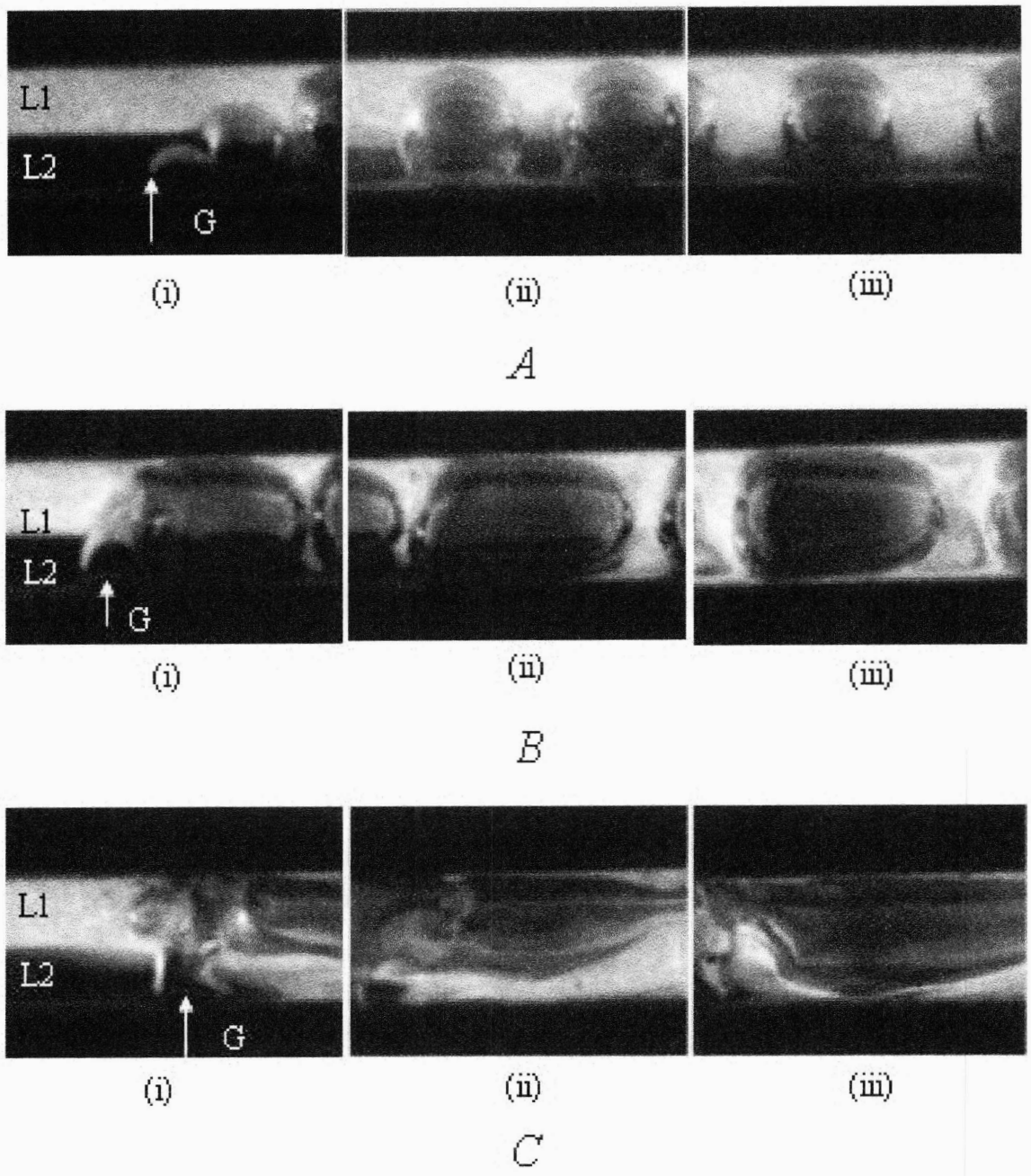

Figure 6-2. Visualization of flow with a gas phase introduced into two liquid streams flowing at a high velocity, for a range of gas velocities and at different locations along the flow path: (A) j_L = 0.065 m/s, j_G = , location (i) showing the point of introduction of gas phase (ii) and (iii) taken 3 and 10 mm downstream from the point of gas introduction (B) j_L = 0.065 m/s, j_G = , location (i) with point of gas-introduction (ii) and (iii) taken 1 and 3 mm downstream (C) j_L = 0.065 m/s, j_G = , with location (i) with point of gas-introduction (ii) and (iii) taken 1 and 3 mm downstream

For estimating the extent of mixing we use two liquid (hexane) streams are seeded with different fluorescent CdSe nanoparticles (quantum dots) with absorption peaks at 514 nm (green), and 590 nm (red) and diffusivities of $1.9X10^{-10}\ m^2/s$ and $2.7X10^{-10}\ m^2/s$. At a location in the channel center, planar scans are obtained for a range of gas and liquid flow rates. The dots are excited at $488\ nm$ and the emitted green and red light is simultaneously collected from separate photomultipliers within $\Delta t_{scan} = 1.6\mu s$, for each of the $512\ x\ 230$ pixels in the scan. Though scanning the entire plane takes too long (1 - $2\ s$) and the instantaneous spatial distribution of gas, L_1 (green) and L_2 (red) across the entire plane cannot be obtained using this methodology the time resolution for a pixel scan is sufficient for all considered velocities, so that the individual pixel data provide accurate measurements. Thus spatial distribution of green and red intensities, $G(x,y)$, $R(x,y)$ are obtained and the ratio $G/(G+R)$ is used to determine the extent of mixing in the liquid using a statistically sufficient number of planar scans.

Experiments for estimating the extent of mixing have been conducted primarily by Dr. Axel Guenther and details can be found elsewhere [67], here we show integration of the developed mixing strategy with reaction and separation of the gas and liquid phases on a single chip.

6.3.Integration of mixing, reaction and phase separation

We use the neutralization reaction between an acid (Sulphuric acid, H_2SO_4), and a basic salt, (Potassium carbonate, K_2CO_3) as a model for our demonstration. Potassium carbonate reacts with an acid almost instantaneously and the reaction proceeds with brisk effervescence of CO_2 gas in addition to formation of potassium salt of the acid and water, the stoiciometry for the reaction is written as:

$K_2CO3 + H_2SO_4 \rightarrow K_2SO_4 + H_2O + CO_2$

Sulphuric acid, 2N (1 M) and potassium carbonate (10 g/100 ml), are filled in two separate 25 ml glass syringes and mounted on a syringe pump (Harvard PHD 2000). 1M sulphuric acid contains 9.8 g of acid/100 ml of solution. For the reaction to go to completion only 7.3 ml of the 1 N acid solution is needed for every 10 ml of the above specified carbonate solution. Potassium carbonate has a high solubility in water (~ 108 g per 100 g of water), compared to sodium bicarbonate (8.15 g/100 g of water) and potassium bicarbonate (27.7 g/100 g water) or sodium carbonate (12.5 g/100 g water), and as a reason is favored over the other salts, for this experiment. We use bromophenol blue as the pH indicator to check the completion of the reaction. The indicator changes color from blue to light yellow as pH of solution changes from 4 to 3. With the concentrations of the two reactants taken here, mixing equal volumes of the two is accompanied change in color for indicator under the influence of excess acid, on completion of reaction. When 10 ml of the above carbonate solution colored with this indicator is taken in a beaker, and even about 8 ml of sulphuric acid added to the solution the solution loses its blue color and changes to yellow almost instantaneously (less than a second), accompanied by brisk effervescence of CO_2. For reaction on microscale the two reactants are pumped at a flow rate of 20 µl/min each, (j_L = 4 mm/s, Re ~ 1) from the two separate inlets of the silicon microfabricated channel detailed in Chapter 3. The reactants meet at the beginning of the 40 mm long main channel, with an outlet at its end. It is observed from the color of the indicator at the outlet that the reactants exit the reactor, only partially converted. In addition the fluid-phase router-array at the end of the channel acts as an indicator to the completion of reaction. If the reaction goes to completion

before the gas-liquid mixture reaches the router array, the liquid is separated from the gas and can be collected as a single phase at the array outlet. However, if the reaction is only partially complete, and continues in the capillaries of the array, it leads to formation of gas bubbles inside the capillaries. In presence of gas inside the capillaries the router is no-longer effective in separation of the gas-liquid mixture into its individual phases. This is due to pressure drop created across any meniscus inside the capillaries, and hence there is no exclusive driving force for the liquid through the capillaries. In this case we indeed find the array to be ineffective in complete-separation of gas and liquid phases and collect a two-phase mixture with gas-bubbles in the liquid phase at the outlet. The residence time of the reactants is about *10* seconds for a reactor channel *40 mm* long. The Reynolds number being small the flow is laminar and mixing between the two liquid reactant streams is diffusion controlled ($\tau_D \sim 100$ seconds). The reaction which starts at the interface of the two reactants cannot go to completion because of insufficient contacting between reactants, and controlled by slow diffusion between liquids. Additionally the small amount of CO_2 gas released due to initial reaction at the interface forms a barrier to good uniform contacting of the two reactants, (Figure 6-3).

Microscale diffusion limitation implies slow and controlled mixing, and has been used to advantage in many microscale applications. However in situations as above, where a good instantaneous mixing is desired it poses a formidable challenge.

We overcome the limitation of insufficient mixing using the developed technique of mixing liquids by introducing an inert or saturated gas phase in the liquid only stream. For the above reaction of sulphuric acid with potassium carbonate solution, we introduce an inert gas (nitrogen) side stream located 5 mm downstream from the beginning of the

main channel where the reactants first contact. We use a gas flow rate of 2.1 sccm into the channel, with both the potassium carbonate and the sulphuric acid flow rates once again at 20 µl/min. Introduction of the gas phase induces mixing of the reactants, and the reaction is observed to go to completion before exiting the main channel at the outlet. We also observe that in this case the router array is capable of separating the individual phases from the two-phase mixture and we collect the liquid phase leading out from the capillaries free of any gas bubbles. This happens despite the decrease in residence time caused by the additional gas used to mix liquids. Thus the positive effect of enhanced mixing and hence increased conversion induced by the gas-phase, dominates the negative effect of reduced residence time on extent of conversion. This example also represents integration of process steps of mixing, reaction and gas-liquid separation on-chip and in sequence. Such a concept is believed to be helpful in construction of microchemical systems, to be used as stand alone entities. The inherently safe nature of microreactors is further advantageous for fast reactions accompanied by release of gas as in the above case.

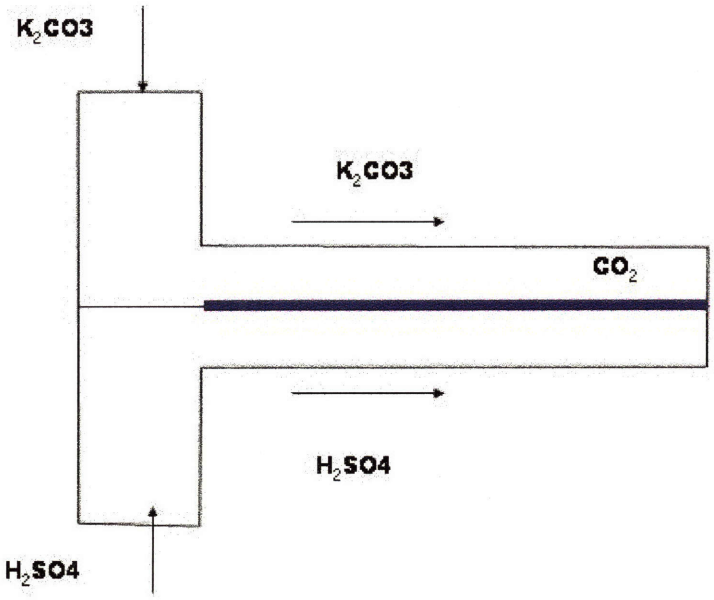

Figure 6-3. Schematic showing the poor contacting between reactants due to slow mixing and a shielding gaseous byproduct (CO_2) layer, leading to only partial completion of the reaction in the channel.

6.4. Summary

Enabled by an available methodology for complete separation of gas and liquid phases from a two-phase gas-liquid mixture in this chapter a novel strategy for mixing liquids on microscale through introduction of a passive gas stream is developed. We also demonstrated the integration of this methodology with reaction and phase separation steps in sequence, all on the same platform on microscale, using a model reaction between an acid and metal salt. In addition to lending itself to convenient integration with processes, we believe a strategy not relying on fabrication of intricate structures but using an operational parameter to effect mixing, will be widely useful for microscale systems.

7. Role of Gravity in Determining Fluid Path on Microscale

7.1. Analysis Using Dimensionless Numbers

We have shown dominance of surface forces over the inertial, viscous and buoyancy forces on microscale using the dimensionless *We, Bo* and *Ca* numbers. We explained how this dominance of surface forces can be used and manipulated to generate inertia in the desired direction while overcoming viscous and buoyancy forces. However, there are common instances when interfacial forces are negligible on microscale. For multiple liquids flowing in a microchannel, two conditions need to be satisfied for this. The first is that the interfacial tension between the different liquids be negligible, and the other that the interfacial energy between the different liquids and the channel walls are comparable. These two ideas are presented in the following equations:

$$\gamma_{i-j} \sim 0 \tag{7.1}$$

$$\gamma_{i-s} \sim \gamma_{j-s} \tag{7.2}$$

i, j is any combination of two liquids in contact inside the channel *S*, containing *n* liquids. Commonly liquids that are miscible satisfy the first criteria and solids that have a similar wettability with different liquids satisfy the second. The two together are easily satisfied for a large section of microscale systems. In such situations consider a channel with characteristic dimension, *L* (*L* is typically the channel diameter, *d*, or the hydraulic diameter, d_h for a channel with non-circular cross-section). Then for the case of two liquids inside the channel with a density difference, $\Delta\rho$, positioned in an unmixed form in

an orientation different from the gravitationally stable one (of the heavier at the bottom and lighter at the top), buoyancy force can be expected to generate flow. Assuming an average density ρ_0, viscosity μ, let U be the order of magnitude of the velocity induced due to buoyancy force. The relative magnitude of the inertial force, $\rho_0 U^2 L$, and the buoyancy force, $\Delta\rho g L^3$, is given by the Froude number:

$$Fr = \frac{Inertial}{Buoyancy} = \frac{U^2}{\frac{\Delta\rho}{\rho_0} gL} \tag{7.3}$$

While that between the viscous, μUL, and the buoyancy force is given by the ratio of Froude and Reynolds number:

$$\frac{Fr}{\mathrm{Re}} = \frac{Viscous}{Buoyancy} = \frac{\mu U}{\Delta\rho g L^2} \tag{7.4}$$

Figure 7-1 is a plot of Fr and Fr/Re numbers against a range of common lengths on microscale, L, for different values of U, plotted for following example values of the fluid physical parameters:

$\rho_0 = 1000\ kg/m^3$, $\Delta\rho/\rho = 0.1$, $\mu = 0.001\ kg/m/s$

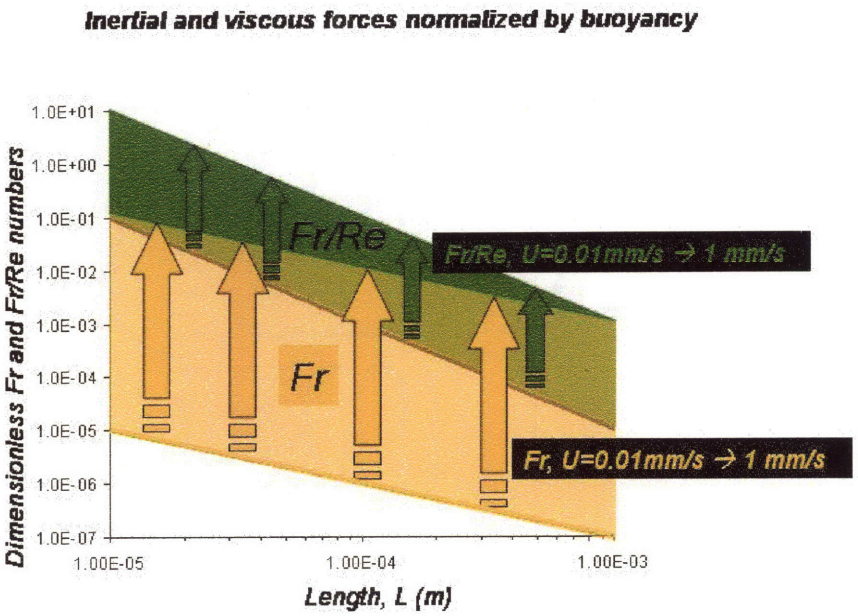

Figure 7-1. Comparison of buoyancy force with inertial and viscous forces for a range of length scales.

The plot clearly illustrates that buoyancy force can overcome the viscous force and act as an important source of inertia on microscale. In the following sections we investigate in some detail to provide answers to two issues: the first is the manner in which the flow generated manifests itself, and its impact on commonly encountered flow situations on microscale. The second is the role of flow and fluid physical parameters in determining the critical velocity and time scales, and the nature of this dependence.

7.2. Experiments in a microchannel

We conducted experiments for studying the path of two liquid streams with a density difference, coflowing in a microchannel. We see reorientation of coflowing fluids in a microchannel under the influence of gravity. A device with two inlets (for introduction of two streams from opposite sides) leading to a *4 cm* long main channel, in

a 'T' configuration is microfabricated in silicon. The inlet and the main channels are *400 μm* wide and *470 μm* deep. Fabrication and design of the device is detailed in Chapter 3. We introduce (ethanol colored with Rhodamine B fluorescent dye for visualization, ρ = 0.79 g/cc) and water (ρ = 1.0 g/cc) streams into the main channel from different inlets. For this miscible liquid system with a density difference we demonstrate a change in fluidic path of streams in the gravitational field through rotation. The rearrangement in the gravitational field is completed in a time much shorter than the time required for streams to mix through diffusion (Figure 7-2). Rotation is caused by the gravitational torque acting on the system of two liquids and results in the repositioning of liquid streams in the channel with the heavier liquid (water) sliding under the lighter (ethanol).

We observe this rotation of different density liquids under gravitational field independent of and unaffected by the inlet geometries, for different angles of *'Y'* shaped and *'T'* shaped configuration of inlet channels. We show complete reorientation through *180* °, for streams of different densities introduced into a channel with the heavier on top and lighter on bottom, proving the redefinition irrespective of the initial configuration of liquid flow paths on microscale (Figure 7-3). In addition, we show the time taken for complete reorientation of the flowing streams is altered with the change in density difference between the streams, (Figure 7-4).

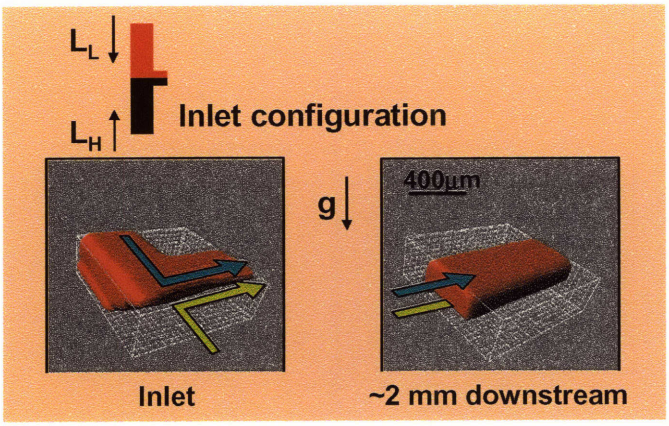

Figure 7-2. Schematic of the contacting of two liquid streams in the silicon channel and 3–D image reconstructed from confocal microscopy scans at two locations: (i) Junction of the inlets carrying the two liquids with the main channel and (ii) At a point ~ *2mm* downstream from the junction in the flow direction. Liquid velocity in the channel is *0.9 cm/s* and the rearrangement of streams in the gravitational field is completed in a distance less than *2mm*, corresponding to a time *<0.2* seconds. Due to laminar flow in the microchannel mixing occurs only by diffusion, with diffusion timescale τ_D ~ *40* seconds ($\tau_D = L^2 / D_{eff}$, where L is the length scale and D_{eff} the diffusivity).

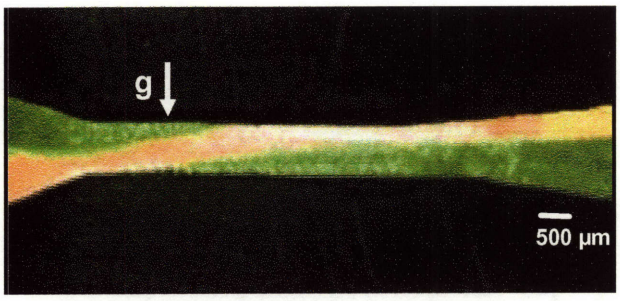

Figure 7-3. Side view of the ethanol (yellow) and water (green) streams introduced from two arms of a Y-channel into a main channel (1 mm wide and 400 μm deep, milled in aluminum). The velocity of liquid in the channel is ~ 0.82 cm/s and the rotation resulting in the heavier stream positioned in the channel bottom while the heavier flows on top, is completed in ~ 0.5 seconds.

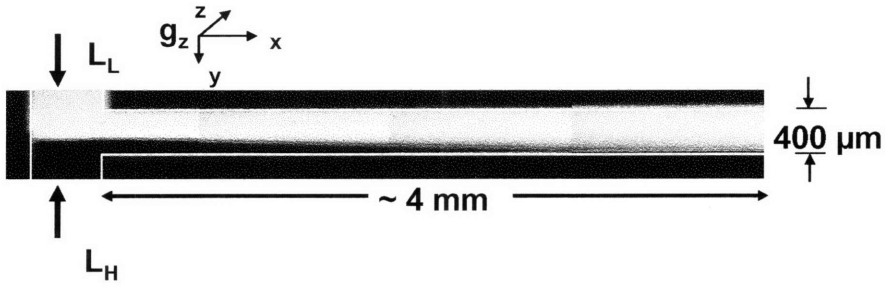

Figure 7-4. Top view of two liquid streams with different densities (lighter liquid, L_L mixture of 25% by volume ethanol and 75% water, $\rho \sim 0.97$ g/cc and colored with fluorescent Rhodamine B dye, heavier liquid, L_H water) contacted in the silicon channel as in Fig. 2. The velocity of streams is 0.4 cm/s and the quarter turn with the flow relocation of heavier liquid to the channel bottom and the lighter to the top takes about1 second, corresponding to an axial distance of about 4 mm. In addition to the density difference between liquids, the time for complete switching of streams is a function of the channel diameter, liquid viscosities and diffusivities.

7.3. Background and Motivation for simulations

Laminar flow of fluids on microscale has been used for microfabrication [68], coating process promoters and inhibitors on specific locations and selective deposition of cells on the coated surface [69], location specific patterning of surface energies [17], controlled transfer of components between streams [70], and is critical to a variety of existent and growing applications across biology and chemistry [71, 72]. Control and definition of fluidic path is at the heart of these processes.

From the experiments conducted we conclude that buoyancy forces arising due to density differences between miscible liquids on microscale can significantly change the path of different coflowing liquids in a microchannel. Additionally, the path of coflowing liquids and the time for reorientation is strongly affected, and can be potentially engineered with the manipulation of the flow and physical parameters of the liquids. The

effect of change in density difference is observed, however, it is important to understand the effect of different fluid flow and physical parameters: ρ, μ, $\Delta\rho$, L, U. The inherently unstable behavior even for small density differences raises an important consideration for design of microfluidic systems. Density differences of a small order could arise between reagent and product stream, between samples and analyte solutions and due to concentration difference between liquids. However, a possibility to vary this switching time can be used to control the distance at which complete switching occurs and the path of two streams inside the channel. Changes in velocity along the channel length by altering the liquid flow rate can also be used to alter the flow path. The dependence of fluid path in a microchannel on the density difference between streams places a constraint on the liquid combinations that can be manipulated using the numerous techniques developed for microfluidic applications. An understanding of this, in designs accounting for the effect would further development of robust systems and those deploying this effect for a localized definition of functionality on channel walls, not attainable otherwise, can open new opportunities.

Flow phenomena resulting when fluids of different density and/or viscosity come together, have been identified in an extraordinary range of natural and industrial settings and have attracted laboratory interest for more than four decades. As gravity currents, they are of importance in mining, discharge of power station effluent, aircraft operations and understanding of natural processes in the atmosphere (sandstorms and volcanoes) and the oceans (large volumes of fresh water less dense than the neighbouring salty water flow very close to the surface determine the distribution of fish, oil slick [73], and as

buoyant or viscous displacements in tubes and porous media with applications in oil recovery, fixed bed regeneration, hydrology, filtration, and lubrication [74].

Fluid layers of different density superposed with the heavier on top and lighter on bottom or with a viscous stratification, form an unstable system [75, 76]]. Taylor, [[77] studied the displacement of a viscous fluid contained in a tube by air blown into the tube and measured the amount of viscous fluid left behind on the walls. The inability of a less viscous fluid in completely displacing a more viscous one due to development of an unfavorable mobility profile, and consequent development of finger like structure was further characterized by [78] and [79] who also found similarities with the Taylor instability, [80]. Since then instabilities due to these viscous displacements in miscible and immiscible systems have been widely studied. Their characterization have been carried out in a variety of geometries and conditions, some incorporating the interaction of gravitationally induced effect when fluids are of different densities but primarily focusing on the viscous contribution [74, 81-87], [88]. Recently the analog for Taylor's experiment for miscible systems was also studied, incorporating the interaction of gravitationally induced effect when fluids are of different densities [89], [90].

Wooding was one of the first (and remains one of the few) to investigate the nature of instability originating primarily due to density differences [91]. He identified the similarity of the wave like instability at the interface of miscible fluids with a density difference, characterized by amplitude that quickly exceeds the wavelength, with the fingers understood earlier [77, 78]. He studied the time propagation of these fingers and analyzed the time evolution of the mean amplitude and wavenumber in a Hele-Shaw cell with a net flow of the heavier liquid maintained from the top. Recent efforts, [92, 93],

investigated early stages of the instability growth and provide growth rate and most amplified wavenmbers as a function of the governing Rayleigh numbers for flow of miscible fluids in a Hele-Shaw cell driven by density difference. In these studies the dimension of the cell along the direction in which the finger amplitude grows (also the direction in which the gravitational force acts), is much greater than the dimensions of the plane normal to this direction. We study displacement of interfaces between miscible fluids in confined microchannels driven solely by buoyancy forces, with the presence of boundaries within sub-millimeter dimensions along the direction of gravitational force, implying small stabilization times for the system.

Our interest is to estimate the time for stabilization and velocity scale for such systems and find dependencies with respect to various fluid flow and system physical parameters. We connect the obtained results from the 2-dimensional simulations to the experimental results described above and the 3-dimensional steady state model. Further, our interest is to be able to derive understanding of the parameters that have an impact on the overall flow situations experimentally described and are of enviable importance to the field of microfluidics.

We study the configurations shown in Figure 7-5 (A and B), identifying them as the '*sideways*' (with the liquid streams oriented sideways at approach), and the '*superposed*' (the liquid streams oriented with the heavier on top and lighter on bottom at approach), configurations respectively.

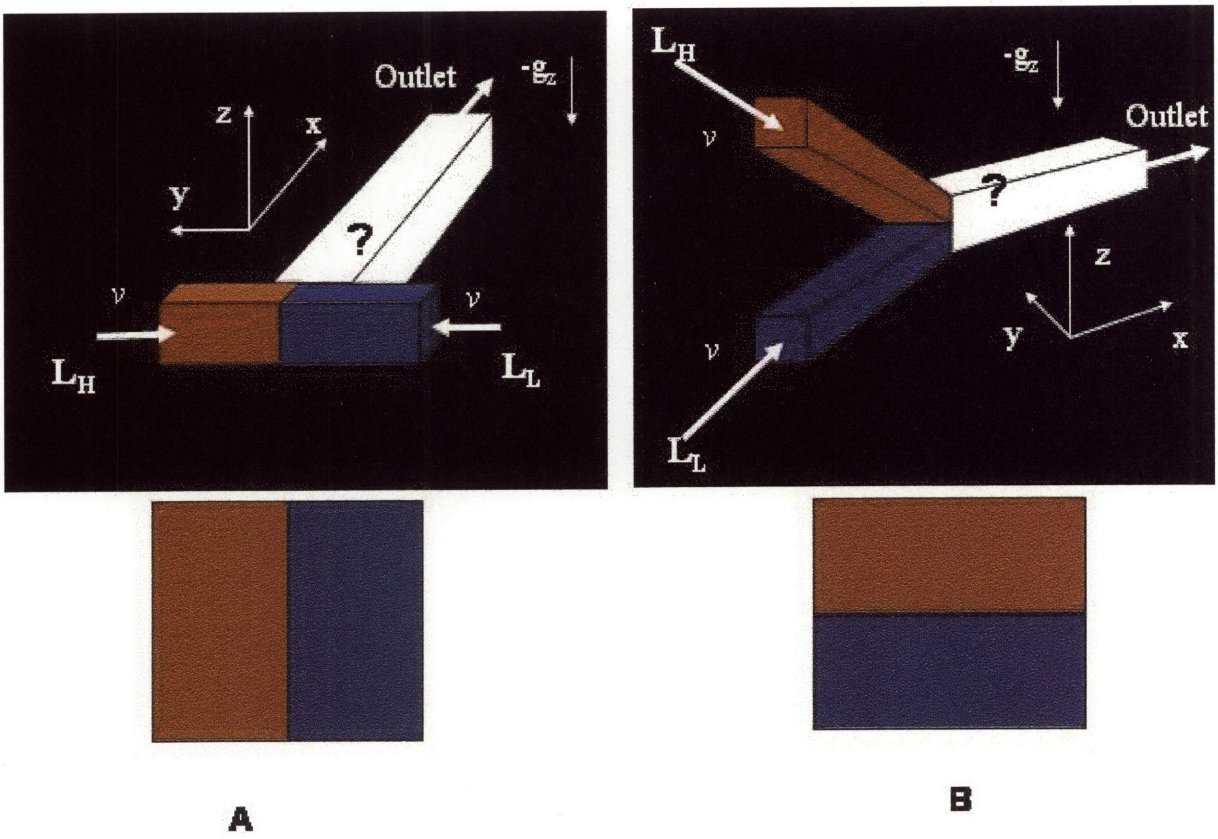

Figure 7-5. The 3-dimensional steady flow configuration and the time dependent problem in 2-dimensions with (A) the sideways and (B) the superposed orientation of liquids.

The dependence of the time to reorient on the relevant parameters is first understood from the dimensionless scaling analysis of the system. We use a finite element scheme (FEMLAB) to model a representative 2-dimensional time dependent system as well as the full 3-dimensional steady state flow situation experimentally studied. We use these models to confirm the dependencies obtained through the analysis of dimensionless numbers and further use it to estimate the time required for reorientation of streams and the velocities induced, for different parameter values, comparing their relative effects.

The 2-dimensional simulations reveal the essential nature of the transfer of fluids on microscale due to density difference. Using these simulations an understanding for the dependency on viscosity, density difference and length scales and the details of time evolution of velocity and concentration fields is obtained. Here the time domain, with a linear transformation using the axial velocity along the channel length, is mapped into the 3rd dimension to derive an understanding of the steady flow path of liquids, as described experimentally. However, even though such a transformation is able to capture the essential dynamics of the flow-situation of interest in 3-dimension it misses on the effects due to presence of the wall and is different in this regard from the 3-dimensional situation. The initial condition of liquids occupying there positions in the channel coupled with the no-slip boundary condition implies that there is significant liquid sticking to the wall with time. On the other hand, a 3-dimensional flow field takes a flow path along the axial direction in a manner such that there is no trace of earlier occupancy along the initial path taken by the fluids in a gravitationally stable orientation. It is to understand the effect of these differences that we carry out simulations in 3-dimension as well.

7.4. The 2-dimensional time evolution problem

7.4.1. Problem definition and equations

The physical situation of interest is the effect of gravity on path of two liquids with a density difference flowing together in a microchannel. The simulations for the sideways and the superposed configurations are presented in this section. While the former is a common pattern of contacting streams in a microchannel the latter is the

opposite form of the stable configuration. The continuity, momentum and the conservation equation for these configurations can be written as:

$$\nabla \cdot \mathbf{v} = 0 \tag{7.5}$$

$$\rho \frac{D\mathbf{v}}{Dt} = -\nabla \mathrm{P} + g\rho e_{\mathrm{g}} + \mu \nabla^2 \mathbf{v} \tag{7.6}$$

$$\frac{DC}{Dt} = D_{eff} \nabla^2 C \tag{7.7}$$

We assume the liquids to be incompressible, miscible in all proportions while the viscosity *(μ, kg/m/s)* and molecular diffusivity *(D_{eff}, m^2/s)* as constants. *C* is the molar concentration of the lighter liquid made dimensionless using the molar concentration of lighter liquid in its pure form, while the density ρ is defined as,

$$\rho = \rho_h - C(\rho_h - \rho_l) \tag{7.8}$$

The density differences under consideration are assumed to be ~ 0.1 or smaller so that the continuity equation can be written as above, without the effect of spatial variation in density. For these density differences considered, we find the results to be unaffected when this variation is included.

With the Boussinesq approximation used, the analysis using dimensionless numbers can be done with the momentum and species conservation equations non-dimensionalized using the following variables,

$$\overline{\mathbf{v}} = \mathbf{v}/U, \bar{t} = t/\tau, \overline{\nabla} = \nabla\ L, \overline{P} = P/\rho_0 U^2 \tag{7.9}$$

where ρ_0 is the density when concentration is zero. *P* is the dynamic pressure and is defined in terms of the actual pressure P as $\nabla P = \nabla \mathrm{P} - \rho_{\mathrm{h}} \mathbf{g}$

$$\frac{D\bar{\mathbf{v}}}{D\bar{t}} = -\bar{\nabla}\bar{P} - g\frac{(\frac{\Delta\rho}{\rho_0})L}{U^2}e_g + \frac{\mu}{\rho_0 UL}\bar{\nabla}^2\bar{\mathbf{v}} \tag{7.10}$$

where $\Delta\rho=\rho_0-\rho$, the deviation in density as concentration changes from zero to C.

$$Fr = Inertial / Buoyancy = \frac{U^2}{(g\frac{\Delta\rho}{\rho_0})L} \tag{7.11}$$

$$\mathrm{Re} = Inertial / Viscous = \frac{LU\rho_0}{\mu} \tag{7.12}$$

On microscale, for Reynolds Number ~ 1 or smaller the inertial terms are unimportant and,

$$U \propto \frac{g(\Delta\rho)L^2}{\mu}, \tag{7.13}$$

$$\tau \propto \frac{\mu}{g(\Delta\rho)L}, \tag{7.14}$$

This dimensionless analysis provides the dependency of the time and the velocity scales for the buoyancy driven flow in microscale on viscosity, density difference, the acceleration due to gravity and the length scale.

The mass conservation equation in the dimensionless form becomes:

$$\frac{DC}{D\bar{t}} = \frac{D_{eff}\tau}{L^2}\nabla^2 C \tag{7.15}$$

$$\text{where } \frac{L^2}{D_{eff}\tau} = Ra = \frac{gL^3\Delta\rho}{\mu D_{eff}} \tag{7.16}$$

The Ra number is the ratio of the diffusion time scale to the critical time scale for momentum transfer. For large Rayleigh numbers the momentum transfer is much faster

compared to diffusion. In cases of small Rayleigh number the diffusion is important and tends to equalize the density across the two liquids.

For large scales, Re>>1 and the viscous term is relatively unimportant initially when the induced velocity is high. However with time, viscous damping decreases the velocity as the system stabilizes and both effects become important, when eventually the inertial effects are completely subdued as the velocity becomes even smaller. For the high Re regime, the dependence of velocity and time scales can be written as,

$$U \propto \sqrt{\frac{g(\Delta\rho)L}{\rho_0}} \tag{7.17}$$

$$\tau \propto \sqrt{\frac{L}{g(\frac{\Delta\rho}{\rho_0})}} \tag{7.18}$$

We solve equations 7.5 through 7.7 using the FEMLAB program for different parameter values for both the superposed and the sideways configuration. The results of simulation are discussed below.

7.4.2. Effect of density difference, viscosity and length scale

We use a cross-section of $400\mu mX400\mu m$, the heavier liquid defined with an initial concentration, $C(t0) = 0$, while the concentration for the lighter liquid defined such that $\Delta\rho/\rho=0.1$, $g = 9.81\ m/s^2$, $\mu=10^{-3}$, $D_{eff}=10^{-9}$, and identify this as the base-case for the parameter system. The no slip and the no flux boundary conditions are used for the momentum and species conservation equations respectively, for all the walls. Additionally, the initial pressure and the velocities in the x and y direction are set to zero, $P(t_0) = v(t_0) = u(t_0)=0$, where u and v are the x and y velocities and P the pressure. An inclined boundary instead of a horizontal (for the superposed configuration) or a vertical

boundary (for the sideways configuration), between the two streams with a small angle of inclination << the expected angle of orientation of the system of liquids (180° for the superposed configuration and 90° for the sideways configuration), is used as an initial perturbation.

We show the time evolution of u and v (x and y components of velocity) induced in the system for the sideways (Figure 7-6), and the superposed (Figure 7-7), configuration.

For both configurations we see the scales of x and y velocities induced are similar, $u \sim v$, a consequence of continuity. Moreover, the velocities peak initially and die out with time. We expect this behavior as a result of the subsequent stabilization and decay of the initial velocities induced by the buoyancy force, as the liquids reorient under the influence of these induced velocities towards the gravitationally stable configuration, with the lighter liquid on top and the heavier on the bottom.

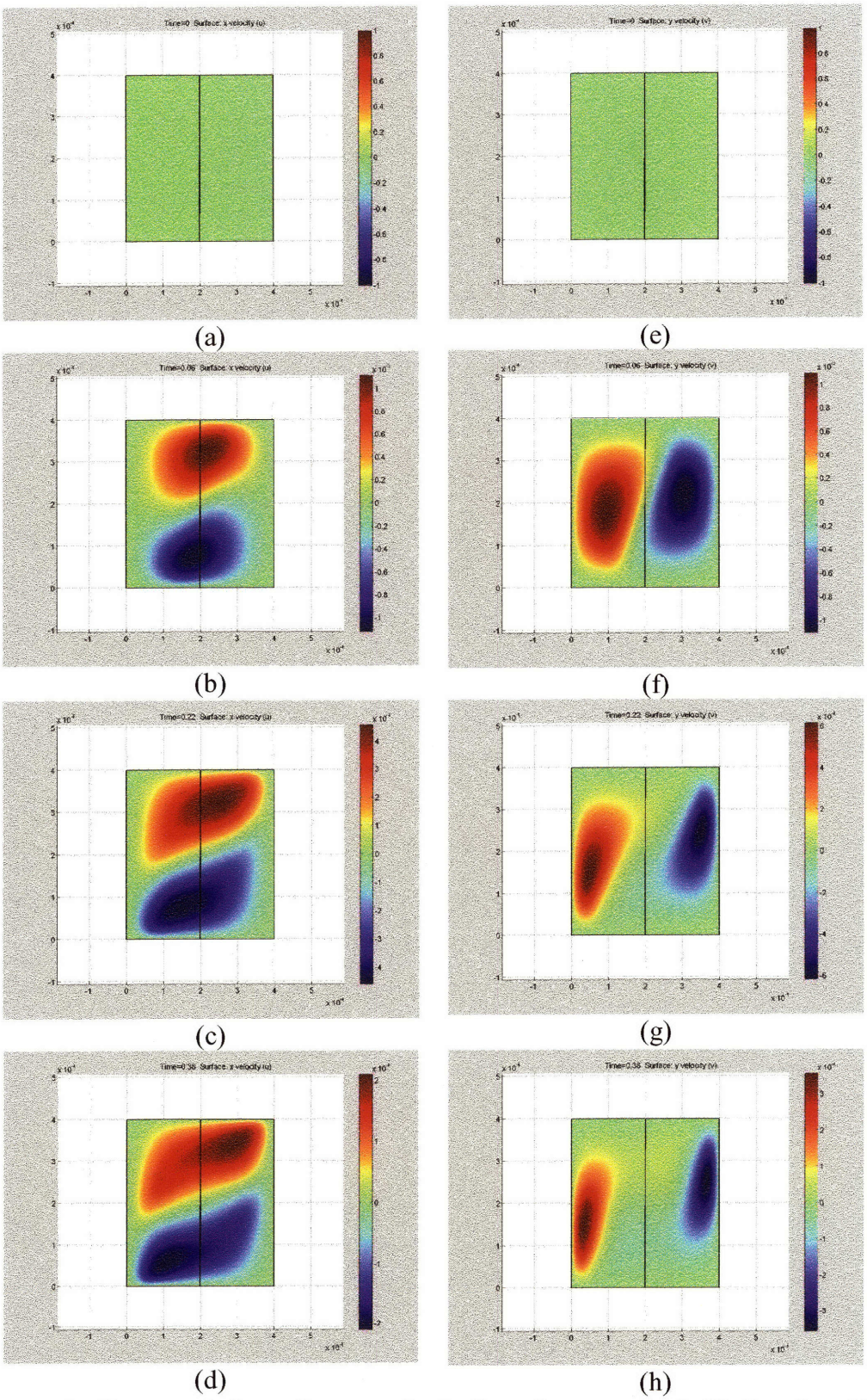

Figure 7-6. Time evolution of u, panels (a-d) and v, panels (e-h) for the sideways orientation.

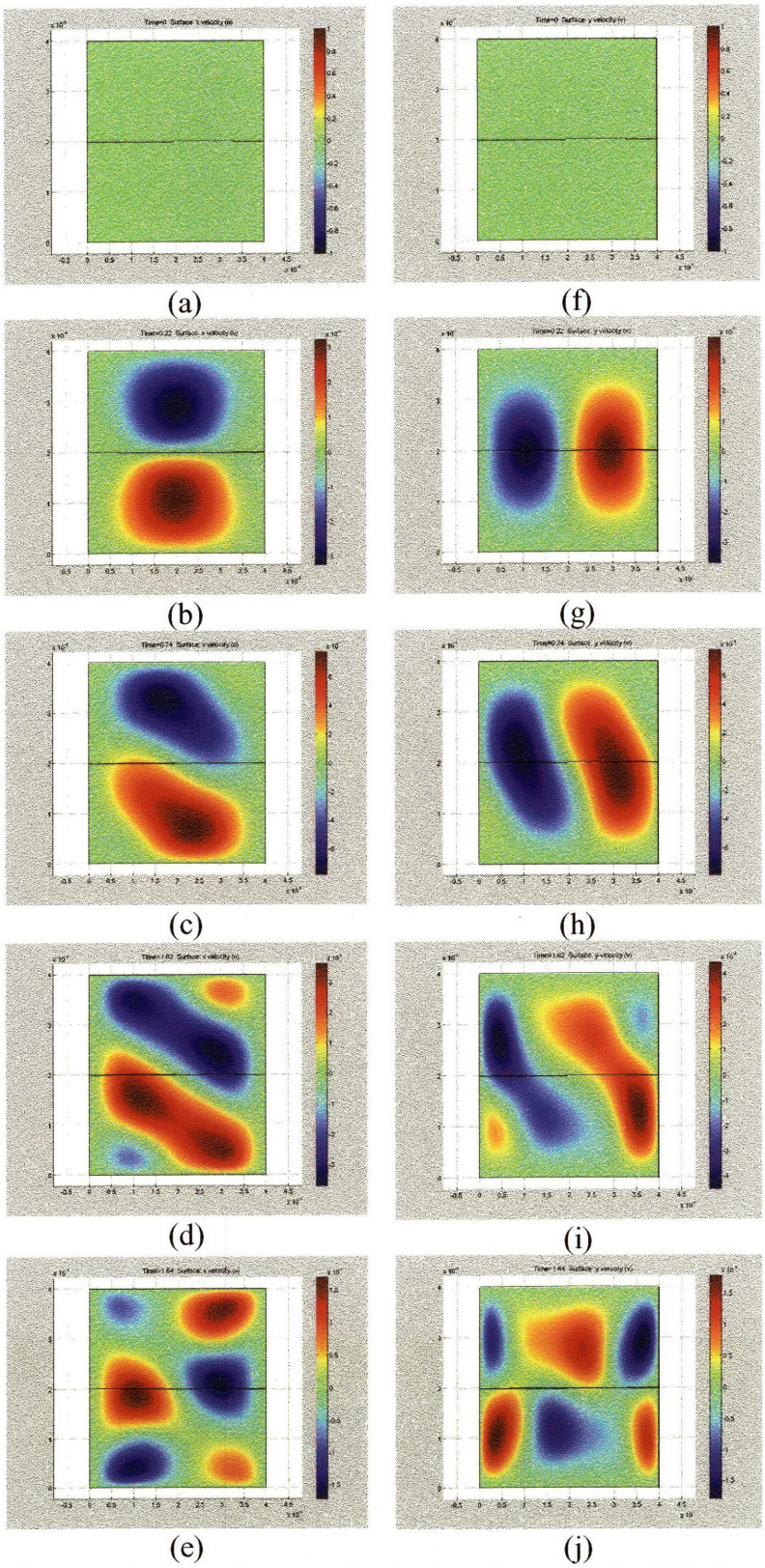

Figure 7-7. Time evolution of u, panels (a-e) and v, panels (f-j) for the superposed orientation.

Plots for the total velocity $U = \sqrt{u^2 + v^2}$ and the concentration C, for the sideways orientation (Figures 7-8 & 7-9) and the superposed orientation (Figures. 7-10 & 7-11) with time, show this decay and the recirculatory nature of the velocity field induced.

An interesting effect observed from the velocity fields is pockets or regions with high velocity emerging close to the wall after the velocity field in the bulk of liquid has decayed. In effect migration of the region with the highest velocity towards the wall is observed. We rationalize this effect: at initial times whereas liquid in the channel away from the wall is strongly affected by the buoyancy force, and have strong induced velocity, the no-slip boundary condition implies that the liquid at the walls remains at rest and there exists a velocity gradient from the bulk to the wall. Thus the liquid away from the wall moves much faster towards the bottom/top of the channel depending on its density, while the liquid sticking at the walls moves slowly and sustains density gradients resisting buoyancy. These density gradients induce velocities that become substantial after velocity in the bulk liquid has decayed, Figure 7-7(e-f) and Fig. 7-9(e-f). There is more liquid sticking to the walls for the superposed configuration than for the sideways one and consequently the observed effect greater for the former.

The viscosity (μ), density difference ($\Delta\rho$), and the length scale L, are identified as critical parameters from the dimensionless analysis. The dependence of Ra number on the length scale is much stronger ($Ra \propto L^3$), than the dependence on viscosity or density difference, $Ra \propto \Delta\rho / \mu$. As a result, when the length scale is reduced to half for studying the dependence of velocity and critical time scales on length scale of the system, the relative importance of the diffusive effects increases 8 fold and diffusion becomes important. We decouple this effect by reducing the diffusivity proportionately here and

discuss the case with the unadjusted diffusivity later. Then, the essential nature of the spatial distribution of the total-velocity U, and its time evolution remains the same with changes in liquid viscosity (Figures 7-12 & 7-13), density difference (Figures 7-14 & 7-15) and the length scale (Figures 7-16 & 7-17) with respect to the base case of μ=*1e-3*, $\Delta\rho/\rho$=*0.1*, *L=400* μ*m*, for both orientations. However, we see that the maximum velocity induced in the system and the time required for the induced velocity fields to decay *are* affected by these parameters.

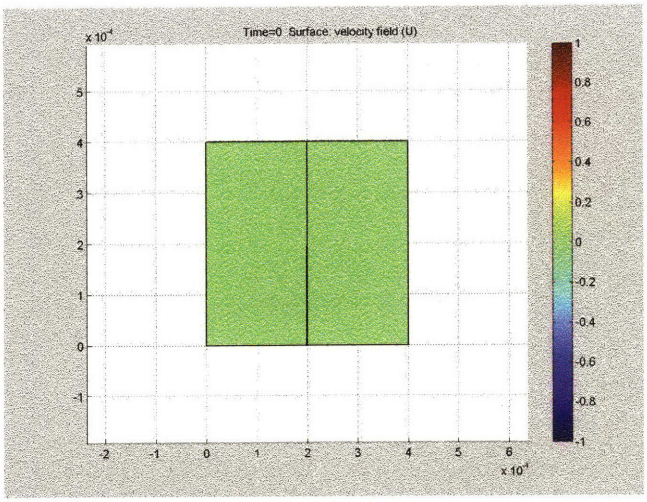

(a)

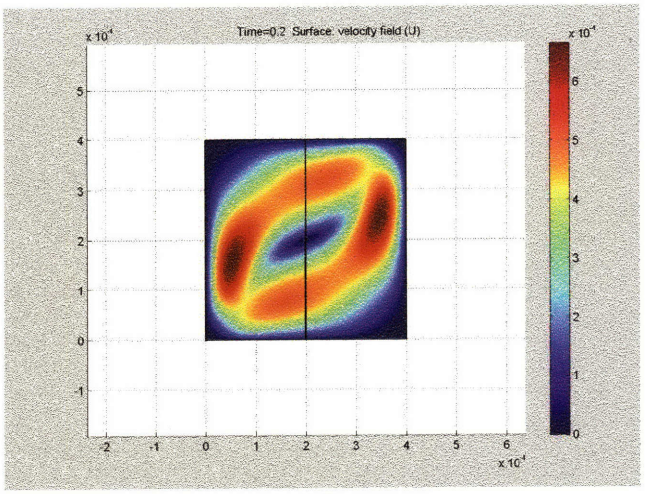

(d)

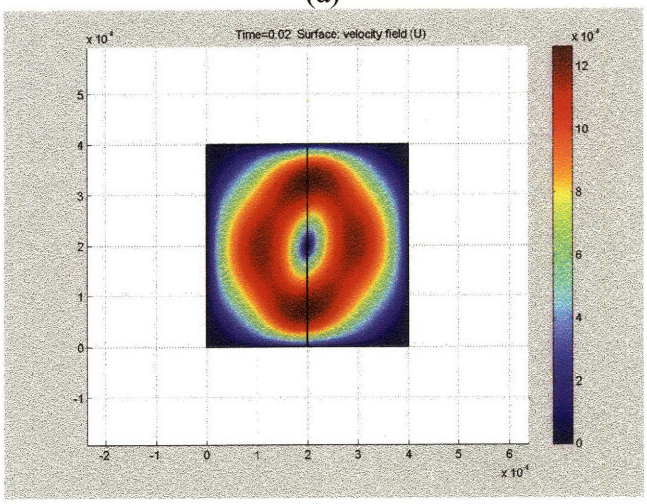

(b)

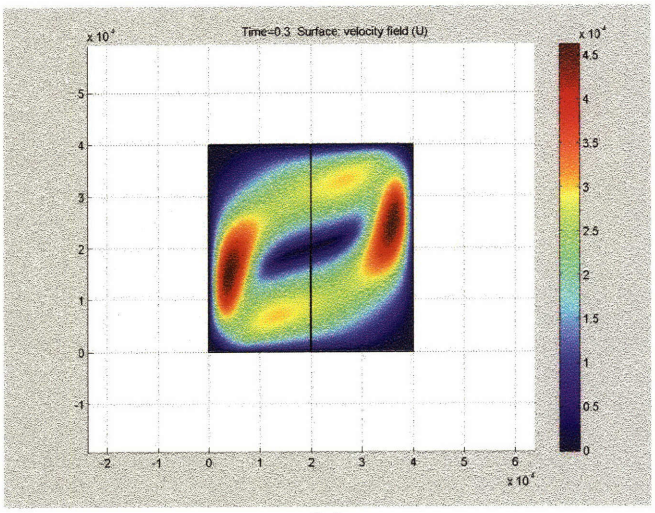

(e)

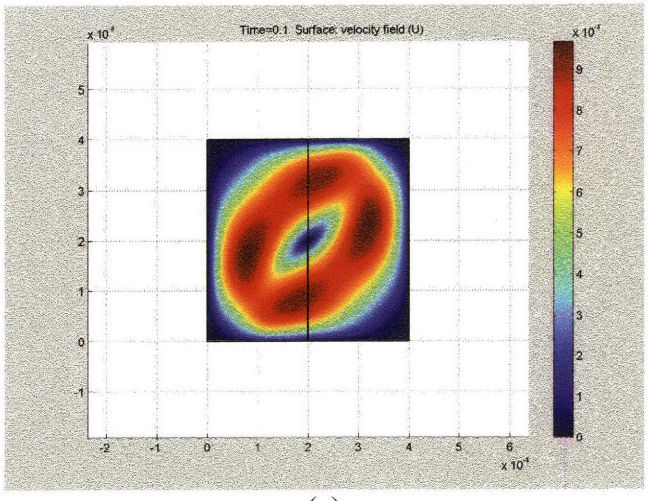

(c)

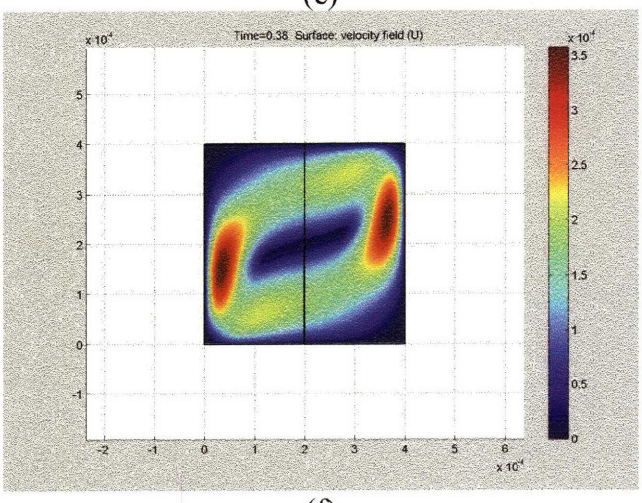

(f)

Figure 7-8. Time evolution of the total velocity *U*, for sideways configuration.

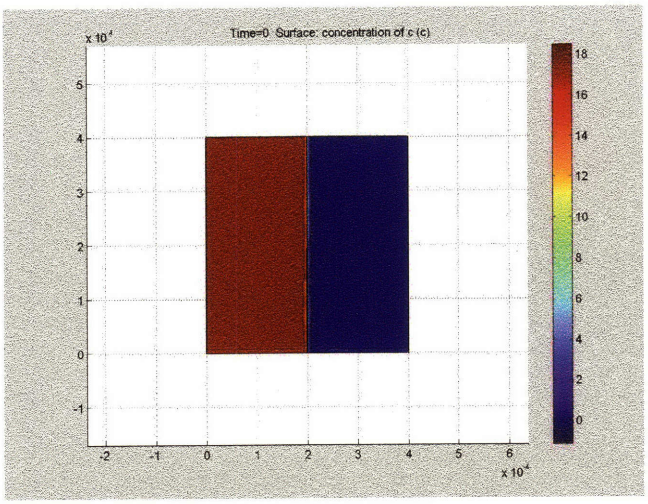

(a)

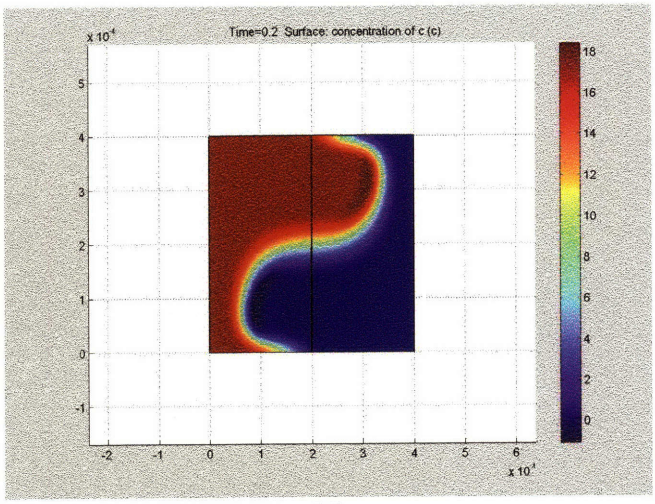

(d)

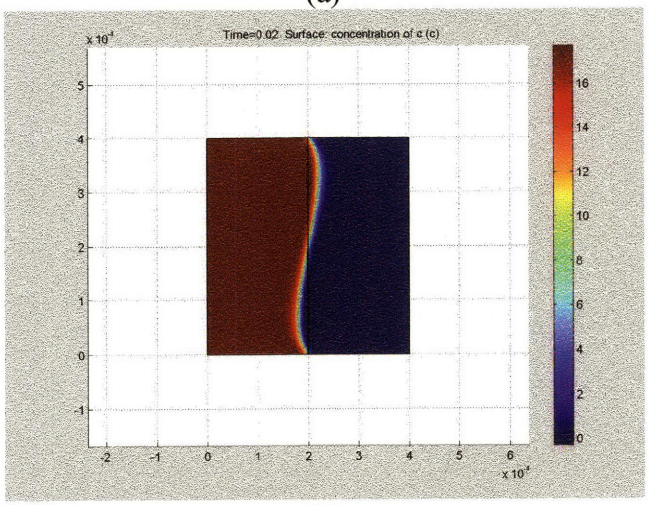

(b)

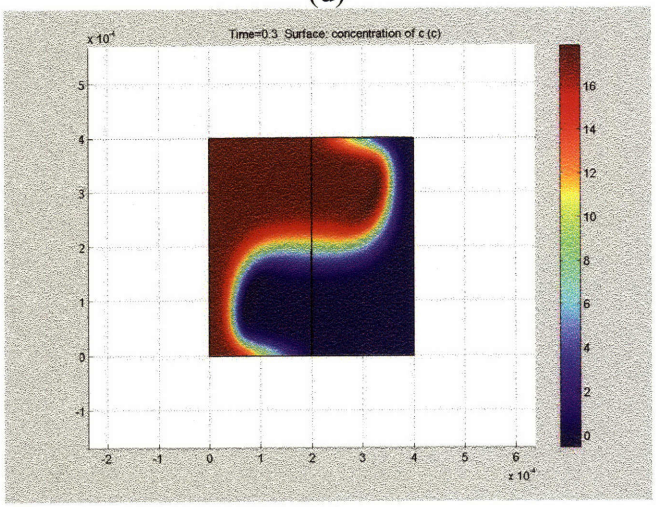

(e)

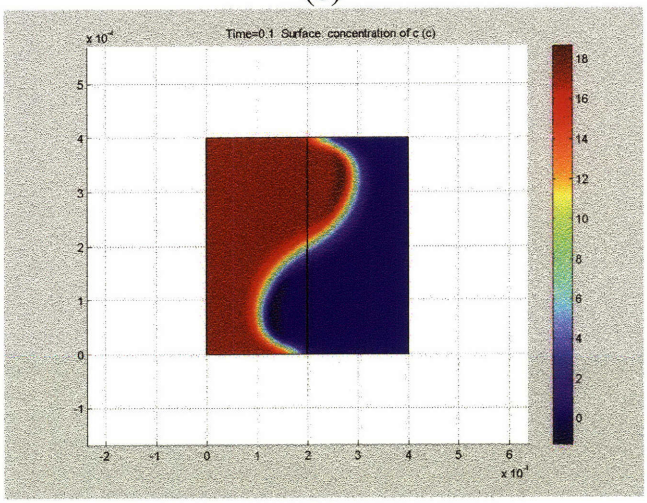

(c)

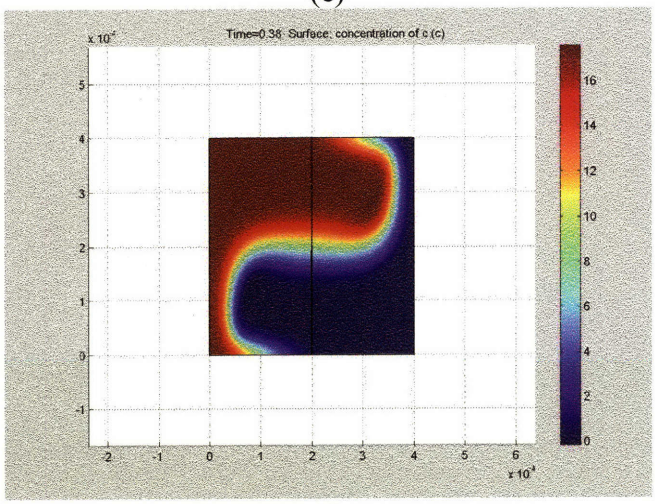

(f)

Figure 7-9. Time evolution of the concentration *C* for sideways configuration.

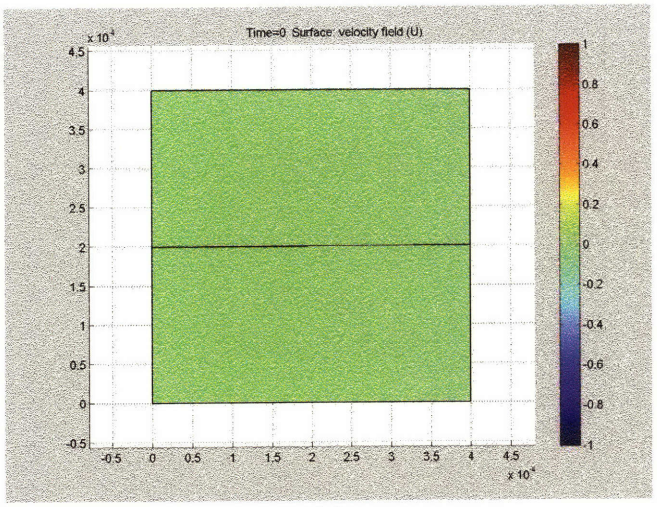

(a)

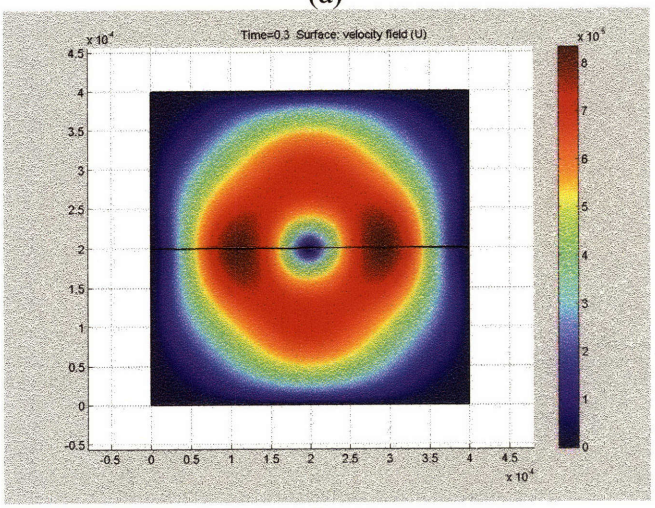

(b)

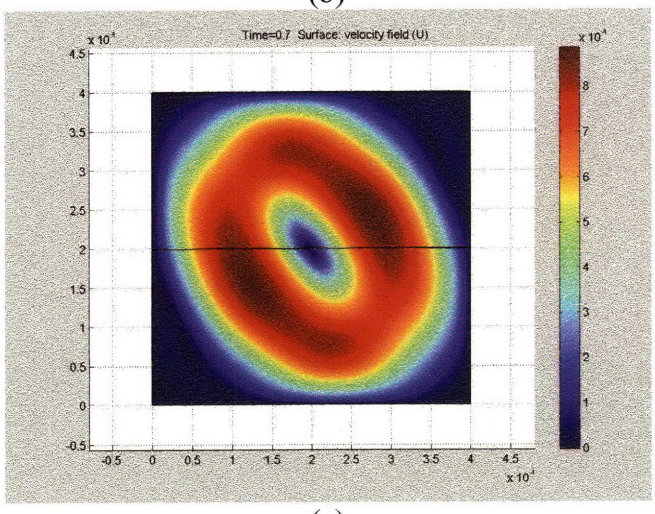

(c)

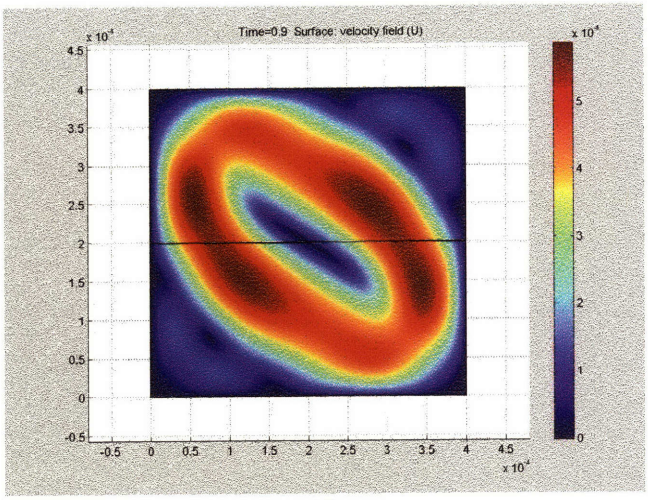

(f)

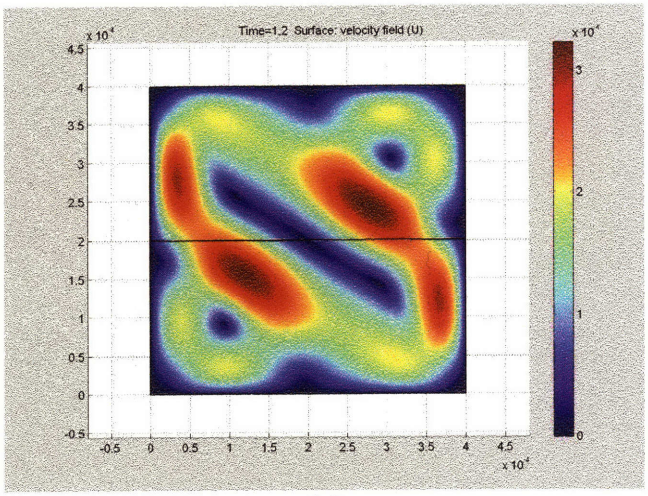

(g)

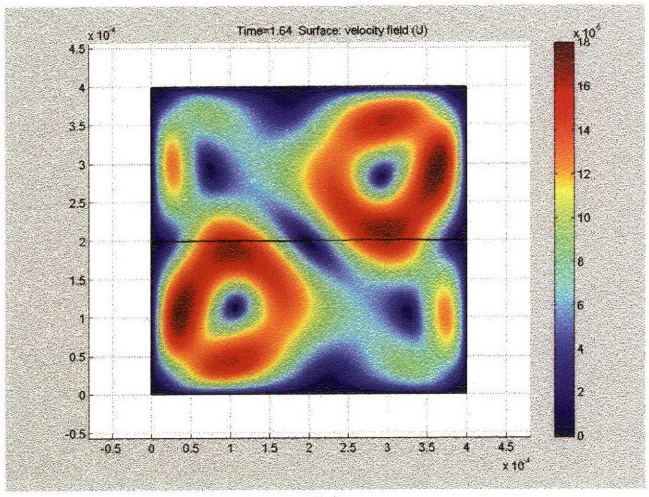

(h)

Figure 7-10. Time evolution of the total velocity U, for superposed configuration.

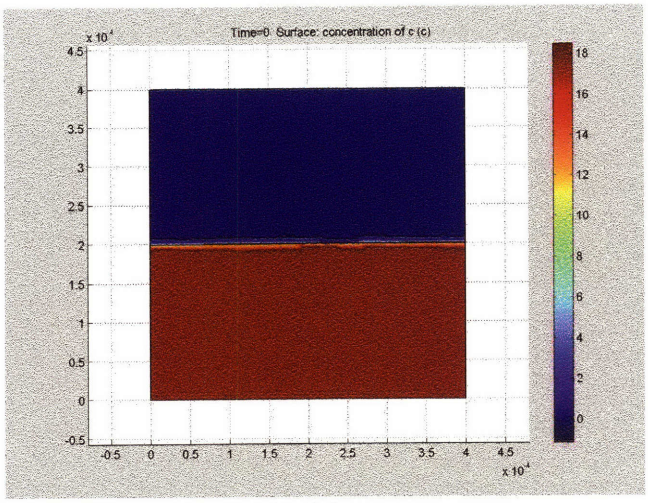

(a)

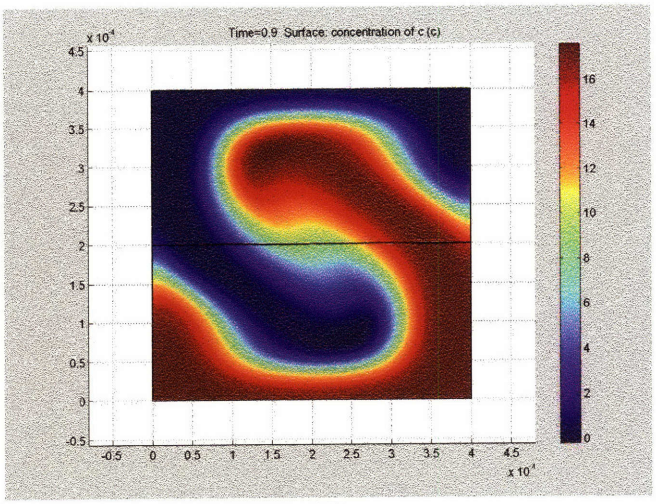

(d)

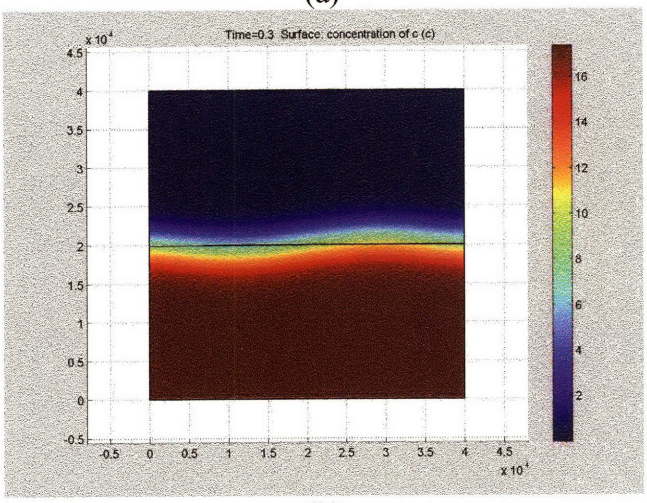

(b)

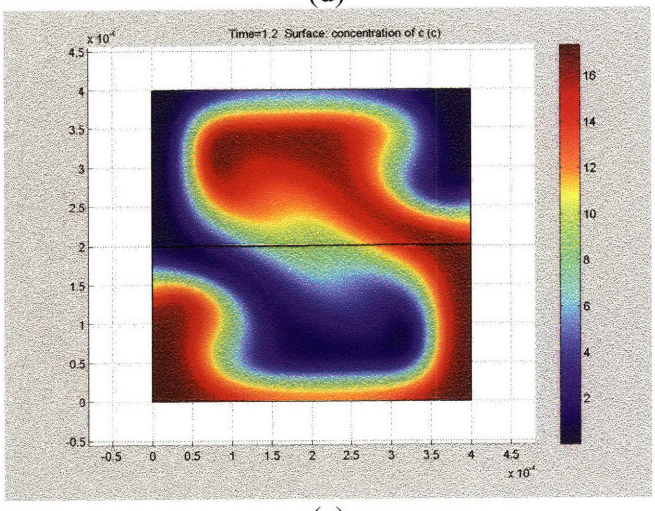

(e)

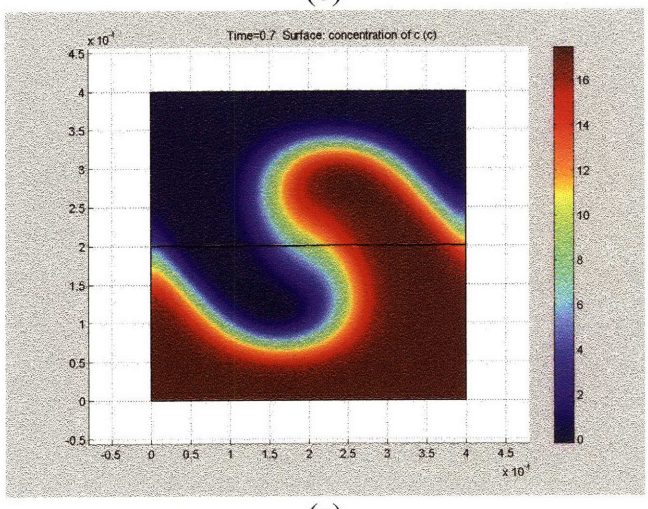

(c)

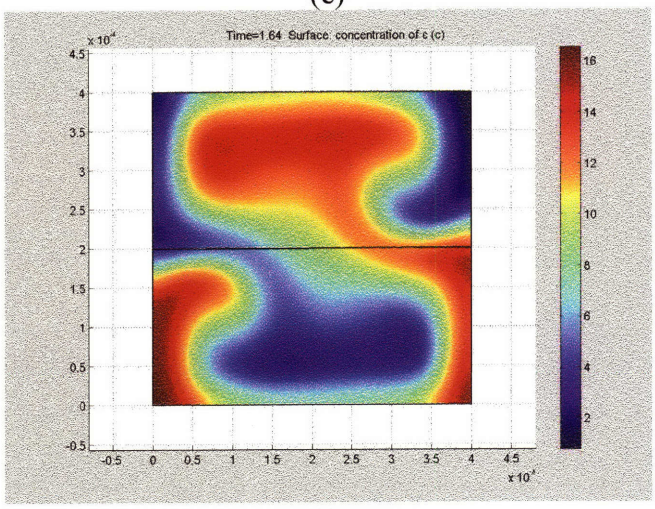

(f)

Figure 7-11. Time evolution of concentration *C* for superposed configuration.

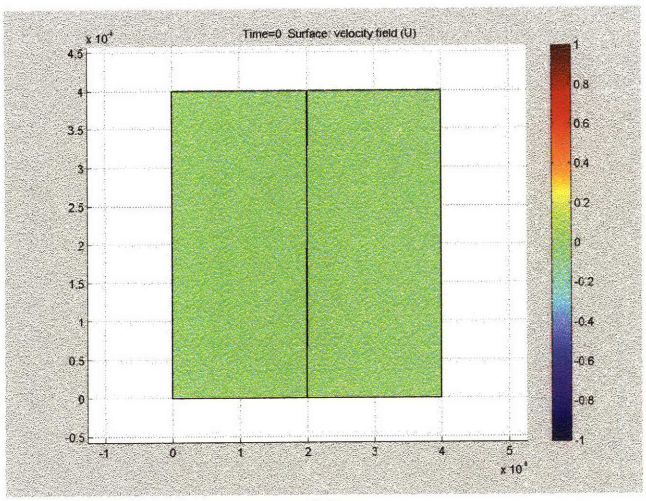

(a)

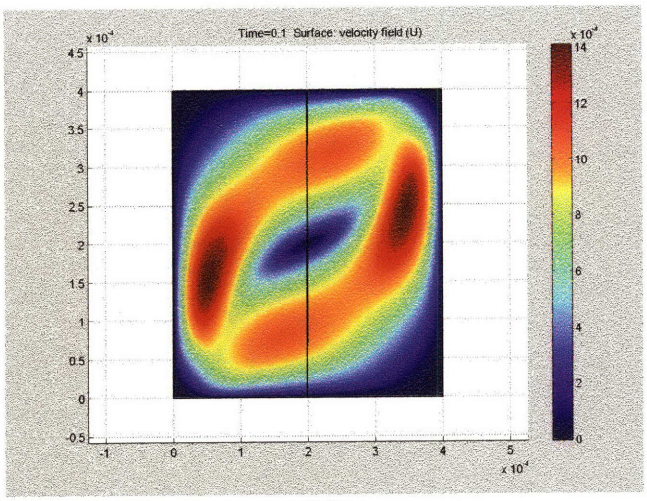

(d)

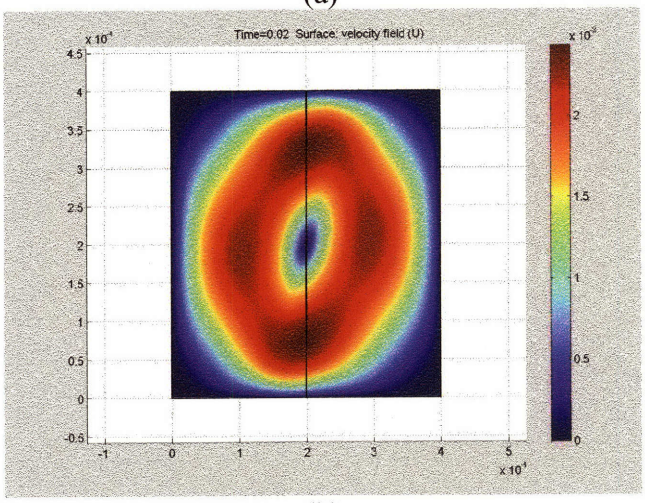

(b)

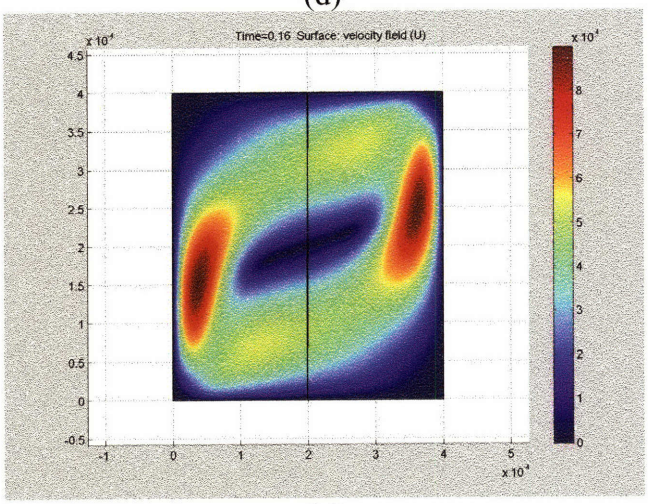

(e)

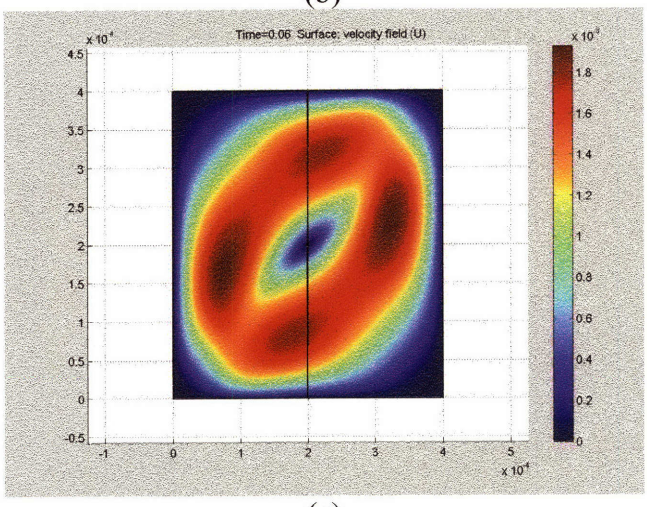

(c)

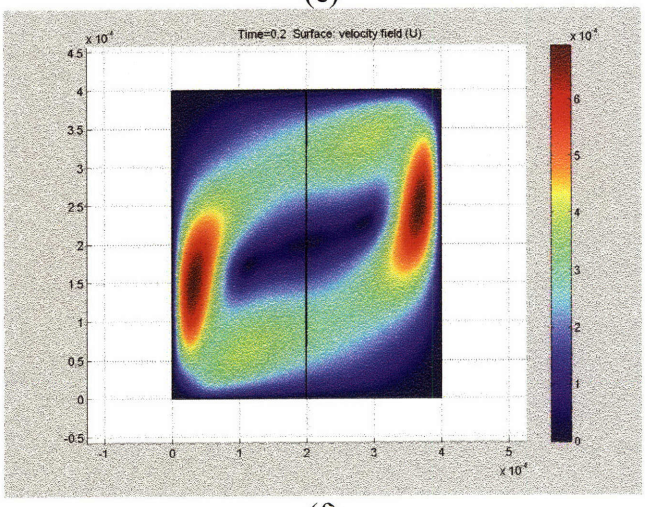

(f)

Figure 7-12. Time evolution of the total velocity U for sideways configuration when liquid viscosity, $\mu = \frac{1}{2}(\mu_{base\ case})$.

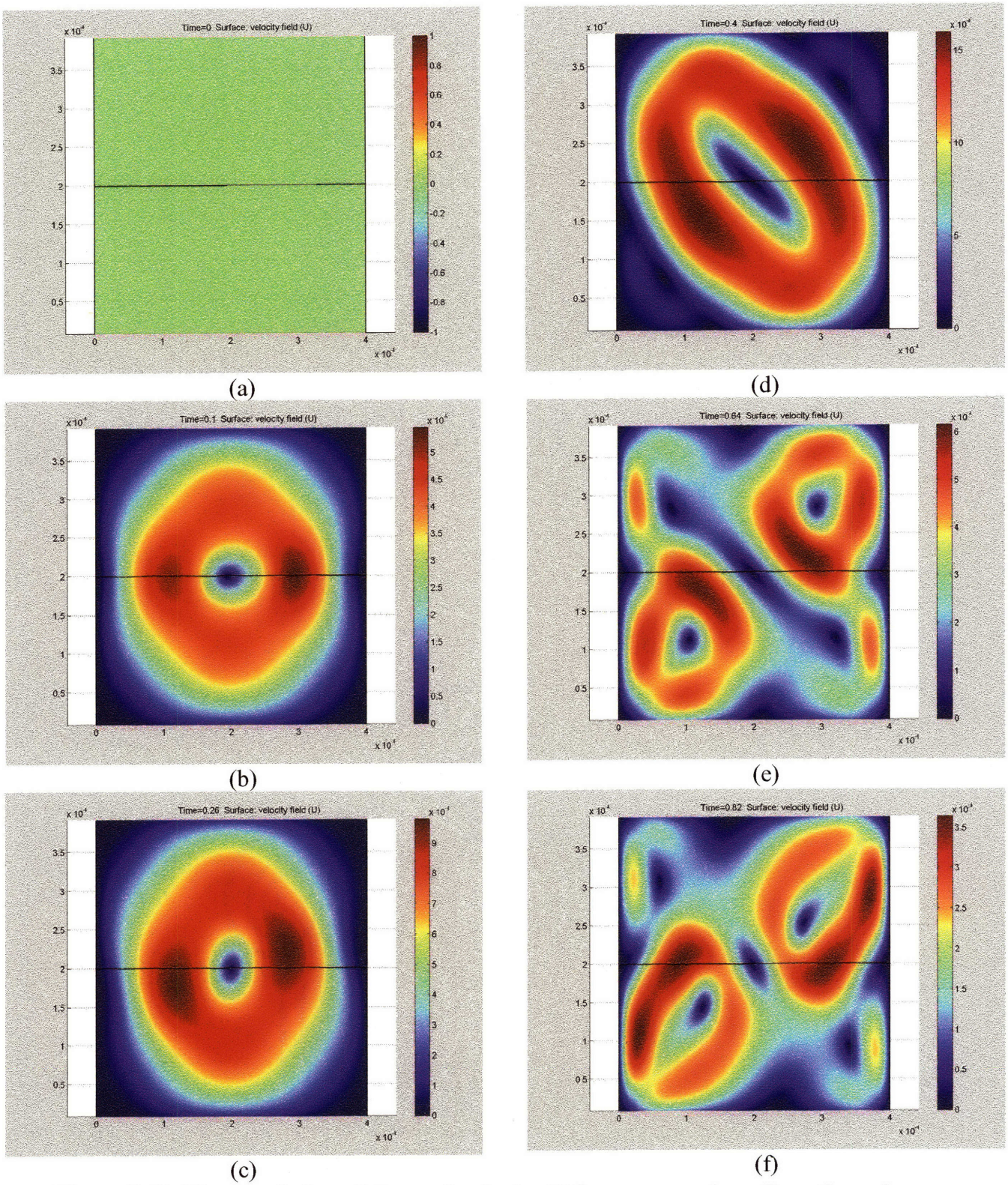

Figure 7-13. Time evolution of the total velocity U for superposed configuration when liquid viscosity, $\mu = \frac{1}{2}(\mu_{base\ case})$.

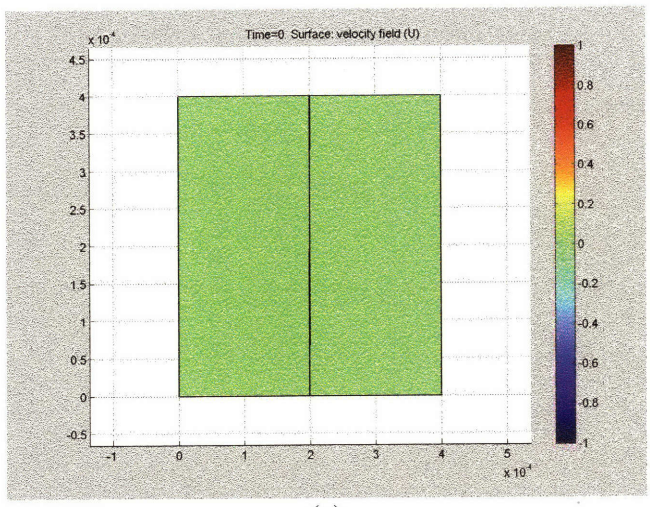

(a)

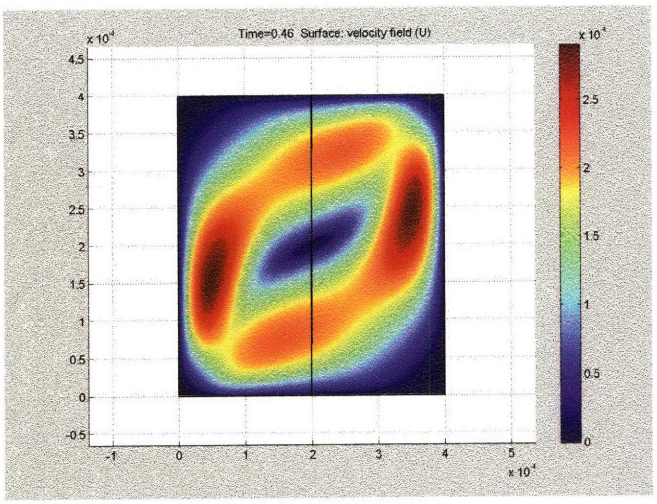

(d)

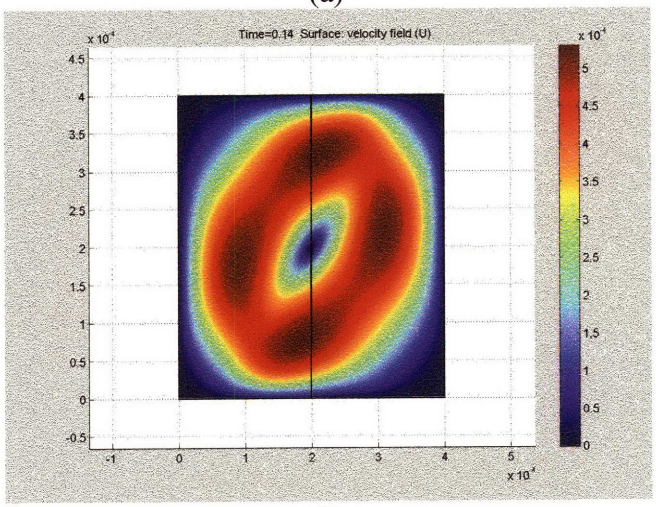

(b)

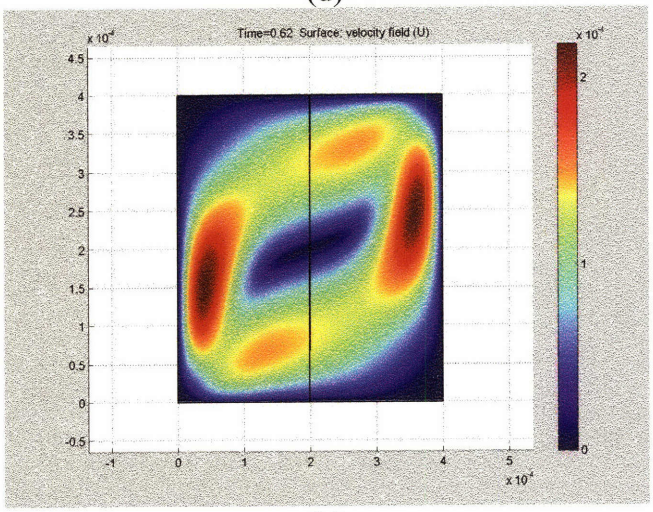

(e)

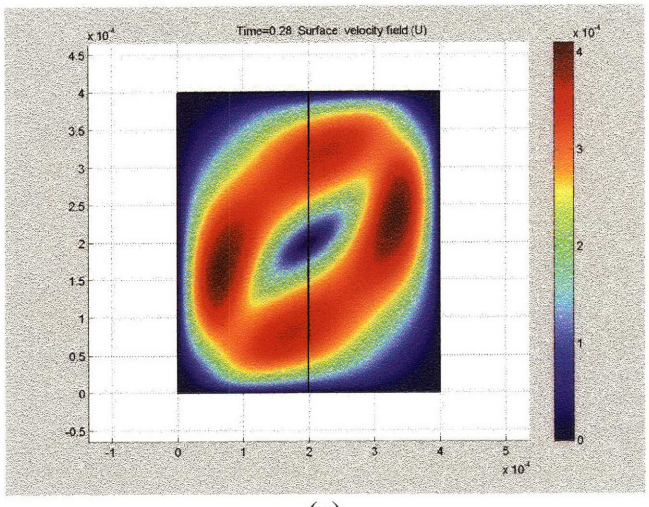

(c)

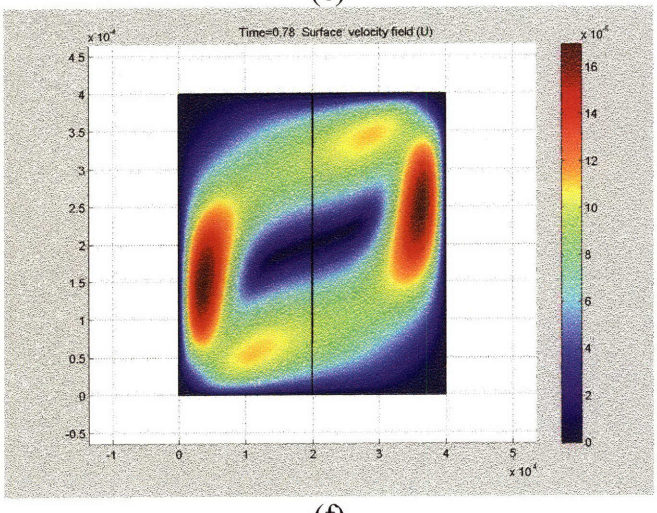

(f)

Figure 7-14. Time evolution of the total velocity U for sideways configuration when the density difference $\Delta\rho=\frac{1}{2}(\Delta\rho_{base\ case})$.

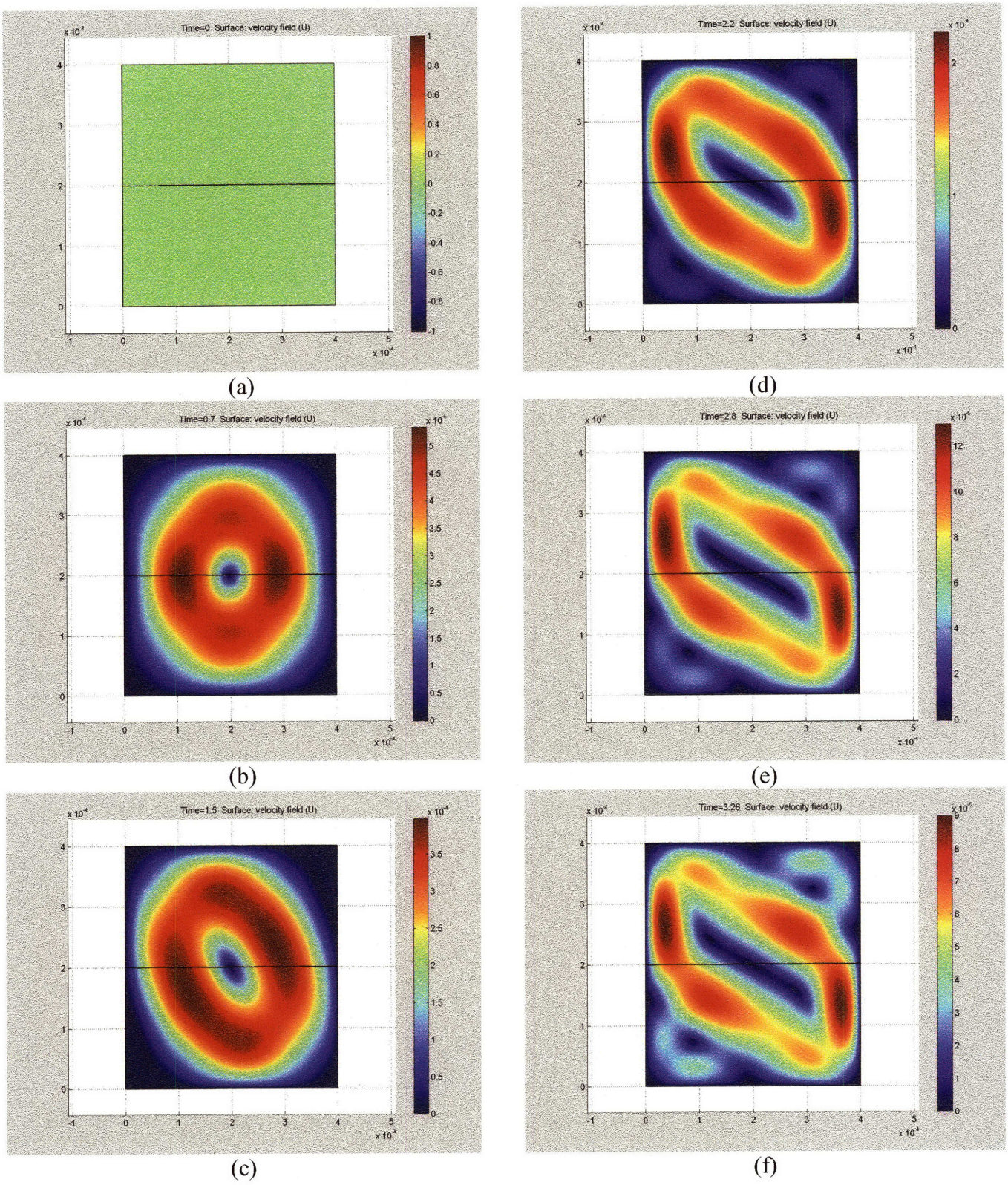

Figure 7-15. Time evolution of the total velocity U for superposed configuration when the density difference $\Delta\rho = \frac{1}{2}(\Delta\rho_{base\ case})$.

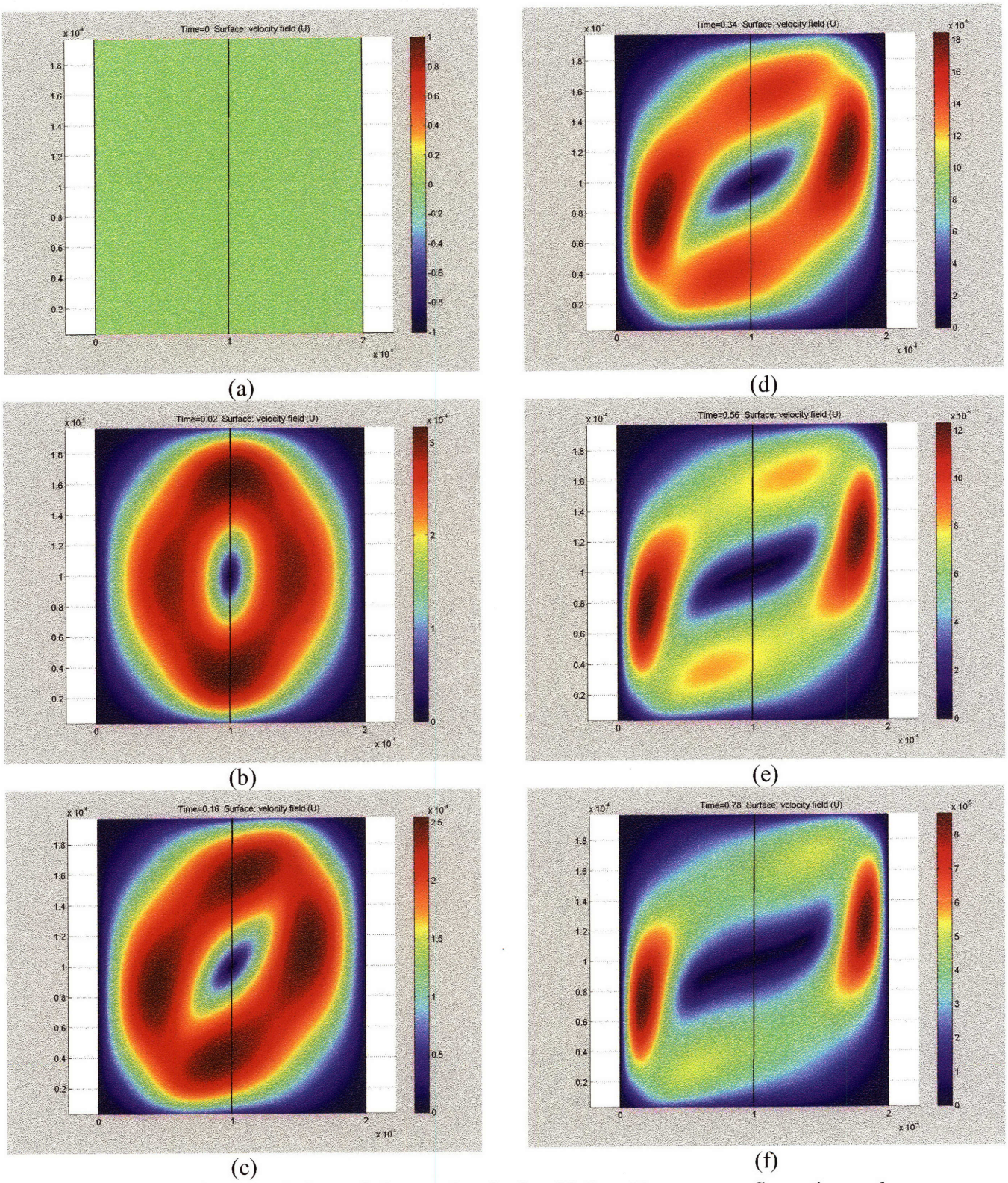

Figure 7-16. Time evolution of the total velocity U for sideways configuration, when Length scale is half of the base case, cross-section = $200X200\mu m$, and diffusivity adjusted so that the Rayleigh number is unchanged

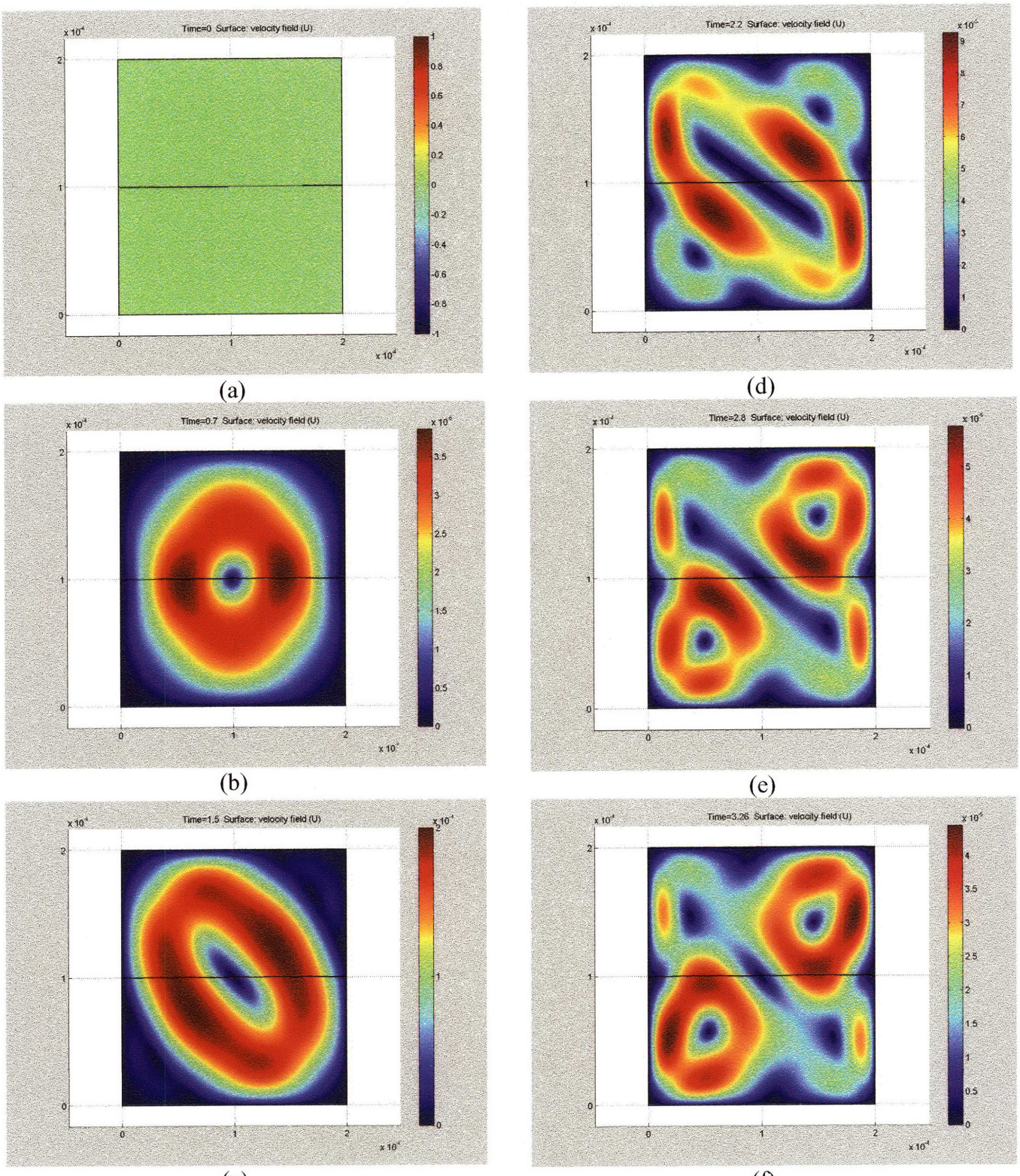

Figure 7-17. Time evolution of the total velocity U for superposed configuration, when length scale is half of the base case, cross-section = *200X200μm,* and diffusivity adjusted so that the Rayleigh number is unchanged.

We calculate an average, $\bar{U}$, of the total velocity U over the cross-section and plot its time evolution to estimate the effect of viscosity, density difference and length scale. Figure 7-18 shows such a time evolution comparing the relative effects of these variables, for a vertical (sideways) configuration. Figure 7-19 shows the same for the superposed configuration.

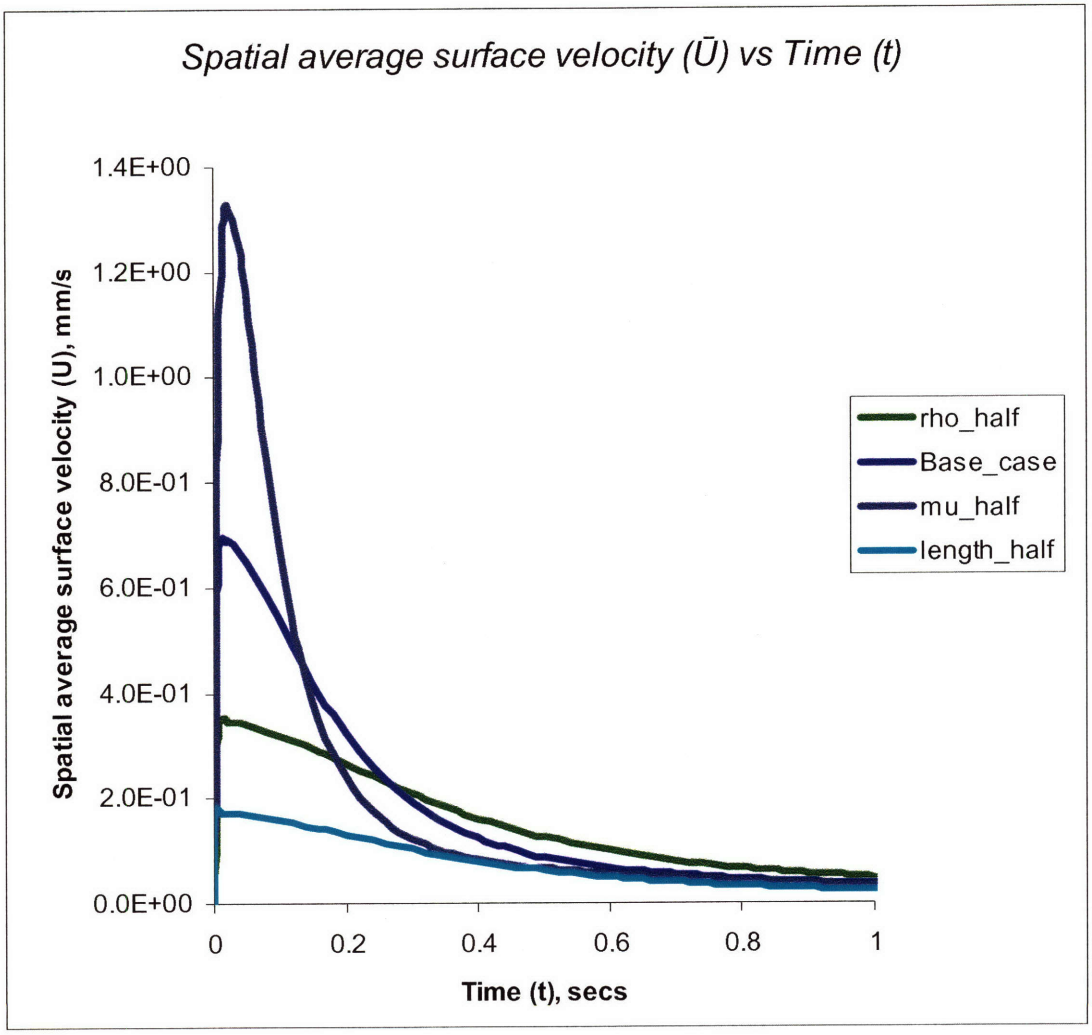

Figure 7-18. Evolution with time of the induced surface average velocity for the sideways configuration, for different density difference, viscosity and length scale, comparing the effect of these parameters.

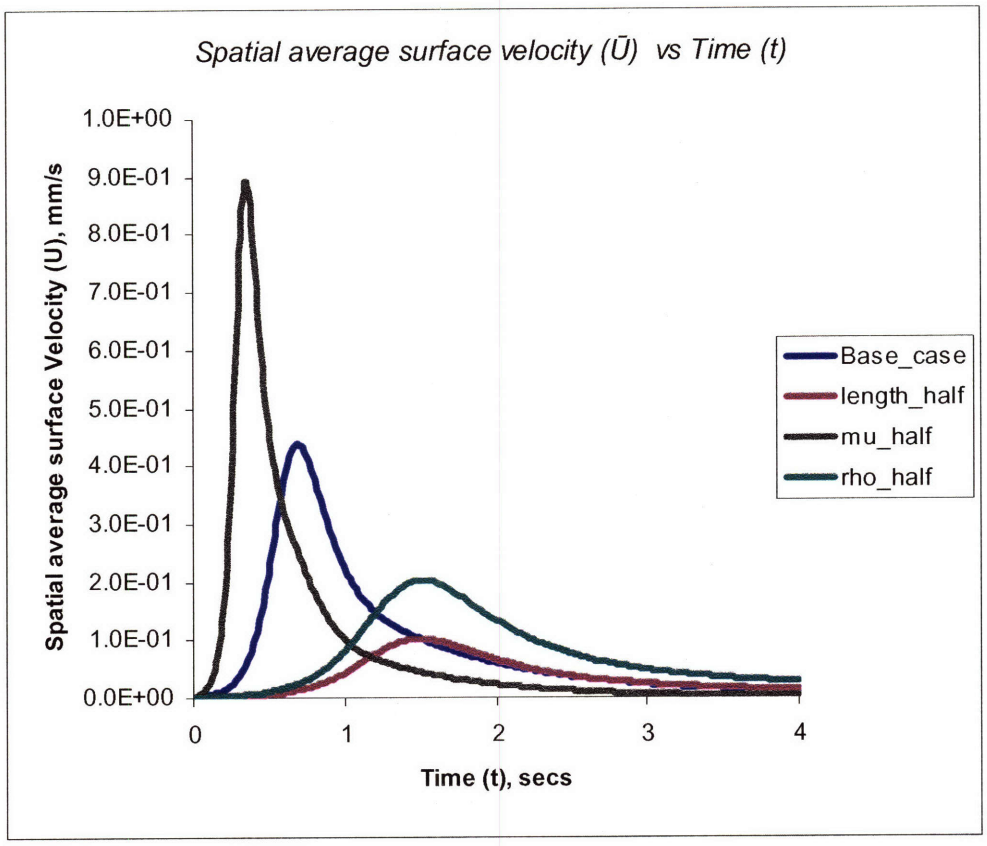

Figure 7-19. Evolution with time of the induced surface average velocity for the superposed configuration, for different density difference, viscosity and length scale, comparing the effect of these parameters.

We define the time required for this surface average velocity to decay by 80% of its original value, $\tau_{80\%}$ as a parameter for comparing the time for reorientation of the liquids. We have shown that the velocity fields are induced because of unstable orientation in the gravitational field and decay as the orientation of liquids to a gravitationally stable configuration progresses. The above choice for estimation and comparison of the time for reorientation is then a physically correct one. Note that even after the reorientation is completed substantial concentration gradients exist and diffusion continues. As a result, this method of calculating the time for reorientation is correct only if diffusion velocity is much smaller than convection velocity (or the diffusion time scale is much larger than the time scale for reorientation), as is indeed the case. The

comparison of the time scale for reorientation and the maximum velocity attained show dependence on the parameters as derived from the dimensionless analysis and are of the same order as the experimentally observed time scales for reorientation of streams.

The maximum velocity and the time for reorientation for different cases are tabulated below for comparison:

	Sideways configuration U_{max} (mm/s)	$\tau_{80\%}$ (secs.)	Sideways configuration U_{max} (mm/s)	$\tau_{80\%}$ (secs.)
Base case	0.69	0.38	0.44	1.64
$\mu=1/2(\mu_{base\ case})$	1.34	0.19	0.89	0.82
$\Delta\rho=1/2(\Delta\rho_{base\ case})$	0.35	0.76	0.21	3.26
$L=1/2(L_{base\ case})$	0.18	0.76	0.11	3.26

The time required for the average surface velocity to reach the maximum in case of the sideways orientation is substantially smaller than in the case of superposed orientation. We use a small initial tilt (angle of tilt << total angular orientation required for stabilization of the liquids in the gravitational field), for the definition of boundary between liquids as the initial perturbation and see that as long as this above condition for choosing the angle of tilt is satisfied, it does not have noticeable effects on the time evolution of the concentration and velocity fields. The sideways orientation can be thought of as a case of superposed orientation with a large perturbation (angle of tilt ~ 90°) for the definition of initial boundary between liquids. Then the maximum effect of gravitational instability (as measured by the maximum of the spatial average velocity), can be seen much faster.

7.4.3. Effect of diffusion on the gravitational instability

The Rayleigh number is the ratio of the diffusive time constant and the time for reorientation for the streams. Thus when *Ra* is small the diffusion is fast and the density gradients are removed before the streams can completely reorient. For large *Ra* the reorientation of streams is much faster than diffusive mixing.

The Rayleigh number being most sensitive to the length scale we studied the effect of change in length scale on the time and velocity scales. Figures 7-20 & 7-21 show the induced velocity fields and the concentration profile for the sideways configuration, when the length scale is reduced by a factor of 2, to $L = 200\ \mu m$, from $L = 400\ \mu m$ of the base case, and the diffusivity unadjusted, so that the *Ra* number is reduced by a factor of 8. It is seen that although the concentration profile becomes more diffused and the initial boundary smooth, the nature of velocity field decay remains the same. Moreover, as for the base case, here too substantial reorientation of the liquid takes place. The time evolution of the spatial average velocity for this case is compared with the case where diffusivity is adjusted to maintain a constant *Ra* number, Figure 7-22, showing little difference between the two cases.

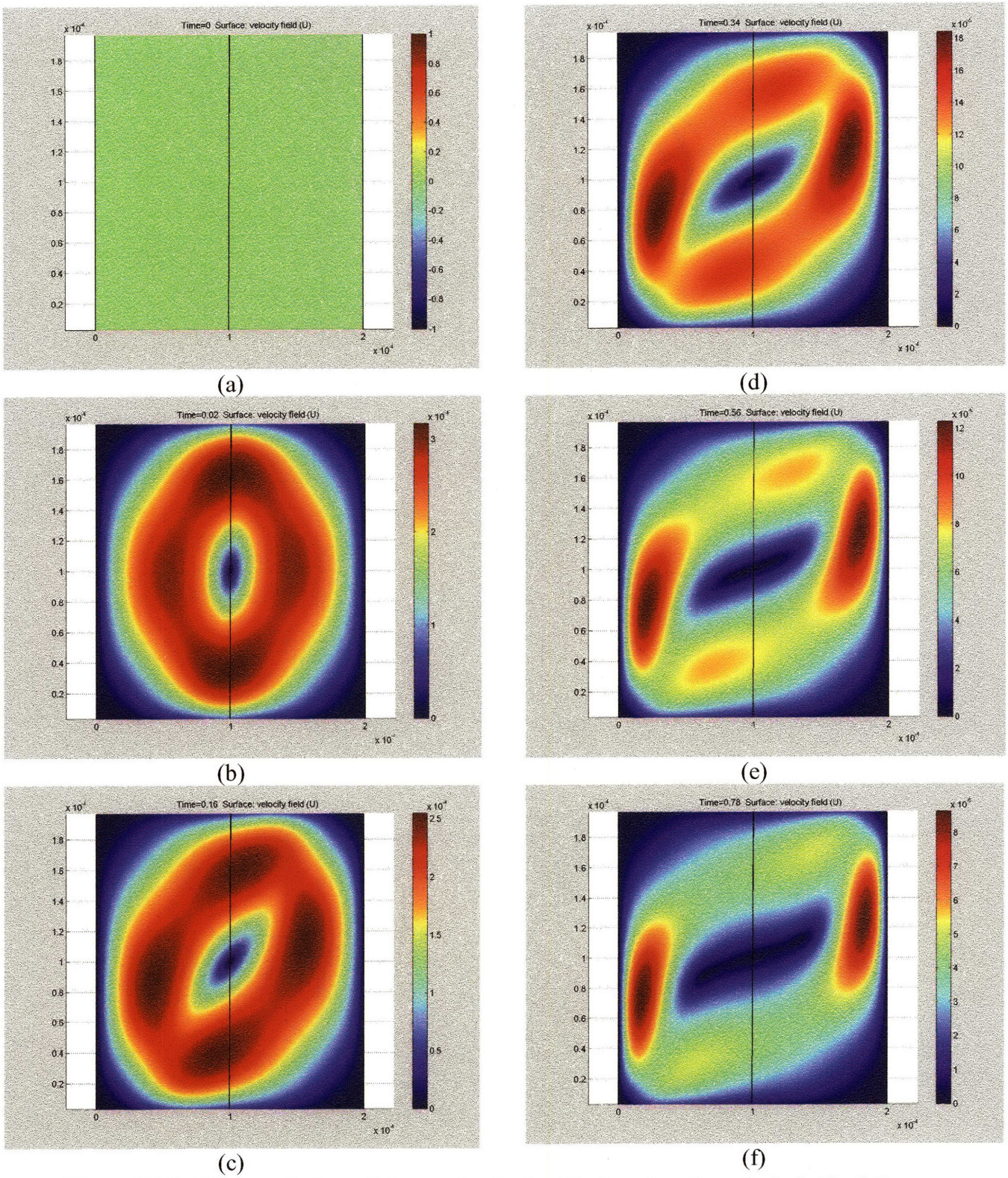

Figure 7-20. Time evolution of the total velocity U when length scale is half of the base case, cross-section = $200X200\mu m$, so that $Ra = 1/8(Ra_{base\ case})$, for sideways configuration.

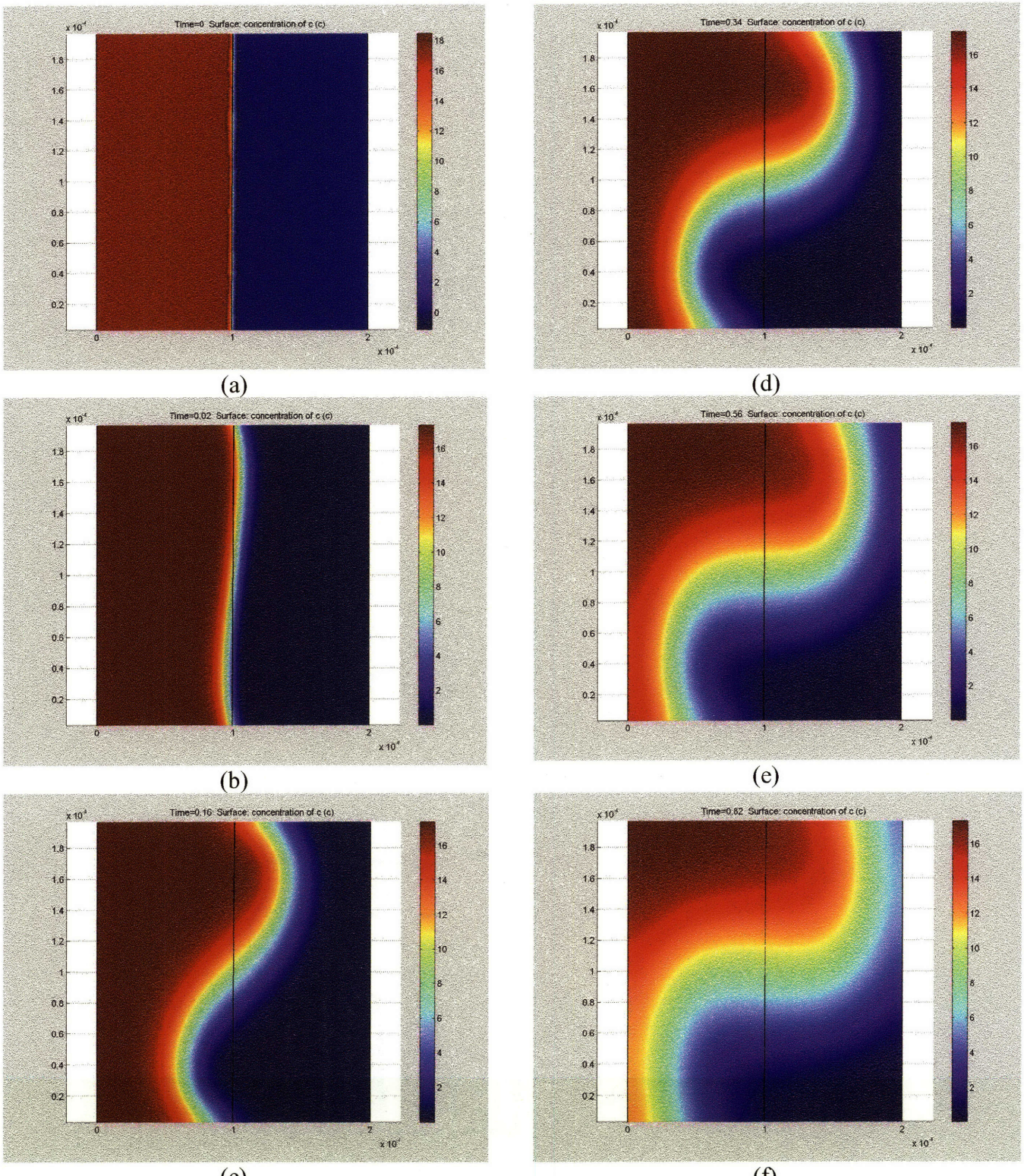

Figure 7-21. Time evolution of the concentration *C,* when length scale is half of the base case, cross-section = *200X200μm*, so that *Ra = 1/8($Ra_{base\ case}$)*, for superposed configuration.

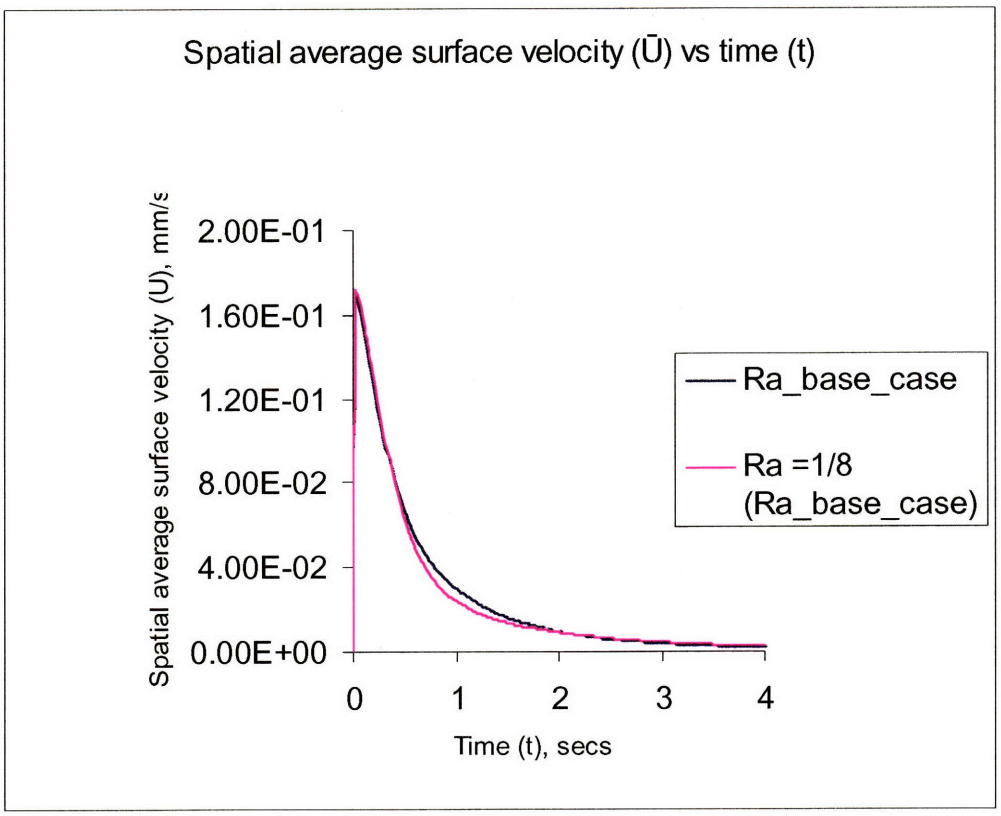

Figure 7-22. The effect of the change in diffusivity on the evolution with time of surface average velocity for the sideways configuration, cross-section *200μmX200μm.*

For the case of superposed orientation the observed effect is more substantial. For this orientation the velocity field takes a much longer time to reach a maximum than for the sideways orientation. This fact coupled with a higher relative importance of diffusion, changes the time evolution of the velocity field considerably, (Figure 7-23). Figures 7-24 & 7-25 show the velocity and concentration fields for this case. For the superposed orientation there is more liquid sticking to the walls than in the sideways orientation. This also leads to a higher component of the diffusive velocity component in the spatial average velocity, once most of the reorientation has been completed or the gradients have died out. Decreasing the *Ra* number affects the concentration profiles, more so for the superposed orientation than for the sideways orientation.

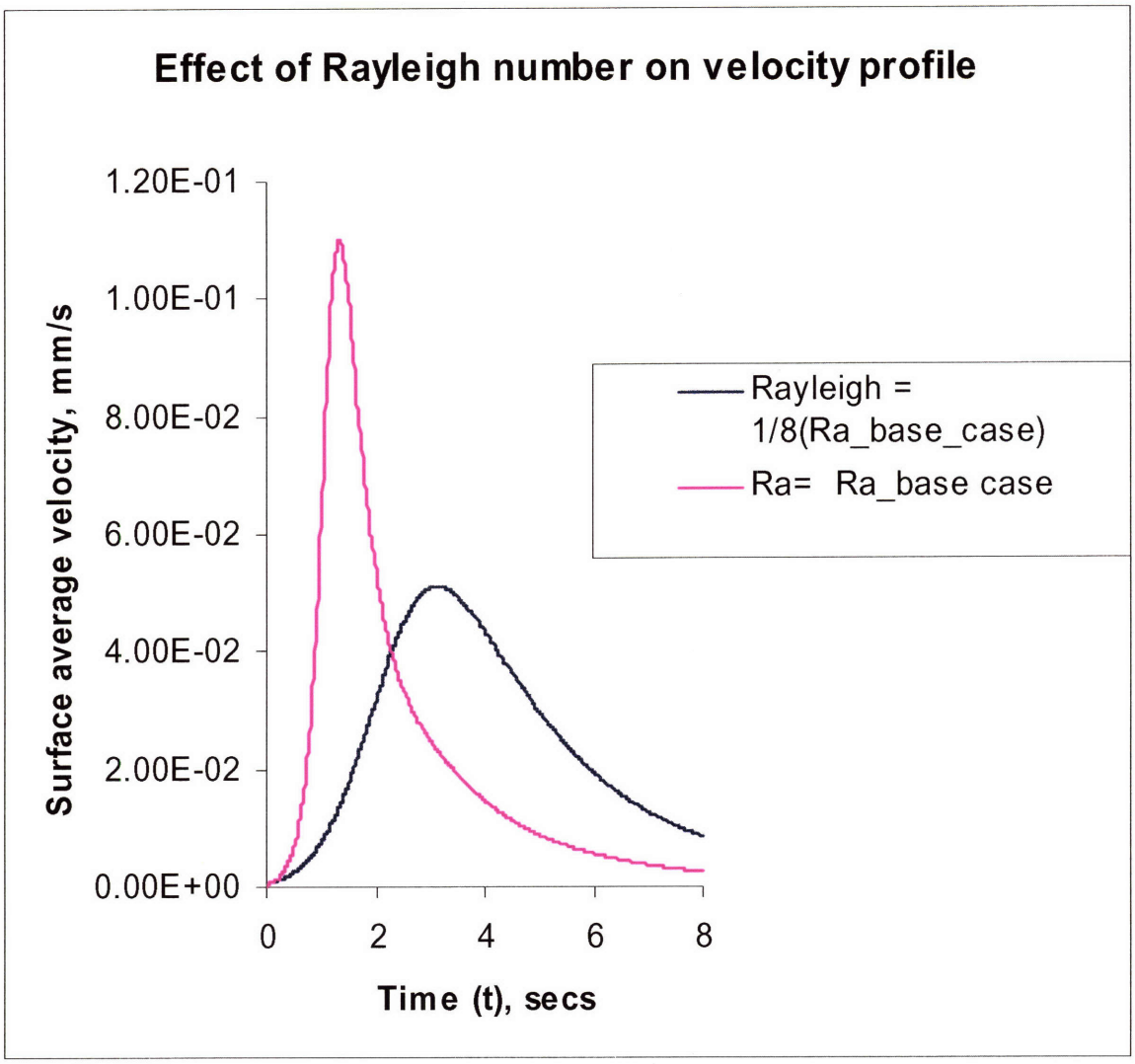

Figure 7-23. The effect of the change in Rayleigh number on the evolution with time of surface average velocity for the superposed configuration, cross-section *200μmX200μm*

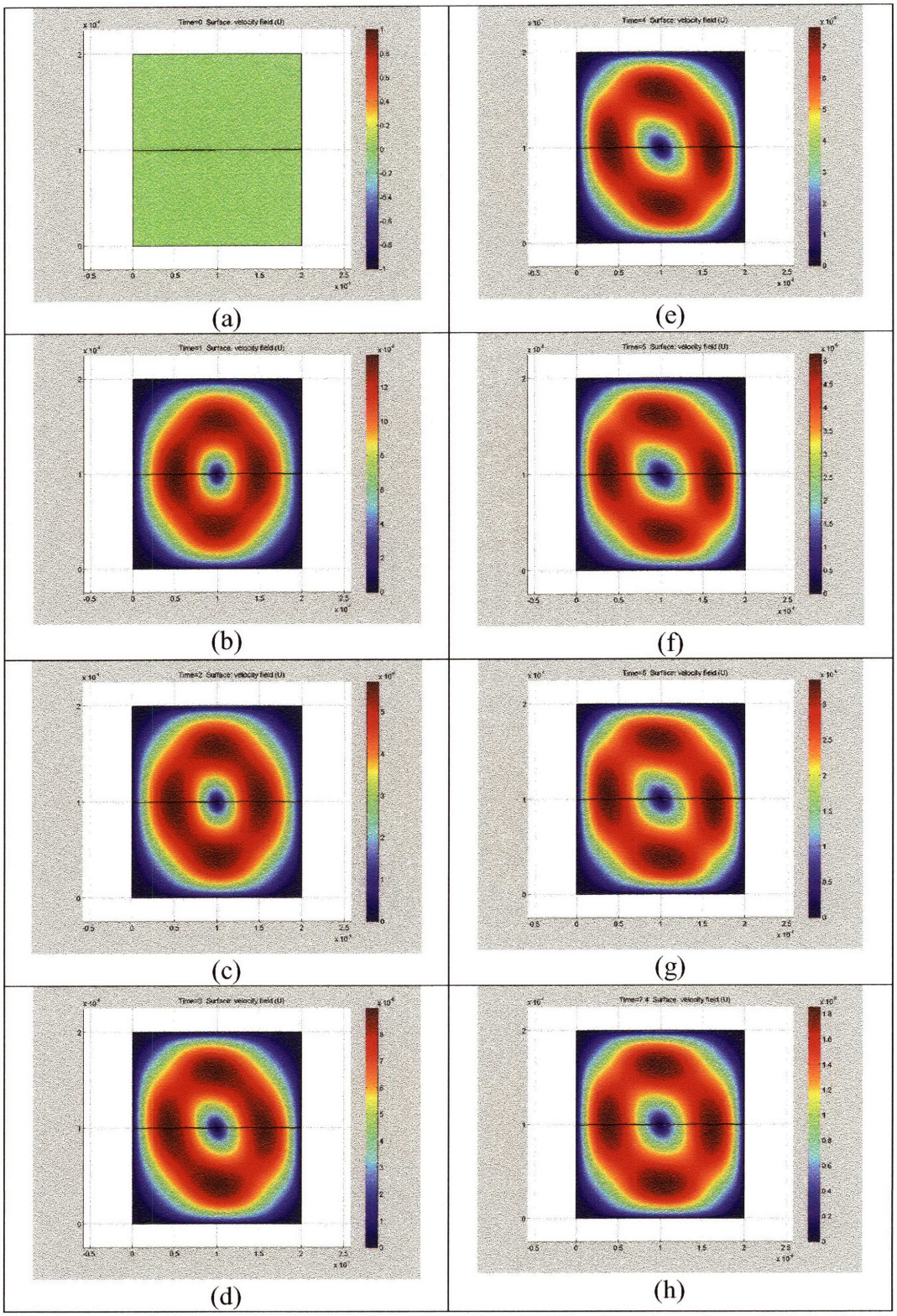

Figure 7-24. Time evolution of the total velocity U when length scale is half of the base case, cross-section = $200X200\mu m$, so that $Ra = 1/8(Ra_{base\ case})$, for superposed configuration.

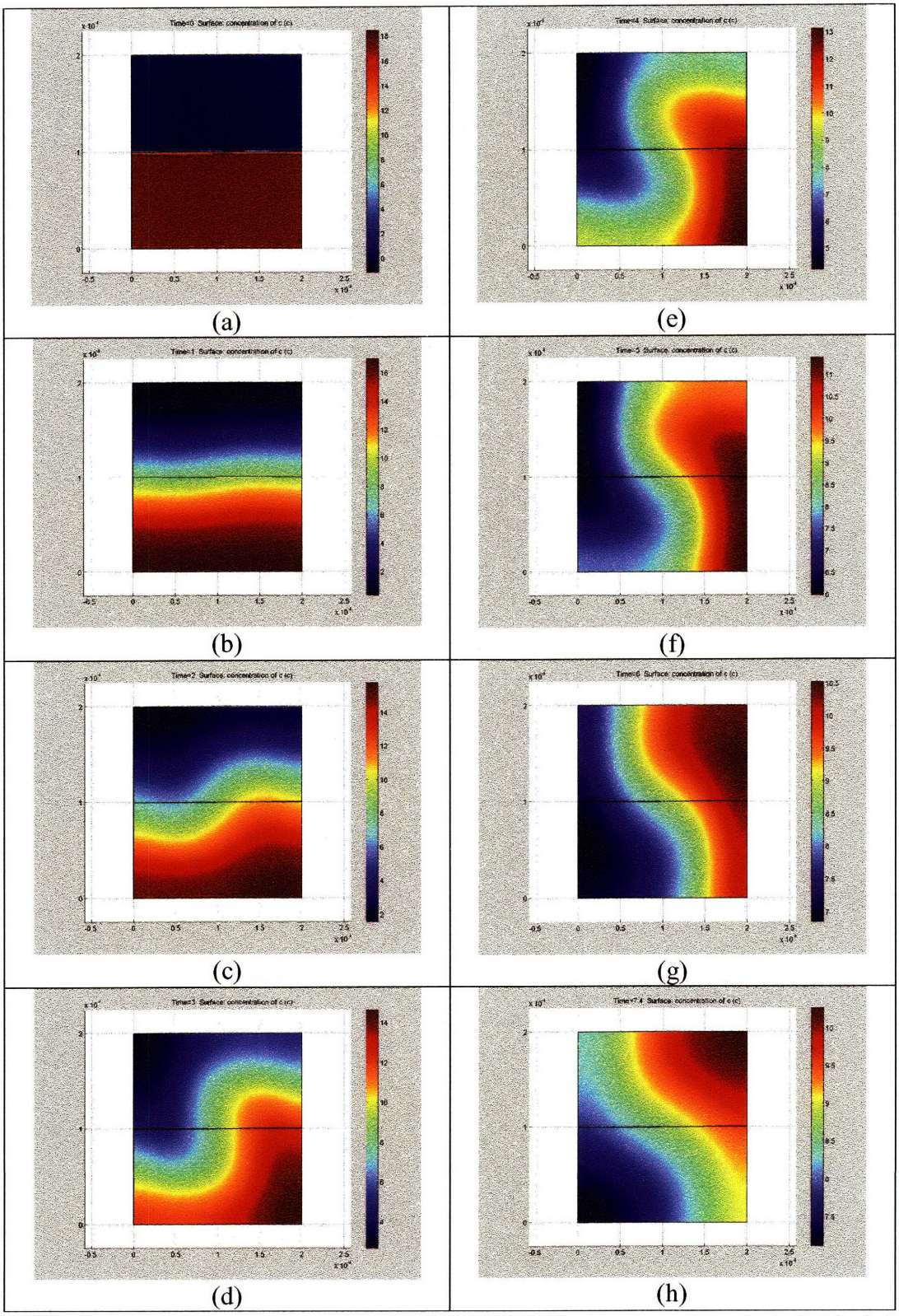

Figure 7-25. Time evolution of the concentration C when length scale is half of the base case, cross-section = $200X200\mu m$, so that $Ra = 1/8(Ra_{base\ case})$, for superposed configuration.

7.4.4. Effect of large length scales

On large scales as Re>>1, the dependence of time and maximum velocity scales are expected to be different from that of small scales, as suggested by the dimensionless analysis. Figure 7-26 shows the total velocity field U at different time instances for a cross-section *1cmX1cm* and *Deff=1e-7,* μ*=1e-3,* $\Delta\rho/\rho$*=0.1* for the vertical (sideways) orientation.

On microscales, where viscous force dominates the inertial force, the velocity reaches a maximum and then decays quickly stabilizing the system. On large scales as the driving buoyancy force reduces progressively because of transfer of heavier fluid elements to the bottom and the lighter to the top, the velocity starts to decrease under the influence of viscous forces. However, as Re>>1 (~ 100 for the case considered above), viscous forces are relatively weak and the surface average of the total velocity decays while still oscillating, as is characteristic of an underdamped system. The maximum velocity attained by the system and the time to reach this velocity must both be governed solely by the interaction between the inertial and the buoyancy forces. We show dependence of the maximum velocity attained and the time to attain this velocity on density difference and length scale, and independence with viscosity, using the time evolution of the surface average velocity, (Figure 7-27). Figure 7-28 shows how the concentration field evolves with time.

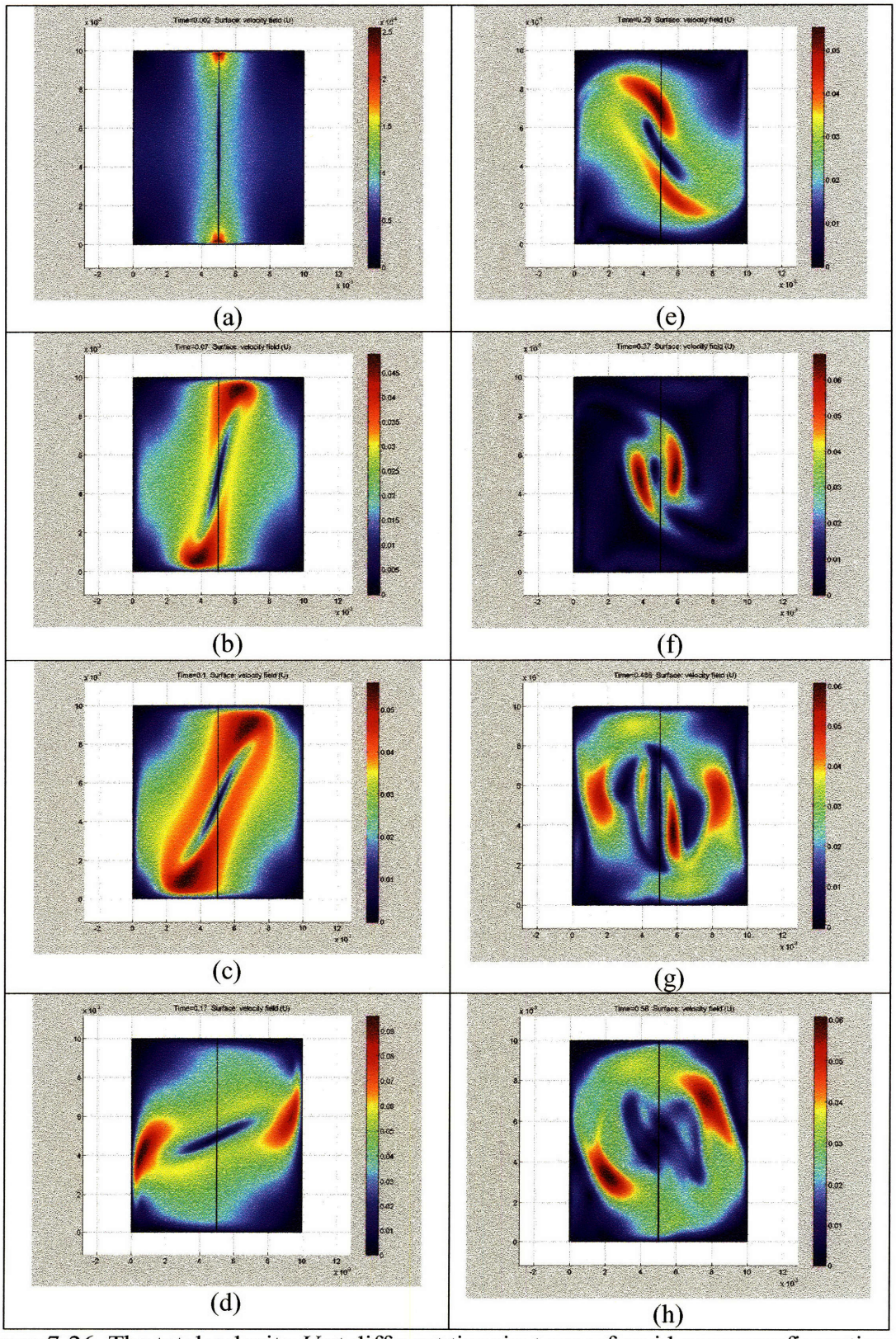

Figure 7-26. The total velocity U at different time instances for sideways configuration.

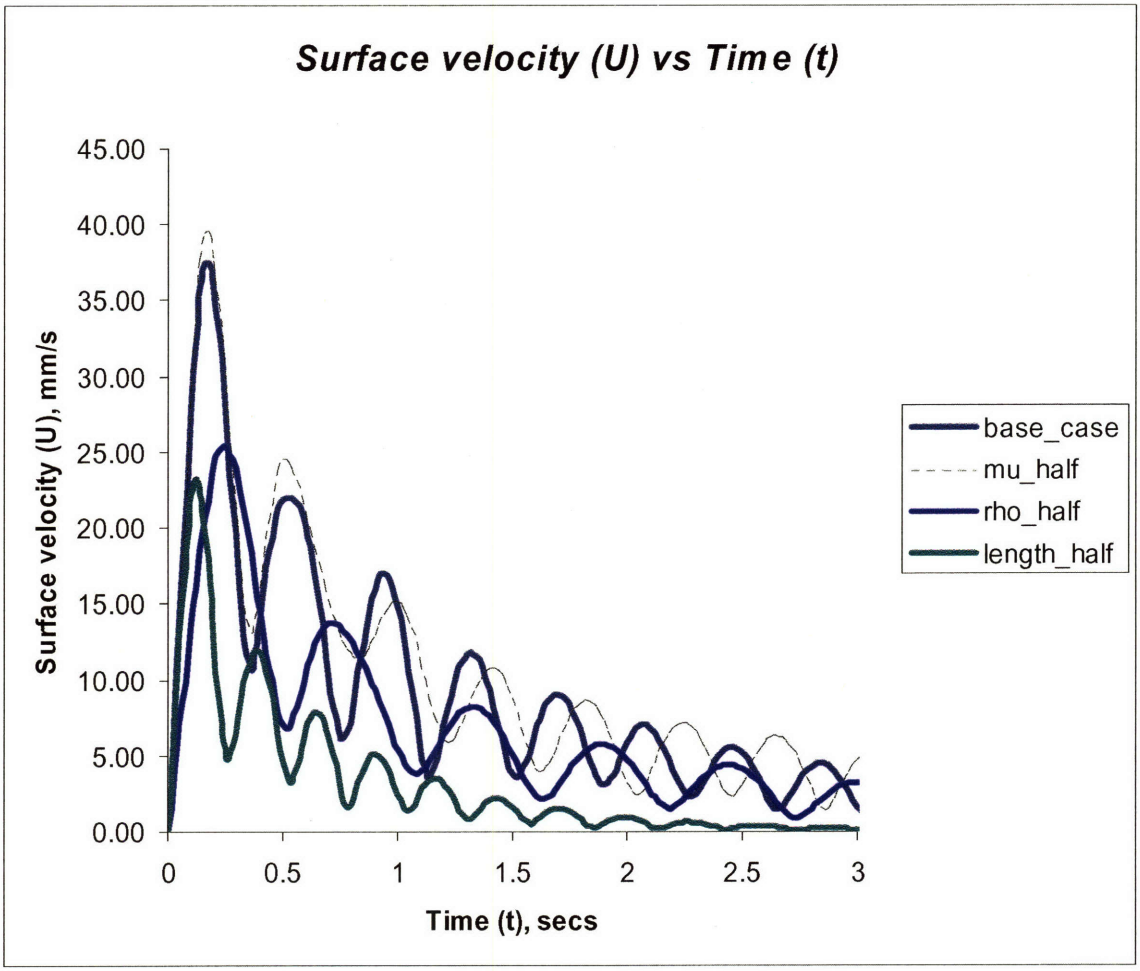

Figure 7-27. Evolution with time of the induced surface average velocity for the sideways configuration, for different density difference, viscosity and length scale, comparing the effect of these parameters, for large scales cross-section *1cmX1cm* and *Re*>>1).

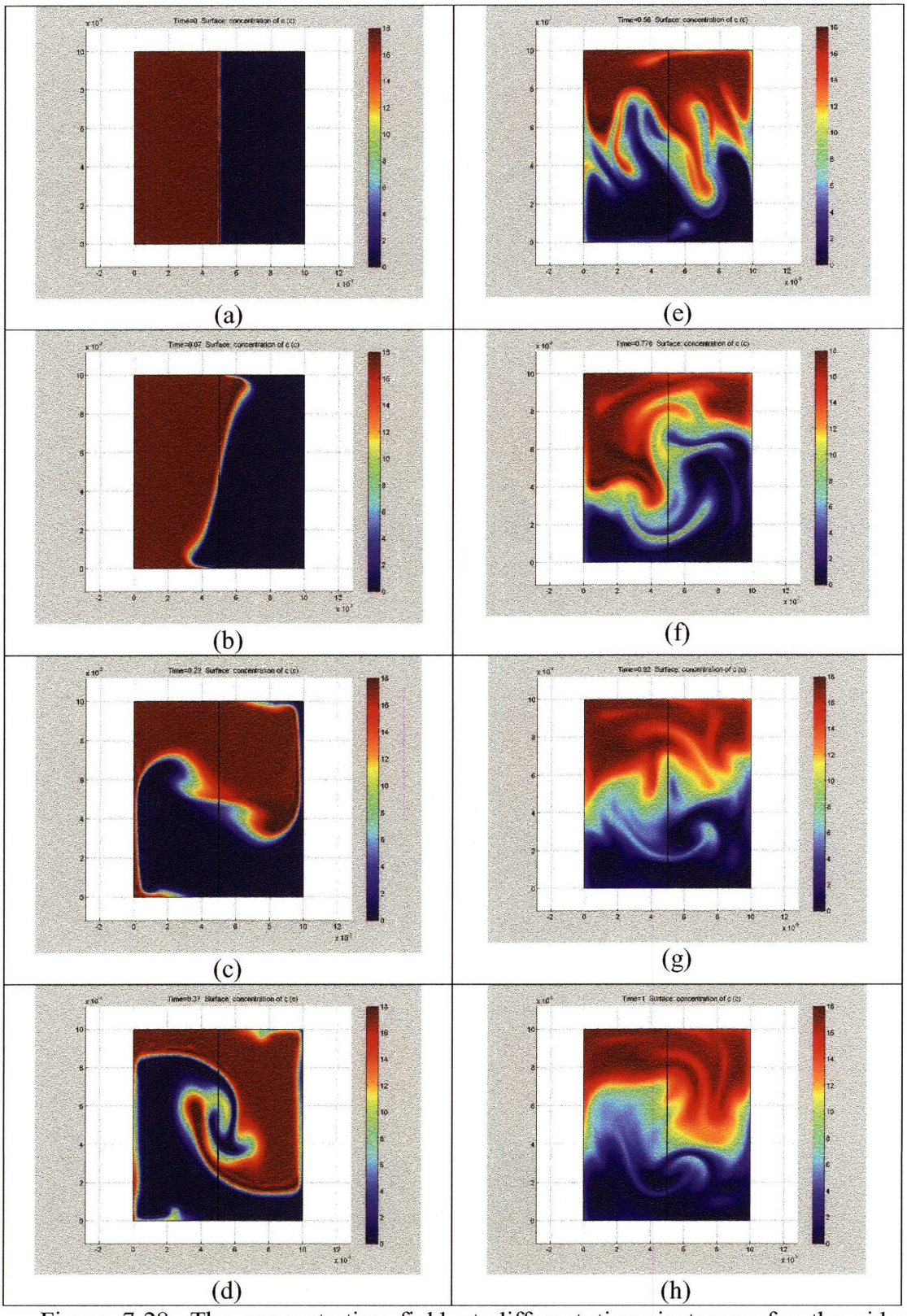

Figure 7-28. The concentration field at different time instances for the sideways orientation of the two liquids for large scale, cross-section *1cmX1cm* and *Deff=1e-7, μ=1e-3, $\Delta\rho/\rho$=0.1.*

Figure 7-29 shows the concentration field at different time instances for the superposed orientation of the two liquids for large length scale (cross-section *1cmX1cm*), with *Deff=1e-7, μ=1e-3, $\Delta\rho/\rho$=0.1*. This is very different from the concentration fields observed on small scale, in terms of multiplicity of finger like projections. However, such origin and propagation of multiple 'finger' like structures is commonly observed on large scales and its nature characterized, (*Wooding, Meiburg*). This essential difference implies that the complete reorientation of streams as observed on microscale is unique. The macroscopic effect observed for larger scale is very different because of the evolution of multiple fingers across the system leading to overall mixing and local recirculation as opposed to complete reorientation on microscale. Figure 7-29(f-h) shows the tendency of adjacent waves to coalesce by mutual entrainment, a process controlled by diffusion [91, 94, 95].

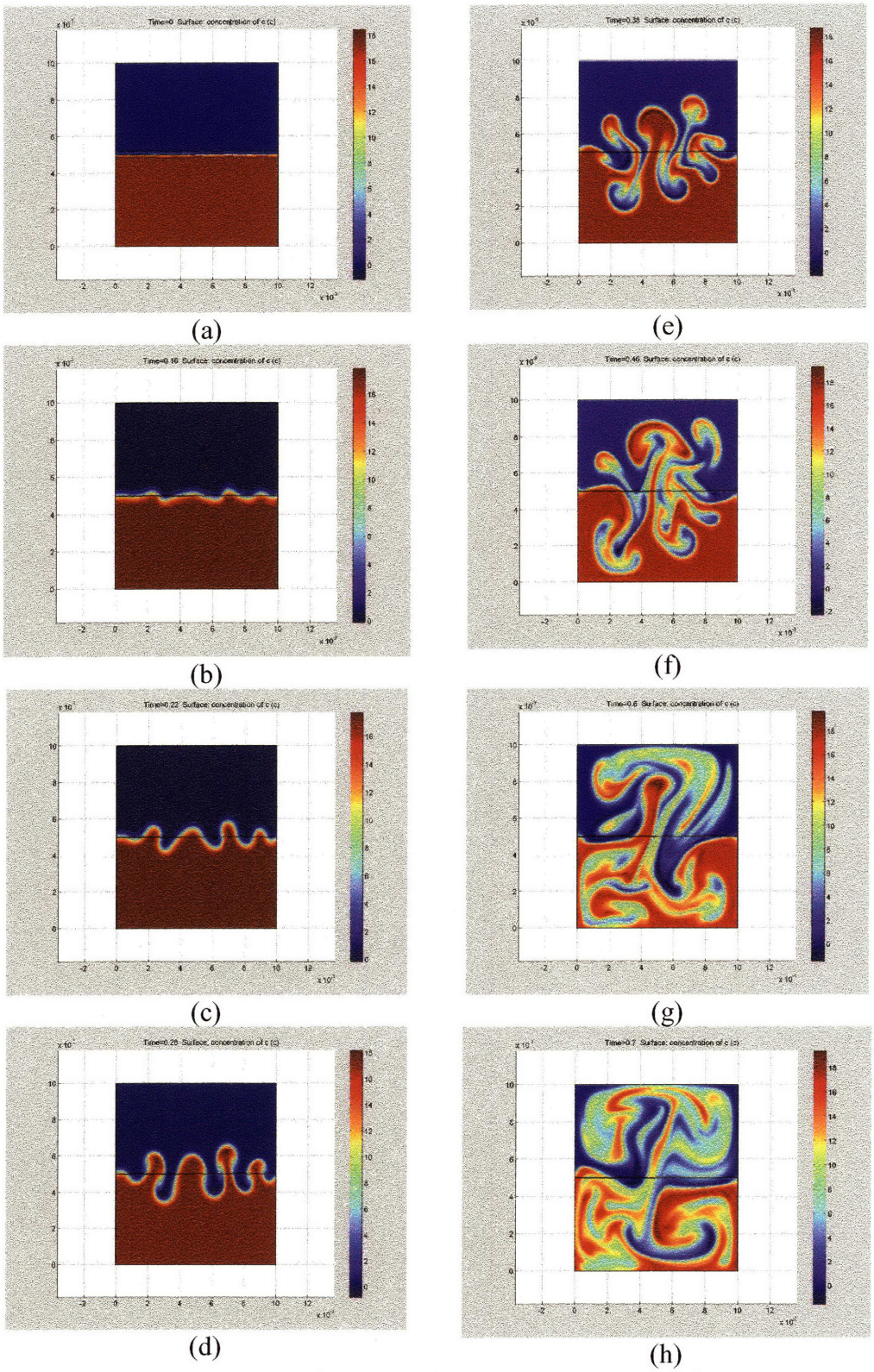

Figure 7-29. The concentration field at different time instances for the superposed configuration of the two liquids for large scale, cross-section *1cmX1cm* and *Deff=1e-7, μ=1e-3, $\Delta\rho/\rho$=0.1.*

7.5. Modeling a Common Microscale Flow Situation

7.5.1. Problem Definition and Equations

The essential difference between the experimentally observed reorientation and the time evolution simulation in 2-diemsnions is the liquid sticking to the walls of the channel in the simulations. We expect this because of the no-slip condition imposed in the 2-dimensional unsteady state simulation and the initial state of the liquids.

We simulate a 3-dimensional steady state flow situation in the superposed configuration, which is a commonly used pattern of contacting liquids on microscale, Figure 7-30. It consists of two inlet sections leading from opposite sides to a main channel, in a 'T' configuration.

The continuity, momentum and the conservation equations solved for this case are:

$$\nabla.\mathbf{v} = 0 \tag{7.19}$$

$$\rho\frac{D\mathbf{v}}{Dt} = -\nabla \mathrm{P} + g\rho e_{\mathrm{g}} + \mu\nabla^2\mathbf{v} \tag{7.20}$$

$$\frac{DC}{Dt} = D_{eff}\nabla^2 C \tag{7.21}$$

with the time derivatives of the variables vanishing for the steady state situation considered here. Once again we assume the liquids to be incompressible, miscible in all proportions while the viscosity (μ) and molecular diffusivity (D_{eff}) as constants. C is dimensionless concentration of the lighter liquid while the density ρ is defined as,

$$\rho = \rho_h - C(\rho_h - \rho_l) \tag{7.22}$$

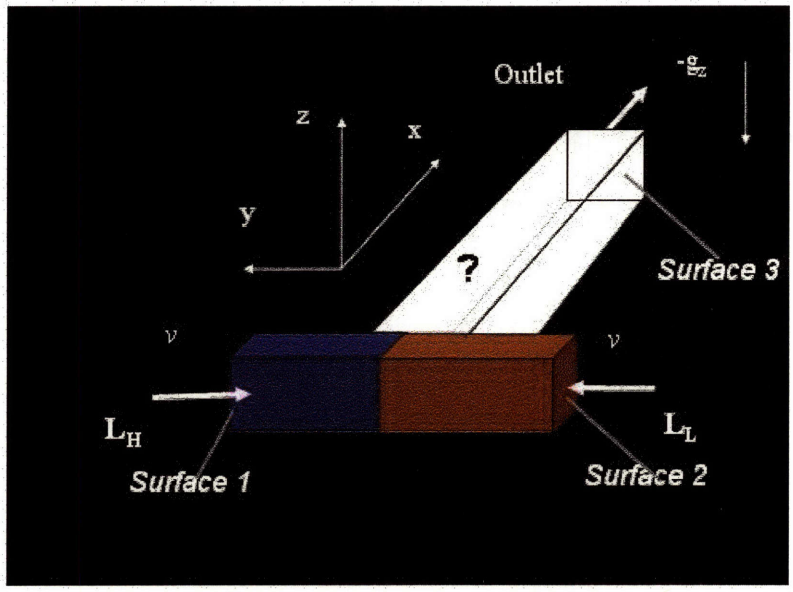

Figure 7-30. 3-dimensional problem for simulation

As earlier the density differences under consideration are assumed to be ~ 0.1 or smaller so that the continuity equation can be written as above, without the effect of spatial variation in density. We confirmed this by including this variation and find the results to be unaffected.

7.5.2. The boundary condition explanation

For the momentum equation a no-slip boundary condition is specified for all surfaces except for *1, 2* and *3*. At surfaces *1* and *2* a plug flow velocity into the channel is specified. Solution of the momentum equation needs a pressure reference specified at some point, we specify pressure at outlet, surface *3*. Specification of the boundary condition at surface *3* needs some explanation. To preclude any velocity components induced due to gravitational head, the pressure boundary condition specified at the outlet must take into account the effect of gravitational head within the channel, and is written

as, $P = -z\rho g$, where ρ is the density at the outlet cross-section. However, this requires knowledge of the distribution of the lighter and heavier liquids at the outlet. We solve this by defining an additional diffusion domain at the end of the region of interest, (Figure 7-30). In the diffusion domain we set the value of diffusivity high enough so that the two liquids can be expected to distribute uniformly across the whole cross-section. This implies that the concentration at the outlet known to be uniform, then the density and hence the pressure boundary condition at the outlet is specified.

For the convection equation the concentration C is specified at surfaces 1, 2 and 3 while a no flux condition is used for all other surfaces.

7.5.3. Solution

The concentration difference between the two streams introduces density difference and couples the momentum conservation with the convection diffusion equations. A large difference in concentration creates a large difference in density, leading to an increased buoyancy force. A large force initiates large spatial gradients in velocity. This makes the system difficult to solve. The desired concentration difference and the density difference can be achieved by solving for a small concentration difference between streams and then increasing the concentration difference in steps while the solution from the previous step is used as the initial guess for the next step. Figure 7-31 shows the solution for concentration difference defined such that the density difference between streams is ~ 5%. To arrive at this solution we first solved the case with an initial density difference of 0.5% between the two streams. The obtained solution was then used as an initial guess to the solution for case with an initial density difference of 1%. We continued progressively in this manner to arrive at a solution for the desired case with a

density difference of about 5%. The streams are seen to reorient as suggested by experimental observations. The time scale for this reorientation is of the order of a second which is in good agreement with the experimental observation and the time scales obtained from the 2-dimensional simulation.

Figure 7-32 shows that the approach velocity of the two streams does not affect the time scale for reorientation of streams, the time to reorient remains the same and the axial distance traveled by the streams along the channels before reorientation is completed, doubles when the velocity is doubled. We also estimate the effect of change in viscosity, density difference and length scale. The time for reorientation and hence the axial distance at which it is completed doubles when viscosity of the system is doubled (Figure 7-33), or when the density difference is halved, (Figure 7-34). It increases four times when the length scale is halved, (Figure 7-35). The time to reorient is estimated from the linear distance traveled along the channel before reorientation, the average linear velocity. These results are once again consistent with the dependency of the time scale obtained from the dimensionless analysis.

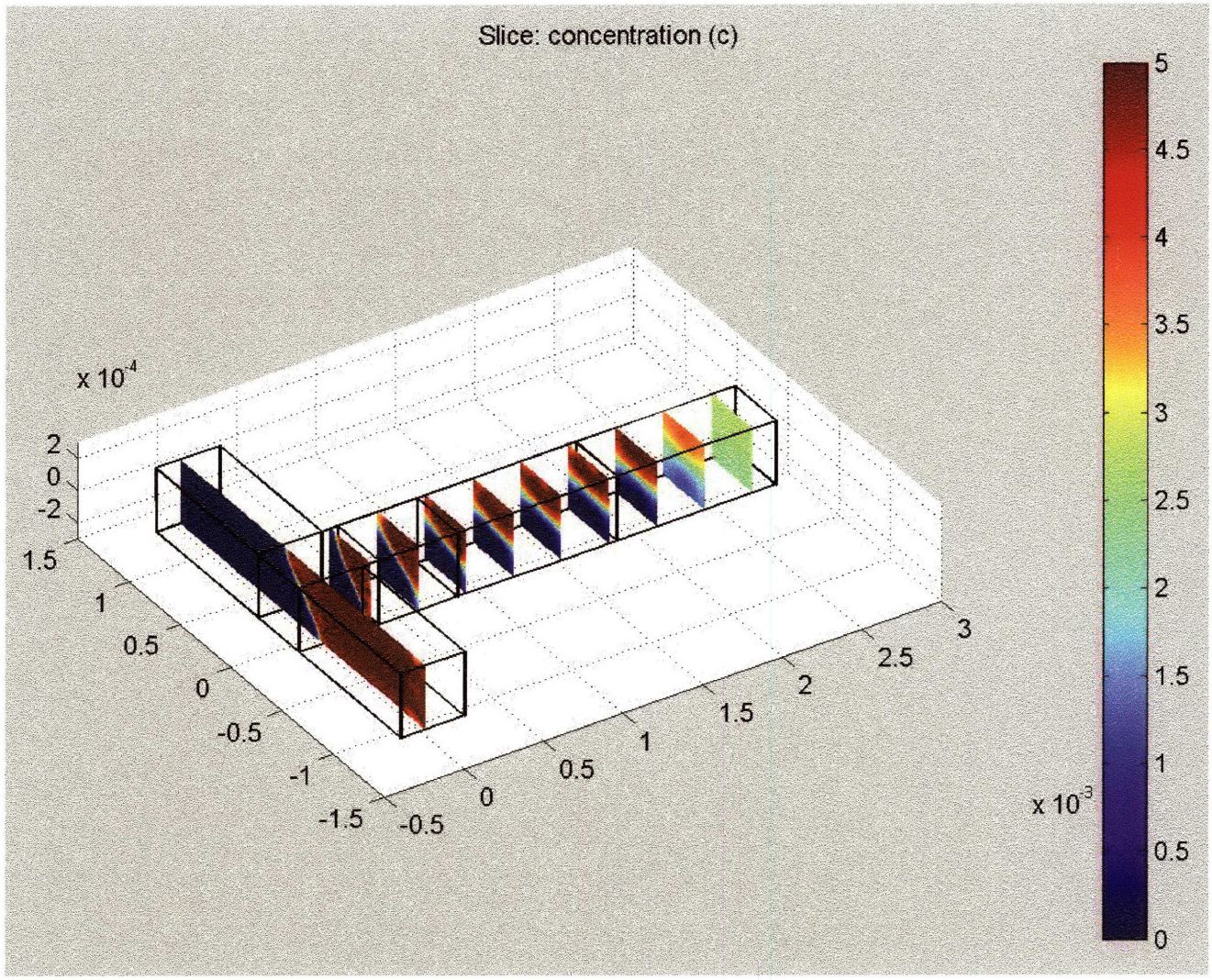

Figure 7-31. 3-dimensional steady state simulation showing reorientation in the gravitational field for streams with a density difference.

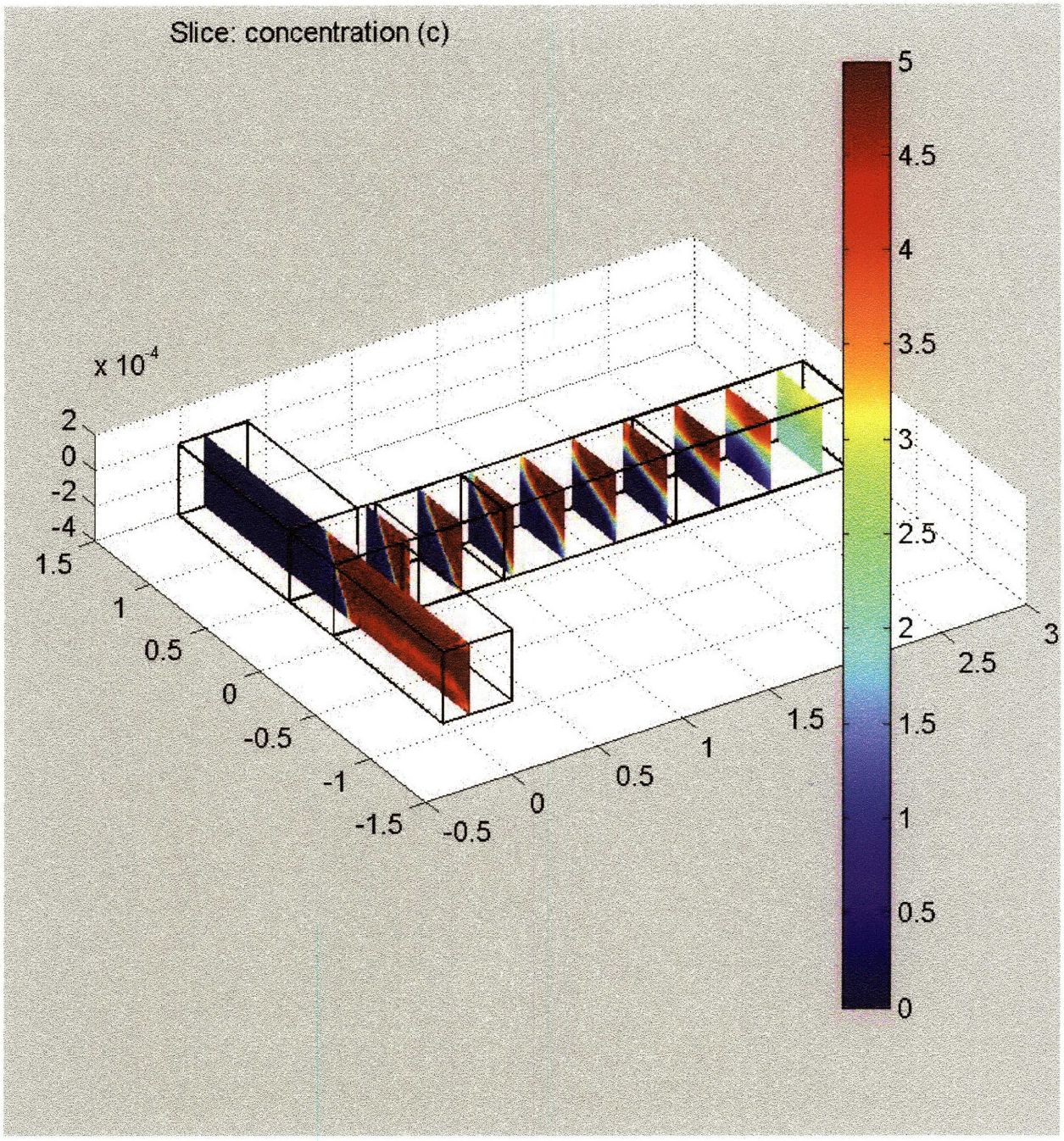

Figure 7-32. 3-dimensional steady state simulation showing reorientation in the gravitational field of streams with a density difference. The approach velocity of the streams being doubled the reorientation being completed at twice the axial distance than for the base-case.

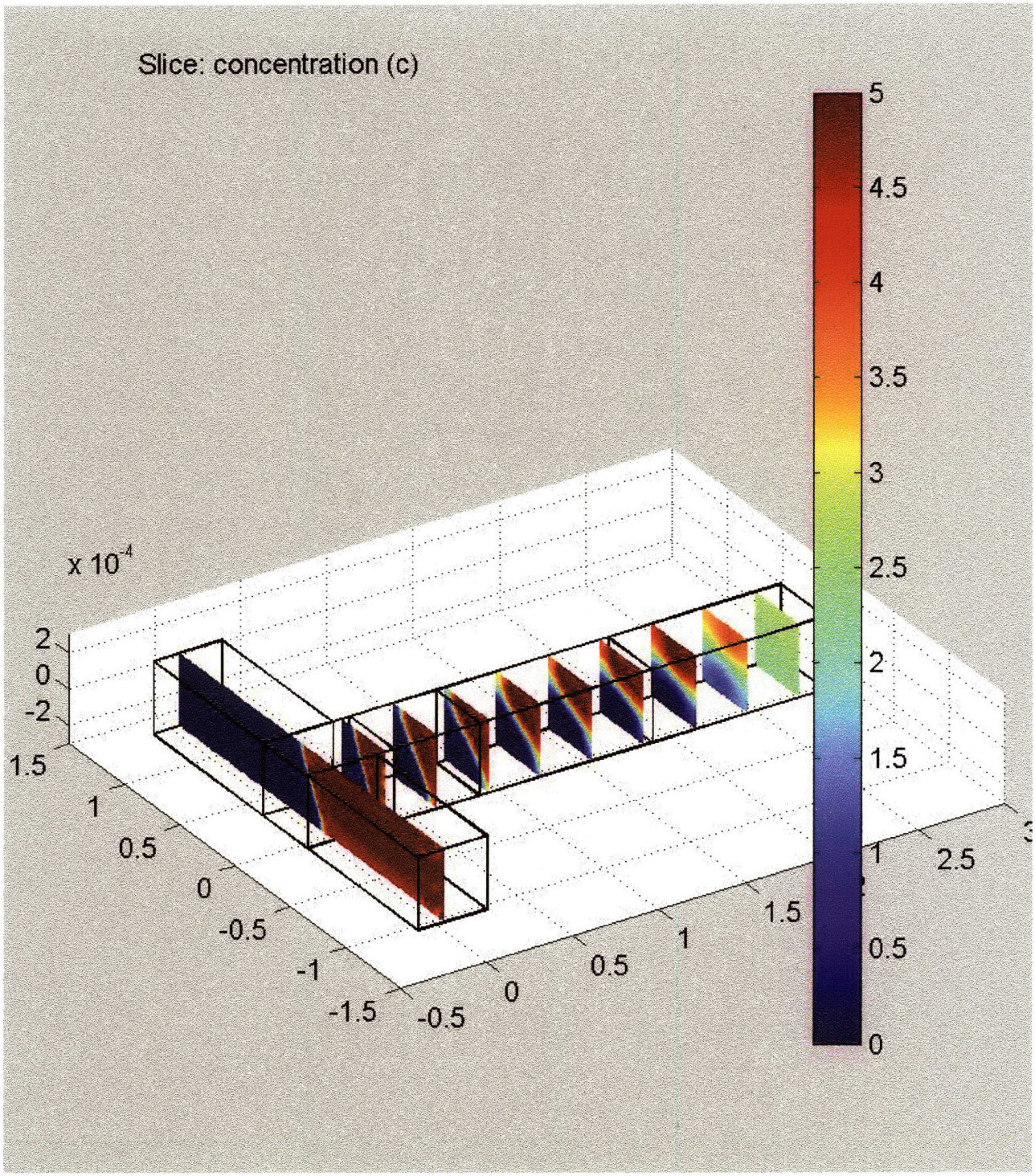

Figure 7-33. 3-dimensional steady state simulation showing reorientation in the gravitational field of streams with a density difference, for viscosity, $\mu = 2(\mu_{base\ case})$. The reorientation of the streams is completed at about twice the axial distance than that for the base-case.

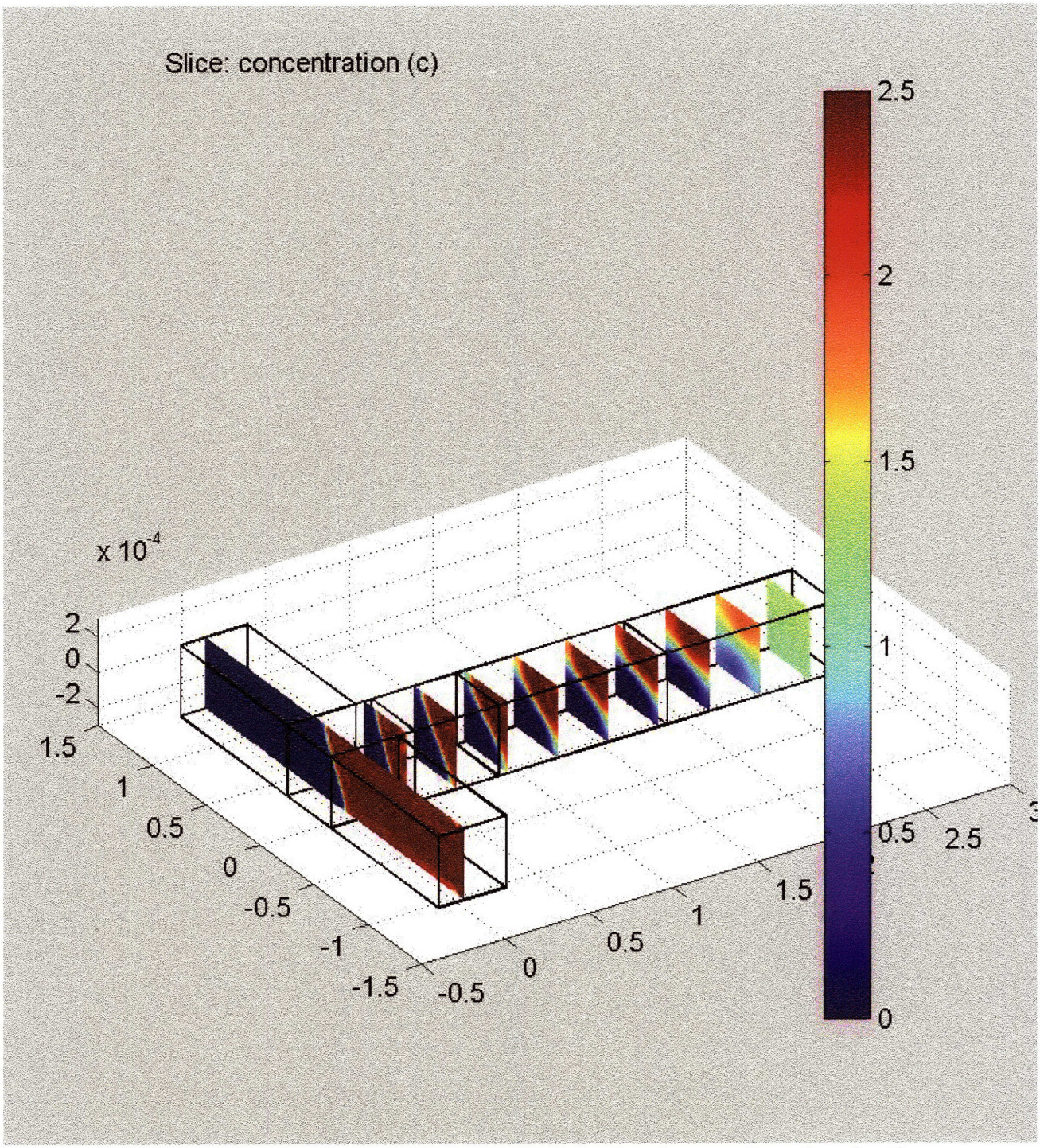

Figure 7-34. 3-dimensional steady state simulation showing reorientation in the gravitational field of streams with a density difference, for the density difference $\Delta\rho = \frac{1}{2}(\Delta\rho_{base\ case})$. The reorientation of the streams is completed at about twice the axial distance than that for the base-case.

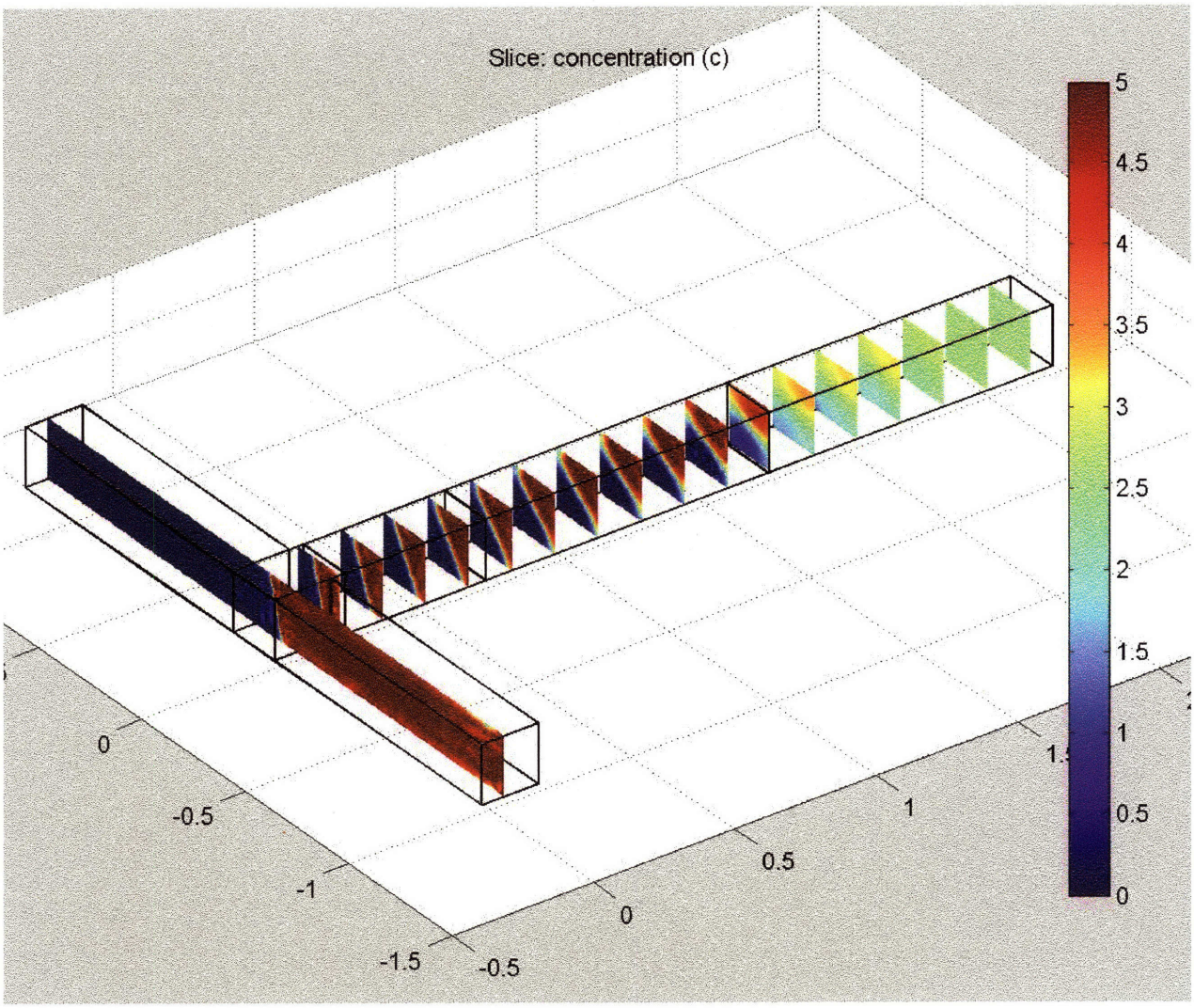

Figure 7-35. 3-dimensional steady state simulation showing reorientation in the gravitational field of streams with a density difference, for the length scale $L = \frac{1}{2}(L_{base\text{-}case})$, cross-section $200\mu mX200\mu m$. About half of the reorientation of the streams is completed at twice the axial distance than that for the base-case.

7.6. Summary

In this chapter we have shown the critical role of gravity in determining path of miscible multiphase systems on microscale. We have shown complete reorientation of miscible liquids coflowing in a microchannel under the influence of buoyancy. We have developed both 2-dimensional time-dependent and 3-dimenisonal finite element models to estimate the critical time and velocity scales for the completion of this orientation for a range of fluid flow and physical parameters and confirming experimental observations. For liquids with a density difference coflowing in a microchannel we find that the time taken for rearrangement of streams with the lighter sliding to the top while the heavier moves to the bottom of the channel, is proportional to the liquid viscosity and inversely proportional to the length scale and the density difference. The approach velocity of the liquids is found not to affect the time for reorientation.

8. Conclusion

8.1. Prime Thesis Accomplishments

8.1.1. Tools and concepts for realization of networks

We have shown routing or separation of individual phases from two-phase gas-liquid and liquid-liquid mixtures for a wide range of mixture velocities and relative fractions of the two phases in the mixture. We also provide an understanding of the underlying principle for the design and functioning of these devices. We extend and generalize the basic principles developed, to design and demonstrate the operation of microscale valves that do not rely on elastic deformation for its operation and can be used even in harsh chemical environments for controlling the flow of fluid between different microscale processes or between a supply and a process. The ability to build computational control in microfluidics rather than using electronic microchips to control the flows is thought of as the ultimate in automation of laboratory-on-a-chip analysis systems [1]. Using suitable configuration for arrangement of these valves we lay out the mechanism for realization of the basic logic gates using microfluidics. These logic gates serve as templates for realization of complex logical computations. Enabled by the phase separation technique, we also develop a novel strategy for mixing liquids on microscale and demonstrate using a model reaction between an acid and a metal salt the integration of the steps of mixing, reaction and phase separation on a single platform. Through the development of fluid-phase routers, valves capable of use in a variety of chemistries and fluid-logic concepts, we provide the tools and concepts that will be useful for interfacing

multiple processes on a microscale platform, for realization and automation of complex chemical/biological networks.

8.1.2. Partial separation in multiphase systems for the purpose of process characterization

We have demonstrated the ability to sample a small quantity of liquid from a gas-liquid mixture and organic phase from an mixture of aqueous and organic phases. We show the general use of this technique for process information retrieval in multiphase systems through measurement of absorption performance in a model two-phase gas (oxygen)-liquid (water) system. Through integration of on-chip sampling and sensing operations we show for the first time direct measurement of gas-liquid mass transfer coefficients on microscale. We compare the estimated coefficients for a range of gas and liquid rates with the absorption mass-transfer coefficient data for large scales. The ability to sample a small quantity of one of the phases from a multiphase system will help further the use of microscale systems as tools for retrieving process knowledge (example chemical kinetics) and characterization and optimization of multiphase systems (example in catalysis).

8.1.3. Role of gravity in determining fluid path on microscale

We have demonstrated the significant role of gravity in determining path of multiphase miscible fluids in microscale flow systems. We show for the first time, a complete change in path of miscible liquids coflowing in a microchannel, driven by buoyancy forces in play due to density difference between the liquids. We also provide an estimate of the time and velocity scales for this redefinition of fluid path, and show the

nature of dependence of the time and velocity scales on critical fluid flow and physical parameters like density difference, viscosity and the critical length scale. Numerous techniques have emerged on microscale with understanding of the path of multiple fluid streams at the heart of these methodologies. With examples in microfabrication, coating/deposition of biologically or chemically active material on the channel walls, controlled transfer of components between streams, these techniques are potentially useful in a variety of existent and rapidly expanding areas across biology and chemistry. Small density differences can arise due to presence of analyte in the solvent, due to concentration difference between fluids or during progress of a chemical reaction. The dependence of fluid path in a microchannel on the density difference between streams places a constraint on the liquid combinations that can be manipulated using the numerous techniques developed for microfluidic applications. Through estimation of the time and velocity scales for these buoyancy driven changes in fluid path and their dependence on critical system parameters, we provide the necessary tools which will be useful for engineering the path of fluids on microscale. Designs accounting for the effect would further development of reliable and flexible systems while those deploying this effect for a localized definition of functionality on channel walls, not attainable otherwise, can open new opportunities. In addition the study connecting the time evolution in unstable 2-dimensional system to 3-dimensional steady state flow situations, presents a novel possibility to investigate other time dependent instabilities in microscale flow situations.

8.2. Future work

Methodology for complete separation of individual phases from two phase gas-liquid and liquid-liquid mixtures opens opportunities for connecting multiphase processes. One of the opportunities for future work is realization of multistage synthesis platforms on microscale. Multistage synthesis is common in fine and speciality chemical and pharmaceutical industries. The inherent advantages of increased speed, reduced cost, ability to handle hazardous chemistry in an easily manageable and safe environment, and handling small quantities of expensive materials for synthesis and analysis in microscale processing are natural attractions to the above niches. The valves presented in this thesis present a unique opportunity to further leverage the safe nature of microscale processes by connecting potentially hazardous but attractive chemistries. It is believed that microfluidic logic built into analysis systems as opposed to interfacing with electronic chips, are the ultimate for realization of integrated microscale systems for analysis. The basic logic-gates presented in this thesis open the doors for realization of complexity in computational logic. Strong potential for impact exists for future endeavors using these tools and interfaces for using these fluid-phase routers, valves and fluid logic components for creation of automated microscale chemical/biological multistage sequences.

The ability to sample one of the phases from a two-phase gas-liquid and liquid-liquid mixtures implies that important multiphase process information can be sampled while only negligibly affecting the process. The small mass transfer limitations achievable on microscale implies that complex chemical kinetics for a range of gas-liquid and liquid-liquid multiphase processes is accessible, with impact to both macro and microscale processing. Specifically the study of multiphase catalytic multiphase

processes for catalyst characterization is attractive. Emulsions are of increasingly growing interest to the pharmaceutical industry and better control over their synthesis through optimization of processing conditions is desirable.

We have underscored the role of gravity in determining fluid path of miscible multiphase flows on microscale. Use of the understanding presented in engineering the flow path of functional chemical/biological materials to gain an improved control and accessibility for location specific patterning of the wall of a microchannel, is attractive. In addition, a number of instabilities have been studied in 2-dimesnions on large scale, and represent an opportunity to study their evolution and impact in a flow situation on microscale.

An improved understanding of the microscale flow phenomena surely has attracted attention of researchers from all disciplines. Chemists working on novel chemistries for synthesis of naturally occurring complex substances is one of these, specifically synthesis of complex carbohydrates have been found to be attractive for discovery of modern day drugs. Most of these syntheses involve multiple steps punctuated by extraction, phase separation and other intermediate steps. The yield of such a multistep sequential synthesis is then a product of the yields for individual steps and this places a strong need for an extremely efficient synthesis path at each step, while taking into account how the methodology used in each step could impact the next steps. For example the overall yield for a 20 step sequential process reduces to about 10% even though the individual yields are 80%. As a result the chemist must test multiple parallel pathways at each step and proceed while trying to battle with the uniformity of the process and environmental conditions across the different pathways. The marriage of

carbohydrate synthesis and microscale processing represents a strong opportunity that can bring the inherent advantages of microscale processing to carbohydrate synthesis and solve many of its problems. In addition study of these complex chemistries provides an opportunity for microscale processing to evolve from the testing of model systems to more modern ones, thus bringing into closer focus the potential advantages from improved selectivity and yield through greater flexibility of the range of process conditions while still achieving better control.

9. Appendix

9.1. Process Flow for the silicon microfabricated device

Purpose: To fabricate micro chemical reactors and separators

Starting material: 1 double-side polished 6-inch silicon wafer. 1, 6-inch 0.762 mm thick Pyrex wafer

General process
Clean silicon wafer and deposit thermal oxide, 1 μm to protect the top side during the etch. Etch port holes to a specified depth 350 μm on the bottom-side of the silicon wafer. Strip all remnant oxide and grow fresh oxide, 1 μm. Etch channels on the top side, aligned with port holes. Passivate the silicon channels by growing a thermal oxide. Bond the pyrex wafer to the top side of the silicon wafer, thereby sealing the flow channels.

Process flow

1. Wafer cleaning and thermal oxide growth

	Lab	Equipment	Description
1.1	TRL	RCA	Wafer cleaning
1.2	TRL	furnace tubeB2	Thermal oxide growth (1 um)

2. Pattern bottom-side silicon wafer

2.1 Photolithography for STS etch

	Lab	Equipment	Description
2.1.1	TRL	HMDS	Coat with HMDS
2.1.2	TRL	coater	Spin Coat New thick resist AZ9620 to 10um
2.1.3	TRL	prebake	Bake 110deg. C for 60minutes.
2.1.4	TRL	EV1	Expose resist for 50 seconds to UV
2.1.5	TRL	photowet-1	Development 3-4 minutes
2.1.6	TRL	prebake	Postbake at 110 deg. C for 60 minutes
2.1.7	TRL	coater	Spin Coat thinresist to 1 um, topside
2.1.8	TRL	prebake	Bake 90deg. C for 30minutes.

2.2 Patterning the oxide for bottom layer

	Lab	Equipment	Description
2.2.1	TRL	Acidhood	BOE etch for 15 minutes

2.3 STS patterning of bottom-side for silicon wafer

	Lab	Equipment	Description
2.3.1	TRL	STS	STS etch, recipe 37A, about 140m – 350 um
2.3.2	TRL	acid hood	Remove resist using piranha

2.4 Removing the oxide and resist from the wafer

	Lab	Equipment	Description
2.4.1	TRL	Acidhood	BOE etch for 15 minutes
2.4.2	TRL	Acidhood	Piranha to remove resist

3. Wafer cleaning and thermal oxide growth

	Lab	Equipment	Description
3.1	TRL	RCA	Wafer cleaning
3.2	TRL	furnace tubeB2	Thermal oxide growth (10000 A)

4. Pattern Top-side silicon wafer

4.1 Photolithography for STS etch, patterning 40 um layer

	Lab	Equipment	Description
4.1.1	TRL	HMDS	Coat with HMDS, recipe for thin resist
4.1.2	TRL	coater	Spin Coat thin resist
4.1.3	TRL	prebake	Bake 90deg. C for 60minutes.
4.1.4	TRL	EV1	Exposure resist for 3-4 seconds to UV, 40 um mask
4.1.5	TRL	photowet-1	Development, 1 min
4.1.6	TRL	prebake	Postbake at 90deg. C for 30 minutes
4.1.7	TRL	coater	Spin coat thin resist on the backside
4.1.8	TRL	prebake	Postbake at 90deg. C for 30 minutes

4.2 Patterning the oxide for 40 um layer

	Lab	Equipment	Description
4.2.1	TRL	Acidhood	BOE etch for 15 minutes

4.3 Wafer cleaning for photolithography of 400 um layer

	Lab	Equipment	Description
4.3.1	TRL	Acidhood	Piranha Clean thin resist

4.4 Photolithography for STS etch,

	Lab	Equipment	Description
4.4.1	TRL	HMDS	Coat with HMDS, recipe 4 for thick resist
4.4.2	TRL	coater	Spin Coat New Thick Resist - 9620 to 10 um
4.4.3	TRL	prebake	Bake 110deg. C for 60minutes
4.4.4	TRL	EV1	Exposure resist for 50 seconds to UV, 400 um mask
4.4.5	TRL	photowet-1	Development, 4 min, AZ 440
4.4.6	TRL	prebake	Postbake at 110deg. C for 60 minutes
4.4.7	TRL	coater	Spin coat thin resist on the backside
4.4.8	TRL	prebake	Postbake at 90deg. C for 30 minutes

4.5 Patterning the oxide for 400 um layer

Lab	Equipment	Description

4.5.1	TRL	Acidhood	BOE etch for 15 minutes

4.6	Attach handle wafer for the through etch		
	Lab	Equipment	Description
4.6.1	TRL	coater	coat handle wafer with resist AZ9620

4.7	STS patterning of top-side for silicon wafer		
	Lab	Equipment	Description
4.7.1	TRL	STS	STS etch, recipe 37A, 144 min for 360 um(2.5um/min)
4.7.2	TRL	acid hood	Remove resist using piranha
4.7.3	TRL	STS	STS etch, recipe 37A, ~15 min for 40 um(2.5 um/min)
4.74	TRL	Acidhood	Piranha to remove resist

5.	Wafer cleaning and thermal oxide growth		
	Lab	Equipment	Description
5.1	TRL	RCA	Wafer cleaning
5.2	TRL	furnace tubeB2	Thermal oxide growth (1000 A)

6.	Attach glass wafer with anodic bond		

6.1	Wafer cleaning - silicon and glass		
	Lab	Equipment	Description
6.1.1	TRL	Acidhood	Piranha in gold compatible

6.2	Contact and bond		
	Lab	Equipment	Description
6.2.1	TRL	evaligner	align/contact
6.2.2	TRL	evbonder	anodic bond (500deg.C, 1000V)

7. Die saw

9.2.Silicon device mask layers

Device with all layers

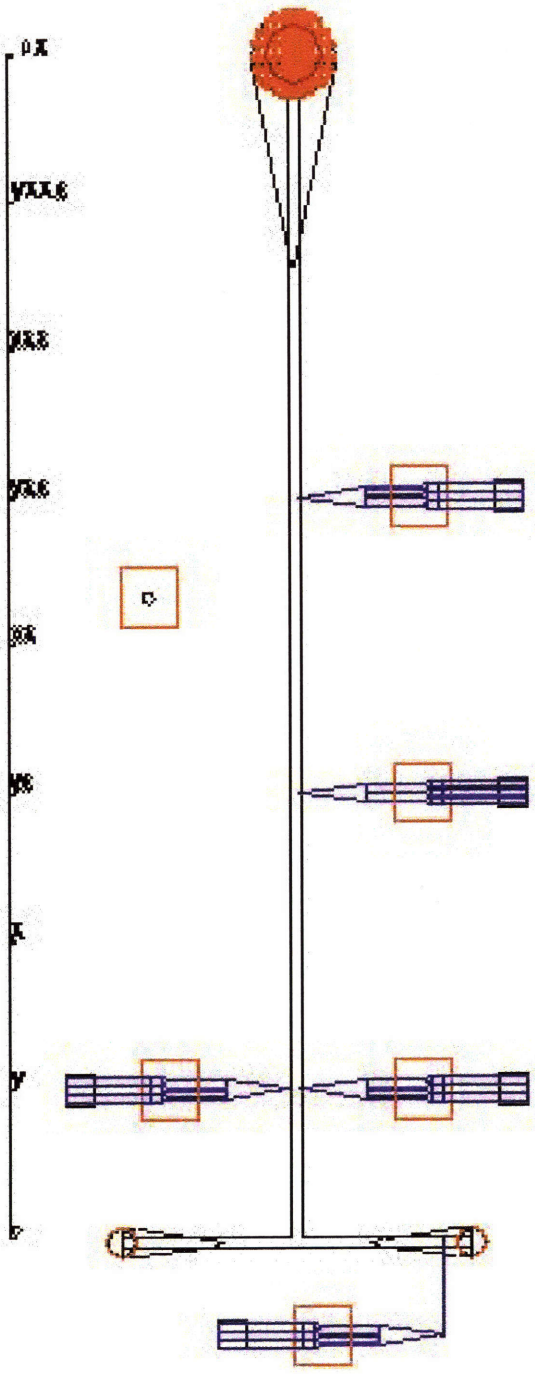

Drawout channel on the 40 micron layer

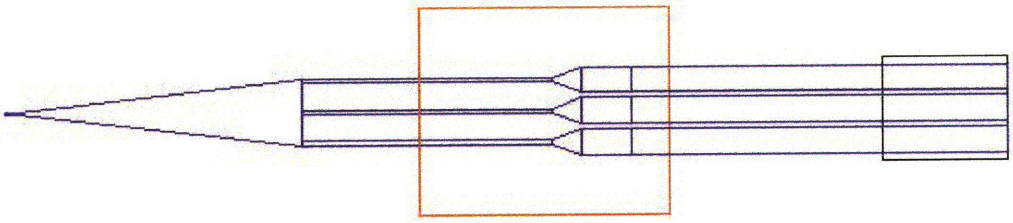

Side Channel

Frontside, 400 micron layer

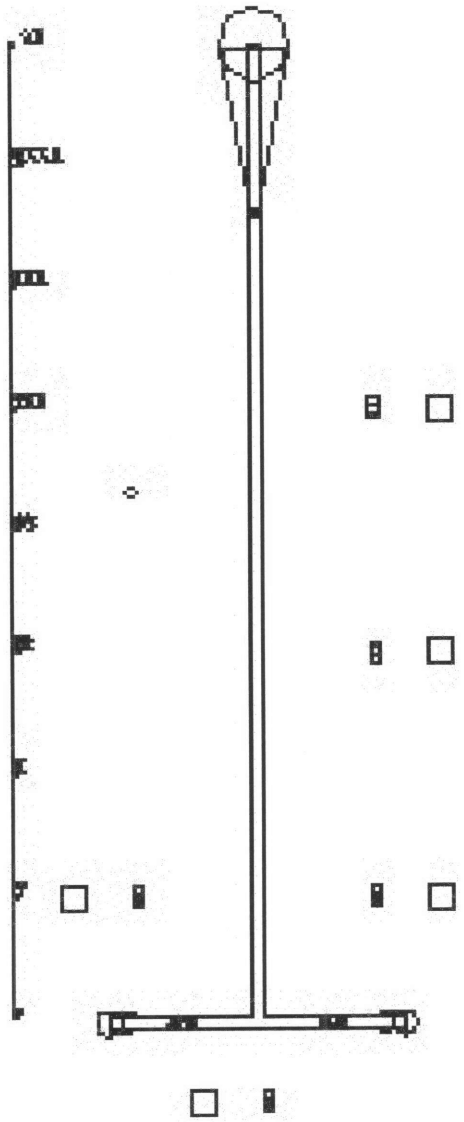

Backside layer and the drawout channel ports

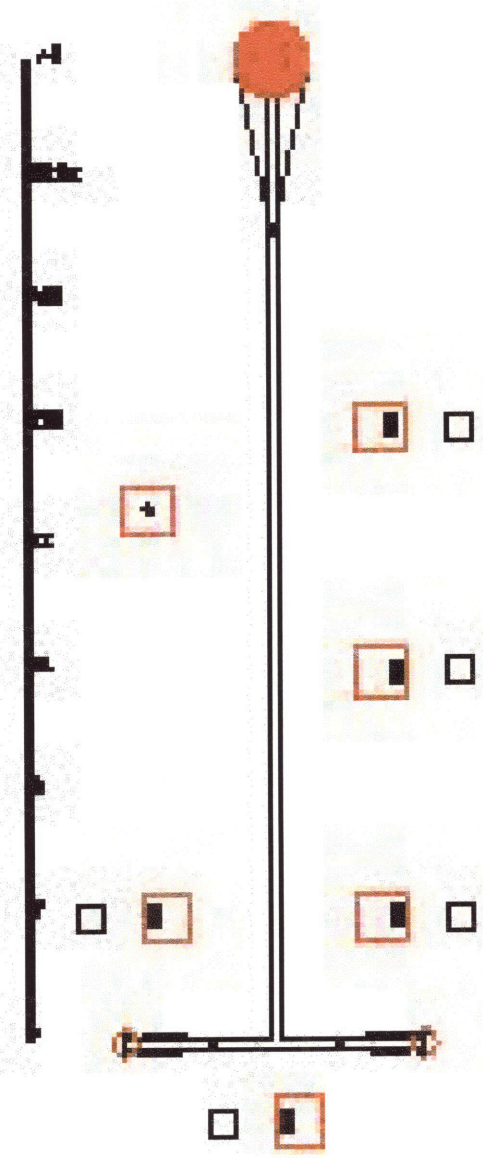

References

1. Ball, P., *Liquid logic.* Nature, Science Update, 2001. **27 March**.
2. Jensen, K.F., *Microreaction engineering - is small better?* Chemical Engineering Science, 2001. **56**(2): p. 293-303.
3. Unger, M.A., H.P. Chou, T. Thorsen, A. Scherer, and S.R. Quake, *Monolithic microfabricated valves and pumps by multilayer soft lithography.* Science, 2000. **288**(5463): p. 113-116.
4. Thorsen, T., S.J. Maerkl, and S.R. Quake, *Microfluidic large-scale integration.* Science, 2002. **298**(5593): p. 580-584.
5. Young, T., Trans. R. Soc. London, 1805. **95**: p. 65.
6. Burns, M.A., C.H. Mastrangelo, T.S. Sammarco, F.P. Man, J.R. Webster, B.N. Johnson, B. Foerster, D. Jones, Y. Fields, A.R. Kaiser, and D.T. Burke, *Microfabricated structures for integrated DNA analysis.* Proceedings of the National Academy of Sciences of the United States of America, 1996. **93**(11): p. 5556-5561.
7. Kataoka, D.E. and S.M. Troian, *Patterning liquid flow on the microscopic scale.* Nature, 1999. **402**(6763): p. 794-797.
8. Daniel, S., M.K. Chaudhury, and J.C. Chen, *Past drop movements resulting from the phase change on a gradient surface.* Science, 2001. **291**(5504): p. 633-636.
9. Chaudhury, M.K. and G.M. Whitesides, *How to Make Water Run Uphill.* Science, 1992. **256**(5063): p. 1539-1541.

10. Gallardo, B.S., V.K. Gupta, F.D. Eagerton, L.I. Jong, V.S. Craig, R.R. Shah, and N.L. Abbott, *ELectrochemical principles for active control of liquids on submillimeter scales.* Science, 1999. **283**(5398): p. 57-60.

11. Lahann, J., S. Mitragotri, T.N. Tran, H. Kaido, J. Sundaram, I.S. Choi, S. Hoffer, G.A. Somorjai, and R. Langer, *A reversibly switching surface.* Science, 2003. **299**(5605): p. 371-374.

12. Prins, M.W.J., W.J.J. Welters, and J.W. Weekamp, *Fluid control in multichannel structures by electrocapillary pressure.* Science, 2001. **291**(5502): p. 277-280.

13. Ichimura, K., S.K. Oh, and M. Nakagawa, *Light-driven motion of liquids on a photoresponsive surface.* Science, 2000. **288**(5471): p. 1624-1626.

14. Beni, G. and M.A. Tenan, *Dynamics of Electrowetting Displays.* Journal of Applied Physics, 1981. **52**(10): p. 6011-6015.

15. Harrison, D.J., K. Fluri, K. Seiler, Z.H. Fan, C.S. Effenhauser, and A. Manz, *Micromachining a Miniaturized Capillary Electrophoresis-Based Chemical-Analysis System on a Chip.* Science, 1993. **261**(5123): p. 895-897.

16. Gau, H., S. Herminghaus, P. Lenz, and R. Lipowsky, *Liquid morphologies on structured surfaces: From microchannels to microchips.* Science, 1999. **283**(5398): p. 46-49.

17. Zhao, B., J.S. Moore, and D.J. Beebe, *Surface-directed liquid flow inside microchannels.* Science, 2001. **291**(5506): p. 1023-1026.

18. Adamson, A.W., Gast. A.P., *Physical Chemistry of Surfaces.* 5 ed. 1999, New York: Wiley.

19. Zhao, T.S. and Q.C. Bi, *Pressure drop characteristics of gas-liquid two-phase flow in vertical miniature triangular channels.* International Journal of Heat and Mass Transfer, 2001. **44**(13): p. 2523-2534.

20. Zhao, T.S. and Q.C. Bi, *Co-current air-water two-phase flow patterns in vertical triangular microchannels.* International Journal of Multiphase Flow, 2001. **27**(5): p. 765-782.

21. Xu, J.L., P. Cheng, and T.S. Zhao, *Gas-liquid two-phase flow regimes in rectangular channels with mini/micro gaps.* International Journal of Multiphase Flow, 1999. **25**(3): p. 411-432.

22. Triplett, K.A., S.M. Ghiaasiaan, S.I. Abdel-Khalik, and D.L. Sadowski, *Gas-liquid two-phase flow in microchannels - Part I: two-phase flow patterns.* International Journal of Multiphase Flow, 1999. **25**(3): p. 377-394.

23. Triplett, K.A., S.M. Ghiaasiaan, S.I. Abdel-Khalik, A. LeMouel, and B.N. McCord, *Gas-liquid two-phase flow in microchannels - Part II: void fraction and pressure drop.* International Journal of Multiphase Flow, 1999. **25**(3): p. 395-410.

24. Coleman, J.W. and S. Garimella, *Characterization of two-phase flow patterns in small diameter round and rectangular tubes.* International Journal of Heat and Mass Transfer, 1999. **42**(15): p. 2869-2881.

25. de Mas, N., A. Gunther, M.A. Schmidt, and K.F. Jensen, *Microfabricated multiphase reactors for the selective direct fluorination of aromatics.* Industrial & Engineering Chemistry Research, 2003. **42**(4): p. 698-710.

26. Dussan, E.B., *Spreading of Liquids on Solid-Surfaces - Static and Dynamic Contact Lines.* Annual Review of Fluid Mechanics, 1979. **11**: p. 371-400.

27. Degennes, P.G., *Wetting - Statics and Dynamics.* Reviews of Modern Physics, 1985. **57**(3): p. 827-863.

28. Heimenz, P.C., Rajagopalan, R., *Principles of clloid and surface chemistry.* 3rd ed. 1997: Marcel Dekker.

29. Campbell, S.A., *The science and engineering of microelectronics fabrication.* 2001: Oxford university press.

30. Madou, M.J., *Fundamentals of microfabrication: The science of miniaturization.* 2002, Ney York: CRC Press.

31. Ayon, A.A., R. Braff, C.C. Lin, H.H. Sawin, and M.A. Schmidt, *Characterization of a time multiplexed inductively coupled plasma etcher.* Journal of the Electrochemical Society, 1999. **146**(1): p. 339-349.

32. Ayon, A.A., R.A. Braff, R. Bayt, H.H. Sawin, and M.A. Schmidt, *Influence of coil power on the etching characteristics in a high density plasma etcher.* Journal of the Electrochemical Society, 1999. **146**(7): p. 2730-2736.

33. Mehra, A., A.A. Ayon, I.A. Waitz, and M.A. Schmidt, *Microfabrication of high-temperature silicon devices using wafer bonding and deep reactive ion etching.* Journal of Microelectromechanical Systems, 1999. **8**(2): p. 152-160.

34. Schmidt, M.A., *Wafer-to-wafer bonding for microstructure formation.* Proceedings of the Ieee, 1998. **86**(8): p. 1575-1585.

35. Weissermel, K., Arpe, H.J., *Industrial organic chemistry, (2nd ed.).* 1993.

36. Dudukovic, M.P., F. Larachi, and P.L. Mills, *Multiphase reactors - revisited.* Chemical Engineering Science, 1999. **54**(13-14): p. 1975-1995.

37. Song, H., J.D. Tice, and R.F. Ismagilov, *A microfluidic system for controlling reaction networks in time.* Angewandte Chemie-International Edition, 2003. **42**(7): p. 768-772.

38. Yonemoto, T., M. Kubo, T. Doi, and T. Tadaki, *Continuous synthesis of titanium dioxide fine particles using a slug flow ageing tube reactor.* Chemical Engineering Research & Design, 1997. **75**(A4): p. 413-419.

39. Burns, J.R. and C. Ramshaw, *The intensification of rapid reactions in multiphase systems using slug flow in capillaries.* Lab on a Chip, 2001. **1**(1): p. 10-15.

40. Losey, M.W., M.A. Schmidt, and K.F. Jensen, *Microfabricated multiphase packed-bed reactors: Characterization of mass transfer and reactions.* Industrial & Engineering Chemistry Research, 2001. **40**(12): p. 2555-2562.

41. Jahnisch, K., M. Baerns, V. Hessel, W. Ehrfeld, V. Haverkamp, H. Lowe, C. Wille, and A. Guber, *Direct fluorination of toluene using elemental fluorine in gas/liquid microreactors.* Journal of Fluorine Chemistry, 2000. **105**(1): p. 117-128.

42. Chambers, R.D., D. Holling, R.C.H. Spink, and G. Sandford, *Elemental fluorine - Part 13. Gas-liquid thin film microreactors for selective direct fluorination.* Lab on a Chip, 2001. **1**(2): p. 132-137.

43. Harms, P., Y. Kostov, and G. Rao, *Bioprocess monitoring.* Current Opinion in Biotechnology, 2002. **13**(2): p. 124-127.

44. Carraway, E.R., J.N. Demas, B.A. Degraff, and J.R. Bacon, *Photophysics and Photochemistry of Oxygen Sensors Based on Luminescent Transition-Metal Complexes.* Analytical Chemistry, 1991. **63**(4): p. 337-342.

45. Mandal, K., T.D.L. Pearson, W.P. Krug, and J.N. Demas, *Singlet Energy-Transfer from the Charge-Transfer Excited-State of Tris(2,2'-Bipyridine)Ruthenium(Ii) to Laser-Dyes.* Journal of the American Chemical Society, 1983. **105**(4): p. 701-707.

46. Douglas, P. and K. Eaton, *Response characteristics of thin film oxygen sensors, Pt and Pd octaethylporphyrins in polymer films.* Sensors and Actuators B-Chemical, 2002. **82**(2-3): p. 200-208.

47. Klimant, I., F. Ruckruh, G. Liebsch, C. Stangelmayer, and O.S. Wolfbeis, *Fast response oxygen micro-optodes based on novel soluble ormosil glasses.* Mikrochimica Acta, 1999. **131**(1-2): p. 35-46.

48. Wales, C.E., *Physical and chemical absorption in two-phase annular and dispersed horizontal flow.* A.I.Ch.E.J., 1966. **12**: p. 1166-1171.

49. Jepsen, C.J., *Mass transfer in two-phase flow in horizontal pipelines.* A.I.Ch.E.J., 1970. **16**: p. 705-711.

50. Tortopidis, P. and V. Bontozoglou, *Mass transfer in gas-liquid flow in small-diameter tubes.* Chemical Engineering Science, 1997. **52**(14): p. 2231-2237.

51. Losey, M.W., *Novel multiphase chemical reaction systems enabled by microfabrication technology*, in *Chemical engineering department.* 2001, MIT: Cambridge.

52. Floyd, T., *A novel microchemical system for rapid liquqid-liquid chemistry*, in *Chemical engineering department.* 2001, MIT: cambridge.

53. Ehrfeld, W., K. Golbig, V. Hessel, H. Lowe, and T. Richter, *Characterization of mixing in micromixers by a test reaction: Single mixing units and mixer arrays.* Industrial & Engineering Chemistry Research, 1999. **38**(3): p. 1075-1082.

54. Knight, J.B., A. Vishwanath, J.P. Brody, and R.H. Austin, *Hydrodynamic focusing on a silicon chip: Mixing nanoliters in microseconds.* Physical Review Letters, 1998. **80**(17): p. 3863-3866.

55. Schwesinger, N., T. Frank, and H. Wurmus, *A modulator microfluid system with an integrated micromixer.* Journal of Micromechanics and Microengineering, 1996. **6**(1): p. 99-102.

56. Ottino, J.M., *The kinematics of mixing: Stretching, chaos, trasnsport.* 1989, Cambridge: Cambridge University Press.

57. Aref, H., *Stirring by Chaotic Advection.* Journal of Fluid Mechanics, 1984. **143**(JUN): p. 1-21.

58. Aref, H. and S. Balachandar, *Chaotic Advection in a Stokes-Flow.* Physics of Fluids, 1986. **29**(11): p. 3515-3521.

59. Stroock, A.D., S.K. Dertinger, G.M. Whitesides, and A. Ajdari, *Patterning flows using grooved surfaces.* Analytical Chemistry, 2002. **74**(20): p. 5306-5312.

60. Stroock, A.D., S.K.W. Dertinger, A. Ajdari, I. Mezic, H.A. Stone, and G.M. Whitesides, *Chaotic mixer for microchannels.* Science, 2002. **295**(5555): p. 647-651.

61. Liu, R.H., M.A. Stremler, K.V. Sharp, M.G. Olsen, J.G. Santiago, R.J. Adrian, H. Aref, and D.J. Beebe, *Passive mixing in a three-dimensional serpentine microchannel.* Journal of Microelectromechanical Systems, 2000. **9**(2): p. 190-197.

62. Therriault, D., S.R. White, and J.A. Lewis, *Chaotic mixing in three-dimensioned microvascular networks fabricated by direct-write assembly (vol 2, pg 265, 2002).* Nature Materials, 2003. **2**(5): p. 347-347.

63. Therriault, D., S.R. White, and J.A. Lewis, *Chaotic mixing in three-dimensional microvascular networks fabricated by direct-write assembly.* Nature Materials, 2003. **2**(4): p. 265-271.

64. Yang, Z., S. Matsumoto, H. Goto, M. Matsumoto, and R. Maeda, *Ultrasonic micromixer for microfluidic systems.* Sensors and Actuators a-Physical, 2001. **93**(3): p. 266-272.

65. Liu, R.H., J.N. Yang, M.Z. Pindera, M. Athavale, and P. Grodzinski, *Bubble-induced acoustic micromixing.* Lab on a Chip, 2002. **2**(3): p. 151-157.

66. Handique, K. and M.A. Burns, *Mathematical modeling of drop mixing in a slit-type microchannel.* Journal of Micromechanics and Microengineering, 2001. **11**(5): p. 548-554.

67. Guenther, A., Jhunjhunwala, M., Schmidt, M.A., Jensen, K.F., *Mixing of miscible liquids using a passive gas stream.* To submit, 2003.

68. Kenis, P.J.A., R.F. Ismagilov, and G.M. Whitesides, *Microfabrication inside capillaries using multiphase laminar flow patterning.* Science, 1999. **285**(5424): p. 83-85.

69. Takayama, S., J.C. McDonald, E. Ostuni, M.N. Liang, P.J.A. Kenis, R.F. Ismagilov, and G.M. Whitesides, *Patterning cells and their environments using multiple laminar fluid flows in capillary networks.* Proceedings of the National

Academy of Sciences of the United States of America, 1999. **96**(10): p. 5545-5548.

70. Weigl, B.H. and P. Yager, *Microfluidics - Microfluidic diffusion-based separation and detection.* Science, 1999. **283**(5400): p. 346-347.

71. DeMello, A.J., *Microfluidics - DNA amplification moves on.* Nature, 2003. **422**(6927): p. 28-29.

72. Knight, J., *Microfluidics: Honey, I shrunk the lab.* Nature, 2002. **418**(6897): p. 474-475.

73. Simpson, J.E., *Gravity Currents*. 2nd Edition ed. 1997: Cambridge University Press.

74. Homsy, G.M., *Viscous Fingering in Porous-Media.* Annual Review of Fluid Mechanics, 1987. **19**: p. 271-311.

75. Chandrasekhar, *Hydrodynamic and Hydromagnetic Stability*. 1961: Clarendon, Oxford.

76. Yih, C.S., *INstability due to viscosity stratification.* Journal of fluid mechanics, 1967. **27**(337).

77. Taylor, *Deposition of a viscous fluid on the wall of a tube.* Journal of fluid mechanics, 1961. **10**: p. 161.

78. Saffman, P.G., Taylor, G.I.,, Proceedings of Royal Society A, 1958. **245**: p. 312.

79. Chouke, R.L., Van Meurs, P., Van Der Poel, C.,, JOurnal of Petroleum Technology, 1959. **11**: p. 64.

80. Taylor, G.I., Proceedings of Royal Society A, 1950. **201**: p. 192.

81. Bensimon, D., L.P. Kadanoff, S.D. Liang, B.I. Shraiman, and C. Tang, *Viscous Flows in 2 Dimensions.* Reviews of Modern Physics, 1986. **58**(4): p. 977-999.

82. Joseph, D.D., R. Bai, K.P. Chen, and Y.Y. Renardy, *Core-annular flows.* Annual Review of Fluid Mechanics, 1997. **29**: p. 65-90.

83. Saffman, P.G., *Viscous Fingering in Hele-Shaw Cells.* Journal of Fluid Mechanics, 1986. **173**: p. 73-94.

84. Jensen, M.H., A. Libchaber, P. Pelce, and G. Zocchi, *Effect of Gravity on the Saffman-Taylor Meniscus - Theory and Experiment.* Physical Review A, 1987. **35**(5): p. 2221-2227.

85. Yang, Z.M. and Y.C. Yortsos, *Asymptotic solutions of miscible displacements in geometries of large aspect ratio.* Physics of Fluids, 1997. **9**(2): p. 286-298.

86. Lajeunesse, E., J. Martin, N. Rakotomalala, and D. Salin, *3D instability of miscible displacements in a Hele-Shaw cell.* Physical Review Letters, 1997. **79**(26): p. 5254-5257.

87. Lajeunesse, E., J. Martin, N. Rakotomalala, D. Salin, and Y.C. Yortsos, *The threshold of the instability in miscible displacements in a Hele-Shaw cell at high rates.* Physics of Fluids, 2001. **13**(3): p. 799-801.

88. Scoffoni, J., E. Lajeunesse, and G.M. Homsy, *Interface instabilities during displacements of two miscible fluids in a vertical pipe.* Physics of Fluids, 2001. **13**(3): p. 553-556.

89. Petitjeans, P. and T. Maxworthy, *Miscible displacements in capillary tubes .1. Experiments.* Journal of Fluid Mechanics, 1996. 326: p. 37-56.

90. Chen, C.Y. and E. Meiburg, Miscible displacements in capillary tubes .2. Numerical simulations. Journal of Fluid Mechanics, 1996. 326: p. 57-90.

91. Wooding, R.A., Growth of fingers at an unstable diffusing interface in a porous medium or Hele-Shaw cell. Journal of fluid mechanics, 1969. 39(3): p. 477-495.

92. Fernandez, J., P. Kurowski, P. Petitjeans, and E. Meiburg, Density-driven unstable flows of miscible fluids in a Hele-Shaw cell. Journal of Fluid Mechanics, 2002. 451: p. 239-260.

93. Graf, F., E. Meiburg, and C. Hartel, Density-driven instabilities of miscible fluids in a Hele-Shaw cell: linear stability analysis of the three-dimensional Stokes equations. Journal of Fluid Mechanics, 2002. 451: p. 261-282.

94. Elder, J.W., Journal of fluid mechanics, 1967. 27: p. 609.

95. Elder, J.W., Journal of fluid mechanics, 1968. 32: p. 69.

1. Appendix: Business of microchemical synthesis..... 2

1. Appendix: Business of microchemical synthesis

1.1.Introduction

In this chapter we analyze the commercial aspects for chemical synthesis on microscale. We discuss the dynamics and main characteristics of the microchemical synthesis industry and highlight the salient characteristics of some of the players. We propose a 'closely collaborative, product and process development for Active Pharmaceutical Ingredient synthesis' as a microchemical synthesis venture and analyze the structure, characteristics and interesting dynamics of such an effort. We show the importance of collaborative development and the mutually beneficial relationship possible between the present API manufacturers and a microchemical synthesis venture. We finally discuss some of the trends from the commercial aspects of the industry which pose challenges for the microchemical industry, while promising solid opportunities for commercial success.

1.2.Industry structure and dynamics

1.2.1. Industry Parts

A number of potential businesses become apparent in consideration of microchemical synthesis on small scale, essentially around the different value addition steps. The 3 broad categories are:

- *Product*: Use of microchemical synthesis for discovery, design of new molecules and material or simply in manufacturing of a known chemical compound with a known process.
- *Process*: Focus on the design of microscale systems, processes and parts that would best allow discovery, testing and/or manufacturing as the *product* need may be.
- *Platform*: Focus on the manufacturing/fabrication of equipment/instruments, nature of interface between micro components and with the macroworld, choice of material to enable the *process*.

1.2.2. State of ferment

The microchemical synthesis industry is in a state of ferment. Multiple platforms exist today, evident in the variety of material of construction/fabrication (plastic, glass, silicon, metal) equipment. Competing technologies also exist for inter-component integration as-well-as interfacing with macroscale (from glass bonding to glues, nut-bolts, screws, plastic thermal bonding). Presently there is no clear dominant or a standard platform for the industry on which most processes must evolve. Although, the silicon and glass platform has proven to be useful for material handling and ease integration of electronic sensing and analysis capability on chip, the design of interface with the macroworld has not been trivial. Polymer and metal platforms on the other hand have had to struggle much more, many a times hopelessly, in dealing with the chemical compatibility issues.

In addition, commonly a variety of designs using these platforms or their combination exist for most processes. Finally few efforts that focus on microsystems for discovery and development of new materials are proprietary in nature and often work in

close collaboration with a partner specializing in process-design or with microscale platform expertise.

It is expected that in future the choice of platform, process and product design methodologies will continue to evolve as competing technologies tussle with each other to emerge more effective than others and a dominant design surfaces, [*A1,A2*].

The question then is which platform to choose and where in the value chain (process, product or platform) to position a potential commercial effort? These are addressed in this section.

1.2.3. Choice of platform

The choice of platform is a critical decision which must be made at a very early stage. It constrains the processes that can be realized with the available technology and hence commands the products that can be processed on the platform. Efforts using plastic or metal as the platform material are unable to process hazardous or corrosive chemistry simply due to material compatibility issues. Such ventures traded-off ease of interfacing within components and with the macroworld for creation of systems with the breadth of chemistry that could be processed in these systems.

To be able to experiment with a wide variety of hazardous chemistry in a continuous flow system is one of the prime advantages of microscale processing over macroscale: attractive for new materials discovery or in developing new pathways. As a result, such platforms are either becoming less popular or forced to develop additional capabilities easily possible with glass or silicon platforms.

Figure 1 below captures the comparison between different platform materials: polymers, glass, silicon and steel along four dimensions of significance: 1. Material

compatibility (capability to handle variety of chemistry) 2. Ease of interfacing between components and with the macroscale 3. Ease of integration of sensing and analysis 4. Difficulty in fabrication and its cost

We believe that silicon and glass have an edge over other platforms because of their natural ability to handle a variety of chemistries easily. As a result, the fabrication process is also more elaborate and adds to the time and cost. However, thanks to the years of advances made in the integrated circuit (IC) industry, the silicon fabrication methodologies today are well known and often need to be slightly modified to suit the fabrication of microscale chemical systems.

Fabrication of microchemical systems in glass has evolved but does not have the direct benefit from the progress of the IC industry. Despite this, we think that the glass platform could evolve to become more widely used than silicon, to some extent motivated by the lower cost. In addition, chemists have traditionally used glassware, consider glass as a natural choice for performing chemistry and hence are more comfortable with adopting systems made in glass. In addition, efforts based on these platforms have come far in overcoming the interfacing hurdles, especially with macroscale (specialized bonding techniques to connect glass tubes at high pressure and temperature to epoxy based adhesives and more recently to adaptation of metal soldering).

Silicon microfabrication has benefited from the IC industry's methodologies for on-chip integration of electronic sensing and analysis instruments. The potential for on-chip control of complex multistep processes has yet to be realized, but could prove to be the determining point in this struggle. Finally, it is possible that before an industry-wide

dominant platform emerges, and this may take a long time, various application-specific standards emerge. Such a trend is common in the innovation cycle, however, once the more commonplace, dominant platform emerges it might replace the different application specific standards. This evolution would be a result of further advancement of the industry-wide standard and its economic attraction. In other instances the individual application specific standards persist for a long time, creating separate protected niches. In the latter case, the niches often have low volumes, require high degree of customization and as a result do not invite big players efficient in the dominant technology.

	Material compatibility	***Ease of interfacing***	***Ease of Integration of sensing, control and analysis***	***Fabrication ease and cost***
Polymers	OK	Very good	OK	Easy and cheap, but slow, large feature size
Glass	Excellent	Good	Very Good	Difficult and cheap, knowledge and popularity limited to few players
Silicon	Excellent	Good	Excellent	Benefits from IC fabrication, expensive but with large economies of scale
Steel	Good	Very good	Not an ideal material for electronic component integration	Easy and cheap, but slow, large feature size

Figure 1. *Comparison of different materials along important dimensions*

1.2.4. Where to position in the struggle

PC industry

The question then is which one is the driving factor: product, process or platform? Where should a venture looking to commercialize the technology position itself. The right material must be chosen along with the interface between components and with the macroworld to allow variety of processes and then for the best to emerge. The most suitable process would then support the best product development, manufacturing or discovery methodology. Platforms enable processes, and processes enable products in the value chain. The product is closest to customer. However, commoditization in one area or innovation and efficiency in another can shift the locus of value elsewhere in the chain. Example exists in the PC industry when IBM was invested in chip design & fabrication, operating systems, peripherals, applications software, network services, memory business and assembly and the industry was vertically integrated in late 70s and early 80s. It allowed Intel in the value chain and Intel commanded power with specialization in IC design and fabrication. Little did IBM expect this. Before Microsoft, IBM did not expect the software business capable of extracting large portion of value in the PC business. Finally Dell showed that even in the so-thought commoditized distribution and assembly of PCs there was value to be extracted. Dell commands significant market power doing just that. The PC industry is horizontally structured today.

Evolving industry structure and locus of market power

The PC industry is not unique in witnessing evolution of industry architecture and shift in the locus of market power. In the consumer products sector Walmart possesses incredible power in dealing with the Procter & Gamble (P&G) or Unilever. This result is

different from the long held thought that a marketing and distribution company has the strongest muscle in consumer products business, a retailer was thought important but never imagined to be strong enough to challenge the likes of a P&G. In the telecommunications industry the integrated operations of Ma Bell gave way to horizontal structure of the Baby Bells and today again Verizon with presence in the wireless, data and land line markets displays some of the vertical structure in the industry. The locus of market power evolves and moves around with time and there is nothing like a permanent competitive advantage, [*A3*].

Companies in a young industry must involve in all parts of value chain

Companies with vision and leadership grow their operations in the direction of the next locus of power. An industry in its infancy, with huge ferment, multiple competing technologies with no clear winner, and uncertainty about its future relies more on leadership for the right direction. An effort within such an industry must keep an eye on all the moving parts, maintain a close involvement with all sources of value addition and make sure that it learns from different parts of the system to update its operations in other areas. Such an effort must strive constantly and repeatedly to differentiate, customize and extract market power at all points.

Irrespective of who wins this evolution struggle, the ferment in the microchemical synthesis industry is clear. Considering this we propose that a successful effort should choose a platform while being closely involved with process design as well as material synthesis and discovery. Such an effort is likely to be the most dynamic, capable to adapt to the best-suited platform and process as it operates on a feedback loop connecting the feedback about the suitability, success or failure of the process or product methodology

with the platform choice. We believe that efforts working through this loop would evolve in the right direction. By doing this, they might be poised to become the Intel inside just as quickly as the Walmart outside.

It is also imperative to be invested in all parts of the value chain while working in close collaboration with the customer to ascertain the success of the system as a whole. The consumer measures her satisfaction through the final product by putting in context the price she had to pay and the utility she derived in return. It is then important even as only a small part of the value chain to ascertain that the final product is of the right quality. In a mature industry and a sophisticated value chain where all the links are well oiled it is possible to play a role in only a few parts of the chain while still entrusting a dominant or a proven player in other parts. In such situations an innovative, unique methodology that serves as a value addition step can benefit from the establishes chain. However in a value chain where there are no proven players, the technological landscape is continually evolving, customer needs are still unfolding it is important to control all parts of the chain. Even when Edison was working on incandescent lamps, what distinguished his approach was the construction of a system (including the lines, generator, insulation, lamps) to deliver the final product the customers cared about, [*A4*]. New ventures must often define, establish and put together the whole value chain, a transfer chain to smoothly deliver intended value without losses.

1.2.5. Industry players

The microchemical synthesis industry consists of a number of companies, primarily in United States, Europe and Japan. Many of them have links to educational or research institutions. Some of them are discussed below.

CPC: Keywords: *modular design in steel; desktop size; macro and inter-component interfaced with number of standard metal fittings; links with Clariant, GSK*

Cellular Process Chemistry (CPC) Systems in Germany was first to develop a modular toolkit system in 1999. The toolkit comes as a desktop system, uses steel as the material of construction and consists of reaction and residence time modules, fluid distribution, delivery as well as collection apparatus integrated with temperature control. Using Steel as the material of construction allowed them to successfully integrate with the macroworld easily and for the first time realize complete, modular system.

Initial sales were met by a handful of chemical suppliers, mainly in Germany and the US. It has been engaged in collaborations with clients such as Clariant and Glaxo (GSK). CPC has helped design and initiate operations of a continuous flow pilot plant for Clariant's Division of Pigments & Additives in Frankfurt. They demonstrated superiority over large scale operations by producing a better material: more uniform size and shape distribution, without any clumping. Ties with GSK, helped synthesis of 'blockbuster substances' by multistep, continuously operated microreaction plant.

Epigem: Keywords: *modular design in plastic, polymers; sensing & control emphasis, integration of thermal, optical analysis*

The company was established in 1995, as an MBO from ICI Materials by a group of chemists, engineers and physicists experienced in polymer product development. Their microfluidic products include the Fluence toolkit: a modular toolkit using plastics and polymers as baseboard and chip material. Functional chips and interconnection choices, with interfacing compatibility and standard sensing, macrofluidic equipment available. Choice for Chip designs, variety of standard modules available. Assembly choice of tiling

vs stacking. Polymers used as material of construction with films, coatings for possible modification of surface characteristics. Fine combination of 'build your own system' from modular toolkit and custom design, development of prototypes through partnerships

Specialty microfluidic products with high standard of prototyping and product development services are also claimed. Emphasize development of integrated microfluidic solutions, with temperature control electrodes and sensor technology. Offer technology integration and consulting services too. Specialize in integration of fluid delivery, control systems along with technologies like micro-optics, micro-electrodes, thin film heating systems and analytical sensors. Collaborative product/process development services offered

Lionix: Keywords: *Design & assembly modularity; wetted materials Si/glass, Teflon; emphasis on optical & electronic sensing, integration; not much chemical synthesis*

Modules used so far include microreactors, chemical sensors (pH,conductivity,ion concentrations), CE-chips, electrodes, flow sensors, micropumps, optical detectors, filters, valves, pressure sensors. Modules can be tested and exchanged just as quickly as IC's and resistors on a printed circuit board (PCB). Integrated optics based sensors and detectors in the works. Alliances in MEMS manufacturing, software, electronics, optics. Design modularity and assembly modularity. Integration of active (electrical) components, read-out and control electronics.

Ehrfeld Mikrotechnik, part of BTS (Bayer Technology Services): Keywords: *Modular architecture in steel; demonstrated numerous reaction and chemical processes; macroworld interface with steel fittings, relatively large in size*

Toolkit: 50 modules choice in stainless steel can be assembled into a miniature chemical plant within six to eight weeks for about £50K. First contracts from specialist developers seeking new reaction pathways for their chemicals. Claim several other multistep synthesis performed, covered by confidentiality agreements with clients. This company was taken over by BTS last year.

IMM: Keywords: *Metal and ceramics standardized components, micromoulding and LIGA*

Funded by a regional German government, Institute for Microtechnology Mainz founded in 1990 is one of the oldest efforts. It offers a catalogue of some 30 'standardized' components including mixers, heat-exchangers and reactors. A number of micro- and nanoscale ventures including CPC, mikroglas and nano solutions, have been spawned by IMM alumni.

Institute of Microchemical Technology: Keywords: *Prof. Kitamori; Glass chips; emphasis on microreactors for information*

Detectors and chips from this venture are commercially available. Kitamori laboratory at the Tokyo University & Kitamori Integrated Chemistry Project at Kanagawa Academy of Science Technology's effort. Glass chips, standard designs and customized options available. Thermal lens microscope for sample detection purposes. Also sell pump, fluidic connections and peripherals as part of solution with focus on information. Supply integration technology and tools required for an ICL (Integrated Chemistry Lab.). Broad range of applications for environment, biochemistry, clinical diagnosis, pharmaceutical science, food science, agriculture and biology as their general-purpose tools for analysis.

Micro Chemical Systems: Keywords: *Electroosmotic flow pumping, glass devices*,

Steve Haswell's group at the University of Hull has developed a kit available from spin-out company Micro Chemical Systems since early 2003. It markets itself as offering specialized services and custom products for pharmaceutical, healthcare, environmental and chemicals industry. Electroosmotic flow pumping is used to drive fluids in the system consisting of glass devices, and hence has limited processing capability.

Caliper: Keywords: *High throughput, analytical systems for discovery, glass chips, publicly traded*

Involved in development and commercialization of life science instruments for pharmaceutical, biotechnology and chemical industries, with focus on the former. Caliper uses liquid handling, automation, and LabChip microfluidics technologies products for use in drug discovery and development, genomics and proteomics, and molecular diagnostics. Products include throughput screening systems, liquid handlers, robotics, storage devices, dissolution, extraction, and evaporation workstations, and software as well as LabChip devices. Selling is through a direct sales force, distributors, and OEMs. Alliances with Affymetrix, Amphora Discovery Corp., Bio-Rad Laboratories. The company's stock is publicly traded, at one time sold in excess of $200/share of stock, now hovers between 5-10 dollars.

1.3. The Active Pharmaceutical Ingredient (API) Business

An Active Pharmaceutical Ingredient is literally the active component of a tablet, capsule or the final formulation. It is the component that has the main therapeutic effect. It is the component that has emerged successful through various clinical trials over several years. For blockbuster drugs this is the chemical compound that a pharmaceutical

company spends hundreds of millions of dollars to discover and develop. The business of manufacturing Active Pharmaceutical Ingredients was about $52 billion in 2003 from $43 billion in 2000 having grown at an annualized rate of 8.4%. The industry is segmented between pharmaceutical companies that manufacture the active ingredient in-house, called captive manufacturers and the fine chemicals manufacturers (60% - 40% in 2003). There is a 75% - 25% split between the API markets for patented branded drugs and the generics segment (including over the counter drugs). In the patented branded drugs market the split between the captive and fine chemical companies is 80% - 20%. This suggests that pharmaceutical companies tend to keep production of active ingredient for the high value patented drugs in-house. This is in sharp contrast to the generics and OTC segments where 90-95% of market goes to fine chemical manufacturers. [*A5, A6*].

The fact that the pharmaceutical companies keep 80% of the API production for branded products in-house implies that they consider it important. We will discuss the value to pharmaceutical companies in detail later.

There are a number of characteristics inherent to the API industry, specially the manufacturing of patented branded drugs, that are unique and point to the suitability of microchemical synthesis to manufacture of APIs. These characteristics are briefly pointed out here and later detailed in context of assessing value of microchemical synthesis to present API manufacturers (captive and fine chemical).

- The demand for an API can completely vanish if the drug fails at any stage during the preclinical or clinical trials. In this case the production has to be shelved. However, quick and predictable scale-up of production is desired if the drug succeeds.

- API volumes for a specific drug rarely exceed 200 metric tones
- Scale up of production, bringing product faster to the market has tremendous benefits because of a fixed period of product patent available.
- Complex multistep synthesis implies alternate pathways that might involve hazardous chemical processing. Such alternate pathways could be important in reduction of waste and byproducts, fewer steps and improved quality, better compatibility with environmental restrictions.
- Pharmaceutical companies' interest in the manufacture of API is strategic and the basis of competition is definitely not cost. These are really those expensive active compounds with the cost of manufacturing being between 5-10% of the sale price.

1.4. Collaborative process, product development and production as a business

We believe that collaborative design, construction and implementation of microchemical systems for pharmaceutical product and process development, refinement and production, represents an attractive opportunity for microscale chemical synthesis. In the following sections we discuss this opportunity from the perspective of a microchemical synthesis venture.

1.4.1. Why close collaboration is critical

We have discussed that the microchemical synthesis technology in a state of ferment with market needs still unraveling, new players entering/leaving frequently while

others eager to enter. Development and delivery of the complete system where the customers care about the product is crucial.

Competitive positioning

In absence of clear/proven product based entry barrier, absence of strong patent protection, alternative ways to create and sustain a competitive edge are necessary. Service and relationship based defense with demonstrated track record, can be constructed

No proven superior product platforms or processes exist, no dominant technology or standard designs are in place. In this situation a close collaboration can serve as source of competitive edge through which an internal position can be carved out. Such entrenchment can make the venture impossible to compete with. Towards this end, it is important concentrate on best possible service to ensure successful experience, build strong relationships with key people and business units.

A close collaboration is also an opportunity to earning a reputation, building a brand for success (better quality of product/service, appropriate pricing: translate into future revenues). In addition it would be possible to ensure customer's success and experience with the microchemical system through education/initiative and appropriate push for resource mobilization.

Successful assignments

A number of big pharmaceutical, chemical companies as well as chemistry research laboratories have expressed interest in the microchemical technology. However, due to inadequate education about the methodology or initial lack of available resources their has been some disappointment. Through close collaboration it will be possible to

help realize the partners complete impact of microchemical systems and prevent intermittent/temporary shelving, unnecessary delay of the project.

Taking Industry, market and technology cues for future revenues

Through close collaboration with the API manufacturer other potential sources of value within the business can be identified. As an example it is expected to be possible to identify key links between business units (research, process development, manufacturing in the pharmaceutical industry) – interfaces where value can be added to function as a business partner. Collaboration will also help keep track of market pulse through close eye to specific customer needs (more important help understand/derive broader customer needs/habits). This will be important for growth in an evolving business climate. Finally technology decisions can be made with an additional level of feedback. Customer relationships will be used as a guide to decisions that continuously match present (tactical), and likely future (strategic) trends. Overall it is a learning and development opportunity, especially indispensable in a fast evolving climate.

1.4.2. Value to pharmaceutical companies

If costs mirror capabilities that are critical to value creation, then consideration of cost of revenue for a typical pharmaceutical company must reflect the company's processing, plant operations, purchasing capabilities. The pharmaceutical business component for a typical large size pharmaceutical company, has about 10-15% cost of goods sold, about 15% as the cost of R&D and about 35% as the marketing, sales, general and administrative costs, leaving, desirably, in excess of 30% of revenues as earnings before interests and taxes (EBIT), [*A7,A8*].

Further zooming into the cost of good sold, especially for the patented drugs reveals that about 30% of the costs come from the cost of starting material. Better processes do not normally lead to higher revenues as there is no reason that a pharmaceutical company will be able to sell larger quantity or charge a higher price in consideration of whether the manufacturing was outsourced versus performed in-house. Moreover, if the effect on the bottom line through lower costs is marginal at best, and actually uncertain considering that the microreactor technology's commercial potential has not been demonstrated before, why should the pharmaceutical companies care about microchemical synthesis? Why should they still retain in excess of 80% of the patented products production in-house in the first place?

Figure 2 depicts the different stages of drug discovery starting from target, lead identification and optimization, to preclinical, clinical and finally product launch, [*A9-A11*]. The figure also shows the long time-span of the drug-discovery stages. Pharmaceutical companies care about manufacturing patented branded drugs in-house because they care a lot about speed and flexibility, quality, control & reliability and safety. They are hesitant about outsourcing of manufacturing for branded patented drugs. Outsourcing is done only when pharmaceutical companies have a strong relationship with the API manufacturer and the API manufacturer has unique expertise with the specific class of chemistry.

There is no major gains to be had either on cost or revenue side from getting the manufacturing right, however, there is a huge cost or a loss in potential gain to decisions that compromise speed or flexibility, safety, reliability and quality. Pharmaceutical

companies maintain in-house manufacturing as a strategic lever for negotiation with the outsourcing companies when they need to.

We believe that microchemical synthesis can impact the pharmaceutical industry in the following areas:

- Speed: Faster progress from research through development to manufacturing will be possible. Better integration of different divisions/different silos in the structure to create business unit type of response and flexibility. As ancillary units to large-scale operations to help information extraction during product and process development. Strategic move towards providing customized therapeutic solutions rather than blockbusters through flexibility in manufacturing will be possible. Synthesis of small amounts of product during development and response experimentation phase will help pharmaceutical strategy.

  Safety & Reliability: Safer processes allowing operation in larger chemistry space, enabling new efficient processes, specificity in synthesis, reducing waste, conforming environmental restrictions, improving quality. Microchemical synthesis will improve process control, decrease disruptions and increase flexibility in operations.

- Strategic lever: Microchemical systems will confer better negotiating power with outsourcing companies through presence of strong state-of-the-art in-house capabilities, possible foray into generics segment.

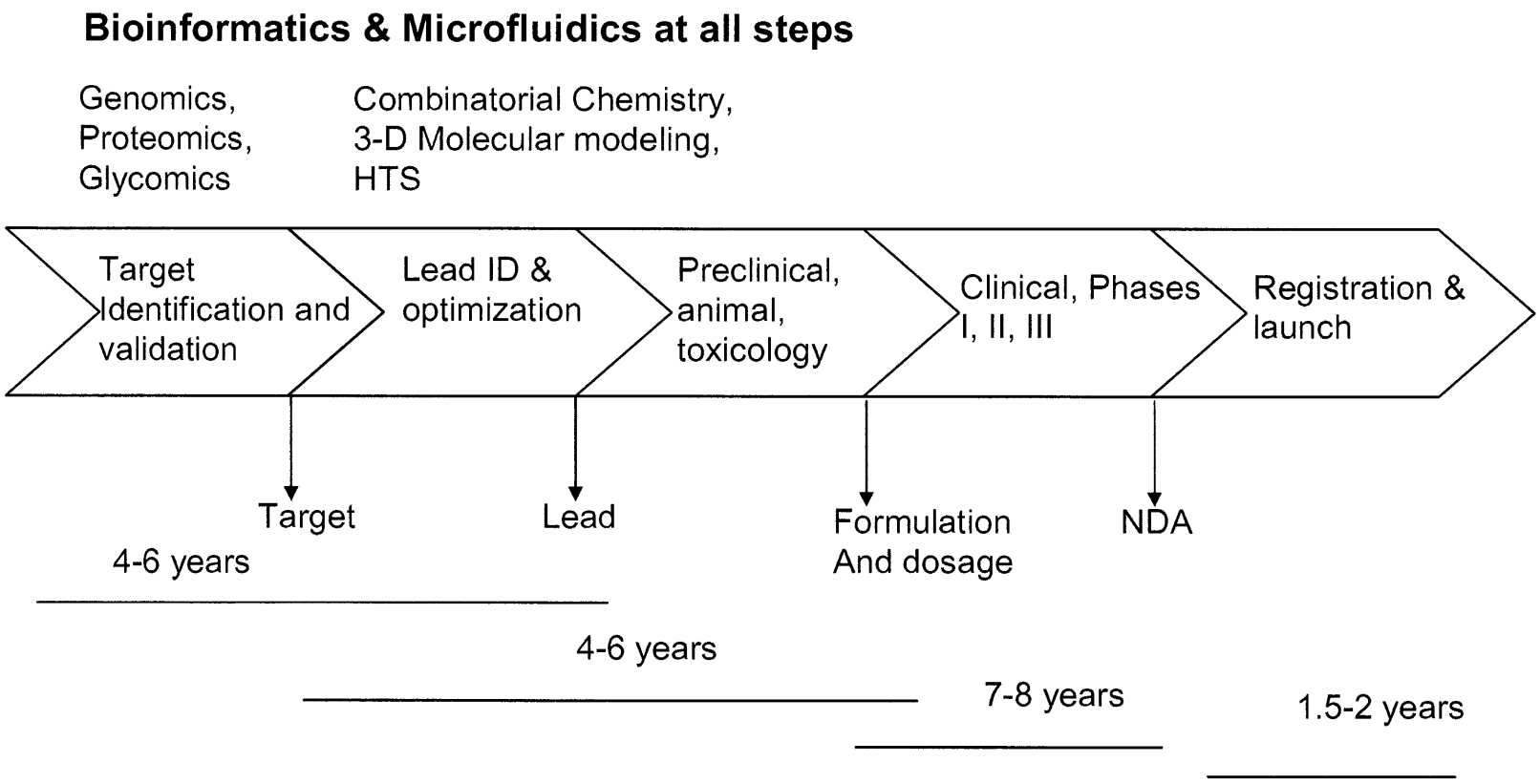

Figure 2: Phases in drug discovery, general time estimates and new technologies used at different stages

- Lower cumulative capital investments: This will be realized through pooling of demand uncertainty for different drugs. Ease of scale-up would allow postponing investment decisions until demand known better.

These are discussed in detail below.

Speed

Microchemical systems will yield faster process & product development due to scale-up by repeating of success and numbering up. Familiarity with the process and equipment from the initial stage, only in larger numbers will ensure predictability. This will also help solve any problem at the outset, remove uncertainty of process transferability when higher volumes are desired. In essence numbering-up and repeating the success is expected to avoid problems in traditional scale-up. Microchemical synthesis would help smoother transition from research through trials to process development and manufacturing. It is expected to encourage tighter integration between divisions, and knowledge transfer due to complete applicability from one stage to the next.

Why is speed important? 3 factors.

- Pharmaceutical companies file patents for discovery of new molecule before preclinical & clinical trials. Currently it takes a long and uncertain, 8-12 years, in the preclinical and clinical phases.
- Pharmaceutical patents get additional fixed period of patent life to compensate time lost in clinical & preclinicals.
- Patented drugs lose as much as 50% of there revenues in the first year of patent expiry.

Uncertain time taken for trials combined with fixed period of patent life extension granted for drug patents, and an expected loss of revenue after patent expiration makes speed of discovery through process development through manufacturing critical.

Why is it critical in the present situation?

Siloed organizational structure for pharmaceutical companies: R&D, engineering, manufacturing work efficiently in with independence thriving on scale, refining competency and coordinating with others. This structure does okay with the blockbuster model, however as pharmaceutical companies grow to an intractable size they stand to learn from the functional unit approach of companies like GE which are more decentralized and based on business unit structure. Each business unit is then responsible for its own profits. In the medical instruments industry Medtronic has succeeded with multiple technology and physician focused business units. Novartis has organized efforts to create some separate business units, such as Oncology while maintaining a backbone of shared services and separating successful brands. Johnson and Johnson is a great example where size is managed effectively through independent business units that are still able to draw from the support structure of the parent while operating independently. We expect that transitory structures may emerge in other large pharmaceutical companies before a more thorough evolution of business-unit structure. Microchemical synthesis venture can gain from and help transition in this direction. Overall this is expected to smoothen transfer of product from one stage, avoiding unnecessary delays while creating a more flexible responsive structure, [*A12*].

Numbering up of micro-reactors, in progressing through different phases requiring increased capacity, would encourage complete transfer of knowledge through divisions for direct application. It would reduce chances of friction between functional units, and hence failure in handover from one stage to the next.

Customized therapeutic solutions:

Genentech's trastuzumab *(Herceptin)* and the Her2-neu gene diagnostic, HIV cocktails and drug medley in cancer treatment are well practiced concepts. These are treatments that address the prescription of a combination of medicines tailored to patient's conditions and response. These instances of combination therapies practiced in treating patients are an exception rather than a rule in the practice of medicine. With increase in patient information storage and ease of access through automated information technology systems, in combination with trends in pharmacogenomics, pharmaceutical companies stand to find in microchemical synthesis a long-term strategic initiative. Ability to synthesize small volumes of chemicals, speed of scale-up and overall flexibility in manufacturing would be assets in implementation of personalized medicine solutions, [*A13, A14*].

In addition to this, pharmaceutical companies stand to benefit from building expertise with microchemical synthesis for the purpose of extracting process or product information eventually used for large-scale systems. Such systems are already in use especially for catalyst testing and high-throughput screening.

Safety & Reliability

Using microchemical systems would allow operation in larger chemistry space, allowing new efficient processes, specificity in synthesis easier conformance with

environmental constraints. Access to safe chemicals processing irrespective of chemistry implies ability to work with a larger space

This will lead to development and practice of new process and pathways with the following benefits:

- Improvement in final product specificity, waste reduction, and final product purity/overall quality, yields.
- Potential reduction in number of process steps required hence lower capital expenditure.
- Overall improved process economics.

In addition inherent micro-reactor processing safety will lead to large scale operations carried out with reduced extreme safeguards required (eg. ability to contain explosions). This will not only help reduce process costs but also allow to operate with increased safety and reduced risk of chemical accidents.

Microchemical synthesis would also allow better control/monitoring, uniform product properties, reduced waste or byproduct production. Overall, systems with each sub-part amenable to more localized automation, sensing and monitoring would lead to better responsive systems with lower probabilities of failure and quick identification and damage control in the event of failure.

These would lead to

- Reduction in off-spec production, waste material
- Improved final product characteristics
- Improved process economics

Strategic Lever

Pharmaceutical companies expect no additional gains from doing the manufacturing right, but face a huge downside from doing it wrong. Speed, quality, control, reliability, safety is key in pharmaceutical manufacturing. Microchemical systems can serve as process development and subsequently manufacturing tools yielding faster and efficient process development across uniform conditions. Coupled with parallel testing and less material required, easy scale up, safety even for explosive hazardous processes they present an attractive tool.

The large costs necessary to develop a novel chemical entity (NCE) will impact the API industry. It costs more than $1 billion and an average of twelve years to conduct research and gain FDA approval for one new drug (this discounted cost also includes investments for failed products), [*A15*]. In addition, generic dose-form competition comes swiftly when products lose patent protection. Typically the original patent holder has about nine years of exclusivity and then will see product price erosion in excess of 50% within the first year after the loss of exclusivity, and within a couple of years of the patent expiration, it will lose the large majority of its market share. In this environment, dose-form pharmaceutical companies are focusing greater efforts on reducing the time to market for NCEs and on protecting their blockbuster products, which are prime candidates for the generic markets, [*A16, A17*].

Strategies used by pharmaceutical companies to maximize revenue and slow or prevent market share erosion after end of patent-protected period:

- Block existing or alternative pathways for manufacture of the API/ drug through secondary patents.

- Another strategy (a version of this was misused in the early 90s before the passage of a law that forced companies to test all optical isomers and file a single patent for all of them) was coming up with a variant/purer form of the patented drug that makes the existent look both ineffective as well as unsafe in comparison. Pure enantiomeric versions of the original racemic mixtures on market fit this category of innovation quite well. An example in hand is: Sepracor patented the single isomer form of fexofenadine hydrochloride, marketed by Hoechst AG as a racemate under the name Seldane. As the generic competition approached, Allegra, the single isomer form jointly developed by Sepracor and Hoechst, received FDA approval and at the same time, the FDA ruled that with Allegra on the market it could not support Seldane because of the risks that were not inherent to Allegra. Even if the FDA officially continues to support the original drug, it can become quite unattractive for generic companies due to lack of popularity, as the generics primarily rely on volumes for significant revenues, [*A6*].

Efficient process and continued product development post discovery of the original drug is key to success of these strategies and for competitiveness in the marketplace once the patent protection is over.

Increased importance of safety, speed and reliability makes pharmaceutical companies hesitant about outsourcing of manufacturing, [*A18*]. For branded patented drugs outsourcing is done when all the following conditions are met:

- The company does not have required in-house capabilities or building capabilities would be more expensive than renting, both from long-term and a short-term

perspective. There is no long-term strategic incentive for manufacturing the particular API in-house.

- Have a strong relationship with the fine API manufacturer.
- The API manufacturer has expertise with the specific class of chemistry.

Manufacturing is a strategic lever for pharmaceutical companies as it allows them a continued better bargaining power with outsourcing companies so that they are never forced to outsource manufacturing. The collaborative development strategy is expected to appeal to them as it allows them to implement a new technology and closely monitor its progress regularly, thus never exposing themselves much to the downside. Close collaboration also means they would have an opportunity to learn the most about the technology and apply it in the best possible way.

State-of-the-art process capabilities are important and go a long way in improving profitability in the follow-on launches. Additionally, improving production efficiencies is critical to compete in the generics segment. With a big lead in terms of proprietary development capabilities, why should the pharmaceutical companies not be the best suited as the lead generic markets player? The generics market is huge and large number of drugs, with market value exceeding $45B is expected to come off-patent over the next 5 years, *[A16, A19]*.

The number of NDAs has been declining:

Foray into generics market and the follow-on strategy is of additional significance in an environment where there is a decline in the number of NDAs. The success of the API industry is tied with that of the pharmaceutical industry. A decline in the new drug output has been observed in the recent years. For example, the number of New Drug

Approvals (NDAs) has dropped from 50 approvals in 1997, to 27 in 2000, to 24 in 2001, to 17 in 2002, and to 20 in 2003), [*A19*]. The value of pharmaceutical companies is primarily tied to the success of their product pipelines. This has created a greater pressure on increasing R&D investments, improving R&D effectiveness. In addition, alternative sources of revenue growth, with less uncertainty, will look more attractive.

Major portion of the API value is in the captive manufacturing by the pharmaceutical companies. With some drug sales of the order of a few million dollars per day, the extension of patent protected life is key to pharmaceutical company profits. When the drug becomes off-patent the companies retain manufacturing primarily to maintain some control over the generics market and to utilize capacity. These companies typically lose out to dominant generic players in terms of efficient manufacturing processes. As a result, when the drug becomes off-patent the fine chemical manufacturers with their core capability in process development and manufacturing typically emerge as the low cost competitor and take over a large fraction of the market from the pharmaceutical companies.

Launching a follow-on drug, a variant of the original & role of microchemical systems:

Introduction of a follow-on drug for a compound becoming off-patent has been an attractive strategy for pharmaceutical companies. Doing this requires development of a product variant of the existing drug, with an increased safety and or effectiveness characteristics and successfully demonstrating this in preclinical and clinical trials. A strong incentive to develop the follow-on, and for being prepared with its process before the original drug becomes off-patent, will favor microchemical systems - as a tool that allows quick product and process development, experimentation and then scale-up. The

manufacturing cost will be a larger fraction of the sales when compared to the case of initial launch of a drug. Efficient processes for the follow-on drug will be useful in extracting larger profits in the wake of competition from the generic form of the original drug.

Foray into the generics market by the branded drug manufacturer and role of microchemical systems:

With the drug pipeline running dry, the pharmaceutical company that is the original innovator of the drug (eg Merck, Novartis), and enjoys exclusive rights to the drug during the period in which it is patented, will find it attractive to keep a large share of the market when the competition is open to generics. In order to do this, pharmaceutical companies will use there exclusive knowledge and lead in understanding the process for the drug to further improve the process, be the best in terms of efficiency to capture the revenues once the drug is open to generic competition. Microchemical systems will be useful as an efficient process development and eventually an excellent manufacturing platform through numbering-up of microreactors.

Capital Cost

Microchemical systems represent investment options. A modular design, will help pooling of demand, reduced investment capacity commitment upfront and hence lower overall cost. Demand uncertainty for APIs is common at all stages, during development (drug might fail trials) as well as market (customer demand may not materialize or lose to competition). Only about 5% of drugs entering the preclinical phase make it to the clinical phase and 20% of the drugs entering the clinical trials make it to the market.

As a result, capacity investment decisions that must be made beforehand are hard and must be made after accounting the possibility of project shelved or the drug cancelled. Modular designs for processes, with each step using numerous micro-reactor units will create investment options across different drugs to tackle uncertainty. They will allow better pooling of demand and require overall lower capacity investments for building same capability to handle demand.

Consider n different products, with a market demand that is normally distributed characterized by expected demand μ_i and standard deviation σ_i. For simplicity we assume that the capacity is proportional to demand desired to be met, with the proportionality constant equal to 1. A decision about the level of capacity, c_i, would be a point where the capital cost, ΔC_{Ci}, incurred per unit time (can be thought of as the annual depreciation expense) due to the incremental capacity of Δc_i is equal to the difference between expected annual incremental revenue in the event the realized demand is greater than the capacity and the expected loss in the event the realized demand is less than the capacity, and can be expressed as: $\Delta C_{Ci} = p_i(c_i)\,\Delta R_i - [1-p_i(c_i)]\,\Delta L_i$, here, $p_i(c_i)$ is the probability that the demand will be greater than the capacity c_i, ΔR_i is the incremental gain when this happens, and ΔL_i is the expected loss in the event the demand is less than c_i, **Figure 3**. In order to understand what probability levels make sense, we can proceed by assuming order of magnitude relationships between ΔC_{Ci}, ΔL_i and ΔR_i. Assuming ΔR_i is ~ 50 ΔC_{Ci} and ΔL_i is ~10 times smaller than ΔC_{Ci} itself, the above equality gives an estimate of $p_i \sim$ 0.02. For a normally distributed demand function this implies that a level of $c_i \sim \mu_i + 2\sigma_i$ would be optimal to set under these conditions.

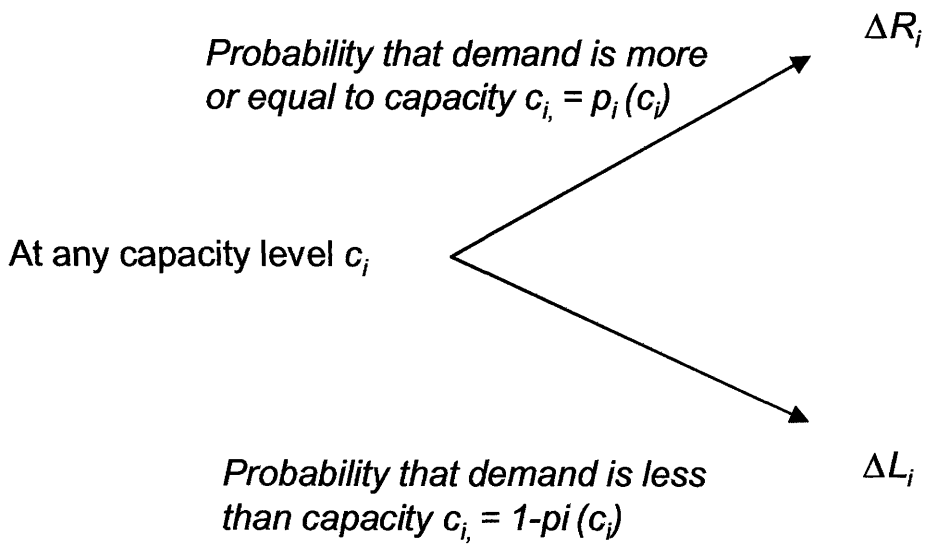

Figure 3: *The two situations that might arise at any capacity level c_i and the tree showing the probabilities and the potential gain or loss in each case. With this the expected value of the situation is derived.*

Now, if each of the n product capacities is set according to this rule, the total committed capacity is $= \Sigma \mu_i + 2 \Sigma\sigma_i$, which reduces to $n\mu + 2n\sigma$ for all μ_i 's equal to μ and all σ_i 's $= \sigma$.

Next consider the case of distributed manufacturing with a modular architecture where the different products use architectures from a common pool of modules. For illustration purposes, assume we have a single module process shared by each of the n products. Here some justification is appropriate: in practice there are possibly tens of modules, with different product processes using a set of these. However, a capacity decision must be made for each module and the following analysis would apply as well to understand how this decision is made.

We assume that the expected demand for the n different products again is normally distributed and that the demand for these n products is independent of each other. Let the demand be characterized by expected value μ_i and standard deviation σ_i, the expected demand for the module = $\Sigma \mu_i$ while the standard deviation is only = $\sqrt{\Sigma\sigma^2_i}$. For the case when all μ_i's = μ and all σ_i 's = σ the expected demand or capacity can be written as = $n\mu$ and the standard deviation for this total expected capacity for the module = $\sigma\sqrt{n}$. This effect is commonly understood as pooling of demand uncertainty, where pooling together independent variables results in the ratio of expected value to standard deviation to improve by a factor =$\sqrt{n}$. Once again we assume incremental revenue, incremental capacity cost and incremental loss ratios same as earlier, the optimal capacity level then is the point where probability of success, $p \sim 0.02$. For a normally distributed demand function a level of $c \sim n\mu + 2\sigma\sqrt{n}$ is obtained. At this level of capacity investment, just as in the first case with separate capacity investments. The comparability arises from the fact that in each case there is a 2.5% probability that the demand will exceed the committed capacity.

Figure 4 plots the ratio of committed capacity for case when demand pooling is not possible to that of modular Microsystems architecture against the number of drugs. Different lines represent varying levels of the ratio of expected demand to the its standard deviation. As shown above the increase in number of independent products decreases the standard deviation of the pooled demand. This effect is evident in the graph as we see that the value of the option to move around resources increases with the number of drugs. Moreover the value of option increases with the increase in standard deviation. For $\mu/\sigma=1$ and with 10 drugs the expected capital investment with the microsystem modular

architecture is only about 55% of that in case when pooling is not allowed. A ratio of 1 between expected value and standard deviation of demand is easily possible and can easily be lower, in the industry fraught with uncertainty.

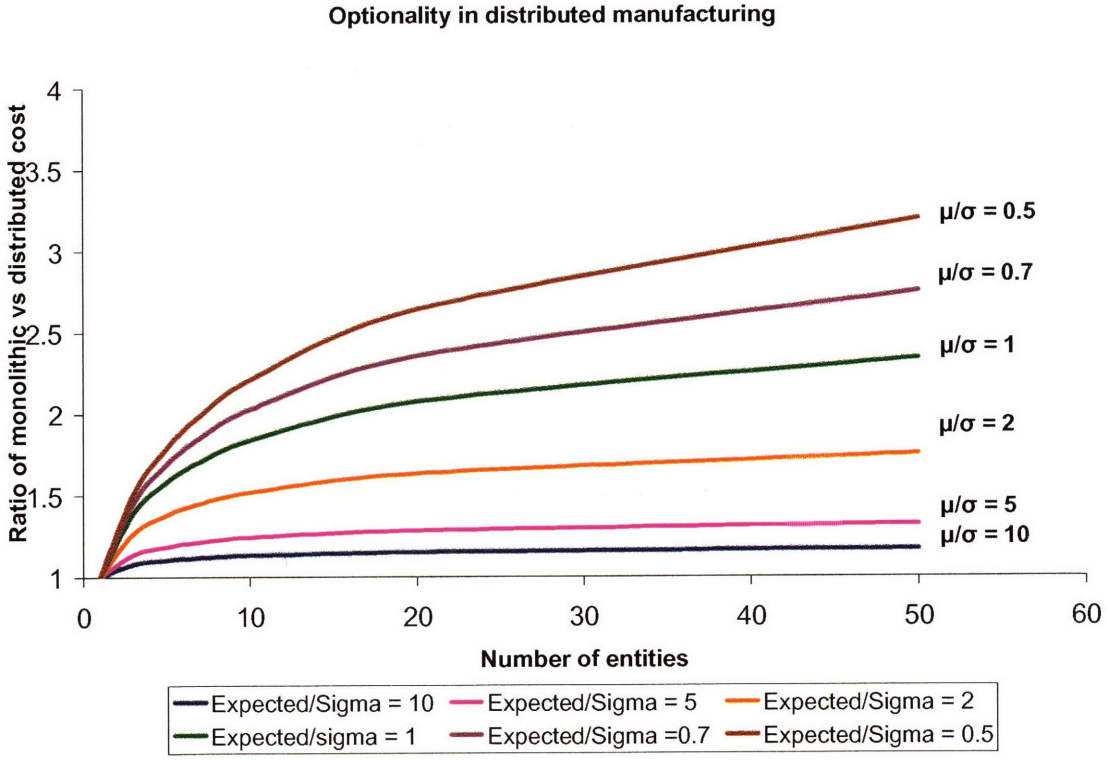

Figure 4: *Ratio of committed capacity in monolithic architecture vs modular one with demand pooling , plotted against number of drugs. Shown for different ratios of expected value and standard deviation of the demand.*

It can also be pointed here that we assume ΔR_i is ~ 50 ΔC_{Ci} and ΔL_i to be an order of magnitude smaller than ΔC_{Ci} , generally ratio between ΔR_i and ΔC_{Ci} can be larger and in that case this optionality in demand pooling would look more attractive. Distributed manufacturing also gives rise to multiple other options which would be captured in

modularity, apart from allowing to move around resources in presence of different demands realized. Ease of process scale-up and reduced uncertainty of success will allow postponement of capacity decisions to a later stage when demand may be better understood, thus further reducing overall excess capacity commitments, [*A20*].

Monolithic structures hence would have to yield to modular architectures in presence of uncertainty and the embedded optionality.

1.4.3. Value to fine-chemical companies

We have discussed in detail the multiple ways in which the small-scale synthesis of chemicals is valuable to the pharmaceutical industry. The industry is extremely fragmented with more than 1000 players, and the top 10 controlling less than 25% of the market. A number of them tend to focus on synthesis of certain class of compounds peptides and oligosaccharides exclusively. Specialization is the key in this industry, differentiation and expertise building are key to present industry structure. This bodes well for microchemical synthesis.

Manufacturing of APIs comprises of almost 50% of the $70 B fine chemicals industry, with a 30%-70% split between manufacturing of branded patented drugs and that of generics (including OTC drugs), [*A21*].

Manufacturing is core capability to the industry and hence process economics, efficiencies are critical here. Speed, safety, reliability, strategic leverage and capital investment hold analogous significance for fine-chemicals companies to continue in the business as about 50% of the industry receives its revenues from the pharmaceutical outsourcing. As opposed to the cost of goods sold at about 15% of sales for the pharmaceutical companies the fine chemical companies have the cost of goods sold at

almost 50% of sales. Benefits of API microchemical synthesis are expected to spill-over to their broader chemicals business, including generics for the fine chemicals manufacturers.

A close collaboration, of the nature described above, with fine chemical companies can be extremely beneficial for the same reasons and represents a solid opportunity. The industry being more fragmented and competitive, process efficiency being the core competency, fine chemical companies may be very eager to collaborate and implement the technology. The challenge here would be to carefully choose the business partners based on interest and initially on the expected applicability of technology to the specific case. Due to their smaller size fine chemical companies may also represent an all round learning opportunity for a new microchemical systems venture without being confounded by the sheer size and complexity of a large pharmaceutical giant.

1.4.4. Metric of success

In working through a close collaboration it will be important to define the deliverables to measure success in different areas, like process development, integration with upstream and downstream. A suitable metric may be defined in terms of time, dollar value saved or generated with respect to a benchmark. We think clear definition and tracking of a metric is extremely important for the success of a collaborative structure explained above. It can be emphasized that it may be a wise decision to not accept projects unless this can be done with satisfaction and mutually agreed upon for the specific project:

For the specific case metrics might emerge through answering basic questions like: Is it going to cost less? (eg. smaller capital investment, more cost effective operation) or generate more revenues (eg. better quality thus allow to charge higher prices or sell to a larger market)? What is the incremental value? Short run? Long run?

Further quantification might require agreement on assumptions about how much excess revenue does saved time (faster scale-up from research through manufacturing) bring. These variables must be quantified to satisfaction, although with assumptions: it is likely to be very specific to the problem. Example, process X cannot be scaled up at all, it results in being able to make something cheaper, sell at a higher price or to a broader market. The discussion on "value to pharmaceutical companies" & " value to fine chemicals company" indicates areas one can probe to define value.

We believe defining and tracking a metric closely is a way to measure, quickly improve upon reactively. It allows to build, publicize credibility and finally transform it into profits. A great tool for future negotiation with customers and in defining a new venture's focus.

1.4.5. Sources of revenue

Having laid out the structure of collaboration and value to collaborating partners, in this section we discuss the different sources of revenue.

- Contract fees & expenses
- Sale of customized systems, accessories, and eventually standard parts
- Licensing fees from IP of processes and systems developed
- On-site production of API

In starting-off with the collaborative development of microchemical systems the main source of revenue will be from the contract revenue, including fees and expenses. The fees itself might be structured based on meeting predetermined levels of success based on defined metrics mutually agreed upon.

In addition to this there is an opportunity for sale of customized systems to a selected few chemistry laboratories. Just as in the case of collaborations, these selections must be made on an understanding that the laboratory has the right interest, understanding and capability to work collaboratively with the microchemical system venture. The microchemical venture must be confident of its ability to find the right time and resources necessary to ensure the laboratory's success as well as learning for itself.

As the microsystem effort matures and gains traction we believe there might be opportunity for revenues from sale of more standardized and popular systems, licensing of patents and finally even conducting on-site production of API. However, we think that clear initial success must be established through collaborative contracts and sale of selected customized systems before that. In context of patent licensing, it is important to point out that although presently microchemical synthesis efforts do not hold strong patents, it will be important to work proactively towards building a portfolio of patents. It is not only a way to get direct licensing fees but also a magnet for future projects and a defensible source of competitive advantage. As a result this should be a conscious imperative going forward.

We discuss specifically the contract fees and expenses and sale of customized systems, as the primary initial ones and of present relevance.

Contract fees & expenses

The contractual agreement should contain two types of remuneration: Contract fees and expenses. Contract fees is a reward for performance and must involve a structure tied clearly to metrics of success defined upfront. In addition expenses covering personnel, materials and development processing must be a fixed non-negotiable portion. We believe that such a structure at the contract level will be useful in aligning the microchemical venture's incentives with that of the collaborating company. It will also help the microchemical venture to pass on similar two-stage remuneration schemes to its personnel, hence aligning incentives at all levels, recruiting the best people and rewarding them for their results.

We think it is best to start with a few contract in the first year (eg. 2-3 contracts) to ensure manageability, success of contracts while developing a process for handling a larger number of assignments.

Apart from the contract remunerations the contractual agreements represent the following benefits or options to advantage from:

- Opportunity to prove potential, earn credibility, win future contracts with present and other customers, grow business in other directions
- Develop cohesive understanding of specific customer needs, integrate learning to draw insights about broader needs, other attractive target customer segments
- Understand in-house capability & limitations, development areas and future desired direction

- Understand what it takes to get the customers to use systems successfully and what level of service, customization is needed. The extent of opportunity and in-house capability

We construct estimates below for the value of the product produced in a model microchemical system as well as annual expenses per project.

Microreactor product value estimates

At a rate of 0.1 ml/min, per single-channel micro-reactor, at a 1M concentration of compound (assuming molecular wt =100) = 10mg/min of product.

For 1 single-channel reactor ~ 6,000 mg/day* .

For 50 mg of dose, this implies 120 doses/day per single-channel reactor made.

For price of $\$P$/50 mg we get \$120 P/day worth of product, at P = \$5 a value of \$120 K/year of product/single-channel reactor is obtained.

For 25 single-channel reactors/wafer we get \$3M of product/wafer/year

Single step reactions will be important for synthesis of critical intermediates. However, if 5 such steps in a sequence are required we get \$0.6M/wafer/year

Assuming 1 person/dose/day implies 1 wafer caters for 600 patients!

*Other assumptions here: For a channel cross-section of 400X250 μm, 0.1 ml/min implies a velocity of ~1.6 cm/s, implying a residence time of about a minute, for channel length ~ 1 m.

**Assuming 200 days/year.

Microreactor development cost estimates

Process design and preliminary testing: 2-3 engineers/chemists for 9-12 months amounting to 36 personnel months to cost $200-300K.

Software, supplies, infrastructure ~ $3000-5000

Wafer + Processing cost ~ $5000/batch of 20 wafers. For 5 different reaction/process steps we get $25,000.

Material for development of system fittings, sensing and system integration capabilities ~ $3000-5000

2-3 process iterations may be justified/needed to optimize the process implying a total wafer processing cost ~ $75,000.

Development cost, if this can be split over 100 wafers (100 wafers with 20 each for 5 different steps, implies 20 wafers worth of reactor systems. Assuming 25 reactors per wafer we get 500 reactor systems) will be $800 per reactor system. This will be ~ $160/wafer if split over 500 wafers (about 300K patients) < 0.15% of the annual value of product/reactor

Cost impact/50mg dose or production ~ 1cent, when concentrated over 1 year of operation/production. If price of 50 mg dose ~ $5, cost ~ 0.15% of price per dose

When put in perspective of a pharmaceutical companies' overall cost of goods sold at ~ 10-15% of sales, while fine chemicals, API manufacturers' cost of goods sold at ~ 50% of sales, this looks reasonable. Additionally, the development cost as percentage of sales would be proportionately less if distributed over several years of production

In addition to the non-negotiable expenses portion of the contract negotiating the compensation tied to performance will be crucial in aligning incentives both with the

collaborating company and within the microchemical venture. Careful negotiation will involve the following:

- Identifying the client's specific compelling need
- Identifying incentives of the people negotiating with, their resources and limitations
- Showing them why it is attractive to them. Careful understanding and agreement on the success metrics as well as analyzing carefully the probabilities of realizing different levels of success per the metric. Clearly identifying deliverables, metric of success: its expected and final measurement
- Identifying personnel within the company who are most affected by the specific compelling need and working through them. Leveraging their pull to impact decision maker's incentives
- Relationships & initial credibility will be important
- For repeat projects past experiences, track record will be critical

Sale of customized synthesizer system, accessories, and eventually standard parts

Examples of partial success in chemists using systems are abound (CPC, Microchemical systems UK). This is definitely not ideal. Ensuring chemist's success through customization instead of force-selling standard designs that end up not being used, is crucial. As product development tools are they easier to penetrate in traditional academic research laboratories or are pharmaceutical company laboratories more attractive target markets?

Academic laboratories may be more keen on trying out new methods/processes in their developmental effort. Example is Peter Seeberger's laboratory. They may be more interested and available to work together without much formal arrangements upfront. However, needs of laboratories in an academic setting, the incentive structure are more exploratory and less efficient. Company laboratories may be more structured and might instill more discipline in a microchemical system venture. Developing a solid knowledge of chemists' specific compelling needs can be used to clearly show a chemist a synthesizer tailored to his chemistry and specific everyday needs such that the advantages are absolutely obvious. This would help succeed in the customized synthesizer market.

Broader market access, penetration and success would require distilling-off important unifying, relevant needs and then developing and offering standard designs that evolve around those needs. Eventually more standardized off-the-shelf systems and parts, may be attractive. However, this also implies commoditization and potential competitive erosion, lower barriers to entry. It will be important to build brand, reputation, distribution channel and good service record before taking this jump. This can be achieved through a conscious focus on excellent after-sales service as a source of differentiation, customer lock-in and service revenues.

Alternative businesses, for example where a microreactor venture designs and passes on the microchemical system for distribution through a chemical company with a strong distribution muscle, may not be a profitable one for the microreactor company. This is especially true in its inception stage. It will be hard for the microreactor company to extract value out of this relationship and make money if it does not have any strong patents or other sources of a defensible edge in the wake of competition. Considering

this, there is little reason why a company with strong distribution muscle pay the microreactor venture once it has the design which is publicly available?

This business involves direct marketing and distribution to consumers and if the distribution company controls the channel and the reach, it is unlikely that the microreactor venture will gain much from supplying the distribution company. The distribution company would pay if there is opportunity for future product development. It could be different if the microreactor company possesses unique and proven record of churning out repeated designs in an environment where consumer demands are changing quickly. In addition, if the microreactor company is able to make and protect critical IP going forward much faster than everybody else, things would be different. In that case, the microreactor company would have the opportunity that players like Intel had in the chip industry, where although consumer cares about the computer, he wants to know what chip goes inside it, and is ready to pay a premium for the perceived qualities therein. It is unclear that a partnership with a distribution company would make such an opportunity available.

So if a distribution company threatens to go ahead and develop the technology on its own, should the microreactor company be scared and choose to be a supplier. We think that the microreactor company may not want to yield to this threat. Even if the distribution company goes ahead and develops the technology for itself it may be better to allow this company to use their marketing and distribution muscle to educate everyone about microreactors. In the meantime, the microreactor company can develop better expertise and be ready with its own superior, more state-of-the-art systems protected by appropriate patents. At that time it might be opportune to actually think about a contract

with the company with a strong distribution system. The microreactor company can then potentially claim the highest margin segment of an educated and developed marketplace. It can operate in the business of customized, state-of-the-art reactors and maintain a competitive edge.

That said, it might be apparent that some chemists in a larger company are interested in the technology. They might be important in identifying customer bases and research laboratories within and outside their company that might be interested in using microchemical systems. In addition, these chemists might recognize the attractiveness of microchemical systems and be interested in building a relationship rather than just finding out what the microreactor company can do and how, and try to do it themselves. Thus overall such companies with a strong distribution arm look like an opportunity with some people within the company who might be interested in a collaborative arrangement.

1.5. Glimpses of pharmaceutical and chemical companies' efforts with microchemical synthesis

- Since August 1998 Merck KGaA is running several microreactors for the production of fine chemicals, in Darmstadt, Germany. For this company flexible production is important as it sells more than 10,000 different chemicals, ~ 2/3 are manufactured at an annual volume of less than 10kg.
- Merck KGaA has used microreaction technology in a full-scale plant facility for around five years, producing 15 tpa of one specialty intermediate in Gernsheim, Germany.

- Since 2002, Merck KGaA has also been running a pilot plant in Darmstadt, built from modular units and designed to yield about 7 tpa of some 10 other key intermediates
- Similarly, at BASF in Ludwigshafen, Germany microreactor syntheses have been studied and the results used to optimize several processes.
- Clariant, DuPont and BASF are using microreactors in process development and/or production.
- BTS (Bayer Technology Services) took over Ehrfeld Microsystems in 2004.
- Siemens automation and drives has been working on the controls/automation aspects of microchemical synthesis.

1.6.Main Trends and opportunities for microchemical synthesis industry

Before closing we want to re-emphasize 3 trends identified, which we understand are critical to be demonstrated to create successful microchemical efforts.

- Design compatibility with macroworld is considered crucial. This facilitates a possibility of using Microsystems in phases alongside their existent systems and will improve adoption.
- Integration of sensing and control, complete automation is considered an imperative for success. As the number of parts increases the system complexity explodes, it will be useful to demonstrate the manageability of complexity in numbering up and repeating the success of single units as well as interfaced with other process steps in a sequence.

Siemens Automation and Drives (A&D) is invested in this effort. Siemens A&D is partnering with Axiva, Merck, Fraunhofer Institute for Chemical Technology (ICT) and sponsored by Germany's Federal Ministry of Education and Research (BMBF) develop a microreaction system for industrial use. They are working on pressure, temperature, mass flow, density control at every stage of the system.

- Better collaboration with reward and responsibility sharing: Hesitation among chemical and pharmaceutical industry because of uncertainty and knowledge gap between them and microchemical systems efforts. A close collaborative arrangement and hand-holding would be a strong word of confidence. It will also help clear any potential lofted notions about microchmical system potential while instilling a strong sense of what is attractive to pursue and achievable.

References

A1. Christensen, C.M., The Innovator's Dilemma, (2000), Harper Business, New York.

A2. Henderson, R, MIT Sloan School of Management , Lectures

A3. Fine, C.H., Clockspeed, 1999, Cambridge, Massachusetts: Perseus Books

A4. Utterback, J.M, Mastering the Dynamics of Innovation, 1996, Harvard Business School Press

A5. Cometta, C et al, Active Pharmaceutical Ingredients, July 2001, Stanford Research Institute

A6. Hajduk, F et al, Active Pharmaceutical Ingredients, August 2004, Stanford Research Institute

A7. Financial Report, Pfizer Inc. 2003

A8. Financial Report Merck & Company 2003

A9. Chow, S., Pong, A., An Overview of the Regulatory Approval Process in Drug Development, Drug Information Journal, Oct-Dec 1998, Vol 32

A10. DiMasi, J.A. et al, The Price of Innovation: New Estimates of Drug Development Costs, Journal of Health Economics, 2003, Vol 22

A11. Somberg, J.C., The Drug Discovery Process: Increasing Efficiency and Cost Effectiveness, 1996, Marcel Dekker New York

A12. Gilbert, J. et al, Rebuilding Big Pharma's Business Model, In Vivo, Nov. 2003, 21(10)

A13. United States Pharmacogenomics Market, Frost & Sullivan, 2001

A14. Barton, C. L., The Future of Personalized Medicine, Reuters Business Insight, 2004

A15. Tufts Center for the Study of drug development, Impact Report, September/October 2002, 4 (5)

A16. Tufts Center for the Study of drug development, Outlook 2004

A17. Coe, J., Pharmaceutical and Biotech Growth Strategies, Reuters Business Insight, 2004

A18. Birch, S., The Pharmaceutical Outsourcing Outlook, Reuters Business Insight, 1999

A19. www.fda.gov

A20. Dixit, A. K., Pindyck, R.S., The Options Approach to Capital Investment, Harvard Business Review, May-June 1995

A21. Zekauskas, J.J., Chemicals Quarterly, JP Morgan Chase & Co., Sep. 2004